# Geology, Mineralogy, Geochemistry, and Petrogenesis of Ni-Cu-(PGE) and PGE-(Cu)-(Ni) Deposits in China

by

Yiguan Lu

A thesis submitted in partial fulfillment
of the requirements for the degree of
Doctor of Philosophy (Ph.D.)
in Mineral Deposits and Precambrian Geology

The Office of Graduate Studies
Laurentian University
Sudbury, Ontario, Canada

**THESIS DEFENCE COMMITTEE/COMITÉ DE SOUTENANCE DE THÈSE**
**Laurentian Université/Université Laurentienne**
Office of Graduate Studies/Bureau des études supérieures

| | |
|---|---|
| Title of Thesis<br>Titre de la thèse | Geology, Mineralogy, Geochemistry, and Petrogenesis of Ni-Cu-(PGE) and PGE-(Cu)-(Ni) Deposits in China |
| Name of Candidate<br>Nom du candidat | Lu, Yiguan |
| Degree<br>Diplôme | Doctor of Philosophy |
| Department/Program<br>Département/Programme | Mineral Deposits and Precambrian Geology |
| Date of Defence<br>Date de la soutenance | April 1, 2023 |

**APPROVED/APPROUVÉ**

Thesis Examiners/Examinateurs de thèse:

Dr. Michael Lesher
(Supervisor/Directeur(trice) de thèse)

Dr. Matthew Leybourne
(Committee member/Membre du comité)

Dr. Pedro Jugo
(Committee member/Membre du comité)

Dr. Chusi Li
(External Examiner/Examinateur externe)

Dr. Daniel Kontak
(Internal Examiner/Examinateur interne)

Approved for the Office of Graduate Studies
Approuvé pour le Bureau des études supérieures
Tammy Eger, PhD
Vice-President Research (Office of Graduate Studies)
Vice-rectrice à la recherche (Bureau des études supérieures)
Laurentian University / Université Laurentienne

**ACCESSIBILITY CLAUSE AND PERMISSION TO USE**

I, **Yiguan Lu**, hereby grant to Laurentian University and/or its agents the non-exclusive license to archive and make accessible my thesis, dissertation, or project report in whole or in part in all forms of media, now or for the duration of my copyright ownership. I retain all other ownership rights to the copyright of the thesis, dissertation or project report. I also reserve the right to use in future works (such as articles or books) all or part of this thesis, dissertation, or project report. I further agree that permission for copying of this thesis in any manner, in whole or in part, for scholarly purposes may be granted by the professor or professors who supervised my thesis work or, in their absence, by the Head of the Department in which my thesis work was done. It is understood that any copying or publication or use of this thesis or parts thereof for financial gain shall not be allowed without my written permission. It is also understood that this copy is being made available in this form by the authority of the copyright owner solely for the purpose of private study and research and may not be copied or reproduced except as permitted by the copyright laws without written authority from the copyright owner.

# ABSTRACT

Nickel, copper, and platinum-group minerals are regarded as “Critical Minerals” that are crucial to the national economy and sustainable development. Magmatic sulfide deposits account for approximately 93% of Chinese nickel resources, 7.3% of Chinese copper resources, and more than 90% of Chinese platinum-group element resources. This study focuses on the mineralogy, geochemistry, and isotope geochemistry of magmatic sulfide deposits in China, including detailed studies of the Jinbaoshan and Bamazhai deposits in the Emeishan Large Igneous Province, leading to a metallogenic model for the spectrum of magmatic sulfide deposits in China.

The 260 Ma Jinbaoshan platinum-group element (PGE) deposit in SW China is a sulfide-poor magmatic PGE deposit that experienced multiple phases of post-magmatic modification. It is characterized by: 1) high-temperature violarite-pyrite1-millerite-chalcopyrite and 2) low-temperature violarite-(polydymite)-pyrite2-chalcopyrite assemblages with more than 16 varieties of platinum-group minerals. Post-magmatic hydrothermal fluids enriched the mineralization in lead, silver, cadmium, and zinc. Cobalt and platinum were also added into violarite, and expelled palladium to the margins of high-temperature violarite and millerite, which also caused the formation of pallidum-enriched minerals. Late-temperature violarite inherited palladium, rhodium, iridium, and osmium from primary pentlandite. Overall, the atypical sulfide assemblages in Jinbaoshan deposit result from multiple overprinted post-magmatic processes, but they did not significantly change the platinum-group element contents of the mineralization, which is interpreted to have formed at high magma:sulfide ratios (500~50000) through interaction of crustal sulfide and a hybrid high-magnesium magma derived by melting of a modified region of the Earth’s mantle.

The ~259 Ma Baimazhai nickel-copper-(platinum-group element) deposit is a typical magmatic sulfide deposit in Emeishan Large Igneous Province. The economic No. 3 intrusion is lenticular and concentrically-zoned from finely dispersed through “net-textured” to massive sulfides (margin to core). The sulfide assemblage comprises pyrrhotite, chalcopyrite, and pentlandite, with lesser magnetite, cobaltite, violarite, and galena. The mineralization is enriched in nickel, copper, and cobalt relative to platinum-group elements. Combined with the geochemical features of Baimzhai host rocks, the sulfides appear to have formed from a PGE-depleted magma derived from mantle source that was modified by

crustal contamination and formed at moderate magma:sulfide ratios (100–1000). Post-magmatic alteration modified the primary sulfide assemblage, resulting in secondary sulfides enriched in nickel-cobalt and antimony-lead-silver-gold. The tectonic and petrogenetic settings of Baimazhai and other deposits in China highlight the potential of nickel-copper deposits to occur in post-subduction settings and exploration potential remains for the Ailaoshan orogenic belt to host additional magmatic sulfide deposits.

Unlike other magmatic sulfide deposits in the world, many of which are older and formed primarily in extensional settings, all known Chinese deposits are younger and many are inferred to have formed in compressional settings. Mineral chemical, whole-rock geochemical, ore geochemical, and isotopic data for 18 typical deposits have been used to aid in the assessment of their genesis and prospectively. Most deposits in mountain belts appear to have been derived from magmas formed by partial melting of a modified but originally PGE-depleted mantle source with minor crustal contamination. Most deposits in the Eemeishan Large Igneous Province appear to be hosted by rocks derived from magmas generated from originally more enriched mantle sources with variable degrees of crustal contamination. Deposits related to the breakup of Rodinia exhibit transitional geochemical characteristics. Taken together with the geochemical and isotopic evidence, it is suggested many Chinese magmatic sulfide deposits were derived by melting modified mantle, most likely produced by interaction of recycled oceanic crust with depleted asthenospheric mantle.

**Key words:** Magmatic sulfide deposit; Jinbaoshan; Baimazhai; Ore genesis; Regional metallogenic features; China

# CO-AUTHORSHIP STATEMENT

The thesis comprises one review paper (Ore Geology Reviews) and two research papers (Canadian Mineralogist) with several co-authors. The project design, general goals, and focus were developed by Prof. C.M. Lesher and Prof. Jun Deng. An initial suite of 85 samples was collected by the candidate. The candidate performed all of the petrographic work, scanning electron microscopy and energy-dispersive X-ray emission spectrometry, electron probe microanalysis, selection and submittal of samples for whole-rock geochemical analysis, and laser ablation inductively-coupled plasma mass spectrometry, with assistance from Dr. William Zhe and Dr. Dongjie Tang (SEM-EDS), Dr. Zhenyu Chen and Mr. David Crabtree (EPMA), and Dr. Joseph Petrus and Prof. Matthew Leybourne (LA-ICP-MS). Interpretation of the data was done by the candidate under the supervision of the co-authors. The first drafts of the thesis, including 3 published journal papers, were completed by the candidate and edited and improved by scientific input and discussions with the co-authors.

# ACKNOWLEDGEMENTS

This PhD project was done under a co-tutelle agreement between Laurentian University in Sudbury, Canada, and China University of Geoscience (Beijing). Funding was provided by a Natural Sciences and Engineering Council of Canada Discovery grant to Prof. Michael Lesher, grants from the National Key Basic Research Development Program (2015CB452606 and 2009CB421008) to Prof. Jun Deng, and grants from the National Natural Science Foundation of China (42002110), SEG Canada Foundation, and a China Scholarship Council award to Yiguan Lu. The field work was supported by Yunnan Gold and Mineral Group Co. Ltd.

I would like to express my sincere gratitude to Prof. Lesher for all his support and supervision. His profound professional knowledge and rigorous academic attitude have deeply affected me. The completion of the thesis benefits from numerous discussions and debate, which gave me a better understanding of the principles of magmatic Ni-Cu-PGE deposits. Prof. Lesher's guidance allowed me to touch a higher academic level and greatly improved self-confidence in my future academic career.

I also greatly thank Prof. Deng for choosing me to work on this project and for always cultivating me attentively. During the postgraduate period, I have been mentored and guided by Prof. Deng all the way, whether in study and life, or in the field work, experimental testing, and study in Canada.

My sincere appreciation goes to Prof. Liqiang Yang. He set an example for me with his professional academic methods and rigorous scientific thinking. During the whole PhD study, Prof. Yang gave me a lot of support and guidance, and inspired me to move forward.

I would like to express my thanks to Prof. Matthew Leybourne, Prof. Andrew McDonald, Dr. Joseph Petrus, Dr. William Zhe, and Mr. David Crabtree for guidance and assistance in the lab.

I also acknowledge the contribution of many friends in Laurentian University and China University of Geoscience (Beijing). We shared happiness and sorrow together, and their help and encouragement during my study was a very rewarding experience for me that I will never forget.

Last, but not the least, I would like to appreciate my family for invaluable support and providing me with good learning conditions and environment along the way. Their health and happiness is my greatest wish.

# TABLE OF CONTENTS

# Chapter 1: Introduction to the thesis

## 1.1 Introduction

Magmatic Ni-Cu-PGE deposits are typically subdivided into: 1) sulfide-rich Ni-Cu-(PGE) deposits (e.g., Kambalda, Noril'sk, Sudbury, Thompson, Voisey's Bay) containing 10-90% sulfide that are mined mainly for Ni-Cu-Co; and 2) sulfide-poor PGE-(Cu)-(Ni) deposits (e.g., Bushveld, Stillwater, Lac des Iles) containing 0.5-5% sulfide minerals that are mined mainly for Pd-Pt. The 260 Ma Emeishan Large Igneous Province (ELIP) in the southwest of China comprises ~$3\times10^5$ $km^3$ of volcanic rocks and associated subvolcanic intrusions, the latter of which contain numerous Ni-Cu-(PGE) deposits, including both sulfide-poor (e.g., Jinbaoshan and Zhubu) and sulfide-rich (e.g., Baimazhai and Limahe) types. These sulfide deposits have variable Ni, Cu, and PGE concentrations and are thought to have formed through concentration of sulfide in magmatic staging chambers and transport to higher levels (Wang et al., 2006; Song et al., 2008; Wang et al., 2018) or in dynamic magma conduits (e.g., Tao et al., 2007, 2010; Wang et al., 2018). The sulfide-poor Jinbaoshan PGE deposit and the sulfide-rich Baimazhai Ni-Cu deposit represent two end-members mineralization types in the ELIP. Jinbaoshan is the largest PGE-(Cu)-(Ni) deposit in China, is hosted mainly by wehrlites, occurs as a stratiform to lenticular body, and is sulfide-poor. Baimazhai contains significant amounts of Cu-Ni-(PGE), occurs as massive to semi-massive sulfide minerals within a zoned (orthopyroxenite-websterite-gabbro) complex, and is sulfide-rich. Like many other deposits in China (e.g., Jinchuan) and a few others worldwide (e.g., Pechenga, Voisey's Bay) but unlike most other deposits worldwide (e.g., Duluth, Kambalda, Noril'sk, Perseverance, Raglan, Thompson, Sudbury), most of the sulfide-rich deposits in the ELIP are enriched in Ni-Co-Cu relative to PGE.

The Jinbaoshan PGE-(Cu)-(Ni) deposit is located in the western Yunnan Province of China and contains resources of 45 t of Pt and Pd with ore grades ranging from 1 to 5 ppm Pt+Pd, occurring as multiple internal stratiform layers in wehrlite. It is the largest PGE-dominant magmatic Ni-Cu-PGE deposit in China (Tao et al., 2007; Wang et al., 2010). The influences of the abundances of PGEs in the mantle sources and parental magmas, multiple sulfide segregation events, and fractional crystallization of sulfide melts in controlling the metal contents of the Jinbaoshan deposit have been studied by Tao et al. (2007), Zhou et al. (2008), Song et al. (2008), Wang et al. (2010, 2018), and Lu and He (2018), however, the

genesis of the Jinbaoshan PGE deposit and the processes that control the distribution of the PGE and other chalcophile elements (e.g., primary and secondary hydrothermal events) are still poorly understood. It is still not clear: 1) which base metal sulfide minerals (BMS) host the PGE; 2) how the BMS formed; and 3) what influences the post-magmatic violarite-polydymite-pyrite-millerite-chalcopyrite assemblages had on the genesis of the PGE mineralization.

The Baimazhai Ni-Cu-(PGE) deposit is located in the middle of the Jinping terrane within the Ailaoshan orogenic belt. It is the largest high-grade Ni-Cu sulfide deposit (>1 wt% Ni) in the Emeishan Large Igneous Province (Li et al., 2019). Previous studies have focused on the tectonic setting (divergent: Zhang, 2006; convergent: Wang et al., 2006; Wang and Zhou, 2006), the composition of the primary magma (high-Mg basalt: Wang and Zhou, 2006; Zhang and Ren, 2013), sulfide saturation mechanisms (Wang and Zhou, 2006; Song et al., 2008), and post-magmatic processes (Zhang et al., 2006) of the deposit. However, many of these aspects are still debated, especially whether PGE and other chalcophile elements were: 1) exsolved from BMS phases (MSS (monosulfide solid solution)-ISS (intermediate solid solution), Po (pyrrhotite)-Pn (pentlandite)-Ccp (chalcopyrite)) during cooling; 2) redistributed during deuteric and/or hydrothermal alteration; or 3) introduced/removed during deuteric and/or hydrothermal alteration.

## 1.2 Research Problems and Objectives

### 1.2.1 Crustal contamination

Mafic magmas that are emplaced at relatively shallow depths are unlikely to be saturated in sulfide and for sulfide saturation to be achieved in the low-pressure environment, either extensive fractionation or the introduction of external sulfur must occur (see discussion by Lesher and Groves, 1986; Mavrogenes and O'Neill, 1999). For this reason, incorporation of crustal S is normally considered to be an essential process in generating large Ni-Cu±PGE deposits (e.g., Lesher et al., 1984; Lesher and Groves, 1986; Ripley, 1986; Lesher and Campbell, 1993; Lesher and Stone, 1996; Naldrett, 2004; Arndt et al., 2005; Barnes and Lightfoot, 2005; Keays and Lightfoot, 2010; Ripley and Li, 2013). PGE-(Cu)-(Ni) deposits normally contain much less sulfide, so there is less (if any) need for an external source of S in those deposits.

Previous studies do not agree on the S saturation mechanism for the Jinbaoshan deposit. Tao et al. (2007) concluded that sulfide saturation occurred at depth due to olivine and chromite crystallization, and that

there is no clear evidence of crustal contamination in the S, Nd, and Os isotopes. Wang et al. (2010) suggested that sulfide saturation was likely triggered by crustal contamination, as previous studies indicated that variable degrees of crustal contamination were effective to trigger immiscible sulfide melts in staging magma chambers during the formation of Ni–Cu-dominated, sulfide-rich deposits elsewhere in the ELIP, such as the Baimazhai and Limahe deposits (Wang et al., 2006; Tao et al., 2008). Ma et al. (2009) noted that $\delta^{34}S$ values at Jinbaoshan vary between +0.6 ‰ and +2.8 ‰, systematically slightly higher than the mantle range of 0 ± 1‰, implying that at least some crustal S is present.

Sun et al. (2008) established an initial $^{187}Os/^{188}Os$ value of 0.456 ± 0.026 for the Baimazhai deposit, which they suggested indicates that the proportion of crustal-derived Os is more than 30 %. Wang et al. (2006) believed that the parental magmas of the intrusion were Si- and Mg-rich, S-undersaturated melts that became S-saturated before emplacement due to strong crustal contamination (up to ~35 %) in a deep-seated staging magma chamber. These are also consistent with the results of high $\delta^{34}S$ values (6.8-7.6 ‰) of disseminated to massive sulfides in the Baimazhai deposit (Zhang, 2005). All these indicate that the Baimazhai intrusion experienced strong crustal contamination and sulfide segregation.

Lesher and Burnham (2001) and Lesher et al. (2001) have noted that it is possible for crustal sulfide xenomelts to be shifted toward mantle S-Os isotopic compositions if the effective magma:sulfide ratios (R factors) are high enough. Thus, what is needed is an integrated mass balance analysis that incorporates S-Nd-Os isotopes, S/Se values, Ni-Cu-Co-PGE metal tenors, and lithophile trace elements (e.g., Nb/Th and Th/Yb values) to establish the degree of crustal contribution to the mineralization in the Jinbaoshan and Baimazhai intrusions.

### 1.2.2 Chalcophile element enrichment mechanisms

Magmatic sulfide deposits are concentrations of sulfide liquids containing economic concentrations of platinum-group and chalcophile elements (Barnes and Lightfoot, 2005; Naldrett, 2004). Platinum-group elements (PGE) are hosted not only by platinum-group minerals (PGM), but also by BMS minerals. Many researchers have studied the influences of the abundances of PGEs in the mantle sources and parental magmas in the ELIP, their behaviour during possible multiple sulfide segregation events, and their behaviour during fractional crystallization of sulfide melts (e.g., Wang and Zhou, 2006; Tao et al., 2007; Song et al., 2008, 2009). However, the relative roles of these processes in controlling the final

abundances of PGE are still debated and there is presently no consensus for the deposits in the ELIP. Importantly, other processes that may control the distribution of the PGE and other chalcophile elements have not been studied as intensively and are only poorly understood, including: 1) early crystallization of platinum-group element alloys; 2) subsolidus diffusion of Pd into pentlandite from MSS, ISS, and/or residual sulfide melt; 3) which BMS minerals are the carriers of PGE and other chalcophile elements; and 4) mobilization in late magmatic/hydrothermal fluids (e.g., Su and Lesher, 2011).

In particular, little work has been done on the on distribution and enrichment mechanisms of PGE and chalcophile elements in the Jinbaoshan and Baimazhai deposits because of analytical limitations. However, it is now possible to measure in situ and with improved detection limits, a full suite of trace elements in each PGE-hosting phase using laser ablation inductively coupled plasma mass spectrometry (LA-ICP-MS). This has led to a better understanding of not only which mineral phases host the PGE but also the petrogenesis of the sulfide in: 1) PGE-rich deposits in large layered mafic-ultramafic intrusions (e.g., Bushveld: Holwell and McDonald, 2007; Godel et al., 2007; Barnes et al., 2008; Hutchinson and McDonald, 2008; Holwell and McDonald, 2010; Stillwater: Godel and Barnes, 2008) and small multiphase intrusions (e.g., Lac des Iles: Djon, 2012); and (2) Ni–Cu–PGE deposits in impact melt sheets (e.g., Sudbury: Huminicki et al., 2005) and relatively small differentiated mafic-ultramafic intrusions (e.g., Noril'sk-Talnakh: Barnes et al., 2006; Aguablanca: Piña et al., 2012; Jinchuan: Chen et al., 2015).

### 1.2.3 Genesis of mineralization

The genesis of the Jinbaoshan PGE deposit has been studied by many workers, most of whom agree on an ultimate magmatic origin (Tao et al., 2007; Song et al., 2008; Wang et al., 2008, 2010). However, some have noted: 1) spatial associations of the PGMs (e.g., moncheite, atokite, sperrylite) with secondary silicate minerals, magnetite, and pyrite (Tao et al., 2007); and 2) the presence of sudburyite in a late vein (Wang et al., 2008), suggesting a significant hydrothermal overprint. Nevertheless, the relationship between mineralization and post-magmatic activity is still poorly understood. Our work shows that the sulfide assemblages in Jinbaoshan are predominantly violarite-pyrite-chalcopyrite and violarite-millerite-pyrite-chalcopyrite, with only rare primary pyrrhotite-pentlandite-chalcopyrite assemblages preserved. A further study on the distribution of PGE and other chalcophile elements in these secondary sulfide minerals will help us better understand element mobilization in late magmatic/hydrothermal stages and the link between mineralization and post-magmatic activities.

Previous work suggests that the Baimazhai Ni-Cu-(PGE) deposit is magmatic in origin, but strongly overprinted by hydrothermal activity (Wang and Zhou, 2006; Zhang et al., 2006). Wang and Zhou (2006) noted that bismuth–tellurium assemblages in the massive ores included native bismuth, parkerite, and hedleyite, believed to be related to later hydrothermal alteration. Zhang et al. (2006) noted that the base metal sulfides locally exhibit peculiar barbed texture, and are intimately associated with hydrothermal biotite, amphibole, and chlorite, suggesting that magmatic sulfide ores were subjected to hydrothermal alteration and subsequent redistribution, resulting in enrichment in Cu, Pd, and Au.

However, the problem with all these models is that few studies include analyses of all components of the system (whole rock, minerals by LA-ICP-MS) and mass balance calculations to establish whether PGE were: 1) exsolved from BMS phases (MSS-ISS, Po-Pn-Ccp) during cooling; 2) redistributed during deuteric and/or hydrothermal alteration; or 3) introduced/removed during deuteric and/or hydrothermal alteration. In addition, our preliminary work has identified several additional PGMs that have not been previously reported, some of which are likely magmatic and some of which may be hydrothermal.

### 1.2.4 Composition of mantle source and primary magma, tectonic settings, and influence on Ni-Cu-PGE mineralization

ELIP basalts have been subdivided into low-Ti and high-Ti types mainly based on Ti contents and Ti/Y values (Xu et al., 2001; Xiao et al., 2004). It is generally accepted that high-Ti basalts are associated with Fe-Ti-V oxide deposits, whereas low-Ti basalts are associated with Ni-Cu-(PGE) sulfide deposits (Tao et al., 2008; Zhou et al., 2008; Wang et al., 2011). Some workers suggest that all Ni-Cu-(PGE) deposits are derived from low-Ti magmas (Tao et al., 2006; Zhou et al., 2008; Wang et al., 2012), whereas others propose that some Ni-Cu-PGE deposits could be derived from high-Ti magmas (e.g., Yangliuping and Limahe: Song et al., 2003; Tao et al., 2008). There is an outstanding need to compile major and trace element geochemical data and Sr-Nd isotopic data from typical Ni-Cu-(PGE) deposits in the ELIP in order to establish the origin of the intrusions and the mineralization.

The Baimazhai Ni-Cu deposit, like many other Chinese Ni-Cu-(PGE) deposits, is more enriched in Ni-Co-Cu than in PGE. To account for this, some authors suggested that PGE depletion was caused by removal of small amounts of sulfide from a magma derived from a peridotitic mantle. For example, Gao et al. (2013) proposed that oxide-poor sulfide mineralization in the Huangshandong intrusion formed

from a magma that had <0.03 % sulfide removed before emplacement and was thus PGE depleted, and that oxide-rich sulfide mineralization formed from a magma that had <0.003 % sulfide removed before emplacement. Zhao et al. (2014) also suggested that the primary magma for the Huangshannan intrusion and its associated sulfide mineralization formed from different pulses of picritic magma with different degrees of crustal contamination and sulfide removals. Other examples include the Kalatongke, Limahe, and Pobei deposits, in which PGE-depletion is attributed to previous episodes of sulfide segregation in a staging chamber (Gao et al., 2012; Tao et al., 2008; Yang, 2011). However, all of these assume a peridotitic mantle source and it is equally possible that the source was pyroxenitic with an inherently higher Ni-Cu-Co and lower PGE contents, as proposed by Tonnelier (2010) for Jinchuan. To solve this problem, more precise models are needed to establish the relative fractionation of Ni-Co-Cu and PGE during sulfide removal and during mantle enrichment processes.

Nearly all the Chinese Ni-Cu-PGE deposits are located at the edge of craton margins (North China craton and Yangtze Craton) or in orogenic belts (Central orogenic belt and East Kunlun orogenic belt), the former of which is considered to be a particularly favourable geological setting to form magmatic Ni-Cu-PGE deposits (e.g., Begg et al., 2010; Maier and Groves, 2011). Jinbaoshan and Baimazhai occur along the margin of Yangtze craton and are considered to have formed in an extensional rift environment (Zhang, 2005; Wang, 2015). However, both deposits also occur in the Ailaoshan Orogenic Belt and the time of deposit formation is interpreted to have already been closed and entered into a period of subduction. Similarly, the Baimazhai deposit has also been suggested to have formed in a convergent setting by previous workers (Wang et al., 2006; Wang and Zhou, 2006). Thus, there are still debates on geological settings of the two deposits, which are located along the margin of the Yangtze Craton and in the Ailaoshan Orogenic Belt. Generally, deposits located along craton margins or in orogenic belts will show different geochemical features. To better understand the tectonic settings of the Jinbaoshan and Baimazhai deposits, a comprehensive geochemical comparison with other typical magmatic sulfide deposits located in craton margins or orogenic belts in China is needed.

## 1.3 Objectives of the Thesis

The objectives of this PhD project are to compare the genesis of sulfide-rich Ni-Cu-(PGE) and sulfide-poor PGE-(Cu)-(Ni) deposits in the ELIP to help us better understand Ni-Cu-PGE mineralization in the

ELIP in particular and LIPs (e.g., Siberia, Karoo, Deccan) in general. The aims of the project are to: 1) determine the abundances of metals in the mantle sources and parental magmas; 2) evaluate the key factors controlling the processes of sulfide segregation; 3) constrain the controls on the mechanism(s) of enrichment of PGE and other chalcophile elements; and 4) establish the relative roles of magmatic and post-magmatic process in the formation of Chinese Ni-Cu-(PGE) and PGE-(Cu)-(Ni) deposits.

## 1.4 Outline of Methodology

It is important to examine the field relationships and the nature of the country rocks, however, the paucity and poor quality of the outcrops hampered geological mapping and sampling. Consequently, most of the samples were colleted from selected representative adits at different levels.

In order to accomplish the objectives, the following methodologies were employed:

1) 85 representative ores, ore-barren mafic-ultramafic rocks, and wall rocks at Jinbaoshan (n = 55) and Baimazhai (n = 30) were collected.
2) All 85 samples were examined in transmitted and reflected light using a compound polarizing microscope to establish their mineralogy and textures.
3) The textures and compositions of platinum-group minerals in six representative polished thin sections were identified and analyzed by scanning electron microscope-based energy-dispersive X-ray emission spectrometry (SEM-ED-XRES).
4) The compositions of silicate minerals, base metal sulfide minerals, and Fe-oxide minerals were analyzed using a combination of SEM-ED-XRES and electron probe microanalyzer (EPMA)-based wavelength-dispersive XRES.
5) Trace elements in base metal sulfide and Fe-oxide minerals in 15 representative sections were analyzed by laser ablation inductively-coupled plasma mass spectrometry (LA-ICP-MS).
6) Whole-rock major, minor, and lithophile trace elements of 55 samples were analyzed on fused glass discs by wavelength-dispersive X-ray fluorescence spectrometry and by solution ICP-MS.
7) Whole-rock PGE compositions of 55 samples were analyzed by inductively coupled plasma-mass spectrometry (ICP-MS) using a Thermo Fisher X-series ICP-MS.
8) S isotopes of 15 samples were analyzed by mass spectrometry using a Thermo Finnigan MAT 253 spectrometer after conversion of sulfide to $SO_2$.

## 1.4 Organization of the Thesis

This thesis consists of this introduction to the thesis (Chapter 1), three published papers (Chapters 2-4), and a concluding chapter (Chapter 5).

Chapter 1 (this chapter) introduces the project, research problems, objectives, and the methodologies applied to solve the research problems.

Chapter 2, entitled “Genesis of the Jinbaoshan PGE-(Cu)-(Ni) deposit: Distribution of Chalcophile Elements and Platinum-Group Minerals” reports new data on BMS and PGMs in the Jinbaoshan deposit using a combination of optical microscopy, SEM-ED-XRES, EPMA-based wavelength-dispersive XRES, and LA-ICP-MS to investigate the origin of the Jinbaoshan deposit and the key factors controlling the PGEs and other chalcophile elements, as well as to enhance the understanding of PGE and PGM in magmatic and post-magmatic systems of similar PGE deposits worldwide. It has been published in a special issue of Canadian Mineralogist dedicated to the memory of Prof. A.J. Naldrett.

Chapter 3, entitled “Genesis and mechanisms of metal enrichment in the Baimazhai Ni-Cu-(PGE) deposit, Ailaoshan orogenic belt, SW China” reports new in situ trace-element analyses of sulfide minerals, new whole-rock PGE and S isotope data, and use this with previously published lithogeochemical, ore geochemical, and Nd-Os isotope data to evaluate the petrogenesis, metallogenesis, and modification of the Baimazhai Ni-Cu-(PGE) deposit. It has also been published in a special issue of Canadian Mineralogist dedicated to the memory of Prof. A.J. Naldrett.

Chapter 4, entitled “Geochemistry and genesis of magmatic Ni-Cu-(PGE) and PGE-(Cu)-(Ni) deposits in China”, compiled mineral chemical, whole-rock lithogeochemical, ore geochemical, and S-Nd-Sr-Os isotopic data from 18 representative Ni-Cu-(PGE) and PGE-(Cu)-(Ni) deposits in China and used the data to generate a comparative view that provides better constraints on the genesis and metallogenesis of Chinese Ni-Cu-(PGE) and PGE-(Cu)-(Ni) deposits. It has been published in Ore Geology Reviews and is Open Access.

Chapter 5 presents the overall conclusions of the project and possible future work.

## 1.5 Statement of Original Contributions

The original contributions made by this study include:

1) This is the first study to report several new PGMs study in the Jinbaoshan PGE-(Cu)-(Ni) deposit, and the first study to report PGE and other trace elements in the base metal sulfide and Fe-oxide minerals.

2) This is the first study to report trace elements in the base metal sulfide and Fe-oxide minerals in the Baimazhai Ni-Cu-(PGE) deposits.

3) This is the first study to report the enrichment and transportation process for the PGEs and/or other chalcophile elements in the Jinbaoshan and Baimazhai deposits.

4) This is the first study to calculate the effective R factor (magma/sulfide value) of the Jinbaoshan and Baimazhai deposits, using a combination of metal contents and S isotopes.

5) This is the first study to evaluate the genesis of both PGE-(Cu)-(Ni) and Ni-Cu-(PGE) mineralization in a single large igneous complex.

6) This is the first study to compile mineral chemical, whole-rock lithogeochemical, ore geochemical, and S-Nd-Sr-Os isotopic data from 18 representative Ni-Cu-(PGE) and PGE-(Cu)-(Ni) deposits in China to generate an integrated basis for providing better constraints on the genesis and metallogenesis of Chinese Ni-Cu-(PGE) and PGE-(Cu)-(Ni) deposits.

## References

Arndt, N., Lesher, C.M., Czamanske, G.K., 2005. Mantle-derived magmas and magmatic Ni-Cu-(PGE) deposits. Economic Geology. 100th Aniversary volume, 5-24.

Barnes, S.-J., Lightfoot, P.C., 2005. Formation of magmatic nickel sulfide ore deposits and processes affecting their copper and platinum group element contents. Economic geology 100th anniversary volume, 34: 179-214.

Barnes, S.J., Prichard, H.M., Cox, R.A., Fisher, P.C., Godel, B., 2008. The location of the chalcophile

and siderophile elements in platinum-group element ore deposits (a textural, microbeam and whole rock geochemical study): implications for the formation of the deposits. Chemical Geology, 248(3): 295-317.

Chen, L.M., Song, X.Y., Danyushevsky, L.V., Wang, Y.S., Tian, Y.L., Xiao, J.F., 2015. A laser ablation ICP-MS study of platinum-group and chalcophile elements in base metal sulfide minerals of the Jinchuan Ni–Cu sulfide deposit, NW China. Ore Geology Reviews, 65: 955-967.

Godel, B., Barnes, S.-J, Maier W.D., 2007. Platinum-group elements in sulphide minerals, platinum-group minerals, and whole-rocks of the Merensky Reef (Bushveld Complex, South Africa): implications for the formation of the reef. Journal of Petrology, 48(8): 1569-1604.

Holwell, D.A., McDonald I, 2007. Distribution of platinum-group elements in the Platreef at Overysel, northern Bushveld Complex: a combined PGM and LA-ICP-MS study. Contributions to Mineralogy and Petrology, 154(2): 171-190.

Keays, R.R., Lightfoot, P.C., 2010. Crustal sulfur is required to form magmatic Ni–Cu sulfide deposits: evidence from chalcophile element signatures of Siberian and Deccan Trap basalts. Mineralium Deposita, 45(3): 241-257.

Lesher C.M., Arndt N.T., Groves D.I., 1984. Genesis of komatiite-associated nickel sulphide deposits at Kambalda, Western Australia: A distal volcanic model. Sulphide deposits in mafic and ultramafic rocks. Institute of Mining and Metallurgy, London: 70-80.

Lesher, C.M., Campbell I.H., 1993. Geochemical and fluid dynamic modeling of compositional variations in Archean komatiite-hosted nickel sulfide ores in Western Australia. Economic Geology, 88(4): 804-816.

Lesher, C.M., Burnham, O.M., 2001. Multicomponent elemental and isotopic mixing in Ni–Cu–(PGE) ores at Kambalda, Western Australia. The Canadian Mineralogist, 39(2): 421-446.

Lesher, C.M., Burnham, O.M., Keays, R.R., Barnes, S.J., Hulbert, L., 2001. Trace-element geochemistry and petrogenesis of barren and ore-associated komatiites. The Canadian Mineralogist, 39(2), 673-696.

Lesher, C.M., Groves, D.I., 1986. Controls on the formation of komatiite-associated nickel-copper sulfide deposits: Geology and metallogeny of copper deposits; Proceedings of the Twenty-Seventh International Geological Congress, Berlin, Springer Verlag, 43–62.

Lesher, C.M., Stone, W.E., 1996. Igneous trace element geochemistry: applications for massive sulphide exploration, Geol Assoc Can, Short Course Notes. Exploration geochemistry of komatiites. 12: 153-204.

Ma, Y.S., Tao, Y., Zhu, F.L., Wang, X.Z., 2009. The sulfur isotopic characteristics and geological significance of Jinbaoshan Pt-Pd Deposit and Limahe nickel deposit. Bulletin of Mineralogy, Petrology and Geochemistry, 28(2): 123-127.

Mavrogenes J.A., O'Neill, H.S.C, 1999. The relative effects of pressure, temperature and oxygen fugacity on the solubility of sulfide in mafic magmas. Geochimica et Cosmochimica Acta, 63(7): 1173-1180.

Naldrett A.J., 2004. Magmatic sulfide deposits—geology, geochemistry and exploration: Berlin, Heidelberg, New York, Springer, 1-727.

Ripley, E.M., Li, C., 2013. Sulfide saturation in mafic magmas: is external sulfur required for magmatic Ni-Cu-(PGE) ore genesis? Economic Geology, 108(1): 45-58.

Song, X.Y., Zhou, M.F., Tao, Y., Xiao, J.F., 2008. Controls on the metal compositions of magmatic sulfide deposits in the Emeishan large igneous province, SW China. Chemical Geology, 253(1), 38-49.

Su, S., Lesher, C.M., 2012. Genesis of PGE mineralization in the Wengeqi mafic–ultramafic complex, Guyang County, Inner Mongolia, China. Mineralium Deposita, 2012, 47(1-2): 197-207.

Sun, X.M, Wang, S.W., Sun, W.D., Shi, G.Y., Sun, Y.L., Xiong, D.X., Qu, W.J., Du, A.D., 2008. PGE geochemistry and Re–Os dating of massive sulfide ores from the Baimazhai Cu–Ni deposit, Yunnan province, China. Lithos, 105(1), 12-24.

Tao, Y., Li, C., Hu, R., Ripley, E.M., Du, A., Zhong, H., 2007. Petrogenesis of the Pt–Pd mineralized Jinbaoshan ultramafic intrusion in the Permian Emeishan large igneous province, SW China. Contributions to Mineralogy and Petrology, 153(3), 321-337.

Tao, Y., Li, C., Song, X.Y., Ripley, E.M., 2008. Mineralogical, petrological, and geochemical studies of the Limahe mafic–ultramatic intrusion and associated Ni–Cu sulfide ores, SW China. Mineralium Deposita, 43(8), 849-872.

Wang, C.Y., Zhou, M.F., 2006. Genesis of the Permian Baimazhai magmatic Ni–Cu–(PGE) sulfide deposit, Yunnan, SW China. Mineralium Deposita, 41(8): 771-783.

Wang, C.Y., Zhou, M.F., Qi, L., 2010. Origin of extremely PGE-rich mafic magma system: an example from the Jinbaoshan ultramafic sill, Emeishan large igneous province, SW China. Lithos, 119(1): 147-161.

Yang, S.H. 2011. The Permian Pobei mafic-ultramafic intrusion (NE Tarim, NW China) and associated sulfide mineralization: Ph.D thesis, Hong Kong University, 1-418.

Zhang, X.S., 2005. Mafic-ultramafic rocks, metallogenetic series and prospecting targeting in the Jinping-Song Da rift: Ph.D thesis, Kunming, China, Kunming University of Science and Technology, 1-284.

# Chapter 2: Genesis of the Jinbaoshan PGE-(Cu)-(Ni) deposit: Distribution of Chalcophile Elements and Platinum-Group Minerals

**Yiguan Lu**[1,2,3,*], **C. Michael Lesher**[2], **Liqiang Yang**[1], **Matthew I. Leybourne**[2,4], **Wenyan He**[1], **Mingwei Yuan**[5], **Zhen Yang**[1], **Xue Gao**[1]

[1] State Key Laboratory of Geological Processes and Mineral Resources, China University of Geosciences, Beijing 100083, China

[2] Mineral Exploration Research Centre, Harquail School of Earth Sciences, Goodman School of Mines, Laurentian University, 935 Ramsey Lake Road, Sudbury, Ontario P3E 2C6, Canada

[3] Current Address: Tianjin Center, China Geological Survey, Tianjin 300170, China

[4] Current Address: Department of Geological Sciences and Geological Engineering, Queen's University, 36 Union Street, Kingston, Ontario K7L 3N6, Canada

[5] Yunnan Gold and Mineral Group Co., Ltd., Kunming 650224, China

* Corresponding Author email: lueyig@gmail.com

## 2.1 Abstract

The Jinbaoshan PGE-(Cu)-(Ni) deposit in SW China is a sulfide-poor magmatic PGE deposit that experienced multiple phases of post-magmatic modification. The sulfide assemblages of most magmatic Ni-Cu-PGE deposits in China and elsewhere in the world are dominated by pentlandite-pyrrhotite-chalcopyrite with lesser magnetite and minor platinum-group minerals (PGMs). However, Jinbaoshan is characterized by: 1) hypogene violarite-pyrite1-millerite-chalcopyrite; and 2) supergene violarite-(polydymite)-pyrite2-chalcopyrite assemblages. Platinum-group minerals are small (0.5-10 μm diameter) and include moncheite $Pt(Te,Bi)_2$, mertieite II $Pd_8(Sb,As)_3$, atokite $(Pd,Pt)_3Sn$, rustenburgite $(Pt,Pd)_3Sn$, irarsite IrAsS, and sperrylite $PtAs_2$, hosted mainly by violarite, silicate minerals (primarily serpentine), and millerite. The PGMs occur in two sulfide assemblages: 1) mertieite II-dominant (with irarsite,

palladium, Pd-alloy) in the hypogene assemblage and 2) moncheite-dominant (with irarsite, sperrylite, atokite) in the supergene assemblage. Palladium and IPGE (Os, Ir, Ru) are concentrated mainly in violarite, polydymite, and pyrite2. Platinum is rarely hosted by base-metal sulfide minerals and occurs mainly as discrete PGMs, such as moncheite, sperrylite, and merenskyite. Violarite and polydymite in Jinbaoshan contain more Pb-Ag than pentlandite and pyrrhotite in the Great Dyke and Lac des Iles deposit. The formation of the sulfide assemblages in Jinbaoshan can be interpreted to have occurred in three stages: (1) a magmatic Fe-Ni-Cu sulfide melt crystallized Fe-Ni monosulfide and Cu-rich intermediate solid solutions, which inverted to a primary pyrrhotite-pentlandite-chalcopyrite-magnetite assemblage; (2) an early-secondary hypogene voilarite-millterite-pyrite1-chalcopyrite assemblage formed by interaction with a lower-temperature magmatic-hydrothermal deuteric fluid; and (3) a late-secondary supergene violarite-polydymite-pyrite2-chalcopyrite assemblage formed during weathering. Late magmatic-hydrothermal fluids enriched the mineralization in Pb-Ag-Cd-Zn, which are incompatible in monosulfide solid solution (MSS), added Co-Pt into violarite, and expelled Pd to the margins of hypogene violarite and millerite, which caused Pd depletion in the hypogene violarite and the formation of mertieite II. Supergene violarite inherited Pd and IPGE from primary pentlandite. Thus, the unusual sulfide assemblages in Jinbaoshan PGE-(Cu)-(Ni) deposit resulted from multiple overprinted post-magmatic processes, but they did not significantly change the chalcophile element contents of the mineralization, which is interpreted to have formed at high magma:sulfide ratios (R factors – give values) through interaction of crustally-derived sulfide and a hybrid picritic-ferropicritic magma derived from subduction-metasomatized pyroxenitic mantle during impingement of the Emeishan plume on the Paleo-Tethyan oceanic subduction system.

Keywords: PGE-(Cu)-(Ni) deposit, Emeishan Large Igneous Province, platinum-group minerals, genesis

## 2.2 Introduction

Magmatic sulfide deposits may be sulfide-rich or sulfide-poor and contain variable contents of Ni, Cu, and platinum-group elements (PGEs). Those of value primarily because of their Ni and Cu contents tend

to be rich in sulfide, with ores containing 10-90 % sulfide. Those of value primarily because of their PGE contents tend to be poor in sulfide, with ores containing 0.5-5 % sulfide (see reviews by Naldrett, 2004, 2010; Barnes and Lightfoot, 2005). There is general agreement that sulfide-rich Ni-Cu-(PGE) deposits formed from crustal sulfide xenomelts that were upgraded by interaction with mafic and ultramafic magmas (e.g., Lesher and Campbell, 1993; Lesher and Burnham, 2001; see reviews by Naldrett, 2004; Arndt et al., 2005; Barnes and Lightfoot, 2005). However, the roles of magma mixing, contamination, and other processes in reducing sulfide solubility and the roles of sulfide melt, alloys, chromite, and PGE clusters in forming PGE-(Cu)-(Ni) deposits are still being debated (see reviews of competing models by Naldrett, 2004; Barnes and Lightfoot, 2005; Yao et al., 2021). A complicating factor is that most PGE-rich deposits have experienced some degree of post-magmatic modification of mineralogy and redistribution of the PGE and base metal sulfides (BMS), and loss of S (e.g., Su and Lesher, 2012; Holwell et al., 2014, 2017; Jenkins et al., 2020), including in some cases loss of Fe (Djon and Barnes, 2012).

The Emeishan Large Igneous Province (ELIP) in China contains several magmatic Ni-Cu-(PGE) sulfide deposits hosted by small mafic–ultramafic intrusions (e.g., Zhou et al., 2002, 2008; Lightfoot and Evans-Lamswood, 2015; Lu et al. 2019). These deposits have variable Ni, Cu, and PGE concentrations and are interpreted to have formed through concentration of sulfide in deeper "staging" magma chambers (Wang et al., 2006, 2010, 2018; Tao et al., 2015) or in dynamic magma conduits (Wang and Zhou, 2006; Tao et al., 2007, 2008; Song et al., 2008). Like many other deposits in China (e.g., Jinchuan) and a few others worldwide (e.g., Pechenga, Voisey's Bay), but unlike most other deposits worldwide (e.g., Kambalda, Noril'sk, Perseverance, Raglan), most of the deposits in the ELIP are sulfide-rich and enriched in Ni-Co-Cu relative to PGE (e.g., Baimazhai, Limahe, Yangliuping and Qingkuangshan) (Lu et al., 2019). The only PGE-rich, sulfide-poor deposit is the Jinbaoshan PGE-(Cu)-(Ni) deposit, which is also China's largest PGE deposit.

The Jinbaoshan PGE-(Cu)-(Ni) deposit is located in the western Yunnan Province of China and contains resources of 45 t of Pt and Pd with ore grades ranging from 1 to 5 ppm Pt+Pd, occurring as multiple internal stratiform layers in wehrlite (Tao et al., 2007; Wang et al., 2010). The influences of the abundances of PGEs in the mantle sources and parental magmas, multiple sulfide segregation events, and fractional crystallization of sulfide melts in controlling the metal contents of the Jinbaoshan deposit

have been studied by Tao et al. (2007), Zhou et al. (2008), Song et al. (2008), Wang et al. (2010, 2018), and Lu and He (2018), however, the genesis of the Jinbaoshan PGE deposit and the processes that control the distribution of the PGE and other chalcophile elements (e.g., primary and secondary hydrothermal events) are still poorly understood. For example, Wang et al. (2008) suggested that hydrothermal fluids were responsible for the release of the PGE from the sulfides to precipitate platinum-group minerals (PGM) at low temperature, and Tao et al. (2007) suggested that hydrothermal alteration affected the final distributions of Pt and Pd in the samples. As a result of hydrothermal alteration, initial PGMs (e.g., moncheite, atokite, cooperite) have been corroded and recrystallized during the formation of serpentine and actinolite/tremolite (Wang et al., 2008). However, it is still not clear: 1) which BMS host the PGE; 2) how the BMS formed; and 3) what influences the post-magmatic violarite-polydymite-pyrite-millerite-chalcopyrite assemblages had on the genesis of the PGE.

In this study, we report new data on BMS and PGMs in the Jinbaoshan deposit using a combination of optical microscopy, scanning electron microscope-based energy-dispersive X-ray emission spectrometry (SEM-EDXS), electron probe microanalyzer-based wavelength-dispersive XRES (EPMA), and laser-ablation inductively-coupled quadrupole mass spectrometry (LA-ICP-QMS) to investigate the origin of the Jinbaoshan deposit and the key factors controlling the PGEs and other chalcophile elements, as well as to enhance the understanding of PGE and PGM in magmatic and post-magmatic systems of similar PGE deposits worldwide.

## 2.3 Geological Setting

The 260 Ma Emeishan Large Igneous Province (ELIP) in south-central China comprises ~$3x10^5$ $km^3$ of volcanic rocks and associated subvolcanic intrusions, the latter of which contain numerous Ni-Cu-(PGE) deposits, including both sulfide-poor (e.g., Jinbaoshan and Zhubu) and sulfide-rich (e.g., Baimazhai, Limahe, Yangliuping) types (**Fig. 1**) (e.g., Chung and Jahn, 1995; Xu et al., 2001; Zhou et al., 2005; Song et al., 2008; Deng et al., 2010; Lu et al., 2019). The ~260 Ma Jinbaoshan PGE deposit is located in the western part of the Yangtze plate, adjacent to the eastern margin of the Red River fault system in the Sanjiang region (Tao et al., 2009; Yang et al., 2010, 2011; Deng et al., 2014a,2014b, 2017). It is hosted by a large sill-like ultramafic intrusion approximately 5 km long, up to 1.2 km wide, and 170 m thick, one of 11 ultramafic and 21 mafic sill-like bodies in the Jinbaoshan area that intrude Devonian and Lower

Permian strata **(Fig. 2**). The Devonian strata consist of interlayered limestone, sandstone, and slate, whereas the Lower Permian strata consist of limestone and sandy slate. The Jinbaoshan intrusion and enclosing rocks were cut by the Lishe River and divided into 2 parts.

The Jinbaoshan intrusion is composed mainly of wehrlite (~90 vol.%) with minor gabbro and clinopyroxenite (Wang et al., 2005; Tao et al., 2007). The olivine and clinopyroxene in the ultramafic rocks have been altered to serpentine and talc. In the contact zone, rocks have been altered to hornfels, marble, and other metamorphic rocks. The PGE mineralized zones occur as stratiform layers and lenses of disseminated sulfide mineralization in wehrlite. Other ultramafic and mafic rocks also contain disseminated mineralization, as well as some country rocks close to the intrusion (Lu et al., 2014). The boundaries between mineralized and unmineralized host and country rocks are transitional. The sulfides in the disseminated ore have hypidiomorphic-xenomorphic textures. The intrusion contains three major PGE-rich horizons, which have average grades of 0.5 ppm Pt + Pd. The largest PGE-rich horizon is near the base of the sill with ~2100 m long, 400 to 600 m wide, and 4 to 16 m thick, and accounts for 44% of the total PGE reserve (Wang et al., 2005).

## 2.4 Research Methods

19 representative samples were collected from Adit 1495 and Adit 1508, including PGE-mineralized samples and unmineralized wehrlite and metagabbro. Of these, 7 PGE-rich samples were selected for PGM identification and determination of BMS compositions.

PGM were identified by energy-dispersive X-ray emission spectrometry (ED-XRES) using a Hitachi S-3400N scanning electron microscope equipped with an Oxford Instruments spectrometer at the State Key Laboratory of Geological Processes and Mineral Resource, China University of Geosciences, Beijing. Analytical procedures followed those described in Yang et al. (2016). Operating conditions were 20 kV accelerating voltage, 19.5 nA beam current, and a working distance of 10 mm.

Mineral compositions were determined by wavelength-dispersive XRES using a JEOL JXA-8230 electron probe microanalyzer equipped with X spectrometers at the Institute of Mineral Resources, Chinese Academy of Geological Sciences in Beijing. Operating conditions were accelerating voltage of 15 kV for silicate and oxide minerals, and 20 kV for sulfide, beam current of 20 nA, beam size of 5 μm,

and counting times of 20 s on peak and 10 s on background. Natural minerals and synthetic materials were used as standards, all of which were tested for homogeneity before their utilization for quantitative analysis. Matrix corrections were carried out using the ZAF correction program supplied by the manufacturer.

Trace elements were analyzed by laser ablation inductively-coupled plasma quadrupole mass spectrometry (LA-ICP-QMS) using a Resonetics RESOlution M50 ArF excimer 193 nm laser coupled to a Thermo-Fisher XSeries II ICP-MS at the Geochemical Fingerprinting Laboratory in the Harquail School of Earth Sciences at Laurentian University. The masses analyzed were: $^{33}S$, $^{55}Mn$, $^{57}Fe$, $^{59}Co$, $^{60}Ni$, $^{61}Ni$, $^{63}Cu$, $^{65}Cu$, $^{68}Zn$, $^{75}As$, $^{77}Se$, $^{99}Ru$, $^{101}Ru$, $^{103}Rh$, $^{105}Pd$, $^{107}Ag$, $^{108}Pd$, $^{111}Cd$, $^{118}Sn$, $^{130}Te$, $^{121}Sb$, $^{185}Re$, $^{189}Os$, $^{193}Ir$, $^{195}Pt$, $^{197}Au$, $^{208}Pb$, and $^{209}Bi$. Dwell times were 10 ms on Fe, 5 ms on major elements, and 15 ms on trace elements. Five line-scan analyses were performed on each phase. The laser beam diameter was set at 19 μm. The laser energy was 60 mJ, the fluence 5 J $cm^{-2}$, and the repetition rate 6 Hz. Ablated material was transferred from the laser to the mass spectrometer with high purity He at 650 ml $min^{-1}$ and $N_2$ at 6 ml $min^{-1}$ via 3 m of tubing. The ICP-QMS was operated at a forward power of 1450 W. The laser has a fast washout dual-volume cell enabling fast ablation without causing laser induced element fractionation (Chew et al., 2017). All instruments were tuned to maximize signal at low oxide rates of < 0.5 % $ThO^+/Th^+$ and a Th/U value higher than 0.9. Certified reference material Po725 pyrrhotite (from Memorial University) was used for $^{99}Ru$, $^{101}Ru$, $^{103}Rh$, $^{189}Os$, $^{193}Ir$, $^{195}Pt$, and $^{197}Au$, and internal standards were S (for violarite), Ni (for millerite) and Fe (pyrite, chalcopyrite) from average of analyses by EPMA. The GSD was used to calibrate all other elements. The NIST 610 glass was used to tune the instrument prior to analyzing the certified reference materials and unknowns. There are some elements that are present in both reference materials, which were used to check accuracy and precision, yielding similar results. For Ni (violarite) and Cu (chalcopyrite), yields were checked based on stoichiometry. To account for the interference of $^{40}Ar^{59}Co^+$, $^{40}Ar^{61}Ni^+$, $^{40}Ar^{63}Cu^+$, and $^{40}Ar^{68}Zn^+$ on $^{99}Ru$, $^{101}Ru$, $^{103}Rh$, and $^{108}Pd$, respectively, a set of natural samples (gersdorffite-cobaltite, millerite, chalcopyrite, and sphalerite) with contents of PGE below detection limits were analyzed at the beginning and at end of each session in order to monitor signal at those masses and correct for peak overlaps. Element distribution maps were created on selected sulfide assemblages. All analyses were processed using Iolite 2.5 for Igor-Pro 6.34A. Each time-resolved spectra obtained was inspected to assess the presence of metalloid-rich nuggets, which appeared as isolated spikes emerging from uniform spectra and became more abundant with

increasing metalloid concentration. To obtain the element concentration in sulfide minerals, only the nugget-free parts of the signal were integrated. Limits of detection were calculated in Iolite using the method of Pettke et al. (2012).

## 2.5 Results

### 2.5.1 Samples and petrography

All samples are strongly altered. Wehrlite has a granular to poikilitic texture and contains ~70% cumulus olivine (up to 2 mm, pervasively altered to serpentine), ~20% intercumulus or oikocrystic clinopyroxene (0.2-0.5 mm, altered to actinolite/tremolite), <5% oikocrystic orthopyroxene (0.2-0.5 mm, altered to talc) and minor intercumulus biotite (**Figs. 3A-E**).

Violarite, pyrite, chalcopyrite, and millerite make up <5% of the mineralized samples and occur as disseminated sulfides in interstitial spaces between serpentine or altered clinopyroxene (**Fig. 4**). According to mineral intergrowth relationships the sulfide assemblages can be divided into 2 assemblages: 1) a hypogene violarite-pyrite1-millerite-chalcopyrite assemblage; and 2) a supergene violarite-pyrite2-chalcopyrite assemblage. Hypogene and supergene violarite (Vl1 and Vl2) can be distinguished based on texture and composition: hypogene violarite (Vl1) is massive, subhedral, and fine-grained with high Co contents (~13 wt%) (**Figs. 4A-E**), whereas supergene violarite (Vl2) is porous, ragged, and coarse-grained with relatively low Co content (~4 wt%) (**Figs. 4A-F**) (see also Nickel, 1973). The two violarites have very sharp contacts, with hypogene violarite preserved as remnants in supergene violarite. Polydymite is texturally similar to supergene violarite and is intergrown with hypogene violarite and chalcopyrite (**Figs. 4E, G**). There are three varieties of pyrite, all anhedral and modified by post-magmatic processes. Pyrite 1 (Py1) occurs in the hypogene violarite-pyrite-chalcopyrite assemblage, is coarse and porous, and is associated with chalcopyrite and millerite (**Fig. 4A**). Pyrite 2 (Py2) occurs only in the supergene violarite-polydymite-pyrite-chalcopyrite assemblage, has a relatively smooth surface, and is intergrown with supergene violarite (**Figs. 4D, F**). Pyrite 3 (Py3) occurs mainly in magnetite-carbonate veins that cut serpentine or tremolite and is subhedral to anhedral (**Fig. 4H**). Millerite forms small (<30 μm) anhedral grains that replace violarite in the hypogene violarite-millerite-pyrite-chalcopyrite assemblage and is commonly intergrown with Py1 and chalcopyrite (**Figs. 4A-B**). The base metal sulfides compositions are shown in Table S2-1.

### 2.5.2 Platinum-group minerals

134 PGM grains (PGE+Au) were identified in 6 polished thin sections containing significant abundances of PGMs: 5 sections dominated by the supergene Viol-Py-Ccp assemblage and 1 section (JBS1495-B6(1)) dominated by the hypogene Viol-Mlr-Py-Ccp assemblage. The PGMs comprise more than 16 different minerals (**Fig. 5**): including moncheite $Pt(Te,Bi)_2$ (38%), mertieite II $Pd_8(Sb,As)_3$ (23%), atokite or rustenburgite $(Pd,Pt)_3Sn$ (6.7%), irarsite IrAsS (6.7%), sperrylite $PtAs_2$ (5.2%), native platinum (4.5%), merenskyite $(Pd,Pt)Te_2$ (2.2%), native palladium (1.5%), palarstanide $Pd_5(Sn,As)_2$ (1.5%), electrum (1.5%), hollingworthite RhAsS (0.7%), and kotulskite Pd(Te, Bi) (0.7%). Other alloys (e.g., Pd-S, Pd-Cu, Pd-As-Hg, Pt-Te, Pt-Au, Pt-As-Te, Au-Pd-Pt-Ag-Sn, Au-Pt-As-Ag) are also present. Some of the PGMs are similar to those reported by Wang et al. (2008) and Tao et al. (2007), but the orders of abundances differ and some PGMs (e.g., mertieite II, palladium) that have genetic significance are reported here for the first time. The compositions of PGMs are shown in Table S2-2.

The PGMs range from 0.5 μm to 10 μm in diameter. The most common occurrences are: (i) PGM along sulfide/silicate boundaries, but they also occur (ii) included in sulfide, (iii) at sulfide/oxide boundaries, (iv) included in oxides, and (v) at oxide/silicate boundaries, and (vi) included in silicates (**Fig. 6**). The main minerals that host PGMs are magnetite, violarite, millerite, serpentine, and chalcopyrite (**Fig. 6**). The dominant PGMs in the Vl2-Py-Ccp assemblage are moncheite with lesser atokite, irarsite, and sperrylite within violarite, chalcopyrite, magnetite, and silicates, whereas the dominant PGMs in the Vl1-Mlr-Py-Ccp assemblage are mertieite II with lesser irarsite, native palladium, and Pd-Cu alloy occurring along the margins of violarite and millerite (**Fig. 6**).

Mertieite II ($Pd_8(Sb,As)_3$) is always present in the hypogene Viol-Mlr-Py-Ccp assemblage and seldom present in the supergene Viol-Pld-Py-Ccp assemblage. It occurs mainly in millerite and commonly in violarite, but never in silicates (**Fig. 6; Figs. 7C-F**). Nearly all mertieite II grains occur as 2-10 μm anhedral to rounded grains along margins of their host minerals (**Figs. 7C-F**). Mertieite II contains ~71% Pd, ~26% Sb, and ~3% As (**Supplemental Table 1**). Moncheite ($Pt(Te,Bi)_2$) is common in the supergene Viol-Py-Ccp assemblage and rare in the hypogene Viol-Mlr-Py-Ccp assemblage. Most moncheite grains also contain some Bi. The main hosts of moncheite are violarite and magnetite, and it is absent in millerite. It occurs as 2-5 μm euhedral to subhedral grains at oxide/silicate contacts, in silicates, or at sulfide/oxide contacts (**Figs. 7A, 8A, 8D**). Moncheite contains 41-56% Pt, 33-55% Te, 0-18% Bi, and small amounts

of Au, Pb, and Rh. Atokite and rustenburgite ($(Pd,Pt)_3Sn$ and $(Pt,Pd)_3Sn$) commonly occur intergrown with other PGMs (e.g., moncheite and electrum) and occur as 5-15 μm ragged grains in chalcopyrite and magnetite (**Fig. 8E, F**). Irarsite (IrAsS) occurs as 1-5 μm clusters of small lath-shaped or triangular grains in silicates and single grains enclosed in magnetite (**Fig. 8B**). In contrast, most sperrylite ($PtAs_2$) grains are 1-3 μm euhedral to anhedral grains included in magnetite, violarite, and cubanite (**Fig. 8D**, **Supplemental Table 1**). 6 grains of native platinum and 2 grains of native palladium have also been identified (**Supplemental Table 1**). Platinum forms 2-12 μm framboidal aggregates or occurs with 5-12 μm composite grains (**Fig. 8G, H**), whereas palladium occurs as 1-5 μm hexagonal to rounded grains along the margins of magnetite (**Figs. 7B, C**). Electrum occurs as 10-20 μm grains intergrown with atokite in magnetite (**Fig. 8F**). Merenskyite ($(Pd,Pt)Te_2$) occurs as 0.5-2 μm grains included in violarite or magnetite (**Fig. 8I**).

### 2.5.3 Chalcophile elements in base metal sulfides

Chalcophile elements in the base metal sulfides are shown in Table 1, and given in detail in Table S2-3. The BMS in Jinbaoshan vary widely in Ni-Cu-Co-PGE content and contain minor amounts of Pb-Ag-Cd-Zn (**Table 1**). Polydymite and violarite generally contain significant PGE, but millerite does not. 15 analyzed supergene violarites contain 0.3-1490 ppm Pd, <LLD-24 ppm Pt, 1-115 ppm Rh, <LLD-12 ppm Ru, <LLD-93 ppm Ir, <LLD-16 ppm Os, <LLD-169 ppm Pb, and 1.6-133 ppm Ag. 11 analyzed hypogene violarites contain <LLD to 9.5 ppm Pd, <LLD to 720 ppm Pt, <LLD to 20 ppm Rh, <LLD to 3.1 ppm Ru, <LLD to 10.2 ppm Ir, <LLD to 5.5 ppm Os, 2.2 to 46.8 ppm Pb, and <LLD to 58 ppm Ag. Supergene and hypogene violarite have similar Rh and IPGE (Ru, Os, Ir) contents, but supergene violarite is characterized by higher Pd and lower Pt than hypogene violarite. 18 analyzed polydymites contain <LLD-820 ppm Pd, <LLD-19.3 ppm Pt, <LLD-31.6 ppm Rh, <LLD-15.4 ppm Ru, <LLD-29.1 ppm Ir, <LLD-15.9 ppm Os, 12.4 to 165 ppm Pb, and 2.2 to 589 ppm Ag (**Table 1**).

Pyrite, chalcopyrite, and millerite have lower PGE contents than polydymite and violarite, and many grains have PGE contents below lower limits of detection (LLD) (**Table 1**). Py1 (n=8) varies from <LLD-19 ppm Pd, <LLD-35 ppm Pt, <LLD-1.3 ppm Rh, <LLD-4.9 ppm Ru, <LLD.1.4 ppm Ir, <LLD-1.2 ppm Os, 5-259 ppm Pb, 0.8-70.2 ppm Ag, <LLD-3300 ppm Zn, and <LLD-14.3 ppm Cd. Py2 (n=5) ranges from <LLD-3.4 ppm Pd, <LLD-25 ppm Pt, <LLD-0.85 ppm Rh, <LLD-0.5 ppm Ru, <LLD-3.5 ppm Ir, and <LLD-0.2 ppm Os, 6.7-48.4 ppm Pb, 0.45-35.8 ppm Ag, and only trace (many <LLD) Zn and Cd.

Py3 (n=7) contains very little (normally <LLD) PGE, and other elements vary from 49.8-257 ppm Pb, 2.7-15.6 ppm Ag, 14-530 ppm Zn, and <LLD-3.3 ppm Cd. Chalcopyrite (n=19) contains very little (many <LLD) PGE, but 4.9-48 ppm Pb, <LLD-104 ppm Ag, 100-3500 ppm Zn, <LLD-26 ppm Cd (**Table 1**). Millerite was difficult to analyze because of its small grain size, but 2 analyzed millerite contain no detectable PGE or other chalcophile elements (**Table S2-3; Fig. 9**).

Zinc and Cd are enriched in chalcopyrite and Py1, but depleted in violarite (polydymite), Py2, and Py3 (**Fig. 10**). Lead is enriched in supergene violarite, polydymite and pyrite. Silver is enriched in polydymite, chalcopyrite, and violarite, but depleted in pyrite (**Fig. 10**).

### 2.5.4 Time resolved spectra

**Figures 11** and **12** show typical time-resolved analytical spectra of pyrite, chalcopyrite, polydymite, millerite, and violarite. Py1 and Py2 have relatively flat Fe-Co-Ni signals with Pt-Pd-Ir-Te-Bi peaks suggesting that a PGM such as $(Pt,Pd)(Te,Bi)_2$ is included in Py1 and Py2 (**Fig. 11**). Because some of the PGMs may have exsolved earlier and migrated to grain boundaries and others may have exsolved later and formed inclusions, we did not attempt to integrate them into the BMS analyses.

Py3 contains no PGE signals, consistent with the spot data. Chalcopyrite contains broad Zn-Cd peaks and relatively high Pb-Ag signals, indicating chalcopyrite is locally enriched in Zn-Cd-Pb-Ag. Polydymite has high and steady Pd signals, together with some other relatively high Rh and IPGE signals, consistent with PGE occurring in solid solution in polydymite. Millerite contains several sharp Pb-As-Sb peaks, suggesting that a PGM like $Pd_8(Sb,As)_3$ occurs as inclusions in millerite.

**Figure 12** shows a comparison between supergene violarite and hypogene violarite. Supergene violarite is enriched in Ni-Co-Pd with insignificant Pt. In contrast, hypogene violarite is enriched in Ni-Co-Pt with insignificant Pd. However, Ni and Co have negative correlations in the signal, suggesting Co is replacing Ni.

### 2.5.5 LA-ICP-MS mapping

Two sulfide assemblages: Viol-Py1-Mlr-Ccp (**Fig. 13**) and Viol-Py2-Ccp **(Fig. 14**) were chosen for LA-ICP-MS mapping. $^{61}Ni^{40}Ar$ and $^{63}Cu^{40}Ar$ interfere with $^{101}Ru$ and $^{103}Rh$ (see e.g., Zhou et al., 2001), we used maps of $^{60}Ni$, $^{63}Cu$, $^{101}Ru$, and $^{103}Rh$ to determine which BMS are enriched in Ru and Rh or

interfered by Ni and Cu. In the Viol-Py1-Mlr-Ccp sulfide assemblage, millerite contains insignificant amounts of PGE. Some As was detected in millerite. Py1 is highly enriched in Co. Cu, Ag, Pb show similar element distributions in the map, suggesting that chalcopyrite is enriched in Ag and Pb (**Fig. 13**). In **Figure 13**, Rh and IPGE have similar distributions, and are concentrated in supergene violarite, ruling out the interference of $^{63}Cu^{40}Ar$ on $^{103}Rh$. Like IPGE, Pd is also mainly concentrated in supergene violarite. Platinum is rarely detected, and only shows a slightly higher concentration in hypogene violarite, which has a weak correlation with Co. Py2 is enriched in Pb and contains some Ag (**Fig. 14**).

## 2.6 Discussion

The key aspects of the formation of the Jinbaoshan deposit are discussed below, broadly in terms of reverse chronology.

### 2.6.1 Post-magmatic alteration

The primary low-temperature sulfide assemblage in magmatic Ni–Cu–(PGE) deposits is typically pyrrhotite-pentlandite-chalcopyrite ± magnetite ± pyrite (Naldrett, 2004), and mineral assemblages containing significant amounts of heazlewoodite, millerite, violarite, and/or pyrite are normally attributed to metamorphic modification (e.g., Groves et al., 1974; Eckstrand, 1975; Donaldson, 1981; Barnes et al. 2009; Konnunaho et al., 2013; Holwell et al., 2017) or supergene alteration (e.g., Nickel, 1974; Thornber, 1975a, b).

At Jinbaoshan, there is abundant evidence for post-magmatic modification of an original pyrrhotite-pentlandite-chalcopyrite-magnetite ± pyrite assemblage to produce: 1) a hypogene violarite-millerite-pyrite-chalcopyrite-magnetite assemblage; and 2) a supergene violarite-(polydymite)-pyrite-chalcopyrite-magnetite assemblage (**Fig. 15**):

a) Vl1 occurs as non-porous high-Co remnants (**Figs. 4A-B**) in the Vl2/Pld-Py2-Cp assemblage (**Figs. 4C-G**).

b) Vl2/Pld occurs as porous and cracked low-Co grains, consistent with it having replaced pentlandite or hypogene violarite.

c) On a Fe-Ni-S diagram (**Fig. 16**) primary magmatic compositions fall in the Po-Pn±Py field (the orange region in the diagram), whereas Jinbaoshan samples fall in the Py-Pld-Mlr field, indicating loss of Fe and/or gain of S (e.g., Djon and Barnes, 2012).

d) The S/Se values of low-S wehrlites and PGE mineralization range 300-2828 (Lu et al., 2014), which is lower than the mantle range of 2850-4350 (e.g., Eckstrand and Hulbert, 1987; McDonough and Sun, 1995) and many other Ni-Cu-PGE deposits (see review by Queffurus and Barnes, 2015). Selenium is less mobile than S, so the lower S/Se values suggest loss of S by breakdown of sulfide minerals (e.g., Peck and Keays, 1990; Maier, 1998; Queffurus and Barnes, 2015). Low S/Se values are commonly caused by low temperature alteration, such as serpentinization and supergene weathering (Queffurus and Barnes, 2015; Smith et al., 2016).

Together, these features indicate the sulfide assemblages in the Jinbaoshan deposit are linked to oxidation during hypogene and supergene alteration.

**Hypogene alteration**

Hypogene Py1 likely formed during sulfidation ± oxidation of pyrrhotite through reactions of the form (**Fig. 15**):

$$\underset{\text{Po}}{FeS} + 1/2S_2(aq) = \underset{\text{Py}}{FeS_2} \quad [1]$$

$$\underset{\text{Po}}{4FeS} + 2O_2(aq) = \underset{\text{Py}}{FeS_2} + \underset{\text{Mgt}}{Fe_3O_4} + S_{2(aq)} \quad [2]$$

Hypogene violarite is distinguished from supergene violarite (below) by its nonporous surface and higher Co contents (e.g., Nickel, 1973; Hudson and Groves, 1974), and has been interpreted to form by low-T oxidation alteration of pentlandite (e.g., Craig, 1971; Vaughan and Craig, 1985; Rodsjo, 1999; Grguric, 2002) through reactions of the form (**Fig. 15**):

$$\underset{\text{Pn}}{2Fe_4Ni_5S_8} + 2O_2(aq) + 2S_2(aq) = \underset{\text{Vio}}{5FeNi_2S_4} + \underset{\text{Mgt}}{Fe_3O_4} \quad [3]$$

Hypogene millerite is commonly attributed to the addition of Ni during serpentinization of olivine (e.g., Nickel, 1973; Groves et al., 1974; Eckstrand, 1975; Donaldson, 1981; Frost, 1985; Barnes et al., 2009, 2011) through reactions of the form (**Fig. 15**):

$$3Fe_4Ni_5S_8 + 9Ni(Ol) + 8O_2(aq) = 24NiS + 4Fe_3O_4 \quad [4]$$
Pn Mlr Mgt

$$3FeNi_2S_4 + 6Ni(Ol) + 2O_2(aq) = 12NiS + Fe_3O_4 \quad [5]$$
Vio Mlr Mgt

but may also represent a more completely equilibrated Py-Vio assemblage (Craig, 1971).

Holwell et al. (2017) modelled the alteration of Po-Pn-Ccp at 200°C using CHILLER (Reed, 1982) and showed that conversion of pyrrhotite to pyrite increases progressively with increasing fluid:rock ratio, but that conversion of pentlandite to millerite occurs more abruptly above a fluid:rock ratio of 3.

**Supergene alteration**

In the primitive mantle-normalized PGE profiles, the PGE patterns of supergene violarite have two patterns (**Fig. 9**), which are characterized by Pd enrichment/depletion, indicating the supergene violarite may be altered from hypogene violarite (Pd depleted) or pentlandite (Pd enriched) directly.

Magnetite is abundant in the Jinbaoshan intrusion and it is likely that most of it formed by oxidation and sulfidation of Po-Pn:

$$FeS + 2Fe_4Ni_5S_8 + 9/2O_2(aq) + 5H_2S(aq) = FeS_2 + 5FeNi_2S_4 + Fe_3O_4 + 5H_2O(aq) \quad [6]$$
Po Pn Py Vio Mgt

Mota e Silva et al. (2016) suggested that pentlandite and pyrrhotite in the Limoeiro Ni-Cu-(PGE) deposit altered to violarite and pyrite by weathering-related oxidation. Similar sulfide assemblages can be also observed at Perseverance, Black Swan, and Kambalda, all of which have been suggested to have undergone supergene alteration (Groves et al., 1974; Nickel et al., 1974, 1977). It seems likely that supergene violarite and pyrite at Jinbaoshan formed under weathering-related oxidization of pentlandite and pyrrhotite, respectively.

Similarly, supergene Vio-Pld-Py2-Ccp assemblages may have formed by Fe-loss from hypogene assemblages brought about by oxidation and the formation of magnetite or hematite (e.g., Craig 1973; Frost 1985) through reactions of the form:

$$6FeNi_2S_4 + 6NiS + 2O_2(aq) = 6Ni_3S_4 + 3FeS_2 + Fe_3O_4 \quad [7]$$

Vio Mlr Pld Py Mgt

In this case, polydymite and Py2 formed from the hypogene violarite-millerite-Py1-Cp assemblage. As a result, PGE-rich minerals like polydymite and Py2 inherited PGEs from hypogene violarite and have similar PGE profiles (**Fig. 9**).

### 2.6.2 Platinum-group elements in base metal sulfides

Platinum-group elements occur in solid solution in BMS or occur as PGMs associated with (exsolved from) BMS (Kinloch et al., 1982; Prichard et al., 2004; Godel et al., 2007). The mineralization at Jinbaoshan is enriched in Pd-Pt-Rh > IPGE > Cu-Ni (Lu et al., 2014). Time resolved LA-ICP-MS analyses of Jinbaoshan minerals confirm that some PGE occur as discrete PGMs (e.g., moncheite, mertieite II) and that some occur in solid solution (e.g., Pd in supergene violarite and polydymite, Rh and Ir in violarite and polydymite).

#### Violarite

Empirical (e.g., Peach et al., 1990; Patten et al., 2013) and experimental studies (e.g., Fleet et al., 1993; Barnes et al., 1997; Mungall et al., 2005) indicate that the PGE and other chalcophile elements fractionate during the crystallization of sulfide liquid: Os-Ir-Ru-Rh partition into monosulfide solid solution (MSS) and Pd-Pt-Cu-Au-Ag-Cd and Te-As-Bi-Sb (TABS) partition into residual sulfide melt. Pentlandite exsolves from MSS during cooling (e.g., Naldrett, 1969; Craig, 1973) and pentlandite may be enriched in Os-Ir-Ru-Rh, especially Rh, relative to pyrrhotite (Mansur et al., 2019, 2020). Although Pd is incompatible in MSS ($D_{Pd}^{MSS/Sul} = 0.01–0.24$: Crocket, 2002), pentlandite hosts Pd in many Ni-Cu-PGE deposits (e.g., Merensky Reef, Bushveld Complex: Godel et al., 2007; J-M Reef, Stillwater Complex: Godel and Barnes, 2008; Aguablanca: Piña et al., 2012; Jinchuan: Chen et al., 2015; Noril'sk: Mansur et al., 2019). This paradox has been explained by later diffusion or peritectic reaction of Pd into pentlandite (Barnes et al., 2006; Mansur et al., 2019).

In magmatic Ni-Cu-PGE deposits, Pd and Rh show a preference for pentlandite relative to other BMS, but Ru, Ir, and Os have similar distributions in pyrrhotite and pentandite (Mansur, 2020). Although most BMS have been altered in this study, it can be inferred that the original pentlandite was enriched in Pd-Rh-Ru-Ir-Os, similar to the whole-rock PGE pattern (**Fig. 9**). Hypogene violarite has similar IPGE patterns as pentlandite but has higher Co-Pt contents and lower Pd contents (**Figs. 9, 12**). The high Co content of hypogene violarite and Py1 has been attributed to modification by high-Co fluids at temperatures of 400-350℃ (Dare et al., 2011; Lu et al., 2020), which may have also introduced Pt. The depletion of Pd in hypogene violarite may reflect dissolution of Pd by hydrothermal fluids and deposition along the margins as Pd-PGMs (e.g., atokite and mertieite II).

Supergene violarite and polydymite in the Jinbaoshan deposit are also enriched in Pd-Rh-Ru-Ir-Os, suggesting that they have been inherited from pentlandite or hypogene violarite (**Figs. 9, 12, 14**). They also have similar but slightly higher PGE patterns contents than the bulk sample, suggesting that violarite and polydymite house most of the PGE (**Fig. 9**).

**Pyrite**

Pyrite is a common minor sulfide in Ni-Cu-PGE deposits. Minor amounts (<3%) may exsolve from MSS at temperatures below 700℃ (e.g., Naldrett et al. 1967; Kullerud et al. 1969; Craig 1973). However, greater abundances require post-magmatic addition of S and there is abundant evidence for addition of S by late-magmatic and/or metamorphic fluids in many Ni-Cu-PGE deposits (e.g., Seccombe et al., 1981; Djon and Barnes 2012; Piña et al. 2013; Vukmanovic et al. 2014). The pyrite in some deposits (e.g., Aguablanca, Great Dyke, Lac des lles) contains significant amounts of IPGE and Pd, which are interpreted to have been inherited from the replaced minerals (mainly pyrrhotite) (Piña et al., 2012, 2013, 2016; Duran et al., 2015). Unlike most BMS, which contain little if any Pt, some pyrite contains Pt (e.g., up to 11 ppm at Lac des lles: Djon and Barne, 2012; Duran et al., 2015). This has been attributed to dissolution of Pt-bearing PGM (e.g., moncheite and sperrylite) by hydrothermal fluids and incorporation into pyrite (Piña et al., 2012, 2016).

Based on textures and PGE contents three pyrite types can be distinguished in the Jinbaoshan deposit. **Py1** is associated with hypogene violarite and millerite and, like hypogene violarite, is enriched in Co but depleted in PGE (**Figs. 4, 9, 12**). Compared to whole-rocks, Py1 is depleted in Ir. This is because Ir

is the least mobile PGE in hydrothermal or metamorphic fluids (e.g., Keays et al., 1981; Lesher and Keays, 1984; 2002), so if BMS were deposited by hydrothermal fluids they would be depleted in Ir. **Py2** is associated with supergene violarite and has similar but slightly lower PGE contents than supergene violarite and host rocks (**Fig. 9**). As discussed above, pyrrhotite may be converted to pyrite under high $fO_2$ and $fS_2$ conditions. In addition, under weathering conditions hypogene violarite+millerite may also be converted to polydymite and Py2. In both cases Py2 could also inherit the IPGEs from pyrrhotite or hypogene violarite, which is relatively enriched in Rh and Ir (**Fig. 9**). This is also consistent with some previous studies on pyrite in Ni-Cu-PGE deposits (Piña et al., 2012, 2013, 2016; Duran et al., 2015). Two analyzed pyrite grains are slightly enriched in Pd (**Supplemental Table 2**), likely because Pd is mobile and may be concentrated during weathering (Mota-E-Silva et al., 2016; Junge et al., 2019). The Py3 occurs in veins associated with magnetite and has PGE contents below the detection limits suggesting that it is not magmatic and may be related to late hydrothermal activity.

### 2.6.3 Other chalcophile elements enrichments in base metal sulfides

Experimental studies (e.g., Li et al., 1996; Barnes et al. 1997; Mungall et al. 2005; Sinyakova and Kosyakov, 2009) indicate that at temperatures of 1200-1000°C, Os-Ir-Ru-Rh and Ni-Co partition into MSS, whereas Te-Bi-As-Sb (TABS) and other weakly chalcophile elements (Pb-Ag-Zn-Cd) partition into residual sulfide melt (e.g., Maclean and Shimazaki, 1976; Helmy et al., 2013; Liu and Brenan 2015; Duran et al., 2017; Helmy and Bragagni, 2017; Mansur et al., 2019). At temperatures of 1000-900°C intermediate solid solution (ISS) crystallizes from the residual melt. Subsequently at temperatures of 650-250°C, pentlandite and pyrrhotite exsolve from MSS and chalcopyrite exsolves from ISS. As a result, Pb-Ag-Zn-Cd are enriched in chalcopyrite but depleted in pentlandite and pyrrhotite.

In the Jinbaoshan deposit, pentlandite and pyrrhotite altered to violarite and pyrite, respectively. So theoretically violarite and pyrite would contain little Pb-Ag-Zn-Cd compared to chalcopyrite. However, Pb-Ag are not depleted in violarite relative to chalcopyrite (**Fig. 10**). Previous studies have shown that Pb-Ag are depleted in pentlandite and pyrrhotite at many Ni-Cu-PGE deposits (e.g., Aguablanca: Piña et al., 2012, 2013; Great Dyke: Piña et al., 2016; Lac des lles: Duran et al., 2016). In the Jinbaoshan deposit, both hypogene violarite and supergene violarite-(polydymite) are enriched in PGE, which appear to have been inherited from pentlandite. But unlike the pentlandite in many Ni-Cu-PGE deposits, the violarite in the Jinbaoshan deposit contains relatively high contents of Pb-Ag, especially supergene violarite

(polydymite). Pb-Ag are highly mobile under a wide range of conditions, including in hydrothermal fluids (Zhong et al., 2015; Yin and Zajacz, 2018) and under weathering conditions (McQueen et al., 2003). In comparison, hypogene violarite contains less Pb than supergene violarite, and Py1 contains more Pb than Py2. Similar to Pd, Pb may have been introduced in hydrothermal fluids and added in hypogene violarite.

### 2.6.4 Crystallization of platinum-group minerals

The principal PGMs in the Jinbaoshan deposit are moncheite (38%), mertieite II (23%), atokite (6.7%), irarsite (6.7%), and sperrylite (5.2%). In the hypogene Vio-Mlr-Py1-Ccp assemblage main PGMs include mertieite II (73.2%), moncheite (7.6%), sperrylite (2.4%) and palladium (2.4%). In the supergene Viol-Pld-Py2-Ccp assemblage main PGMs include moncheite (66.7%), atokite (11.1%), sperrylite (6.9%) and Pt-O compound (5.6%).

Experimental work suggests that the PGE sulfarsenides crystallize at high temperatures (e.g., sperrylite at ~1400℃: Hansen et al, 1958; Bennett and Heyding, 1966), especially if As contents in the initial sulfide melt are high (Dare et al., 2010; Helmy et al., 2013). Mineralized rocks in the Jinbaoshan deposit have high As/S values ($1.6\times10^{-4}$ to $8.5\times10^{-4}$, ave. $4.0\times10^{-4}$, **Supplemental Table 3**), higher than Jinchuan ($0.1\times10^{-4}$ to $3.1\times10^{-4}$, ave. $0.8\times10^{-4}$: Jiang et al., 2014), Heishan ($0.5\times10^{-4}$ to $8\times10^{-4}$ average: $2.0\times10^{-4}$: Xie et al., 2014), and even Yangliuping ($0.13\times10^{-4}$ to $11\times10^{-4}$, ave. $1.7\times10^{-4}$: Song et al., 2004; Liang et al., 2019), which contains abundant PGE-arsenides and sulfarsenides (Liang et al., 2019). Like the Creighton deposit in Sudbury and the Yangliuping deposit in ELIP, PGMs such as sperrylite, irarsite, and hollingworthite at Jinbaoshan likely crystallized directly from the sulfide melt at temperatures between 1400℃ and 850℃ (Hansen et al, 1958; Bennett and Heyding, 1966; Makovicky, 2002).

The dominant PGM in Jinbaoshan is moncheite, which is also widely distributed in many Ni-Cu-PGE deposits worldwide (e.g., Platreef, Merensky, Aguablanca). Previous studies (Holwell and McDonald, 2007, 2010; Helmy et al., 2007, 2010) have shown that semimetals like Te-Bi-Sn partition into residual Cu-rich liquid during crystallization of MSS at around 900℃, which may exsolve from subsequently crystallized ISS or migrate and crystallize with PGEs (especially Pt-Pd) in other areas of the system over temperatures of 650℃ to 250℃. In the Jinbaoshan deposit, mertieite II is commonly associated with hypogene violarite, millerite, and Py1 (**Fig. 7**), suggesting the mertieite II formed during hypogene

alteration, after sulfarsenide PGMs and Pt-Pd-Te-Bi-Sn minerals. Nearly all mertieite II grains occur at the margins of BMS, probably because Pt and Pd formed As- and Sb-bearing PGMs that would be expelled to the margins of sulfide droplets if the degree of contamination was high (Hutchinson and McDonald, 2008). Hypogene violarite is depleted in Pd (**Fig. 9**). As discussed above, Pd is enriched in MSS and later pentlandite, in addition, Pd is one of the most soluble PGEs in fluids, so it is likely that Pd from MSS/pentlandite was carried by fluids and deposited as mertieite II at the margins of hypogene violarite.

In the Jinbaoshan deposit, moncheite is strongly associated with magnetite and supergene violarite, which suggests that moncheite formed during the alteration event. Atokite is more often associated with chalcopyrite because Pd partitions into ISS, although some Pd will also partition into MSS and cause violarite to have relatively high Pd contents.

### 2.6.5 Sulfide melt formation

Mantle-derived magmas more mafic than MORB are undersaturated in sulfide (e.g., Keays, 1982; Lesher and Groves, 1986; Naldrett and Barnes, 1986). In order for sulfide saturation to be achieved, the magma must be contaminated and/or crystallize significant amounts of silicates, but because mafic magmas only dissolve 0.05-0.2% S (e.g., Haughton et al., 1974; Wendlandt, 1982; Mavrogenes and O'Neill, 1999) and because S cannot be removed quantitatively, this generates only very small amounts of sulfide (<1-2%) even if accumulated with silicate phases. For this reason, incorporation of crustal S is normally considered to be an essential process in generating S-rich Ni-Cu-(PGE) deposits (e.g., Lesher, et al, 1989; Lesher and Campbell, 1993; Lesher and Groves, 1986; Lesher et al., 1984, 2001; Keays and Lightfoot, 2010; Ripley and Li, 2013; He et al., 2014; Lesher, 2017, 2019).

The wehrlites in the Jinbaoshan deposit are cumulate rocks that contain up to 2% S as Fe-Ni-Cu sulfides (Lu et al., 2014), such high abundances of sulfide could not have crystallized from trapped intercumulus liquid, but some could have segregated and accumulated with pyroxene. Tao et al. (2007) report $\delta^{34}S$ values of 1-2‰, which are close to mantle values (0.1 ± 0.3‰: Sakai et al., 1984) and much lighter than the S in the country rocks (18‰ for a dolomite xenolith: Tao et al., 2007; 12‰ for a pyrite vein in footwall dolomite: Tao et al., 2007) (**Supplemental Table 4**). They suggest that little or no S was contributed from the country rocks and that the slightly high values can be attributed to hydrothermal modification. The

values for our samples range up to 7‰ and are still below the country-rock values, but it is possible for crustal sulfide xenomelts to be shifted toward mantle S isotopic compositions if the effective silicate liquid:sulfide liquid mass ratios (R factors) are high enough (see Lesher and Burnham, 2001). For example, reacting sulfide xenomelts containing 38% S and 18-12‰ $\delta^{34}S$ with a mafic magma containing 0.05 wt% S (see Lesher and Stone, 1996) and 0.1 ± 0.3‰ (Sakai et al., 1984) will produce the observed range of S isotopic compositions at R factors of 800 (low-PGE samples) to 40,000 (high-PGE samples) (**Fig. 17**).

The range of R factors may have also produced the observed range of ore tenors. The final abundance of metal i in a magmatic Ni-Cu-PGE sulfide melt $Y_i^f$ is controlled by the abundance of i in the initial magma ($X_i^o$), the sulfide liquid/silicate liquid partition coefficient ($Di^{Sul/Sil}$), the silicate liquid: sulfide liquid mass ratio (R: Campbell and Naldrett, 1979), and the abundance of i (if any) in the crustal sulfide xenomelt ($Y_i^o$: Lesher and Burnham, 2001):

$$Y_i^f = (X_i^o R + Y_i^o) D_i^{Sul/Sil} / (R+D_i^{Sul/Sil})$$

For simplicity, we will ignore the small amounts of metal in the external sulfide (Naldrett, 1981):

$$Y_i^f = (X_i^o R D_i^{Sul/Sil}) / (R+D_i^{Sul/Sil})$$

$Di^{Sul/Sil}$ values vary with composition, temperature, $fO_2$, and $fS_2$ (see reviews by Naldrett, 2004; Barnes and Lightfoot, 2005; Fonseca et al., 2009; Mungall and Brenan, 2014; Barnes and Ripley, 2016), but in basaltic magmas are of the order of 300-1000 for Ni, 900-1400 for Cu, $10^4$-$10^6$ or even higher for PGE. In order to compare samples with different sulfide contents, we have recalculated the metal abundances to 100% sulfide. Compared with samples collected close to the bottom of the intrusion from Wang et al. (2010), those collected for this study (see also Lu, 2014; Lu and He, 2018) are more enriched in Ni (**Fig. 18A**), which may be caused by alteration of pentlandite to Ni-rich violarite. We have recalculated them to 100% sulfide assuming that all of Cu is in chalcopyrite (34.6 wt% Cu), the Ni is divided between olivine/serpentine (0.02~0.1 wt% Ni) and violarite (38.9 wt% Ni), the remaining S is in pyrite (53.5 wt% S), but this will not significantly change the metal tenors.

Zhou et al. (2008) and Wang et al. (2018) suggested that the ores in the Jinbaoshan deposit formed from a PGE-enriched low-Ti picritic magma containing 10 ppb Pd (Wang et al., 2007, 2010) and 1 ppb Ir (Li

et al., 2012). However, Lu et al. (2019) showed that the trace element and Nd-Os isotopic characteristics of the host rocks in ELIP deposits require them to have formed from a magma derived from subduction-modified mantle, albeit less modified than the mantle from which the magmas at most other deposits in China formed. This suggests interaction between the ELIP plume and subduction-modified asthenospheric mantle and that the magma had Ni-Cu-PGE abundances intermediate between those of low-Ti picritic and basaltic magma (**Fig. 19**), of the order of 970 ppm Ni, 90 ppm Cu, 4.9 ppb Pd, and 1.1 ppb Ir. The Jinbaoshan has much lower Ru and Ni values than the modelled PGE pattern (Fig. 19), which is interpreted to reflect ~25% olivine and lesser spinel crystallization.

Returning to the ore compositions, the $Ir_{100}$ vs $Pd_{100}$ plot shows that lower-PGE samples at Jinbaoshan appear to have formed at lower R (500~2000), consistent with their high $\delta^{34}S$ values (4.4‰-6.7‰), whereas the higher-PGE samples appear to have formed at higher R (>10000), consistent with their lower $\delta^{34}S$ values (1.3‰-1.5‰) (**Fig. 18B**). Thus, the high PGE tenor of the Jinbaoshan mineralization appears to have been produced by a high R factor, not a high-PGE magma. The fairly uniform PGE pattern (Lu et al., 2014, 2019) suggests that alteration did not introduce the metals or modify them significantly.

### 2.6.6 Ore style and localization

The major, trace-element, and Nd-Sr-Os isotope chemistry of the rocks in the Jinbaoshan intrusion are similar to the other intrusions in the ELIP that host Ni-Cu-(PGE) mineralization. Thus, the composition of the magma does not appear to have determined whether the intrusions in the ELIP formed Ni-Cu-(PGE) or PGE-(Cu)-(Ni) mineralization. Baimazhai, Limahe, and Yangliuping are sulfide-rich Ni-Cu-(PGE) deposits, Zhubu is a sulfide-poor Ni-Cu-(PGE) deposit, and Jinbaoshan is a sulfide-poor PGE-(Cu)-(Ni) deposit. Thus, the amount of sulfide in the system also does not appear to have determined whether these deposits formed Ni-Cu-(PGE) or PGE-(Cu)-(Ni) mineralization.

Baimazhai, Limahe, and Zhubu have diamond-shaped plans and funnel-shaped cross sections and may represent subvertical pipes (Lightfoot and Evans-Lamswood, 2015) or they may represent subhorizontal blade-shaped dikes (Lu et al., 2019; see also Barnes and Mungall, 2018), whereas Jinbaoshan and Yangliuping are subhorizontal sills (Song et al., 2008; Lu et al., 2019). Thus, there does not appear to be any correlation with intrusion geometry.

Yangliuping is composed of peridotite, olivine websterite, and olivine clinopyroxenite-gabbro; Zhubu is

composed of lherzolite, olivine websterite, gabbro, and gabbrodiorite; Limhae is composed of wehrlite, gabbro, and diorite; Baimazhai is composed of peridotite, olivine pyroxenite, pyroxenite-gabbro; Jinbaoshan is composed primarily of wehrlite (see Lu et al., 2019; Song et al., 2008; Tao et al., 2008; Tang et al., 2013; Wang et al., 2018). Jinbaoshan is the least differentiated and contains the lowest amounts of sulfides, similar to many poorly differentiated systems that host low-grade Ni-Cu-(PGE) deposits (e.g., Dumont, Mt Keith, parts of Thompson and Raglan). Thus, there is a weak correlation between degree of differentiation and amount of mineralization.

The reason why Jinbaoshan formed PGE-(Cu)-(Ni) mineralization and the other deposits in the ELIP formed Ni-Cu-(PGE) mineralization most likely reflects a more dynamic system (more flow-through) and a correspondingly high R factor (~800 to 40000, **Figs. 17, 18B**), leading to enrichment in PGE >>> Cu > Ni.

### 2.6.7 Genesis of base metal sulfides and platinum-group minerals in the Jinbaoshan deposit

Experimental studies have shown that natural sulfide liquids at magmatic temperatures approaching 1200 ℃ may contain significant amounts of dissolved Fe, Ni, Cu, PGEs, and semi-metals (e.g., McLean and Shimazaki, 1976; Fleet et al., 1996; Barnes et al. 1997; Helmy et al., 2013; Cafagna and Jugo, 2016). Depending on O content (Naldrett, 1969; Doyle and Naldrett, 1987) they will crystallize Fe-Ni-Co-IPGE-bearing MSS ± magnetite.

If As contents are high enough, As-bearing PGMs (e.g., sperrylite, irarsite) or As-rich melts may also form at the magmatic stage (e.g., Mackovicky, 2002; Dare et al., 2010; Liu and Brenan, 2015). Although Pt and As are generally below saturation concentration, sperrylite is stable and crystallizes before MSS if the melt is As-rich (Helmy et al., 2013). At 1200℃ PGE sulfarsenides (e.g., irarsite, hollingworthite) grow in the sulfide melt, and PGM grains could grow slightly larger as the temperature falls to around 1020℃ (Helmy and Bragagni, 2017). In the Jinbaoshan deposit, micrometer-size sperrylite and PGE sulfarsenides are associated with BMS, magnetite and silicates. The whole rock As/S (~4) is higher than the Yangliuping deposit (~1.7) in ELIP, where abundant PGE-arsenides and sulfarsenides crystallized at high temperature (Liang et al., 2019). Thus, it is likely that the PGM arsenides in Jinbaoshan (e.g., sperrylite, irarsite) crystallized directly from a sulfide melt at an early magmatic stage at temperatures between 1200-1000℃ (see discussion by Dare et al., 2010; **Fig. 20A**).

At temperatures below 1190°C, IPGE-Co-Ni-bearing MSS crystallizes and PPGE-Cu-Au-Ag-Zn-Pb-Cd-Te-As-Bi-Sn partition into the residual sulfide liquid. On further cooling to around 900°C, Cu-Ag-Pb-Zn bearing ISS crystallizes and the remaining incompatible chalcophile elements partition into the residual sulfide liquid (**Fig. 20B**). Although MSS/liquid and ISS/liquid partition coefficients for PPGE (Rh, Pt, Pd) and semi-metals are very low, small amounts of these elements may be included in ISS and MSS (Liu and Brenan, 2015; Mansur and Barnes, 2020). During this interval, PPGE are concentrated in immiscible rich melts in both MSS and ISS, and excess Pd will also enter into MSS if the Pd:semimetal ratio is sufficiently high (Holwell and McDonald, 2010), or by peritectic reaction at high temperature (Mansur et al., 2019). Thus, at an early stage Pd-Pt-Bi-Te inclusions form in both ISS and MSS, which will recrystallize as moncheite and atokite associated with the formation of the original Pn-Po-Ccp sulfide assemblage (**Fig. 20C**).

The occurrence of violarite-pyrite-magnetite indicates it formed in a relatively high $fO_2$ and $fS_2$ environment, as a result, pentlandite and pyrrhotite altered to violarite, pyrite, millerite, polydymite, and magnetite. In the hypogene stage (<540°C) hydrothermal fluids overprinted into the sulfide system and convert it to hypogene violarite-millerite-pyrite (**Fig. 20D**). Many Pd-PGMs formed in this stage, including palladium, mertieite II, and some other Pd-alloy (**Supplemental Table 1**). At this stage Pd-minerals are most abundant because Pd is the most mobile PGE. Mertieite II is the dominant PGM in violarite-millerite-pyrite assemblage. Nearly all mertieite II grains are anhedral, forming at the edge of millerite or violarite, suggesting that mertieite II has been expelled to the edge of sulfides by hydrothermal fluids. Although it therefore appears that hydrothermal fluids dissolved and reprecipitated some PGMs, the process does not appear to have affected the whole-rock composition significantly.

When the temperature continues to decrease (supergene stage, lower than 250°C), Pt and Pd were mobile and transported as complexes with soft (e.g., $HS^-$) or borderline (e.g., $Cl^-$) ligands (Wood, 2002). Late stage calcite is associated with some Pd-PGMs such as atokite, palarstanide, and kotulskite (**Fig. 20E**, **Supplemental Table 1**). In the stage the unstable PGM may suffer destruction from the weathering and many of the early formed PGMs are modified by fluids and anhedral in morphology (Oberthür et al., 2018; **Figs. 8C, 8F**). Fluid activities also led to the development of pyrite and magnetite (Duran et al., 2017; **Fig. 20E**). Moncheite and atokite are the dominant PGMs, which are mainly associated with magnetite, supergene violarite, and polydymite (**Fig. 20E**). Anhedral irarsite also formed in magnetite.

Merenskyite is commonly associated with magnetite or violarite, because Pd and some other semimetals enter into MSS at an early stage, which makes Pd-Te mineral crystallized from MSS evolved minerals (**Fig. 20E**).

## 2.7 Conclusions

1) The parental magma to the Jinbaoshan deposit formed through interaction of crustally-derived sulfide and a hybrid picritic-ferropicritic magma derived from subduction-metasomatized pyroxenitic mantle during impingement of the Emeishan plume and the Paleo-Tethyan oceanic subduction system.
2) Some of the S in the deposit may have been derived from the magma, but S isotopic data indicate that some was derived from the country rocks.
3) A high R factor (magma:sulfide ratio) in a dynamic system was the key factor in generating the high PGE tenors and enrichment in PGE >>> Cu > Ni in the Jinbaoshan intrusion.
4) The formation of the sulfide assemblages in Jinbaoshan appear to have occurred in three stages: (1) a magmatic Fe-Ni-Cu sulfide melt crystallized Fe-Ni monosulfide and Cu-rich intermediate solid solutions that inverted to a primary pyrrhotite-pentlandite-chalcopyrite-magnetite assemblage; (2) an early-secondary hypogene voilarite-millterite-pyrite1-chalcopyrite assemblage formed by interaction with a lower-temperature deuteric magmatic-hydrothermal fluid; (3) a late-secondary supergene violarite-polydymite-pyrite2-chalcopyrite assemblage formed during weathering.
5) The Jinbaoshan PGE-(Cu)-(Ni) deposit is dominated by two sulfide assemblages: 1) hypogene violarite-pyrite1-millerite-chalcopyrite; and 2) supergene violarite-(polydymite)-pyrite2-chalcopyrite. The principal PGMs in the Jinbaoshan deposit are moncheite (38%), mertieite II (23%), atokite (6.7%), irarsite (6.7%), and sperrylite (5.2%).
6) Violarite, polydymite, and Py1 are the main BMS that host PGEs, mainly Pd and IPGE. Pt is seldom hosted by BMS, which occurs mainly as discrete Pt minerals. PGE-hosted BMS are more enriched in magmatically incompatible chalcophile elements (Ag, Pb, Zn, Cd) than traditional Pn-Po minerals in other PGE deposits.

7) During the hypogene stage, fluids introduced Co and Pt into violarite, expelling Pd to the edges of BMSs, which caused Pd depletion in the high-Co violarite and the formation of mertieite II. Fluids in the supergene stage further led to the development of pyrite and magnetite and many PGMs are associated with supergene violarite and magnetite.
8) The hypogene and supergene alteration dissolved and precipitated PGMs, but did not change the PGE contents significantly.

## Acknowledgements

This paper is dedicated to the memory of Prof AJ Naldrett, who was a long-time mentor to CML and an inspiration to YL and two generations of magmatic ore deposit geologists in China and worldwide. This research has been supported by the National Natural Science Foundation of China (No. 42002110), the National Key Technologies R&D Program (2019YFA0708603), the National Key Basic Research Development Program of China (No. 2015CB452606, 2009CB421008), the Geological Investigation Work project of China Geological Survey (No. 12120114013501, DD20190439), Project 111 of the Ministry of Education, China (Grant No. B07011), a Natural Sciences and Engineering Council of Canada Discovery grant to CML, and a SEG Canada Foundation grant and a China Scholarship Council award to YL. We are grateful to Sarah-Jane Barnes, Malte Junge, Christopher Jenkins, and an anonymous reviewer for comments that led to substantial improvements in the paper. This is Mineral Exploration Research Centre publication number MERC-2021-05.

## References

Arndt, N.T., Lesher, C.M., Czamanske, G.K., 2005, Mantle-derived magmas and magmatic Ni-Cu-(PGE) deposits: 100th Anniversary Volume. *Society of Economic Geologists,* 5–24.

Barnes, S.-J., Cox, R.A., Zientek, M.L., 2006, Platinum-group element, Gold, Silver and Base Metal distribution in compositionally zoned sulfide droplets from the Medvezky Creek Mine, Noril'sk, Russia: *Contributions to Mineralogy and Petrology* 152, 187-200.

Barnes, S.J., Makovicky, E., Makovicky, M., Rose-Hansen, J., Karup-Moller, S., 1997, Partition

coefficients for Ni, Cu, Pd, Pt, Rh, and Ir between monosulfide solid solution and sulfide liquid and the formation of compositionally zoned Ni–Cu sulfide bodies by fractional crystallization of sulfide liquid: *Canadian Journal of Earth Sciences* 34, 366-374.

Barnes, S.J., Wells, M.A., Verrall, M.R., 2009, Effects of magmatic processes, serpentinization, and talc-carbonate alteration on sulfide mineralogy and ore textures in the Black Swan disseminated nickel sulfide deposit, Yilgarn Craton: *Economic Geology* 104, 539-562.

Barnes, S.-J., Lightfoot, P.C., 2005, Formation of magmatic nickel sulfide ore deposits and processes affecting their copper and platinum group element contents: *Economic geology*, 100th anniversary volume 34, 179-214.

Barnes, S.J., Mungall, J.E., 2018, Blade-shaped dikes and nickel sulfide deposits: A model for the emplacement of ore-bearing small intrusions: *Economic Geology* 113, 789-798.

Barnes, S.-J., Ripley, E.M., 2016, Highly siderophile and strongly chalcophile elements in magmatic ore deposits: *Reviews in Mineralogy and Geochemistry* 81, 725-774.

Barnes, S.J., Godel, B.M., Locmelis, M., Fiorentini, M.L., Ryan, C. G., 2011, Extremely Ni-rich Fe–Ni sulfide assemblages in komatiitic dunite at Betheno, Western Australia: results from synchrotron X-ray fluorescence mapping: *Australian Journal of Earth Sciences* 58, 691-709.

Bennett, S.L., Heyding, R.D., 1966, Arsenides of the transition metals: viii. some binary and ternary group viii diarsenides and their magnetic and electrical properties: *Canadian Journal of Chemistry* 44, 3017-3030.

Campbell, I.H., Naldrett, A.J., 1979, The influence of silicate: sulfide ratios on the geochemistry of magmatic sulfides: *Economic Geology* 74, 1503-1506.

Cafagna, F., Jugo, P.J., 2016, An experimental study on the geochemical behavior of highly siderophile elements (HSE) and metalloids (As, Se, Sb, Te, Bi) in a mss-iss-pyrite system at 650° C: a possible magmatic origin for Co-HSE-bearing pyrite and the role of metalloid-rich phases in the fractionation of HSE: *Geochimica et Cosmochimica Acta* 178, 233-258.

Chen, L.M., Song, X.Y., Danyushevsky, L.V., Wang, Y.S., Tian, Y.L., Xiao, J.F., 2015, A laser ablation ICP-MS study of platinum-group and chalcophile elements in base metal sulfide minerals of the Jinchuan Ni–Cu sulfide deposit, NW China: *Ore Geology Reviews* 65, 955-967.

Chung, S.L., Jahn, B.M., 1995, Plume-lithosphere interaction in generation of the Emeishan flood basalts at the Permian-Triassic boundary: *Geology* 23, 889-892.

Craig, J. R., 1973, Pyrite-pentlandite assemblages and other low temperature relations in the Fe-Ni-S system: *American Journal of Science* 273, 496-510.

Craig, J.R., 1971, Violarite stability relations. American Mineralogist: *Journal of Earth and Planetary Materials* 56, 1303-1311.

Crocket, J.H., 2002, Platinum-group element geochemistry of mafic and ultramafic rocks: *The Geology, Geochemistry and Mineral Beneficiation of Platinum-Group Elements. Special Volume* 54, 177-210.

Deng, J., Wang, Q., Li, G., 2017, Tectonic evolution, superimposed orogeny, and composite metallogenic system in China: *Gondwana Research* 50, 216-266.

Deng, J., Wang, Q., Yang, L., Wang, Y., Gong, Q., Liu, H. 2010. Delineation and explanation of geochemical anomalies using fractal models in the Heqing area, Yunnan Province, China. *Journal of Geochemical Exploration*, 105(3), 95-105.

Deng, J., Wang, Q.F., Li, G.J., Li, C., Wang, C.M., 2014a, Tethys tectonic evolution and its bearing on the distribution of important mineral deposits in the Sanjiang region, SW China: *Gondwana Research* 26, 419-437.

Deng, J., Wang, Q.F., Li, G.J., Santosh, M., 2014b, Cenozoic tectono-magmatic and metallogenic processes in the Sanjiang region, southwestern China: *Earth Science Review* 138, 268-299.

Djon, M.L.N., Barnes, S.-J., 2012, Changes in sulfides and platinum-group minerals with the degree of alteration in the Roby, Twilight, and High Grade Zones of the Lac des Iles Complex, Ontario, Canada: *Mineralium Deposita* 47, 875-896.

Donaldson, M.J., 1981, Redistribution of ore elements during serpentinization and talc-carbonate alteration of some Archean dunites, Western Australia: *Economic Geology* 76, 1698-1713.

Doyle, C.D., Naldrett, A.J., 1987, The oxygen content of "sulfide" magma and its effect on the partitioning of nickel between coexisting olivine and molten ores: *Economic Geology* 82, 208-211.

Duran, C.J., Barnes, S.-J., Corkery, J.T., 2015, Chalcophile and platinum-group element distribution in pyrites from the sulfide-rich pods of the Lac des Iles Pd deposits, Western Ontario, Canada: Implications for post-cumulus re-equilibration of the ore and the use of pyrite compositions in exploration. *Journal of Geochemical Exploration* 158, 223-242.

Duran, C.J., Barnes, S.-J, Corkery, J.T., 2016, Geology, petrography, geochemistry, and genesis of sulfide-rich pods in the Lac des Iles palladium deposits, western Ontario, Canada: *Mineralium Deposita* 51, 509-532.

Duran, C.J., Barnes, S.J., Pleše, P., Prašek, M.K., Zientek, M.L., Pagé, P., 2017, Fractional crystallization-induced variations in sulfides from the Noril'sk-Talnakh mining district (polar Siberia, Russia): *Ore Geology Reviews* 90, 326-351.

Eckstrand, O.R., Hulbert, L.J., 1987, Selenium and the source of sulfur in magmatic nickel and platinum deposits: *Geological Association of Canada-Mineralogical Association Canada Program with Abstracts* 12, 40.

Eckstrand, O.R., 1975, The Dumont serpentinite: a model for control of nickeliferous opaque mineral assemblages by alteration reactions in ultramafic rocks.: *Economic Geology* 70, 183-201.

Fleet, M.E., Chryssoulis, S.L., Stone, W.E., Weisener, C.G., 1993, Partitioning of platinum-group elements and Au in the Fe−Ni−Cu−S system: experiments on the fractional crystallization of sulfide melt: *Contributions to Mineralogy and Petrology* 115, 36-44.

Fleet, M. E., Crocket, J. H., Stone, W. E., 1996, Partitioning of platinum-group elements (Os, Ir, Ru, Pt, Pd) and gold between sulfide liquid and basalt melt: *Geochimica et Cosmochimica Acta* 60, 2397-2412.

Frost, B.R., 1985, On the stability of sulfides, oxides, and native metals in serpentinite: *Journal of Petrology* 26, 31-63.

Godel, B., Barnes, S.-J, Maier, W.D., 2007, Platinum-Group Elements in Sulphide Minerals, Platinum-Group Minerals, and Whole-Rocks of the Merensky Reef (Bushveld Complex, South Africa): Implications for the Formation of the Reef: *Journal of Petrology* 48, 1569-1604.

Godel, B., Barnes, S.-J., 2008, Platinum-group elements in sulfide minerals and the whole rocks of the JM Reef (Stillwater Complex): Implication for the formation of the reef: *Chemical Geology* 248, 272-294.

Grguric, B.A., 2002, Hypogene violarite of exsolution origin from Mount Keith, Western Australia: field evidence for a stable pentlandite–violarite tie line: *Mineralogical Magazine* 66, 313-326.

Groves, D.I., Hudson, D.R., Hack, T.B., 1974, Modification of iron-nickel sulfides during serpentinization and talc-carbonate alteration at Black Swan, Western Australia: *Economic Geology* 69, 1265-1281.

Hansen, M., Anderko, K., Salzberg, H.W. 1958. Constitution of binary alloys. *Journal of the Electrochemical Society* 105.12 (1958): 260C.

Haughton, D. R., Roeder, P. L., Skinner, B. J., 1974, Solubility of sulfur in mafic magmas. *Economic Geology* 69(4), 451-467.

He, S.F., Sun, K., Wang, J., Ren, J.P., Liu, X.Y, 2014, New Progress on the Kabanga Cu-Ni Sulphide Deposits Research, Northwestern Tanzania. *Geological Survey and Research*, 37(1), 6-12 (in Chinese with English abstract).

Helmy, H.M., Bragagni, A., 2017, Platinum-group elements fractionation by selective complexing, the Os, Ir, Ru, Rh-arsenide-sulfide systems above 1020° C: *Geochimica et Cosmochimica Acta*, 216, 169-183.

Helmy, H.M., Ballhaus, C., Fonseca, R.O.C., Nagel, T.J., 2013, Fractionation of platinum, palladium, nickel, and copper in sulfide–arsenide systems at magmatic temperature: *Contributions to*

*Mineralogy and Petrology* 166, 1725-1737.

Helmy, H. M., Ballhaus, C., Wohlgemuth-Ueberwasser, C., Fonseca, R. O., Laurenz, V. 2010. Partitioning of Se, As, Sb, Te and Bi between monosulfide solid solution and sulfide melt–application to magmatic sulfide deposits. *Geochimica et Cosmochimica Acta*, 74(21), 6174-6179.

Helmy, H. M., Ballhaus, C., Berndt, J., Bockrath, C., Wohlgemuth-Ueberwasser, C. 2007. Formation of Pt, Pd and Ni tellurides: experiments in sulfide–telluride systems. *Contributions to Mineralogy and Petrology 153*(5), 577-591.

Holwell, D.A., Mcdonald, I., 2010, A Review of the Behaviour of Platinum Group Elements within Natural Magmatic Sulfide Ore Systems: *Platinum Metals Review* 54, 26-36.

Holwell, D.A., Keays, R.R., Firth, E.A., Findlay, J, 2014, Geochemistry and Mineralogy of Platinum Group Element Mineralization in the River Valley Intrusion, Ontario, Canada: A Model for Early-Stage Sulfur Saturation and Multistage Emplacement and the Implications for "Contact-Type" Ni-Cu-PGE Sulfide Mineralization: *Economic Geology* 109, 689-712.

Holwell, D.A., McDonald, I., 2007, Distribution of platinum-group elements in the Platreef at Overysel, northern Bushveld Complex: a combined PGM and LA-ICP-MS study: *Contributions to Mineralogy and Petrology* 154, 171-190.

Holwell, D.A., Adeyemi, Z., Ward, L.A., Smith, D.J., Graham, S.D., McDonald, I., Smith, J.W. 2017, Low temperature alteration of magmatic Ni-Cu-PGE sulfides as a source for hydrothermal Ni and PGE ores: A quantitative approach using automated mineralogy: *Ore Geology Reviews* 91, 718-740.

Hudson, D.R., Groves, D.I., 1974, The composition of violarite coexisting with vaesite, pyrite, and millerite: *Economic Geology* 69, 1335-1340.

Hutchinson, D., McDonald, I., 2008, Laser ablation ICP-MS study of platinum-group elements in sulphides from the Platreef at Turfspruit, northern limb of the Bushveld Complex, South Africa: *Mineralium Deposita* 43, 695-711.

Christopher Jenkins, M., Mungall, J. E., Zientek, M. L., Holick, P., Butak, K., 2020, The Nature and

Composition of the JM Reef, Stillwater Complex, Montana, USA. *Economic Geology* 115(8), 1799-1826.

Jiang, J., Song, X.Y., Chen, L.M., Wang, L., Fu, Z.Q, 2014, Geochemistry and Petrogenetic Significances of Semimetal and Platinum Group Elements of the Longshou Mine of the Jinchuan Ni-Cu Sulfide Deposit: *Bulletin of Mineralogy, Petrology and Geochemistry* 33, 882-892.

Junge, M., Oberthür, T., Kraemer, D., Melcher, F., Piña, R., Derrey, I. T., Manyeruke, T., Strauss, H., 2019, Distribution of platinum-group elements in pristine and near-surface oxidized Platreef ore and the variation along strike, northern Bushveld Complex, South Africa. *Mineralium Deposita* 54(6), 885-912.

Keays, R.R., Lightfoot, P.C., 2010, Crustal sulfur is required to form magmatic Ni-Cu sulfde deposits: evidence from chalcophile element signatures of Siberian and Deccan Trap basalts. *Mineralium Deposita* 45, 241-257.

Keays, R.R., Ross, J.R., and Woolrich P., 1981, Precious metals in volcanic peridotite associated nickel sulfide deposits in Western Australia, II: Distribution within ores and host rocks at Kambalda, *Economic Geology* 76, 1645-1674.

Keays, R.R., Nickel, E.H., Groves, D.I., McGoldrick, P.J., 1982, Iridium and palladium as discriminants of volcanic-exhalative, hydrothermal, and magmatic nickel sulfide mineralization: *Economic Geology* 77, 1535-1547.

Kinloch, E.D., 1982, Regional trends in the platinum-group mineralogy of the critical zone of the Bushveld Complex, South Africa: *Economic Geology* 77, 1328-1347.

Konnunaho, J.P., Hanski, E.J., Bekker, A., Halkoaho, T.A.A., Hiebert, R.S., Wing, B.A., 2013, The Archean komatiite-hosted, PGE-bearing Ni–Cu sulfide deposit at Vaara, eastern Finland: evidence for assimilation of external sulfur and post-depositional desulfurization: *Mineralium Deposita* 48, 967-989.

Kullerud, G., Yund, R.A., Moh, G.H., 1969, Phase relations in the Cu–Fe–S, Cu–Ni–S and Fe–Ni–S systems: *Economic Geology*, Monograph 4, 323–343.

Lesher, C.M., Arndt, N.T., Groves, D.I., 1984, Genesis of komatiite-associated nickel sulphide deposits at Kambalda, Western Australia: a distal volcanic model. In: Buchanan, D.L., Jones, M.J. (Eds.), Sulphide Deposits in Mafic and Ultramafic Rocks. *Institution of Mining and Metallurgy, London*, 70–80.

Lesher, C.M., Keays, R.R., 2002, Discrimination between magmatic and hydrothermal Ni–Cu–PGE and PGE mineralization: *9th International platinum symposium*, Stillwater, USA.

Lesher, C.M., 2019, Up, down, or sideways: emplacement of magmatic Fe–Ni–Cu–PGE sulfide melts in large igneous provinces. *Canadian Journal of Earth Sciences* 56, 756-773.

Lesher, C.M., Burnham, O.M., 2001, Multicomponent elemental and isotopic mixing in Ni-Cu-(PGE) ores at Kambalda, Western Australia: *The Canadian Mineralogist* 39, 421-446.

Lesher, C.M., Campbell, I.H., 1993, Geochemical and fluid dynamic modeling of compositional variations in Archean komatiite-hosted nickel sulfide ores in Western Australia: *Economic Geology* 88, 804-816.

Lesher, C.M., Groves, D.I., 1986, Controls on the formation of komatiite-associated nickel copper sulfide deposits: In: Friedrich, G.H., Genkin, A.D., Naldrett, A.J. (Eds.), *Geology and Metallogeny of Copper Deposits*. Springer, 43–62.

Lesher, C.M., Burnham, O.M., Keays, R.R., Barnes, S.J., Hulbert, L., 2001, Trace-element geochemistry and petrogenesis of barren and ore-associated komatiites: *Canadian Mineralogist* 39, 673–696

Lesher, C.M., 2017, Roles of xenomelts, xenoliths, xenocrysts, xenovolatiles, residues, and skarns in the genesis, transport, and localization of magmatic Fe-Ni-Cu-PGE sulfides and chromite: *Ore Geology Reviews* 90, 465-484.

Lesher, C.M., Stone, W.E., 1996, Exploration geochemistry of komatiites, in Wyman D (Ed.), Igneous Trace Element Geochemistry: Applications for Massive Sulphide Exploration, *Geological Association of Canada, Short Course Notes* 12, 153–204.

Lesher, C. M., Whitney, J. A., Naldrett, A. J., 1989, Komatiite-associated nickel sulfide deposits. *Reviews*

*in Economic Geology* 4, 45-101.

Li, C., Tao, Y., Qi, L., Ripley, E.M., 2012, Controls on PGE fractionation in the Emeishan picrites and basalts: constraints from integrated lithophile-siderophile elements and Sr-Nd isotopes: *Geochimica et Cosmochimica Acta* 90, 12-32.

Li, C., Ripley, E.M., Tao, Y., Hu, R.Z., 2016, The significance of PGE variations with Sr-Nd isotopes and lithophile elements in the Emeishan flood basalt province from SW China to northern Vietnam: *Lithos* 248, 1-11.

Li, C., Barnes, S. J., Makovicky, E., Rose-Hansen, J., Makovicky, M., 1996, Partitioning of Ni, Cu, Ir, Rh, Pt and Pd between monosulfide solid solution and sulfide liquid: effects of composition and temperature. *Geochimica et Cosmochimica Acta*, 60(7), 1231-1238.

Liang, Q.L., Song, X.Y., Wirth, R., Chen, L.M., Dai, Z.H., 2019, Implications of nano-and micrometer-size platinum-group element minerals in base metal sulfides of the Yangliuping Ni-Cu-PGE sulfide deposit, SW China: *Chemical Geology* 517, 7-21.

Lightfoot, P.C., Evans-Lamswood, D., 2015, Structural controls on the primary distribution of mafic–ultramafic intrusions containing Ni–Cu–Co–(PGE) sulfide mineralization in the roots of large igneous provinces: *Ore Geology Reviews* 64, 354-386.

Liu, Y., Brenan, J., 2015, Partitioning of platinum-group elements (PGE) and chalcogens (Se, Te, As, Sb, Bi) between monosulfide-solid solution (MSS), intermediate solid solution (ISS) and sulfide liquid at controlled $fO_2$–$fS_2$ conditions: *Geochimica et Cosmochimica Acta* 159, 139-161.

Lu, Y. G., He, W.Y., 2018, Characteristics of S-Os isotopes and its constraints on the mineralization for the Jinbaoshan Pt-Pd deposit, western Yunnan, China: *Acta Petrologica Sinica* 34, 1258-1270 (in Chinese with English abstract).

Lu, Y.G., Zhao, K., Xiong, Y.Q., Li, P., Du, D.Y., Yuan M.W., 2014, Elements geochemistry of Jinbaoshan Pt-Pd deposit, western Yunnan, China: *Acta Petrologica Sinica* 30, 2681-2694 (in Chinese with English abstract).

Lu, Y., Lesher, C.M., Deng, J., 2019, Geochemistry and genesis of magmatic Ni-Cu-(PGE) and PGE-(Cu)-(Ni) deposits in China: *Ore Geology Reviews* 107, 863-887.

Lu, Y.G., Hao, B., Sun, K., He, S.F., Xu, K.K., Gong, P.H., Zhang, H., 2020, General situation of cobalt resource and its utilization analysis. *Geological Survey and Research*, 43(01):72-80 (in Chinese with English abstract).

MacLean, W.H., Shimazaki, H., 1976, The partition of Co, Ni, Cu, and Zn between sulfide and silicate liquids: *Economic Geology* 71, 1049-1057.

Maier, W.D., Barnes, S.J., De Waal, S.A., 1998, Exploration for magmatic Ni-Cu-PGE sulphide deposits: A review of recent advances in the use of geochemical tools, and their application to some South African ores: *South African Journal of Geology* 101, 237-253.

Makovicky, E.M.I.L., Cabri, L.J., 2002, Ternary and quaternary phase systems with PGE: *Canadian Institute of Mining, Metallurgy and Petroleum Montreal* 54, 131-175)

Mansur, E.T., Barnes, S.-J., 2020, The role of Te, As, Bi, Sn and Sb during the formation of platinum-group-element reef deposits: examples from the Bushveld and Stillwater complexes: *Geochimica et Cosmochimica Acta* 272, 235-258.

Mansur, E.T., Barnes, S.-J., Duran, C.J., 2019, Textural and compositional evidence for the formation of pentlandite via peritectic reaction: Implications for the distribution of highly siderophile elements: *Geology* 47, 351-354.

Mansur, E.T., Barnes, S.-J., Duran, C.J., 2020, An overview of chalcophile element contents of pyrrhotite, pentlandite, chalcopyrite, and pyrite from magmatic Ni-Cu-PGE sulfide deposits: *Mineralium Deposita*, 1-26.

Mavrogenes, J.A., O'Neill, H.S.C., 1999, The relative effects of pressure, temperature and oxygen fugacity on the solubility of sulfide in mafic magmas: *Geochimica et Cosmochimica Acta* 63, 1173-1180.

McDonough, W.F., Sun, S.S., 1995, The composition of the Earth: *Chemical geology* 120, 223-253.

McQueen, K.G., Munro, D.C., 2003, Weathering-controlled fractionation of ore and pathfinder elements at Cobar, NSW: *Advances in Regolith. CRC LEME*, 296-300.

Mota-E-Silva, J., Prichard, H.M., Suárez, S., Ferreira, Filho, C.F., Fisher, P.C., 2016, Supergene Alteration of Platinum-Group Minerals and the Formation of Pd-Cu-O and Pd-I-O Compounds In the Limoeiro Ni-Cu-(PGE) Deposit, Brazil: *Canadian Mineralogist* 54, 755-778.

Mungall, J. E., Andrews, D. R., Cabri, L. J., Sylvester, P. J., Tubrett, M. 2005. Partitioning of Cu, Ni, Au, and platinum-group elements between monosulfide solid solution and sulfide melt under controlled oxygen and sulfur fugacities. *Geochimica et Cosmochimica Acta 69*(17), 4349-4360.

Mungall, J. E., Brenan, J. M. 2014. Partitioning of platinum-group elements and Au between sulfide liquid and basalt and the origins of mantle-crust fractionation of the chalcophile elements. *Geochimica et Cosmochimica Acta 125*, 265-289.

Naldrett, A.J., 1969, A Portion of the System Fe–S–O between 900 and 1080 °C and its Application to Sulfide Ore Magmas: *Journal of Petrology* 10, 171-201.

Naldrett, A.J., 1981. Nickel sulfide deposits: Classification, composition and genesis. In Seventy-Fifth Anniversary Volume. Edited by B.J. Skinner. *Economic Geology Publishing Company*, 628-685.

Naldrett, A.J., 2004, Magmatic Sulfide Deposits: Geology, Geochemistry and Exploration: Springer, 1-727.

Naldrett, A.J., 2010, Secular variation of magmatic sulfide deposits and their source magmas. *Economic Geology* 105, 669-688.

Naldrett, A.J., Craig, J.R., Kullerud, G., 1967, The central portion of the Fe-Ni-S system and its bearing on pentlandite exsolution in iron-nickel sulfide ores: *Economic Geology*, 826-847.

Nickel, E.H.,1973, Violarite-a key mineral in the supergene alteration of nickel sulphide ores: *Australasian Institute of Mining and Metallurgy, Perth Conference*, 111-116.

Nickel, E.H., Allchurch, P.D., Mason, M.G., Wilmshurst, J.R., 1977, Supergene alteration at the

Perseverance nickel deposit, Agnew, Western Australia: *Economic Geology* 72, 184-203.

Nickel, E.H., Ross, J.R., Thornber, M.R., 1974, The supergene alteration of pyrrhotite-pentlandite ore at Kambalda, Western Australia: *Economic Geology* 69, 93-107.

Oberthür, T., 2018, The fate of platinum-group minerals in the exogenic environment—From sulfide ores via oxidized ores into placers: Case studies Bushveld complex, South Africa, and Great Dyke, Zimbabwe. *Minerals*, 8(12), 581.

Patten, C., Barnes, S.-J., Mathez, E.A., Jenner, F.E., 2013, Partition coefficients of chalcophile elements between sulfide and silicate melts and the early crystallization history of sulfide liquid: LA-ICP-MS analysis of MORB sulfide droplets: *Chemical Geology* 358, 170-188.

Peach, C.L., Mathez, E.A., Keays, R.R., 1990, Sulfide melt-silicate melt distribution coefficients for noble metals and other chalcophile elements as deduced from MORB: Implications for partial melting: *Geochimica et Cosmochimica Acta* 54, 3379-3389.

Peck, D.C., Keays, R.R., 1990, Insights into the behavior of precious metals in primitive, S-undersaturated magmas; evidence from the Heazlewood River complex, Tasmania: *The Canadian Mineralogist* 28, 553-577.

Petrus, J. A., Chew, D. M., Leybourne, M. I., Kamber, B. S., 2017, A new approach to laser-ablation inductively-coupled-plasma mass-spectrometry (LA-ICP-MS) using the flexible map interrogation tool 'Monocle'. *Chemical Geology* 463, 76-93.

Pettke, T., Oberli, F., Audétat, A., Guillong, M., Simon, A. C., Hanley, J. J., Klemm, L. M., 2012, Recent developments in element concentration and isotope ratio analysis of individual fluid inclusions by laser ablation single and multiple collector ICP-MS. *Ore Geology Reviews* 44, 10-38.

Pina, R., Gervilla, F., Barnes, S.-J, Ortega, L., Lunar, R., 2012, Distribution of platinum-group and chalcophile elements in the Aguablanca Ni–Cu sulfide deposit (SW Spain): Evidence from a LA-ICP-MS study: *Chemical Geology* 302-303, 61-75.

Pina, R., Gervilla, F., Barnes, S.-J., Oberthür, T., Lunar, R., 2016, Platinum-group element concentrations

in pyrite from the Main Sulfide Zone of the Great Dyke of Zimbabwe. *Mineralium Deposita* 51, 853-872.

Pina, R., Gervilla, F., Barnes, S.-J., Ortega, L., Lunar, R. 2013. Platinum-group elements-bearing pyrite from the Aguablanca Ni-Cu sulphide deposit (SW Spain): a LA-ICP-MS study: *European Journal of Mineralogy* 25, 241-252.

Prichard, H.M., Barnes, S.-J., Maier, W.D., Fisher, P.C., 2004, Variations in the nature of the platinum-group minerals in a cross-section through the Merensky Reef at Impala Platinum: Implications for the mode of formation of the reef: *The Canadian Mineralogist* 42, 423-437.

Queffurus, M., Barnes, S.-J., 2015, A review of sulfur to selenium ratios in magmatic nickel–copper and platinum-group element deposit: *Ore Geology Reviews* 69, 301-324.

Reed, M.H.,1982, Calculation of multicomponent chemical equilibria and reaction processes in systems involving minerals, gases and an aqueous phase: *Geochimica et Cosmochimica Acta*, 513-528.

Ripley, E.M., Li, C., 2013, Sulfide saturation in mafic magmas: is external sulfur required for magmatic Ni-Cu-(PGE) ore genesis? *Economic Geology* 108, 45-58.

Rodsjo, L., 1999, The alteration history of the Agnew-Wiluna Greenstone Belt, Western Australia, and the impacts on nickel sulphide mineralisation (Doctoral dissertation, University of Western Australia).

Sakai, H., Des Marais, D. J., Ueda, A., Moore, J. G., 1984, Concentrations and isotope ratios of carbon, nitrogen and sulfur in ocean-floor basalts: *Geochimica et Cosmochimica Acta* 48, 2433-2441.

Seccombe, P. K., Groves, D. I., Marston, R. J., Barrett, F. M., 1981, Sulfide paragenesis and sulfur mobility in Fe-Ni-Cu sulfide ores at Lunnon and Juan Main shoots, Kambalda; textural and sulfur isotopic evidence: *Economic Geology* 76, 1675-1685.

Sinyakova, E.F., Kosyakov, V.I., 2009, Experimental modeling of zonality of copper-rich sulfide ores in copper-nickel deposits. *Doklady Earth Sciences* 427, 787-792.

Song, X.Y., Zhou, M.F., Tao, Y., Xiao, J.F., 2008, Controls on the metal compositions of magmatic sulfide deposits in the Emeishan large igneous province, SW China. *Chemical Geology* 253, 38-49.

Song, X.Y., Zhou, M.F., Cao, Z.M., 2004, Genetic relationships between base-metal sulfides and platinum-group minerals in the Yangliuping Ni-Cu-(PGE) sulfide deposit, southwestern China: *Canadian Mineralogist* 42, 469-483.

Su, S.G., Lesher, C.M., 2012, Genesis of PGE mineralization in the Wengeqi mafic–ultramafic complex, Guyang County, Inner Mongolia, China: *Mineralium Deposita* 47, 197-207.

Tang, Q., Ma, Y., Zhang, M., Li, C., Zhu, D., Tao, Y., 2013, The origin of Ni-Cu-PGE sulfide mineralization in the margin of the Zhubu mafic-ultramafic Intrusion in the Emeishan large igneous province, southwestern China: *Economic Geology* 108, 1889-1901.

Tao, Y., Li, C., Hu, R.Z, Ripley, E.M., Du, A.D, Zhong, H., 2007, Petrogenesis of the Pt-Pd mineralized Jinbaoshan ultramafc intrusion in the Permian Emeishan large igneous province, SW China. *Contributions to Mineralogy and Petrology* 153, 321–337.

Tao, Y., Li, C., Song, X.Y., Ripley, E.M., 2008, Mineralogical, petrological, and geochemical studies of the Limahe mafic–ultramatic intrusion and associated Ni-Cu sulfide ores, SW China: *Mineralium Deposita*, v. 43, p. 849-872.

Tao, Y., Putirka, K., Hu, R.Z., Li, C., 2015, The magma plumbing system of the Emeishan large igneous province and its role in basaltic magma differentiation in a continental setting. *American Mineralogist* 100, 2509-2517.

Tao, Y., Ma, Y.S., Miao, L.C., Zhu, F.L., 2009, SHRIMP U-Pb zircon age of the Jinbaoshan ultramafc intrusion, Yunnan Province, SW China. *Chinese Science Bulletin* 54, 168–172.

Thornber, M.R., 1975a, Supergene alteration of sulphides, I. A chemical model based on massive nickel sulphide deposits at Kambalda, Western Australia: *Chemical Geology* 15, 1-14.

Thornber, M.R. 1975b, Supergene alteration of sulphides, II. A chemical study of the Kambalda nickel deposits: *Chemical Geology* 15, 117-144.

Vaughan, D.J., Craig, J.R., 1985, The crystal chemistry of iron-nickel thiospinels: *American Mineralogist* 70, 1036-1043.

Vukmanovic, Z., Reddy, S.M., Godel, B., Barnes, S.J., Fiorentini, M.L., Barnes, S.J., Kilburn, M.R. 2014, Relationship between microstructures and grain-scale trace element distribution in komatiite-hosted magmatic sulphide ores: *Lithos* 184, 42-61.

Wang, C.Y., Zhou, M.F., Keays, R.R., 2006, Geochemical constraints on the origin of the Permian Baimazhai mafic-ultramafic intrusion, SW China: *Contributions to Mineralogy and Petrology* 152, 309-321.

Wang, C.Y., Prichard, H.M., Zhou, M.F., Fisher, P.C., 2008, Platinum-group minerals from the Jinbaoshan Pd–Pt deposit, SW China: evidence for magmatic origin and hydrothermal alteration: *Mineralium Deposita* 43, 791-803.

Wang, C.Y., Zhou, M.F., Qi, L., 2007, Permian flood basalts and mafic intrusions in the Jinping (SW China)-Song Da (northern Vietnam) district: mantle sources, crustal contamination and sulfide segregation: *Chemical Geology* 243, 317-343.

Wang, C.Y., Zhou, M.F., Qi, L., 2010, Origin of extremely PGE-rich mafic magma system: an example from the Jinbaoshan ultramafic sill, Emeishan large igneous province, SW China. *Lithos*119, 147-161.

Wang C.Y., Zhou, M.F., Zhao, D.G., 2005, Mineral chemistry of chromite from the Permian Jinbaoshan Pt–Pd–sulphide-bearing ultramafic intrusion in SW China with petrogenetic implications: *Lithos* 83, 47-66.

Wang, C.Y., Zhou, M.F., 2006, Genesis of the Permian Baimazhai magmatic Ni-Cu-(PGE) sulfide deposit, Yunnan, SW China: *Mineralium Deposita* 41, 771-783.

Wang, C.Y., Wei, B., Zhou, M.F., Minh, D.H., Qi, L., 2018, A synthesis of magmatic Ni-Cu-(PGE) sulfide deposits in the 260 Ma Emeishan large igneous province, SW China and northern Vietnam: *Journal of Asian Earth Sciences* 154, 162-186.

Wendlandt, R.F., 1982, Sulfide saturation of basalt and andesite melts at high pressures and temperatures: *American Mineralogist* 67, 877–885.

Wood, S.A., 2002, The aqueous geochemistry of the platinum group elements with applications to ore deposits. In: Cabri LJ (ed) The geology, geochemistry, mineralogy and mineral beneficiation of platinum-group elements: *Canadian Institute of Mining, Metallurgy Special Publication* 54, 211–249.

Xie, W., Song, X.Y., Chen, L.M., Deng, Y.F., Zheng, W.Q., Wang, Y. S., Ba, D. H., Yin, M. H., Luan, Y., 2014, Geochemistry insights on the genesis of the subduction-related Heishan magmatic Ni-Cu-(PGE) deposit, Gansu, northwestern China, at the southern margin of the Central Asian Orogenic Belt: *Economic Geology* 109, 1563-1583.

Xu, Y.G., Chung, S.L., Jahn, B.M., Wu GY., 2001, Petrologic and geochemical constraints on the petrogenesis of Permian–Triassic Emeishan flood basalts in southwestern China: *Lithos* 58, 145-168.

Yang, L,Q., Deng, J., Wang, Z.L., Guo, L.N., Li, R.H., Groves, D.I., Danyushevsky, L.V., Zhang, C., Zheng, X.L., Zhao, H., 2016, Relationships between gold and pyrite at the Xincheng gold deposit, Jiaodong Peninsula, China: implications for gold source and deposition in a brittle epizonal environment. *Economic Geology* 111(1): 105-126.

Yang L.Q., Liu, J.T., Zhang. C., Wang. Q.F., Ge, L.S., Wang, Z.L., Zhang, J., Gong, Q.J., 2010, Superimposed orogenesis and metallogenesis An example from the orogenic gold deposits in Ailaoshan gold belt, Southwest China. *Acta Petrologica Sinica* 26(6): 1723-1739 (in Chinese with English abstract)

Yang. L.Q., Deng, J., Zhao, K., Liu, J.T., 2011, Tectono-thermochronology and gold mineralization events of orogenic gold deposits in Ailaoshan orogenic belt, Southwest China: Geochronological constraints. *Acta Petrologica Sinica* 27(9): 2519-2532 (in Chinese with English abstract)

Yao, Z., Mungall, J. E., Jenkins, M. C., 2021, The Rustenburg Layered Suite formed as a stack of mush with transient magma chambers. *Nature communications* 12(1), 1-13.

Yin, Y., Zajacz, Z., 2018, The solubility of silver in magmatic fluids: Implications for silver transfer to the magmatic-hydrothermal ore-forming environment. *Geochimica et Cosmochimica Acta* 238, 235-251.

Zhou, M.F., Arndt, N.T., Malpas, J., Wang, C.Y., Kennedy, A.K., 2008, Two magma series and associated ore deposit types in the Permian Emeishan large igneous province, SW China: *Lithos* 103, 352-368.

Zhou, M.F., Malpas, J., Song, X.Y., Robinson, P.T., Sun, M., Kennedy, A.K., Lesher, CM., Keays, R.R., 2002, A temporal link between the Emeishan large igneous province (SW China) and the end-Guadalupian mass extinction: *Earth Planetary Science Letters* 196, 113-122.

Zhou, M.F., Robinson, P.T., Lesher, C.M., Keays, R.R., Zhang, C.J., Malpas, J., 2005, Geochemistry, petrogenesis and metallogenesis of the Panzhihua gabbroic layered intrusion and associated Fe–Ti–V oxide deposits, Sichuan Province, SW China. *Journal of Petrology* 46, 2253-2280.

Zhou, M. F., Malpas, J., Sun, M., Liu, Y., & Fu, X., 2001, A new method to correct Ni-and Cu-argide interference in the determination of the platinum-group elements, Ru, Rh, and Pd, by ICP-MS. *Geochemical Journal* 35(6), 413-420.

Zhong, R., Brugger, J., Chen, Y., Li, W., 2015, Contrasting regimes of Cu, Zn and Pb transport in ore-forming hydrothermal fluids. *Chemical Geology* 395, 154-164.

**Figure captions**

**Figure 1. Distribution of continental flood basalts and contemporaneous magmatic sulfide deposits in the Emeishan large igneous province, SW China (after Song et al., 2008; Li et al., 2016).**

**Figure 2. Sketch geological map of the Jinbaoshan PGE-(Cu)-(Ni) deposit (after Wang et al., 2010).**

**Figure 3. Photomicrographs of A: clinopyroxene interstitial to serpentine, B: orthopyroxene and amphibole interstitial to serpentine, C: amphibole interstitial to serpentine, D: talc associated with serpentine, E: biotite interstitial to serpentine. F: actinolite after pyroxene, interstitial to clinopyroxene. Serpentine is pseudomorphous after olivine in A-C. Abbreviations: Srp-serpentine; Cpx-clinopyroxene; Opx-orthopyroxene; Amp-amphibole; Tlc-talc; Bt-biotite; Act-actinolite.**

**Figure 4. Photomicrographs of (A) millerite associated with pyrite 1 and chalcopyrite, (B) millerite replacing hypogene violarite, (C) hypogene violarite intergrown with supergene violarite, (D) violarite associated with pyrite 2 and chalcopyrite, (E) polydymite associated with hypogene violarite, (F) pyrite 2 associated with supergene violarite, (G) polydymite associated with chalcopyrite, and (H) pyrite 3 in magnetite-carbonate vein. Abbreviations: Py – pyrite; Cp – chalcopyrite; Vio– violarite; Pld – polydymite; Mlr – millerite.**

**Figure 5. Pie diagram showing the relative proportions of PGMs in 6 representative Jinbaoshan PGE-(Cu)-(Ni) samples.**

**Figure 6. Bar charts showing the frequency of minerals in contact with PGMs (top) and the frequency of each PGM in the two main sulfide assemblages (bottom). Abbreviations: Vl1-hypogene violarite; Vl2-supergene violarite; Py1-pyrite 1; Py2-pyrite 2; Cp-chalcopyrite; Vio-violarite; Mlr-millerite; Mag-magnetite; Sil-silicates.**

**Figure 7. Backscattered electron images of PGMs in Viol-Mlr-Py-Ccp assemblage (Style 1). A: Lath-shaped moncheite included in chalcopyrite, B: Hexagonal palladium associated with magnetite, C: Anhedral palladium and mertieite II at the edge of violarite, D-E: Anhedral mertieite II at the edge of millerite and violarite, F) Mertieite II, irarsite and Pd-Hg-As associated with violarite and magnetite. Abbreviations: Py-pyrite; Vio-violarite; Mlr-millerite; Cp-chalcopyrite; Mgt-magnetite.**

**Figure 8. Backscattered electron images of PGMs in Vio-Py-Cp assemblage (Style 2). A: oval moncheite at the boundary of violarite and magnetite, B: irarsite grains occurring as clusters in silicate, C: anhedral lath-shaped irarsite grain in magnetite; D: subhedral sperrylite and moncheite in magnetite, E: atokite intergrown with other electrum and moncheite, F: atokite intergrown with electrum in magnetite; G: secondary framboidal native platinum in a secondary electron image. H: Pt alloy surrounded by moncheite in chalcopyrite. I: elongated merenskyite in supergene violarite and magnetite. Abbreviations: Py - pyrite; Vio - violarite; Cp - chalcopyrite; Mgt - magnetite; Sil - silicate; Cal - calcite.**

**Figure 9. Primitive mantle-normalized PGE profiles of base metal sulfides in representative Jinbaoshan samples.**

**Figure 10. Box plots of Pb, Ag, Zn, and Cd concentration in the base metal sulfides. Abbreviations: Vl1-hypogene violarite; Vl2-supergene violarite; Py-pyrite; Cp-chalcopyrite; Pld-polydymite.**

**Figure 11. Time-resolved LA-ICP-MS spectra showing metal counts in the three generations pyrite and in chalcopyrite, polydymite, and millerite. Abbreviations: Py-pyrite; Cp-chalcopyrite; Pld-polydymite; Mlr-millerite.**

**Figure 12. Time-resolved LA-ICP-MS spectra showing metal counts in supergene two grains of hypogene violarite (Vl1) and two grains of supergene violarite (Vl2).**

**Figure 13. Element distribution maps (left) and reflected light image (right) for the Viol-Py1-Ccp assemblage. Abbreviations: Mlr-millerite; Py-pyrite; Cp-chalcopyrite.**

**Figure 14. Element distribution maps for the Viol-Py2-Mlr-Cp assemblage. Abbreviations: Vl1-hypogene violarite; Vl2-supergene violarite; Py-pyrite; Cp-chalcopyrite.**

**Figure 15. Approximate $fO_2$ vs $fS_2$ diagram for the Fe-Ni-S-O system under conditions of common equilibration in altered ultramafic rocks, probably less than 200°C (after Eckstrand 1975).**

**Figure 16. Phase equilibria in the Fe–Ni–S system below 350°C, modified from Craig (1973). Fields for Cygnet and Black Swan from Barnes et al. (2009); field for Lac des lles from Djon and Barnes (2012). Abbreviations: Po-pyrrhotite, Py-pyrite, Pn-pentlandite, Mlr-millerite, Viol-violarite, Pd-polydymite.**

**Figure 17. R factor vs $\delta^{34}S$ histogram (blue bars) for 28 mineralized samples from the Jinbaoshan intrusion. Variations in $\delta^{34}S$ with varying magma:sulfide ratios (R factors) have been calculated for a magma containing 0.05% S with 0.1‰ $\delta^{34}S$ equilibrated with a sulfide xenomelts (derived from country-rock sandstone) containing 38% S with 18‰ $\delta^{34}S$ (red line) and 12‰ $\delta^{34}S$ (blue line).**

**Figure 18. A: S vs. Ni and B: $Ir_{100}$ vs. $Pd_{100}$ and R factor model (parameters in text) for mineralized samples from the Jinbaoshan intrusion. The differences between the S-Ni trends in the Wang et al. (2010) and Lu et al. (2014), Lu and He (2018) datasets are attributed to differences in the nature and degree of post-magmatic alteration (see Figure 16).**

**Figure 19. Primitive mantle-normalized chalcophile element patterns for average composition of mineralized samples from the Jinbaoshan deposit (black pattern) and models for varying amounts of a hybrid magma containing 96% ELIP picrite magma and 4% ELIP low-Ti (LT1) basalt interacting with different amounts of sulfide xenomelt (R – magma:sulfide ratio). Compositions of picrite (Li et al., 2012) and LT basalt (Wang et al., 2011) given in text. Normalizing values after McDonough and Sun (1995)**

**Figure 20. Schematic model for the formation of PGMs and base metal sulfides from the Jinbaoshan deposit (adapted from Holwell and McDonald, 2010; Dare et al., 2010, 2011). Abbreviations: Cp-chalcopyrite; Pn-pentlandite; Po-pyrrhotite; Vl1-hypogene violarite; Vl2-supergene violarite; Py-pyrite; Mlr-millerite; Pld-polydymite; Mgt-magnetite.**

**Table caption**

**Table 1 LA-ICP-MS analyses of maximum, minimum and median values for the base metal sulfides in the Jinbaoshan deposit.**

## Figures

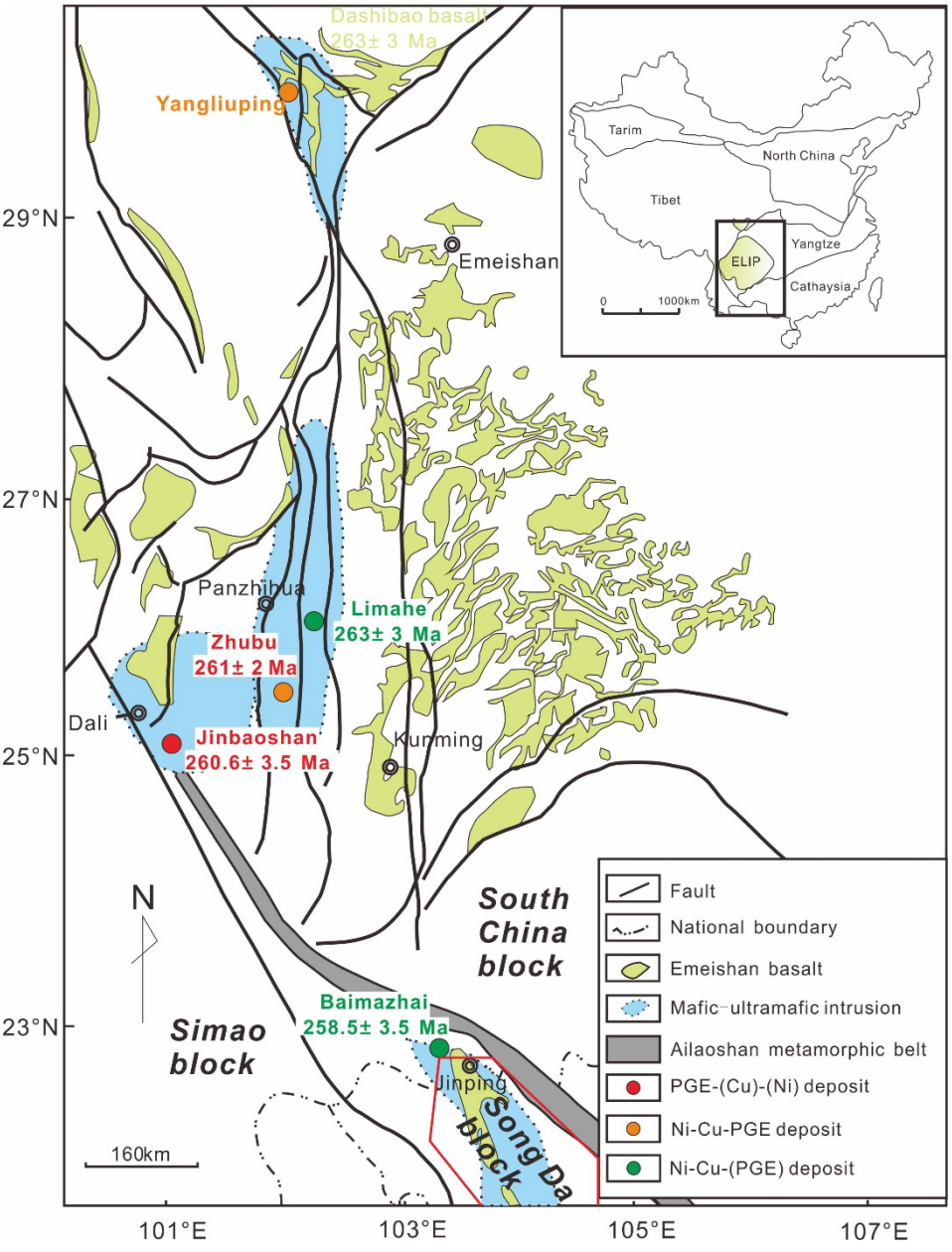


**Figure 1**

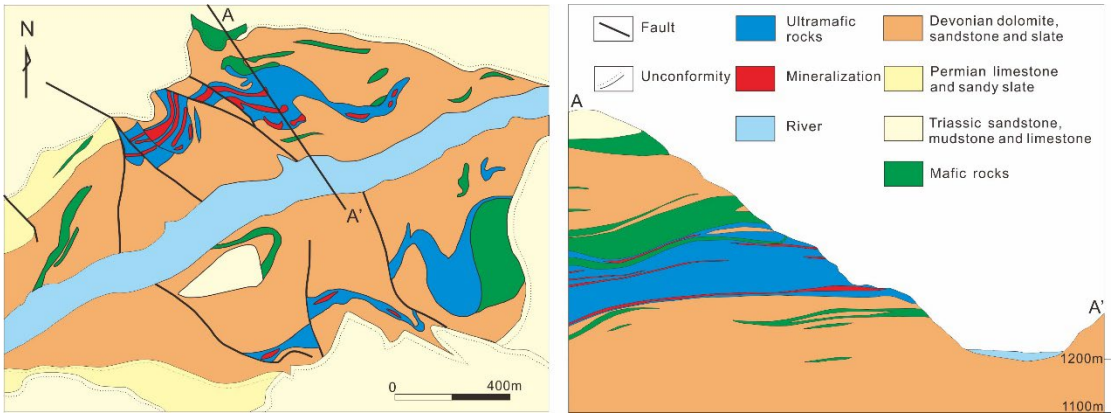
N
A
A'
0
400m
Fault
Unconformity
Ultramafic rocks
Mineralization
River
Devonian dolomite, sandstone and slate
Permian limestone and sandy slate
Triassic sandstone, mudstone and limestone
Mafic rocks
A
A'
1200m
1100m

**Figure 2**

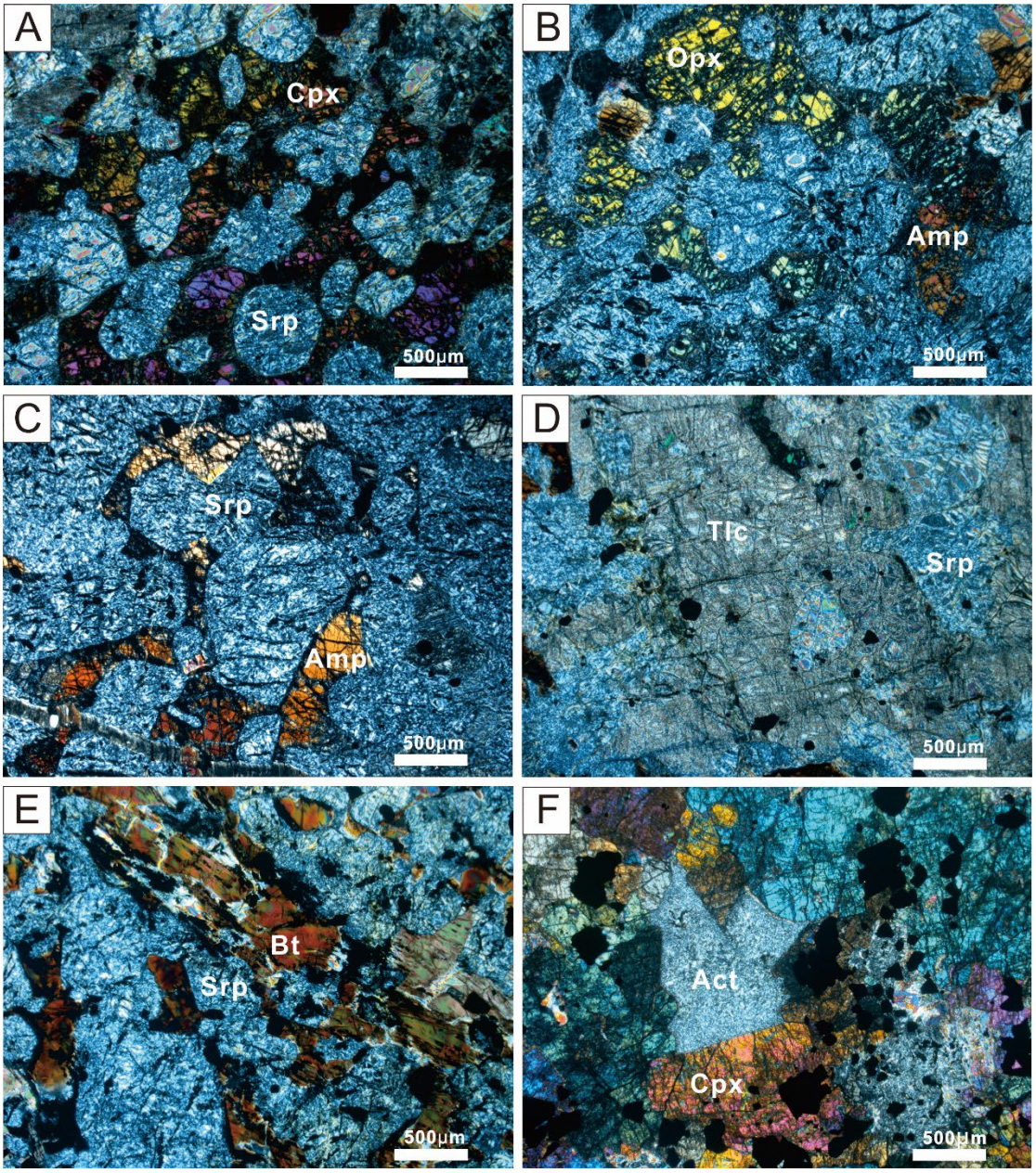
A
Cpx
Srp
500µm
B
Opx
Amp
500µm
C
Srp
Amp
500µm
D
Tlc
Srp
500µm
E
Bt
Srp
500µm
F
Act
Cpx
500µm

**Figure 3**

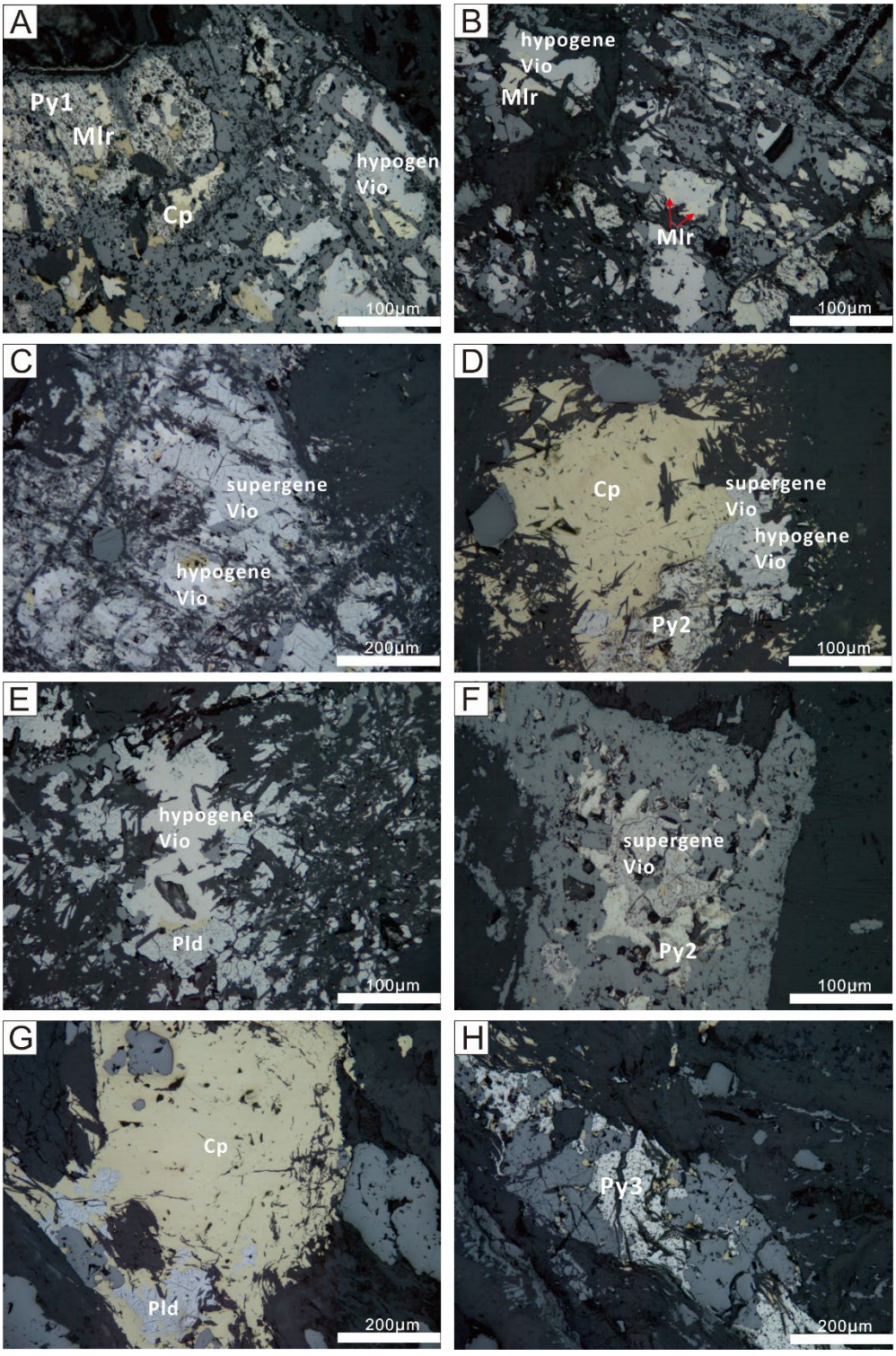
A
Py1
Mlr
hypogen
Vio
Cp
100µm
B
hypogene
Vio
Mlr
Mlr
100µm
C
supergene
Vio
hypogene
Vio
200µm
D
Cp
supergene
Vio
hypogene
Vio
Py2
100µm
E
hypogene
Vio
Pld
100µm
F
supergene
Vio
Py2
100µm
G
Cp
Pld
200µm
H
Py3
200µm

**Figure 4**

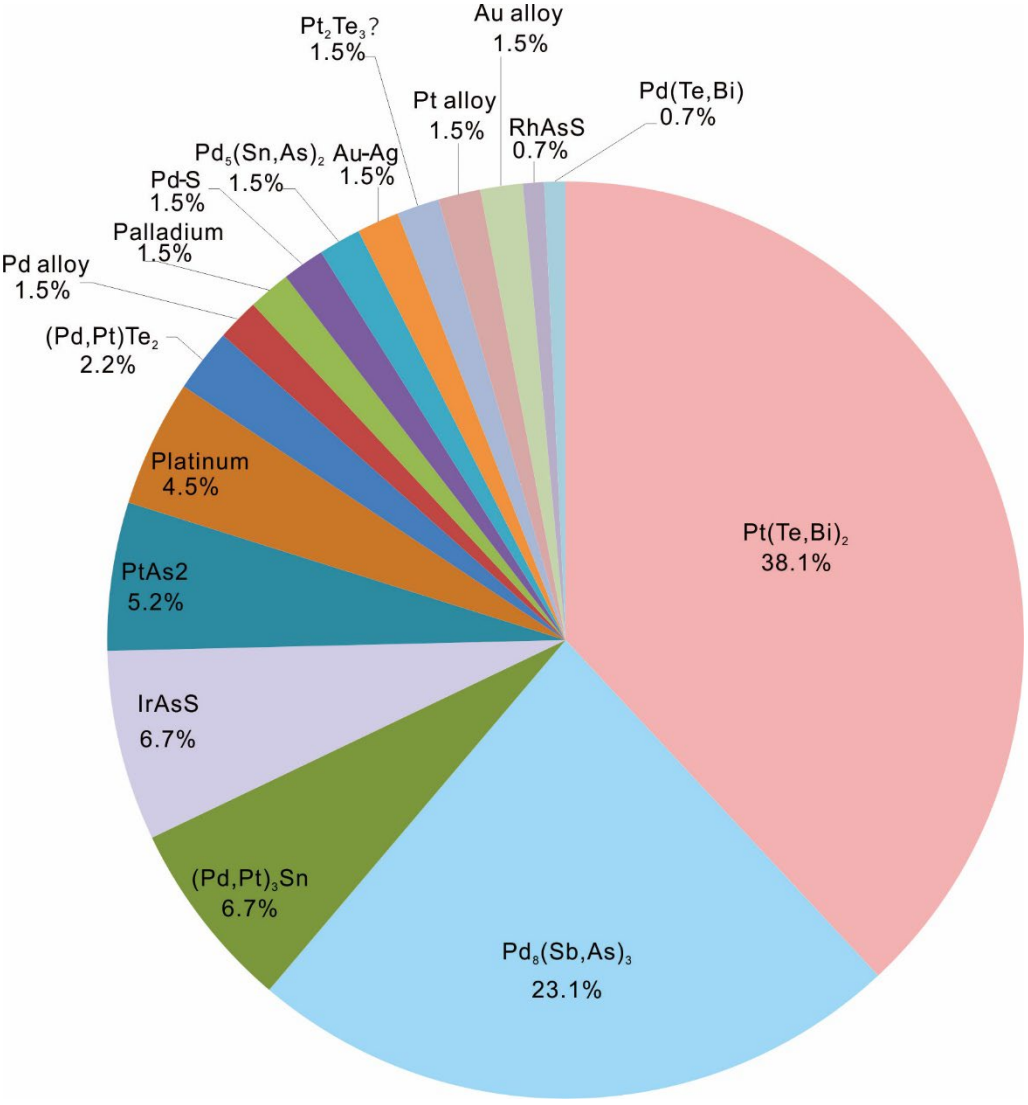
Pt2Te3? 1.5%
Au alloy 1.5%
Pt alloy 1.5%
RhAsS 0.7%
Pd(Te,Bi) 0.7%
Pd5(Sn,As)2 1.5%
Au-Ag 1.5%
Pd-S 1.5%
Palladium 1.5%
Pd alloy 1.5%
(Pd,Pt)Te2 2.2%
Platinum 4.5%
PtAs2 5.2%
IrAsS 6.7%
(Pd,Pt)3Sn 6.7%
Pd8(Sb,As)3 23.1%
Pt(Te,Bi)2 38.1%

**Figure 5**

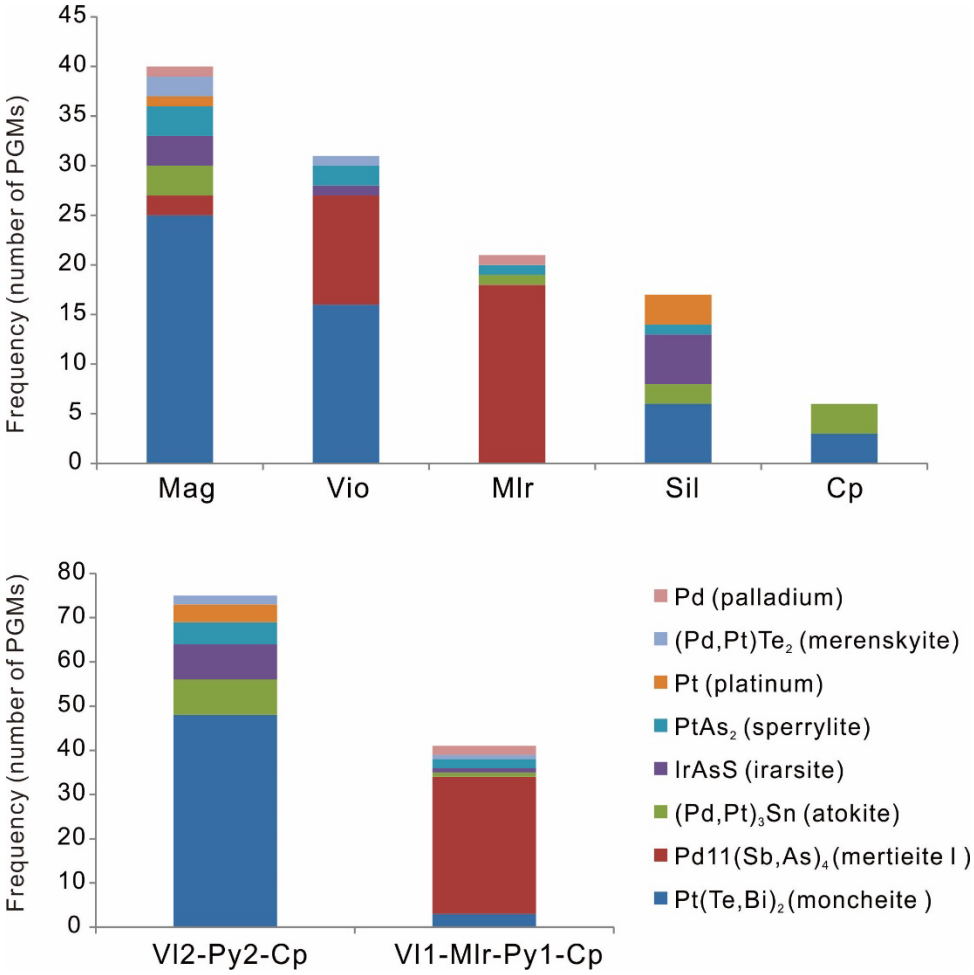
Frequency (number of PGMs)
45
40
35
30
25
20
15
10
5
0
Mag
Vio
Mlr
Sil
Cp
Frequency (number of PGMs)
80
70
60
50
40
30
20
10
0
Vl2-Py2-Cp
Vl1-Mlr-Py1-Cp
Pd (palladium)
(Pd,Pt)Te2 (merenskyite)
Pt (platinum)
PtAs2 (sperrylite)
IrAsS (irarsite)
(Pd,Pt)3Sn (atokite)
Pd11(Sb,As)4 (mertieite I )
Pt(Te,Bi)2 (moncheite )

**Figure 6**

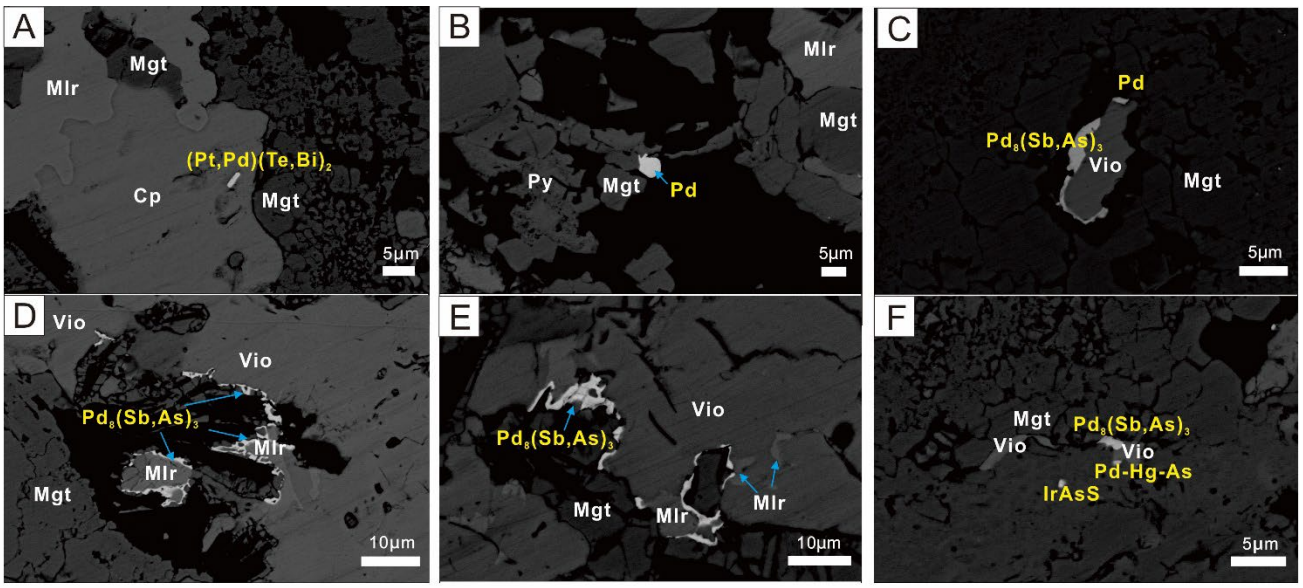
A
Mlr
Mgt
(Pt,Pd)(Te,Bi)2
Cp
Mgt
5μm
B
Mlr
Mgt
Py
Mgt
Pd
5μm
C
Pd
Pd8(Sb,As)3
Vio
Mgt
5μm
D
Vio
Vio
Pd8(Sb,As)3
Mlr
Mlr
Mgt
10μm
E
Vio
Pd8(Sb,As)3
Mgt
Mlr
Mlr
10μm
F
Mgt
Pd8(Sb,As)3
Vio
Vio
Pd-Hg-As
IrAsS
5μm

**Figure 7**

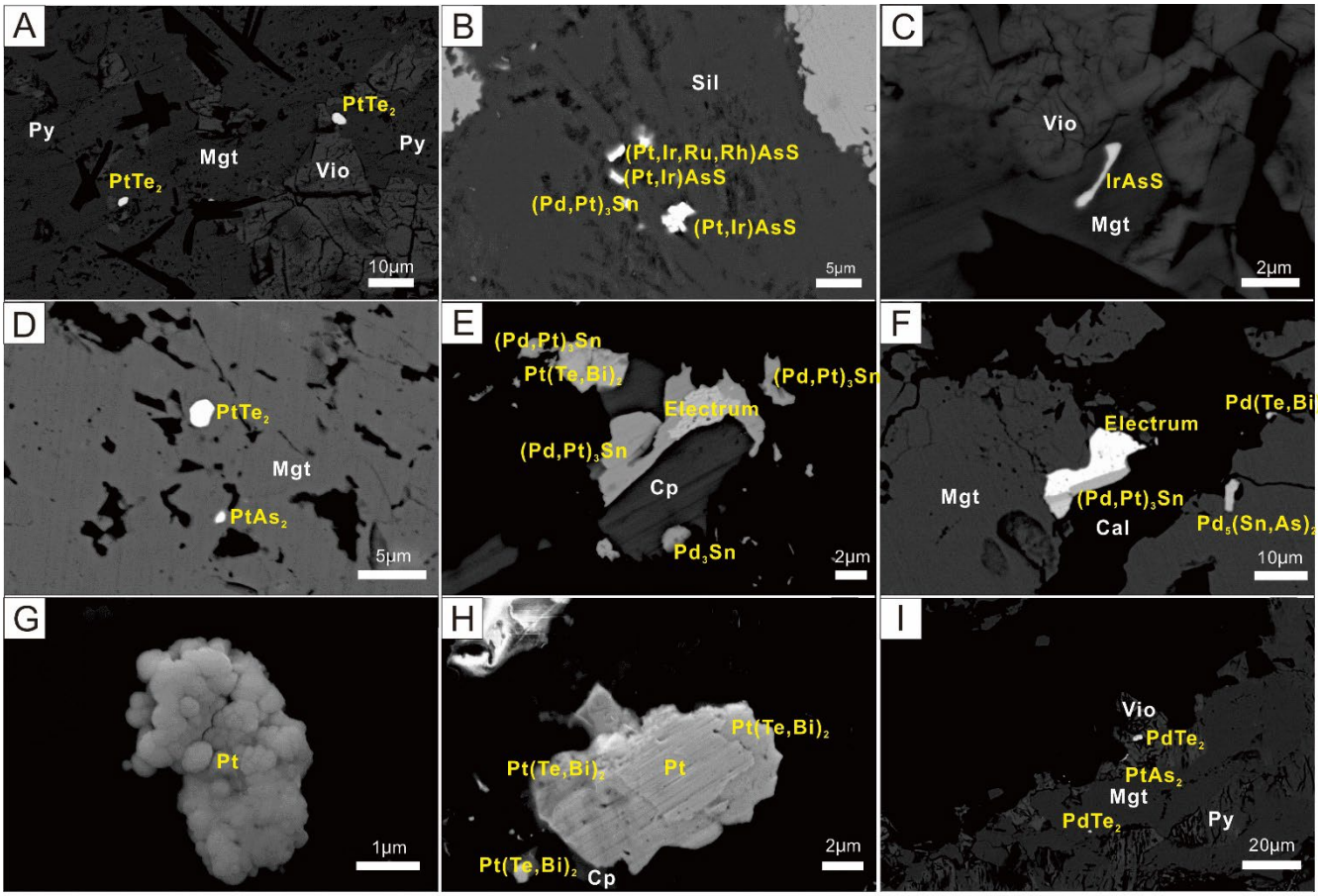
A
Py
PtTe2
Mgt
Py
PtTe2
Vio
10μm
B
Sil
(Pt,Ir,Ru,Rh)AsS
(Pt,Ir)AsS
(Pd,Pt)3Sn
(Pt,Ir)AsS
5μm
C
Vio
IrAsS
Mgt
2μm
D
PtTe2
Mgt
PtAs2
5μm
E
(Pd,Pt)3Sn
Pt(Te,Bi)2
(Pd,Pt)3Sn
Electrum
(Pd,Pt)3Sn
Cp
Pd3Sn
2μm
F
Pd(Te,Bi)
Electrum
Mgt
(Pd,Pt)3Sn
Cal
Pd5(Sn,As)2
10μm
G
Pt
1μm
H
Pt(Te,Bi)2
Pt(Te,Bi)2
Pt
Pt(Te,Bi)2
Cp
2μm
I
Vio
PdTe2
PtAs2
Mgt
PdTe2
Py
20μm

**Figure 8**

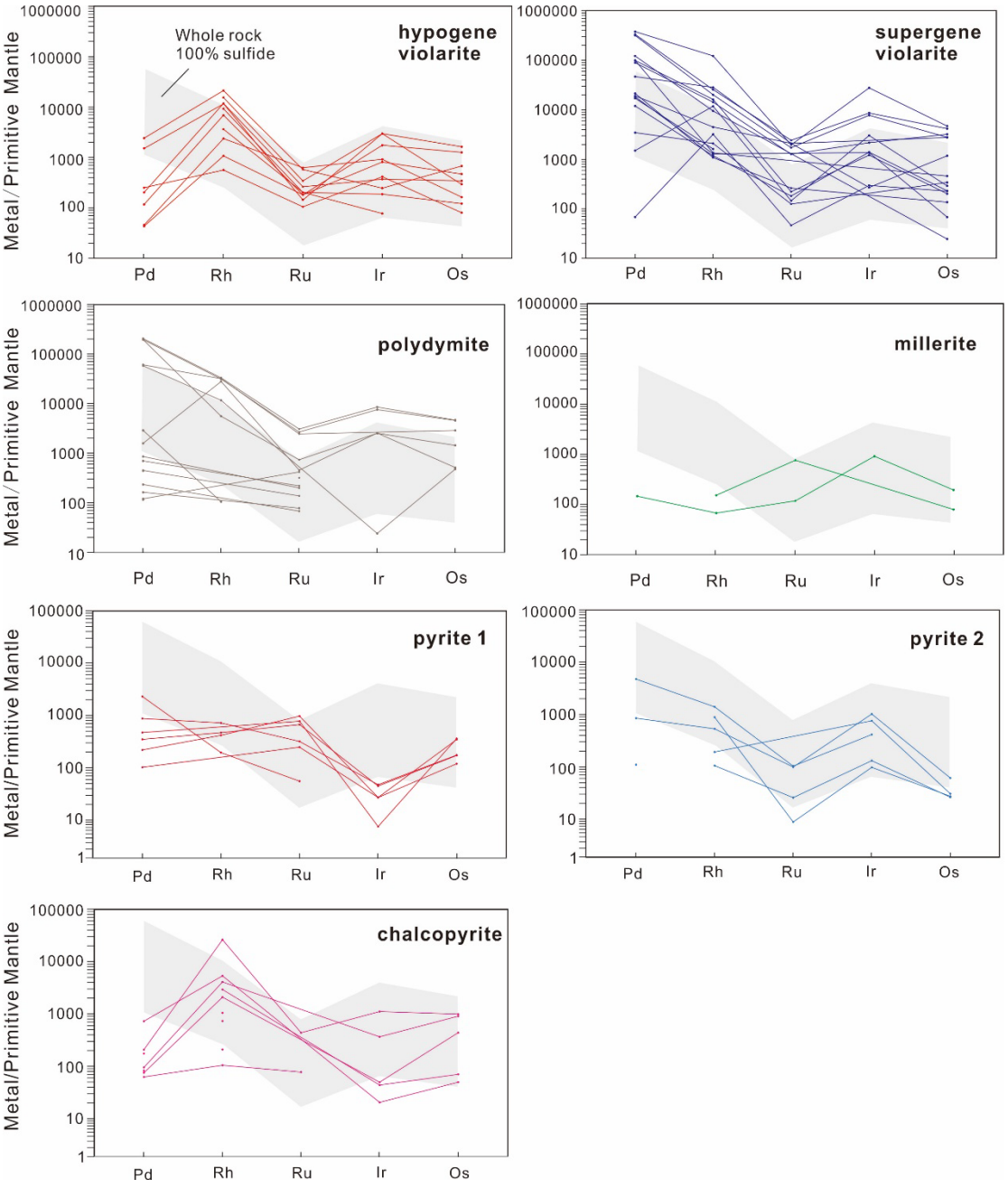
Metal/Primitive Mantle
1000000
100000
10000
1000
100
10
1
Pd
Rh
Ru
Ir
Os
Whole rock
100% sulfide
hypogene
violarite
supergene
violarite
polydymite
millerite
pyrite 1
pyrite 2
chalcopyrite

**Figure 9**

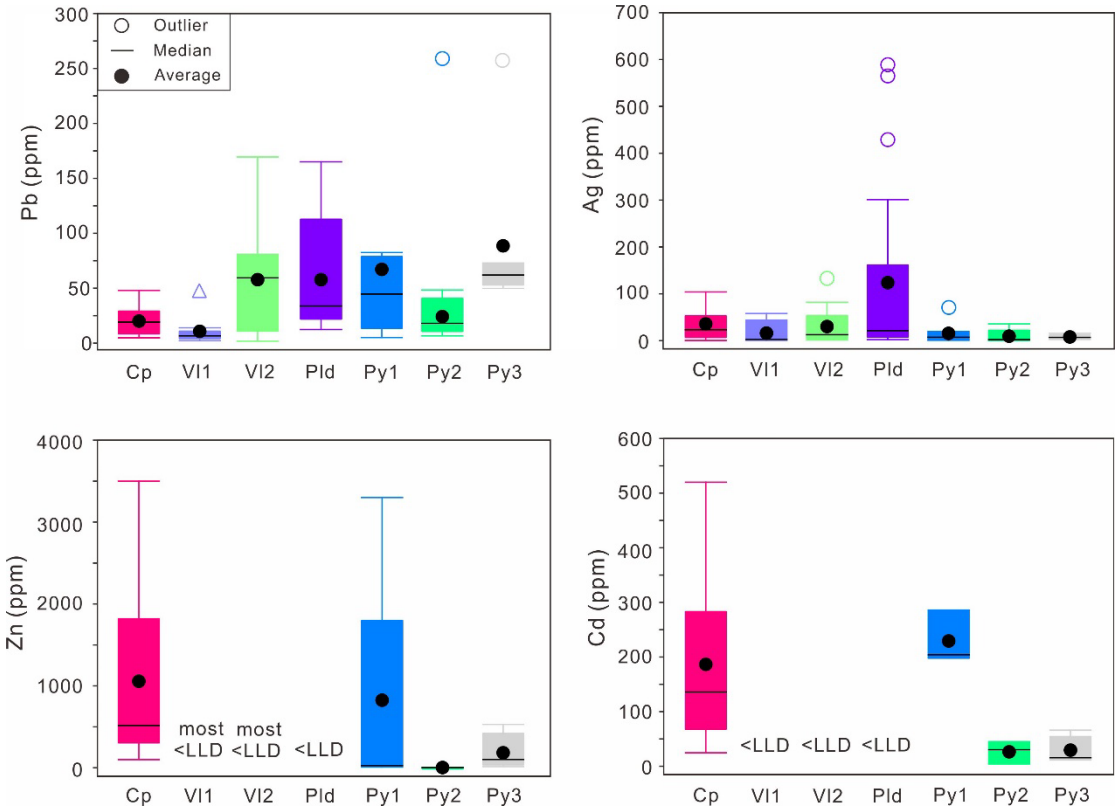
Outlier
Median
Average
Pb (ppm)
Ag (ppm)
Zn (ppm)
Cd (ppm)
Cp
Vl1
Vl2
Pld
Py1
Py2
Py3
most <LLD
most <LLD
<LLD
<LLD
<LLD
<LLD

**Figure 10**

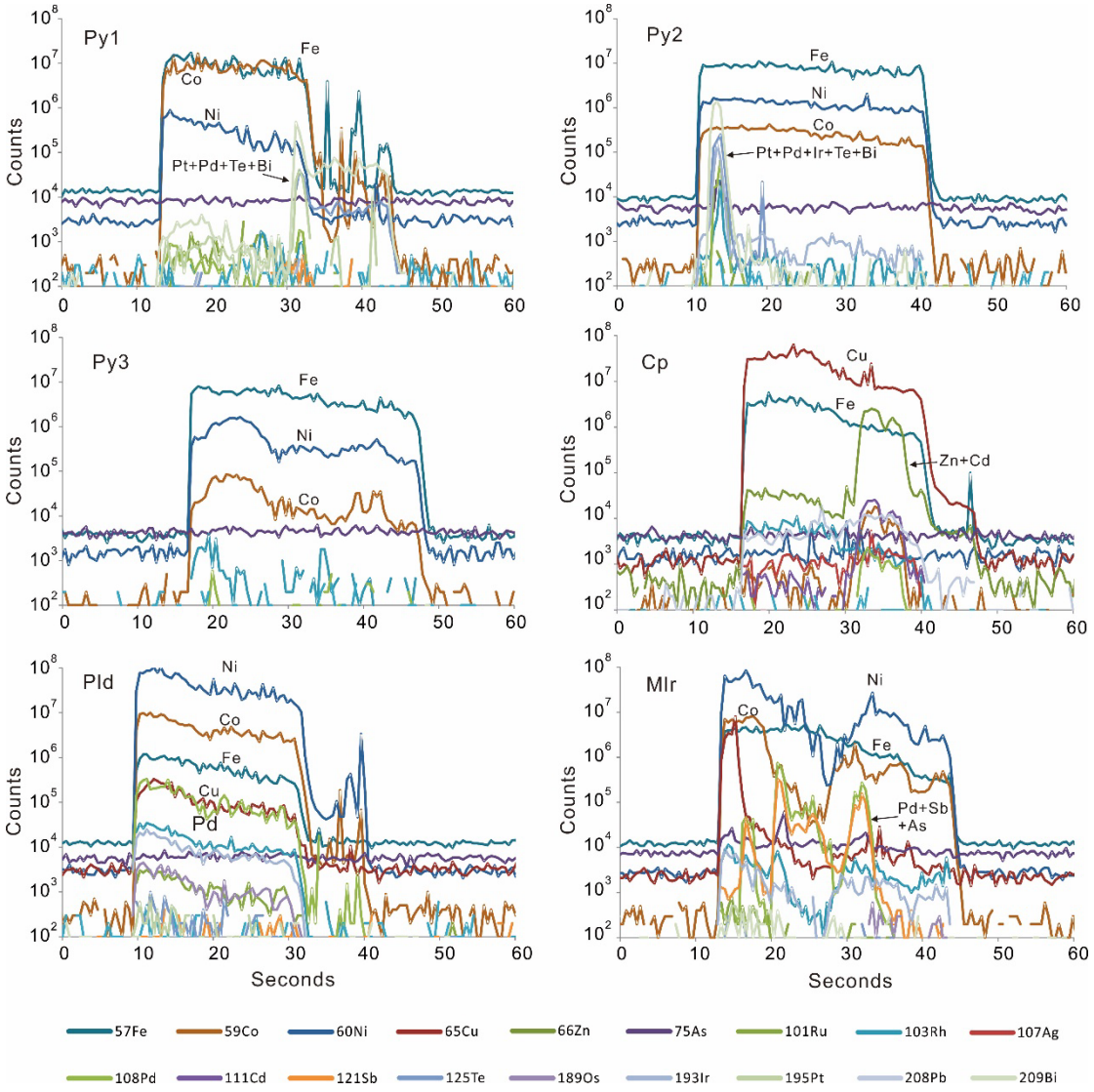
Py1
Fe
Co
Ni
Pt+Pd+Te+Bi
Py2
Fe
Ni
Co
Pt+Pd+Ir+Te+Bi
Py3
Fe
Ni
Co
Cp
Cu
Fe
Zn+Cd
Pld
Ni
Co
Fe
Cu
Pd
Mlr
Ni
Co
Fe
Pd+Sb
+As
Counts
Seconds
57Fe
59Co
60Ni
65Cu
66Zn
75As
101Ru
103Rh
107Ag
108Pd
111Cd
121Sb
125Te
189Os
193Ir
195Pt
208Pb
209Bi

**Figure 11**

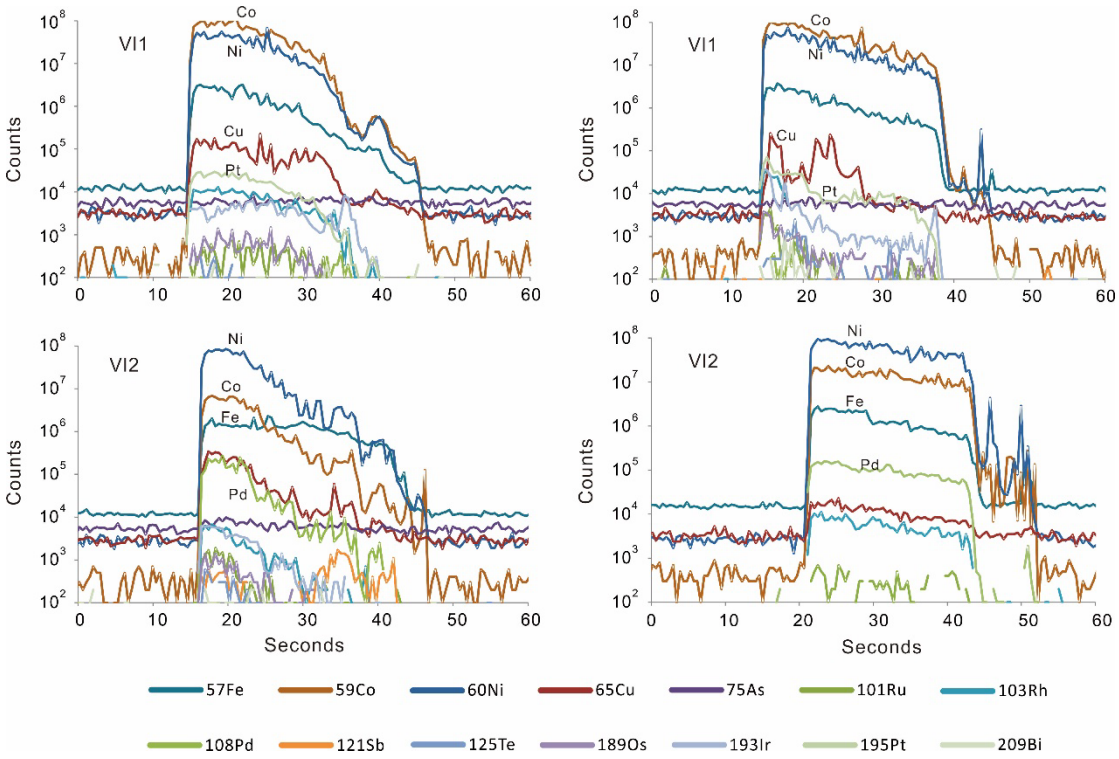
VI1
Co
Ni
Cu
Pt
VI2
Ni
Co
Fe
Pd
Counts
Seconds
57Fe
59Co
60Ni
65Cu
75As
101Ru
103Rh
108Pd
121Sb
125Te
189Os
193Ir
195Pt
209Bi

**Figure 12**

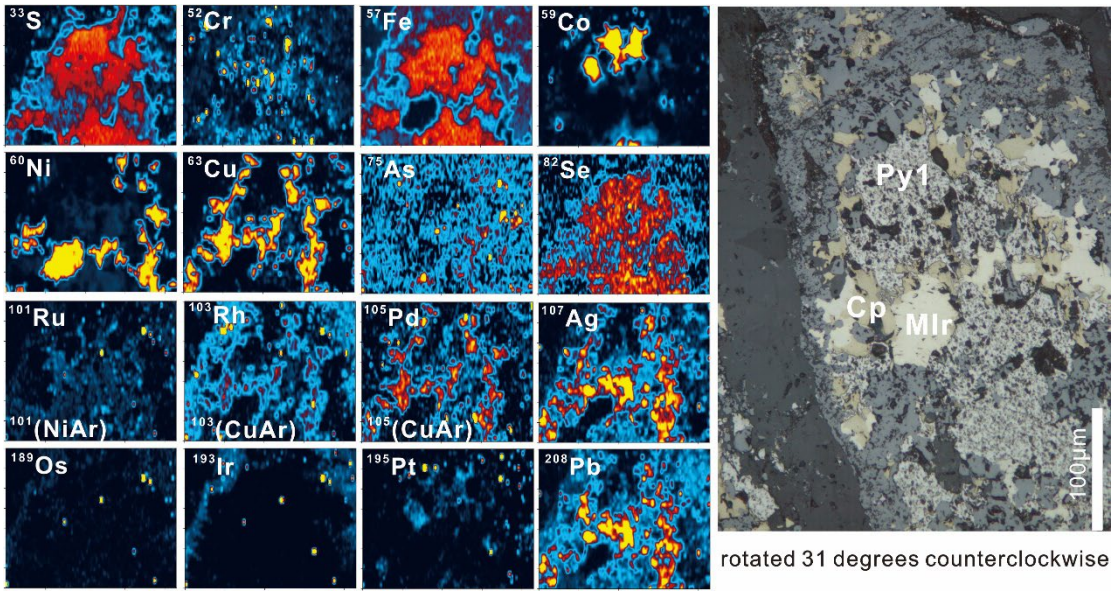
33S
52Cr
57Fe
59Co
60Ni
63Cu
75As
82Se
101Ru
101(NiAr)
103Rh
103(CuAr)
105Pd
105(CuAr)
107Ag
189Os
193Ir
195Pt
208Pb
Py1
Cp
Mlr
100µm
rotated 31 degrees counterclockwise

**Figure 13**

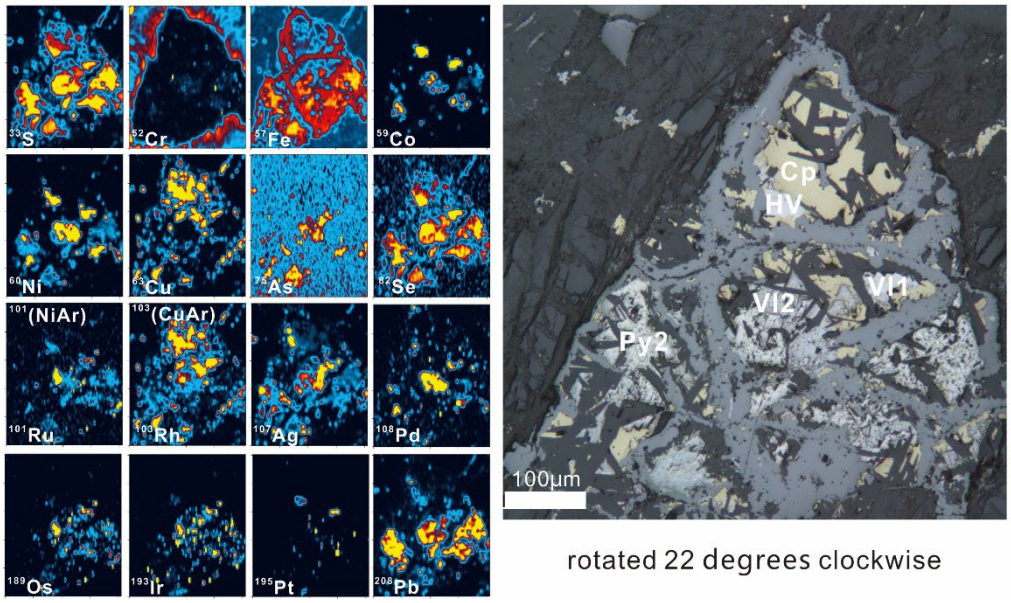
33S
52Cr
57Fe
59Co
60Ni
63Cu
75As
82Se
101(NiAr)
103(CuAr)
101Ru
103Rh
107Ag
108Pd
189Os
193Ir
195Pt
208Pb
Cp
HV
Vl2
Vl1
Py2
100µm
rotated 22 degrees clockwise

**Figure 14**

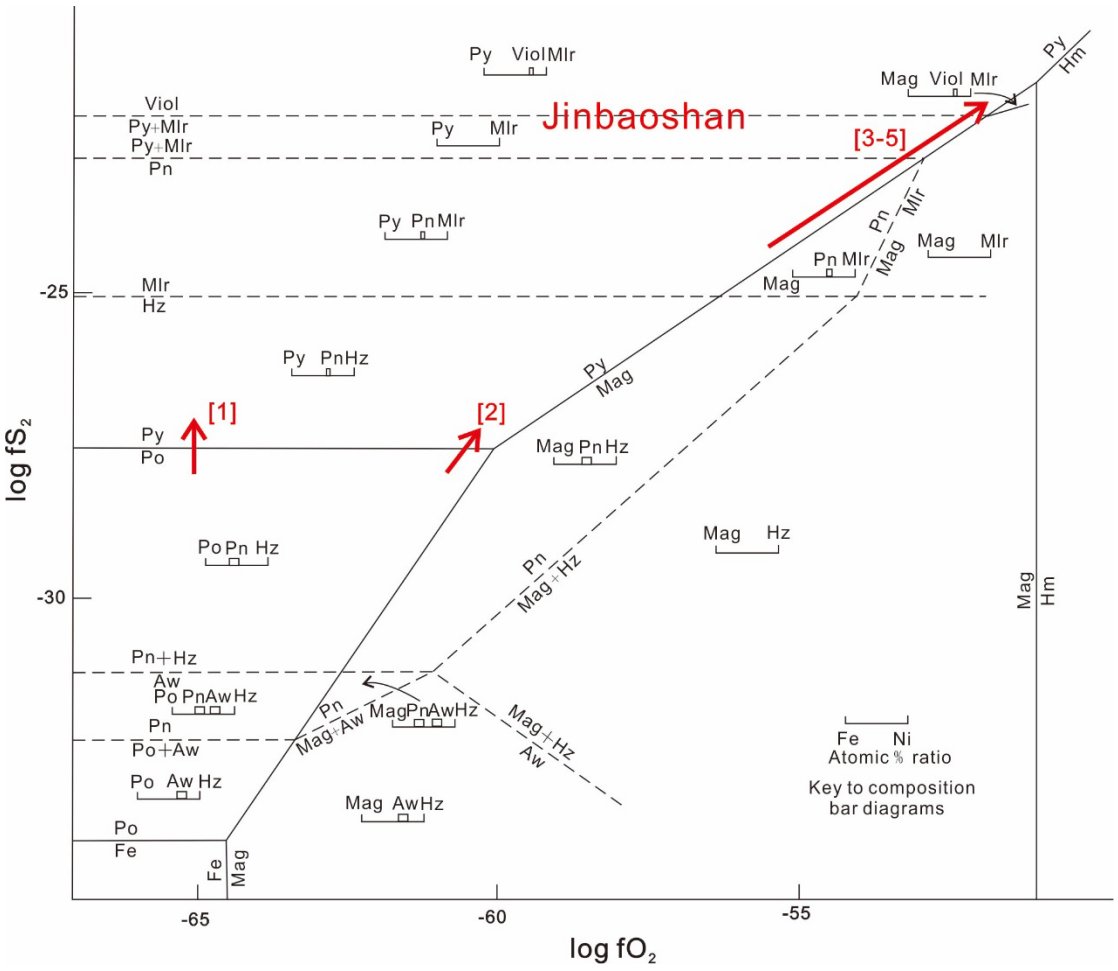
Jinbaoshan
[1]
[2]
[3-5]
Py Viol Mlr
Viol
Py+Mlr
Py+Mlr
Pn
Py Mlr
Py Pn Mlr
Mlr
Hz
Py PnHz
Py
Po
Po Pn Hz
Pn+Hz
Aw
Po PnAwHz
Pn
Po+Aw
Po Aw Hz
Po
Fe
Fe
Mag
Mag AwHz
Py
Mag
Mag Pn Hz
Pn
Mag+Hz
Mag Hz
Pn
Mag+Aw
MagPnAwHz
Mag+Hz
Aw
Mag Viol Mlr
Py
Hm
Pn Mlr
Mag
Pn
Mlr
Mag
Mag Mlr
Mag
Hm
Fe Ni
Atomic % ratio
Key to composition
bar diagrams
-25
-30
-65
-60
-55
log fS2
log fO2

**Figure 15**

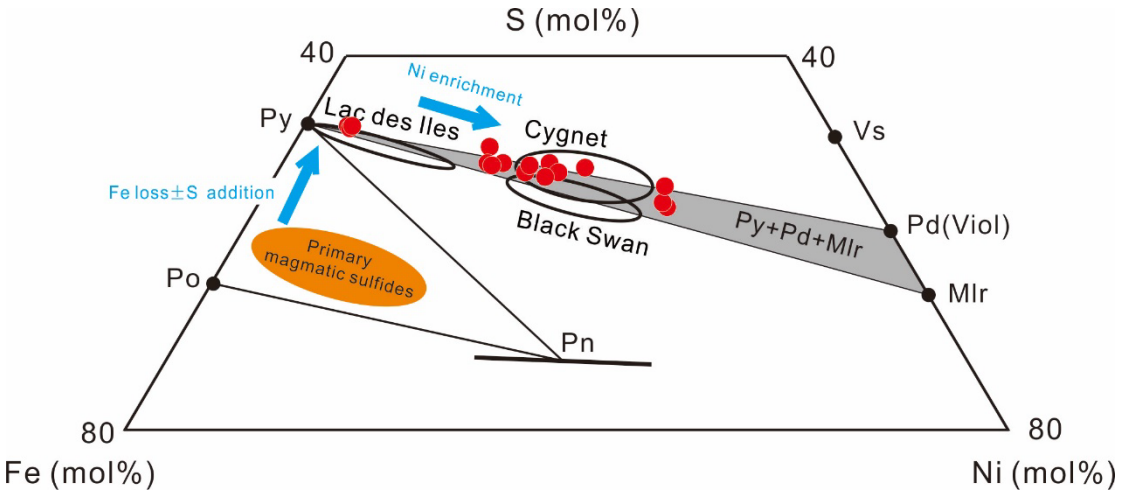
S (mol%)
40
40
Ni enrichment
Py
Lac des Iles
Cygnet
Vs
Fe loss±S addition
Black Swan
Py+Pd+Mlr
Pd(Viol)
Primary magmatic sulfides
Po
Mlr
Pn
80
80
Fe (mol%)
Ni (mol%)

**Figure 16**

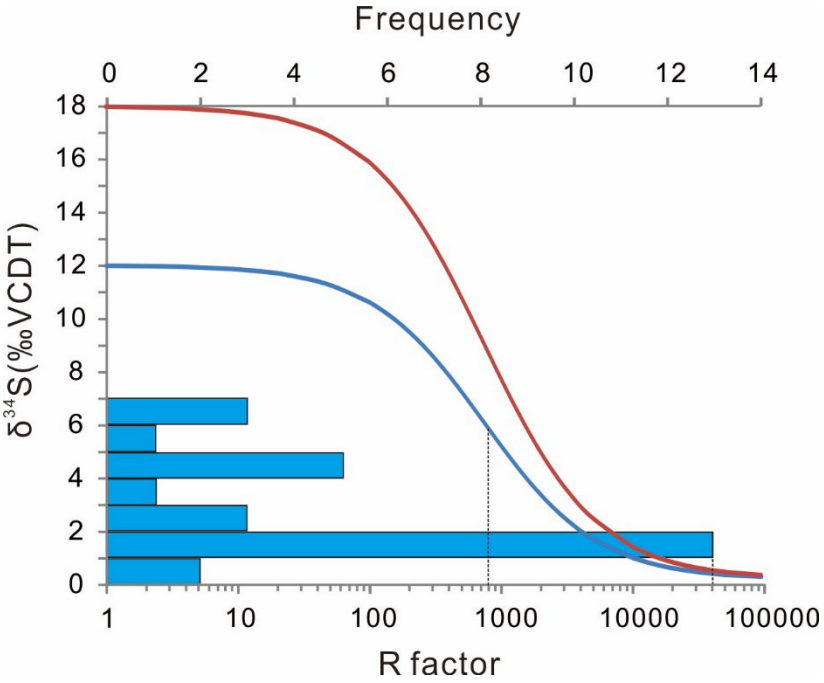
Frequency
0
2
4
6
8
10
12
14
18
16
14
12
10
8
6
4
2
0
δ34S(‰VCDT)
1
10
100
1000
10000
100000
R factor

**Figure 17**

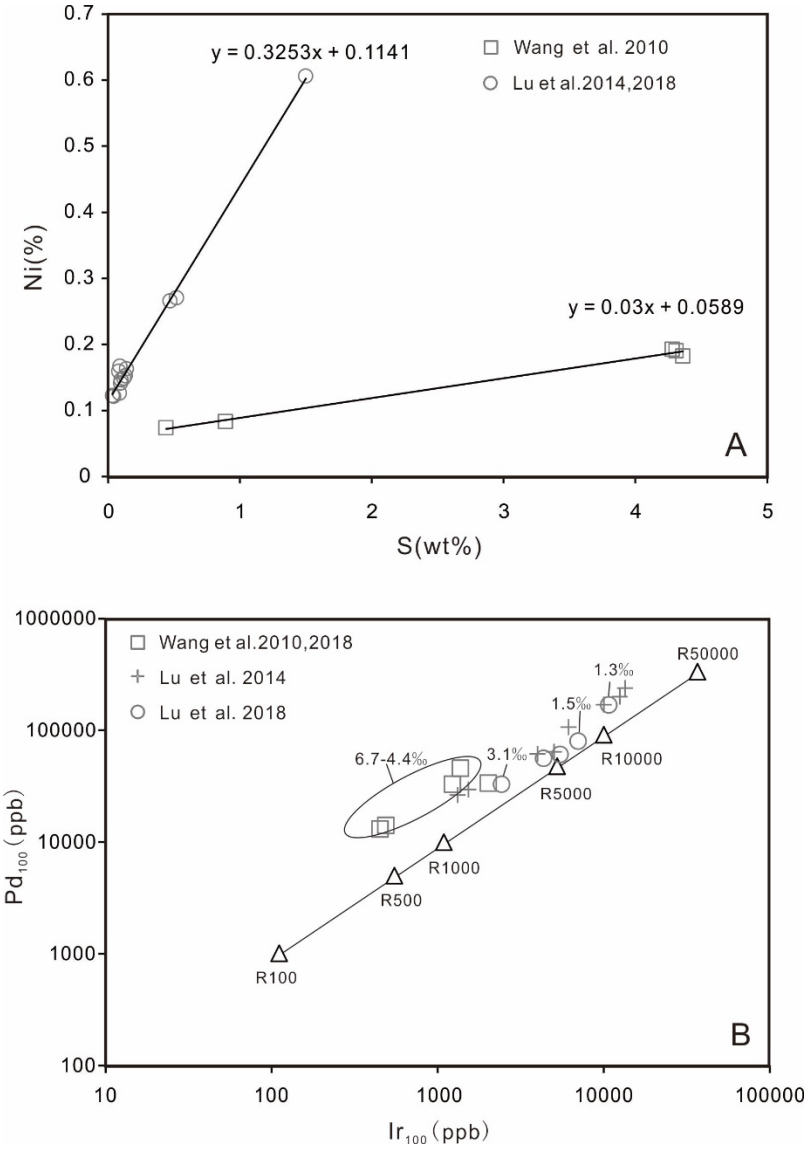
y = 0.3253x + 0.1141
Wang et al. 2010
Lu et al.2014,2018
y = 0.03x + 0.0589
Ni(%)
S(wt%)
A
Wang et al.2010,2018
Lu et al. 2014
Lu et al. 2018
R50000
1.3‰
1.5‰
6.7-4.4‰
3.1‰
R10000
R5000
R1000
R500
R100
$Pd_{100}$ (ppb)
$Ir_{100}$ (ppb)
B

**Figure 18**

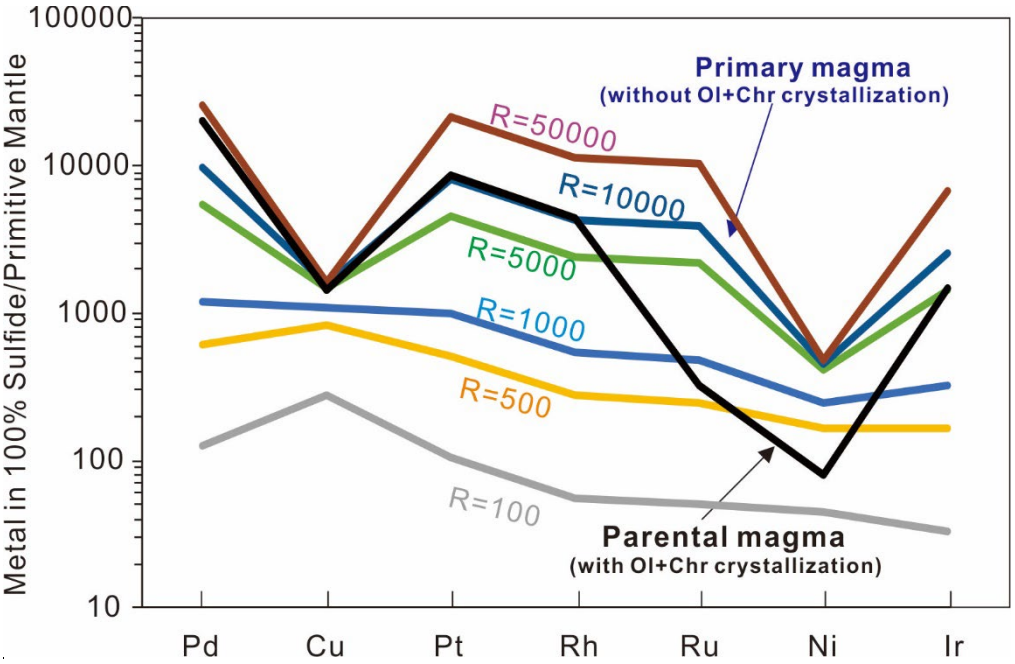
100000
10000
1000
100
10
Metal in 100% Sulfide/Primitive Mantle
Pd
Cu
Pt
Rh
Ru
Ni
Ir
Primary magma
(without Ol+Chr crystallization)
R=50000
R=10000
R=5000
R=1000
R=500
R=100
Parental magma
(with Ol+Chr crystallization)

**Figure 19**

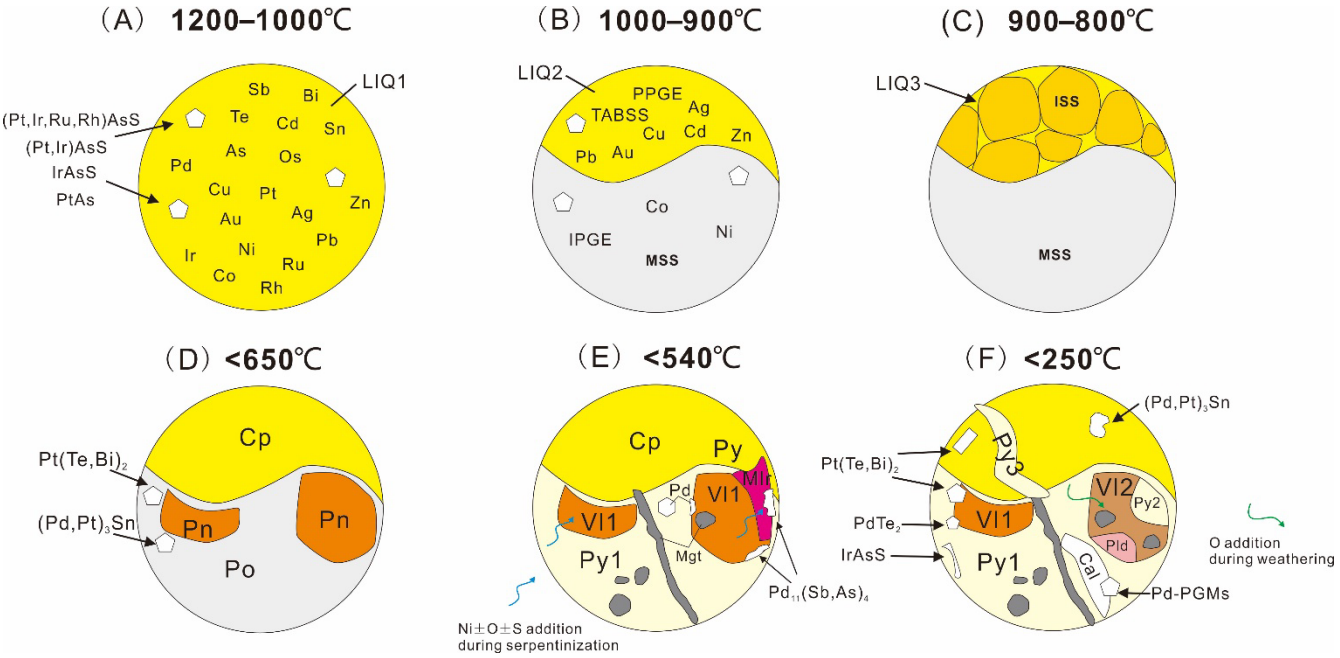
(A) 1200–1000℃
LIQ1
Sb
Bi
Te
Cd
Sn
As
Os
Pd
Cu
Pt
Ag
Au
Zn
Pb
Ir
Ni
Ru
Co
Rh
(Pt,Ir,Ru,Rh)AsS
(Pt,Ir)AsS
IrAsS
PtAs
(B) 1000–900℃
LIQ2
PPGE
TABSS
Ag
Cu
Cd
Zn
Pb
Au
Co
Ni
IPGE
MSS
(C) 900–800℃
LIQ3
ISS
MSS
(D) <650℃
Cp
Pt(Te,Bi)2
(Pd,Pt)3Sn
Pn
Pn
Po
(E) <540℃
Cp
Py
Mlr
Pd
Vl1
Vl1
Py1
Mgt
Pd11(Sb,As)4
Ni±O±S addition
during serpentinization
(F) <250℃
(Pd,Pt)3Sn
Py3
Pt(Te,Bi)2
Vl2
Py2
PdTe2
Vl1
Pld
IrAsS
Py1
Cal
Pd-PGMs
O addition
during weathering

**Figure 20**

## Tables

**Table 1 LA-ICP-MS analyses of maximum, minimum and median values for the base metal sulfides in the Jinbaoshan deposit**

| Mineral | Mineral type | | Cd ppm | Pb ppm | Ag ppm | Pd ppm | Cu ppm | Pt ppm | Rh ppm | Ru ppm | Ni ppm | Ir ppm | Os ppm | Co ppm | Zn ppm |
|---|---|---|---|---|---|---|---|---|---|---|---|---|---|---|---|
| Vio | Vl1 | Max | <LLD | 46.8 | 58 | 9.5 | 9980 | 720 | 20 | 3.1 | 318000 | 10.2 | 5.5 | 167600 | 1200 |
| | | Min | <LLD | 2.24 | <LLD | <LLD | 180 | <LLD | <LLD | <LLD | 225000 | <LLD | <LLD | 40700 | <LLD |
| | | Median | <LLD | 6.17 | 2.6 | 0.895 | 630 | 32.2 | 7.6 | 1.005 | 246000 | 2.07 | 1.16 | 126200 | 625 |
| Vio | Vl2 | Max | <LLD | 170 | 133 | 1490 | 4850 | 24 | 115 | 12 | 436600 | 93.3 | 15.8 | 38400 | 82 |
| | | Min | <LLD | <LLD | 1.62 | 0.27 | 14.1 | <LLD | 1.02 | <LLD | 195000 | <LLD | <LLD | 1561 | <LLD |
| | | Median | <LLD | 65.3 | 13.6 | 184 | 151 | 0.73 | 4.22 | 6.3 | 338000 | 4.7 | 1.35 | 16800 | 82 |
| Pld | | Max | <LLD | 165 | 589 | 820 | 7800 | 19.3 | 31.6 | 15.4 | 512100 | 29.1 | 15.9 | 42700 | <LLD |
| | | Min | <LLD | 12.4 | 2.24 | <LLD | 62.5 | <LLD | <LLD | <LLD | 399100 | <LLD | <LLD | 3190 | <LLD |
| | | Median | <LLD | 33.9 | 21.3 | 4.86 | 646 | 2.84 | 26.7 | 1.85 | 485050 | 8.7 | 7.35 | 13550 | <LLD |
| Py | Py2 | Max | 2.24 | 48.4 | 35.8 | 3.4 | 1179 | 25 | 0.85 | 0.5 | 36900 | 3.5 | 0.21 | 820 | 3.1 |
| | | Min | <LLD | 6.7 | 0.45 | <LLD | 9 | <LLD | <LLD | <LLD | 2240 | <LLD | <LLD | 6.3 | <LLD |
| | | Median | 1.51 | 18 | 2.27 | 1.92 | 299 | 0.28 | 0.35 | 0.13 | 7600 | 1.53 | 0.1 | 416 | 3.1 |
| Py | Py1 | Max | 14.3 | 259 | 70.2 | 19 | 20600 | 35 | 1.34 | 4.9 | 11030 | 1.42 | 1.24 | 24100 | 3300 |
| | | Min | <LLD | 5.1 | 0.82 | <LLD | 43 | <LLD | <LLD | <LLD | 864 | <LLD | <LLD | 91 | <LLD |
| | | Median | 10.2 | 44.7 | 7.4 | 1.89 | 1645 | 4.16 | 0.45 | 1.61 | 3880 | 0.124 | 0.6 | 12550 | 27 |
| Py | Py3 | Max | 3.3 | 257 | 15.6 | 0.25 | 5500 | <LLD | 0.07 | 0.55 | 9900 | <LLD | <LLD | 14900 | 530 |
| | | Min | <LLD | 49.8 | 2.74 | <LLD | 1160 | <LLD | <LLD | <LLD | 3730 | <LLD | <LLD | 940 | 14.1 |
| | | Median | 0.78 | 62 | 6.9 | 0.25 | 2400 | <LLD | 0.07 | 0.55 | 5480 | <LLD | <LLD | 5400 | 102 |
| Cp | | Max | 26 | 48 | 104 | 2.9 | 442000 | 0.86 | 25 | 2.2 | 350 | 3.8 | 3.4 | 18 | 3500 |
| | | Min | <LLD | 4.85 | <LLD | <LLD | 264000 | <LLD | <LLD | <LLD | <LLD | <LLD | <LLD | <LLD | 100 |
| | | Median | 6.8 | 19.1 | 23.2 | 0.38 | 315000 | 0.6 | 2 | 1.3 | 15.9 | 0.17 | 1.5 | 1.61 | 517 |
| Mlr | | Max | <LLD | <LLD | <LLD | 0.58 | 90 | <LLD | 0.145 | 3.8 | | 3.1 | 0.66 | 244 | <LLD |
| | | Min | <LLD | <LLD | <LLD | <LLD | 60 | <LLD | 0.064 | 0.59 | | <LLD | 0.27 | 17.9 | <LLD |
| | | Median | <LLD | <LLD | <LLD | 0.58 | 75 | <LLD | 0.105 | 2.2 | | 3.1 | 0.47 | 131 | <LLD |

# Chapter 3: Genesis and mechanisms of metal enrichment in the Baimazhai Ni-Cu-(PGE) deposit, Ailaoshan orogenic belt, SW China

**Yiguan Lu[1,2,3,*], C. Michael Lesher[1], Liqiang Yang[2], Matthew I. Leybourne[1,4], Wenyan He[2]**

[1] Mineral Exploration Research Centre, Harquail School of Earth Sciences, Goodman School of Mines, Laurentian University, 935 Ramsey Lake Road, Sudbury, Ontario P3E 2C6, Canada

[2] State Key Laboratory of Geological Processes and Mineral Resources, China University of Geosciences, Beijing 100083, China

[3] Current Address: Tianjin Center, China Geological Survey, Tianjin 300170, China

[4] Current Address: Department of Geological Sciences and Geological Engineering, Queen's University, 36 Union Street, Kingston, Ontario K7L 3N6, Canada

* Corresponding Author email: lueyig@gmail.com;

## 3.1 Abstract

The ~259 Ma Baimazhai Ni-Cu-(platinum-group element) (PGE) deposit is located in the Ailaoshan-Red River fault zone on the southwest margin of the Yangtze Plate in the Jinping area of southeastern Yunnan Province. The intrusion is lenticular (~530 m long x 190 m wide x 24-64 m thick) and concentrically-zoned (margin to core) from gabbro through pyroxenite to peridotite. It contains ~50 kt of Ni-Cu-(PGE) mineralization, concentrically zoned (margin to core) from disseminated through net-textured to massive sulfides with an average grade of 1.03 wt% Ni, 0.81 wt% Cu, and 0.02~0.69 ppm Pd+Pt. The sulfide

assemblage comprises pyrrhotite, chalcopyrite, and pentlandite, with lesser magnetite, violarite, galena, and cobaltite. The mineralization is enriched in Ni-Cu-Co relative to PGE and the host rocks are enriched in highly incompatible lithophile elements relative to moderately incompatible lithophile elements with high Th/Yb and intermediate Nb/Yb values. These host rocks, and those at most other Ni-Cu-PGE deposits in the Emeishan Large Igneous Province, have high γOs and intermediate εNd values, indicating that they crystallized from a magma derived from a subduction-modified pyroxenite mantle source and modified by crustal contamination. The initial concentrations of metals in the primary magma are estimated to have been of the order of 200 ppm Ni and 100 ppm Cu, but only 0.4 ppb Pd, 0.2 ppb Pt, 0.005 ppb Rh, 0.02 ppb Ru, and 0.01 ppb Ir. The $\delta^{34}S$ values of ores and separated sulfides range from 5.8‰ to 8.6‰, between the ~10‰ value of sulfides in the metasedimentary country rocks and the 0 ± 0.5‰ value expected for magmas derived from MORB-type mantle or the -2.5 ± 0.3‰ value expected for subduction-modified mantle, consistent with equilibration at magma:sulfide mass ratios (R factors) of 100-1000. Variations in $Ir_{100}$ and $Pd_{100}$ (metals in 100% sulfide) are consistent with 40-60% fractional crystallization of monosulfide solid solution to form Ni-Co-IPGE-rich (IPGE: Ru, Os, Ir) massive ores and Cu-PPGE-Au-rich (PPGE: Pt, Pd, Rh) residual sulfide liquids. This process is also recorded by magnetite: Type I (early magmatic), type II (late magmatic), and type III (secondary) magnetites exhibit progressively lower Cr-Ti-V concentrations. The PGE contents in base-metal minerals are low, and only pentlandite, violarite, and cobaltite contain detectable concentrations of Pd, Rh, and Ru. There is abundant textural evidence for metamorphic-hydrothermal alteration of sulfides in the Baimazhai intrusion, with secondary violarite, chalcopyrite, and pentlandite being enriched (Ag, Sb, Au, Pb) or depleted (Sn) in more mobile chalcophile elements. The different tectonic and petrogenetic settings of the Baimazhai and other deposits in China highlight the potential of Ni-Cu-(PGE) deposits to occur in post-subduction settings and demonstrate that the key controls are magma flux and access to crustal S. Exploration potential remains for the Ailaoshan orogenic belt to host additional magmatic Ni-Cu deposits.

Keywords: genesis, metal enrichment mechanism, Ni-Cu-(PGE) deposit, Baimazhai, SW China

## 3.2 Introduction

Magmatic Ni-Cu-platinum-group element (PGE) deposits are typically related to mantle plumes (e.g., Arndt et al., 2005; Barnes and Lightfoot, 2005) and occur along the thinner margins of cratons (e.g., Kerrich et al., 2005; Sleep, 2006; Begg et al., 2010; Maier and Groves, 2011), trans-lithospheric faults (e.g. Naldrett, 2004; Barnes and Lightfoot, 2005), or crustal sutures (Cassidy et al., 2006; Champion and Cassidy, 2007; Mole et al., 2013). Subduction-related environments are generally considered to be poor targets for Ni-Cu-(PGE) deposits (e.g., Naldrett, 2004; Ripley, 2010; Manor et al., 2016), however, Ni-Cu-(PGE) mineralization occurs in several convergent environments, including Aguablanca in southwestern Spain (e.g., Tornos et al., 2001, 2006; Piña et al., 2008), Duke Island in Alaska (e.g., Stifter et al., 2014; Thakurta et al., 2014), and especially in China, where numerous Ni-Cu-PGE deposits occur in convergent orogenic belts (e.g., Zhou et al., 2004; Song and Li, 2009; Wei et al., 2013; Li et al., 2015; Lu et al., 2019).

Continental China is located at the junction of the Central Asian orogenic belt (CAOB), the Tethyan orogenic belt, and the Pacific oceanic subduction zone (Deng et al., 2017). Nickel-Cu-PGE deposits associated with convergent tectonic settings contribute 40% of the Ni resources of all magmatic Ni-Cu-PGE deposits in China (Li, 2017). These deposits occur mainly in the Central Asian (e.g., Huangshandong, Kalatongke, Pobei, Tianyu, and Heishan), East Kunlun (e.g., Xiarihamu), and Southern Qilian (e.g., Lashuixia and Yulonggou) orogenic belts. The genesis of these deposits is thought to be linked to magmas derived from melting of metasomatized mantle in a subduction or post-subduction environment (Tonnelier, 2010; Li et al., 2012a; Song et al., 2013, 2016; Xie et al., 2014; Lu et al., 2019).

The Sanjiang region in Southwest China is a collage of Paleozoic arc terranes and Gondwana-derived micro-continental blocks formed by oceanic subduction followed by continental collision during the Paleozoic to Mesozoic (Deng et al., 2014a, 2014b, 2017). It is also one of the most important metallogenic regions in China, containing significant Cu-Au-Pb-Zn-Ag-Sn-W mineralization (e.g., magmatic-hydrothermal Au-Cu-Mo-Sn-W deposits, porphyry-skarn Au-Cu-Mo deposits, volcanogenic massive sulfide (VMS) + Mississippi valley-type (MVT) + magmatic-hydrothermal Pb-Zn-Cu-Ag deposits, and orogenic Au deposits) (Zhang et al., 2014; He et al., 2015, 2016; Deng et al., 2015a, 2015b, 2017; Deng and Wang, 2016; Yang et al., 2016, 2017) and magmatic Ni-Cu-PGE mineralization (e.g.,

Jinbaoshan, Baimazhai, Niulanchong, and Xinanli: Zhang, 2006; Wang and Zhou, 2006; Lu et al., 2014; Lu and He, 2018). The Baimazhai Ni-Cu-(PGE) deposit is located in the middle of the Jinping terrane within the Ailaoshan orogenic belt. It is the largest high-grade Ni-Cu sulfide deposit (>1 wt% Ni) in the Emeishan Large Igneous Province (Li et al., 2019). Previous studies have focused on the tectonic setting (divergent: Zhang, 2006; convergent: Wang et al., 2006; Wang and Zhou, 2006), the composition of the primary magma (high-Mg basalt: Wang and Zhou, 2006; Zhang and Ren, 2013), sulfide saturation mechanisms (Wang and Zhou, 2006; Song et al., 2008), and post-magmatic processes (Zhang et al., 2006) of the deposit, however, many of these aspects are still debated.

In this paper, we report new in situ trace-element analyses of sulfide minerals, new whole-rock PGE and S isotope data, and use this with previously published lithogeochemical, ore geochemical, and Nd-Os isotope data to evaluate the petrogenesis, metallogenesis, and modification of the Baimazhai Ni-Cu-(PGE) deposit.

## 3.3 Geological Background

The South China Block formed through the amalgamation between the Yangtze Craton and Cathaysia Block along the Jiangnan orogen, with the western portion of the South China Block being affected by the Tethyan orogen and Emeishan plume (Deng et al., 2017). The Emeishan Large Igneous Province (ELIP) in southwest China (mainly the Yunnan, Sichuan, and Guizhou Provinces) and Northern Vietnam comprises ~$3\times10^5$ $km^3$ of volcanic rocks and associated subvolcanic intrusions (e.g., Chung and Jahn, 1995; Xu et al., 2001). It is bound to the northwest by the Longmenshan thrust belt, to southwest by the Ailaoshan-Red River strike-slip fault, and to the southeast by the Mile-Shizong fault; the east boundary is located in the Duyun-Weng'an area, east of Guiyang (Li, et al., 2012b; Xu et al., 2013). The ELIP consists predominantly of tholeiite basalts, minor picritic, rhyolitic, and related pyroclastic rocks, mafic-ultramafic layered intrusions, sills, dikes, syenite, and alkalic and A-type granitic intrusions (Xu et al., 2001; Xiao et al., 2004). The mafic-ultramafic intrusions in the ELIP have been dated at 263-259 Ma using U-Pb single zircon Sensitive High Resolution Ion Microprobe (SHRIMP) methods (Zhou et al., 2002, 2008; He et al., 2007; Zhong et al., 2007). The ELIP contains numerous magmatic Ni-Cu-(PGE) deposits hosted by small mafic-ultramafic intrusions (e.g., Zhou et al., 2002; Song et al., 2008; Wang et al., 2018) and world-class Fe-Ti-V oxide deposits (e.g., Zhou et al., 2005; Bai et al., 2012; Liu et al.,

2015).

The Baimazhai Ni-Cu-(PGE) deposit is located in the northern portion of the wedge-shaped Jinping terrane between the Lvchun nappe and the Ailaoshan basement nappe (**Fig. 1**). The Jinping terrane is a triangular wedge, bounded to the southeast by the Tengtiaohe fault and to the northwest by the Ailaoshan fault (Zhang et al., 2017). The magmatic and metallogenic processes appear to have been controlled by a series of NW-NNW-trending faults (Zhang et al., 2017; Shen et al., 2019). The strata in the Jinping area mainly include Lower Ordovician clastic and Upper Silurian-Permian carbonate rocks (Zhang et al., 2014, 2017). Numerous ELIP basalts and later mafic dykes occur in this region (Guan et al., 2005; Li et al., 2008), which are considered to be related to the Cu-Ni-Au mineralization in this area (Yang et al., 2011). Wang et al. (2007) suggested that the unmineralized Permian flood basalts and mafic intrusions in the Jinping area crystallized from a high-Ti magma that was derived from a deep, enriched mantle source, and which subsequently underwent fractional crystallization without crustal contamination. In contrast, they suggested that the associated unmineralized low-Ti picritic basalts formed by melting of a source that was not enriched, and which subsequently experienced fractional crystallization with extensive crustal contamination. The Baimazhai Ni-Cu-(PGE) mineralized intrusions have been dated at 258.5 ± 3.5 Ma by U-Pb single zircon SHRIMP methods (Wang et al., 2006) and at 259 ± 20 Ma by Re-Os dating of massive sulfides (Sun et al., 2008), consistent with their formation from magmas that originated from the Emeishan mantle plume.

## 3.4 Geology of the Baimazhai deposit and sample descriptions

More than 10 mafic-ultramafic intrusions occur in the Baimazhai area, which are composed of gabbro, pyroxenite, and peridotite, and lesser diabase, syenite, and lamprophyre. Mineralization is hosted by three of the intrusions (Nos. 1, 2, and 3), which were emplaced discordantly into Ordovician slates, sandstones, and shales of the Baimazhai Formation (Wang et al., 2006; Zhang et al., 2006). All three contain disseminated Fe-Ni-Cu sulfides, but only the No. 2 and No. 3 intrusions contain massive sulfides, and only the No. 3 intrusion contains economically viable grades (up to 3.5% Ni, up to 2.3% Cu).

The No. 3 intrusion contains 50,000 tonnes of Ni in massive ores, with an average grade of 1.03 wt% Ni and 0.81 wt% Cu (Wang and Zhou, 2006), accounting for approximately 50% of the total Ni resource for the Baimazhai deposit (Zhang et al., 2006). It has a surface exposure of 0.1 $km^2$ and is ~530 m in

length, ~190 m in width, and up to 64 m thick (Wang et al., 2006). It is a lens-shaped, concentrically zoned mafic-ultramafic complex (folded saucer in plan: Lightfoot and Evans-Lamswood, 2015; planar saucer in cross section: **Fig. 2**) composed of (from exterior to interior) 2-55 m of gabbro, 2 to 9.5 m of pyroxenite, 0.5 to 13 m of olivine pyroxenite, and 9 m of peridotite, and contains an outer disseminated and inner massive Ni-Cu-(PGE) zone (Zhang, 2006; **Fig. 2**). The No. 3 intrusion is cut by a ~32 Ma lamprophyre (Guan et al., 2005; Li et al., 2008).

The marginal gabbro is fine-grained, with a hypidiomorphic-granular texture, and consists mainly of 45% (modal) albite and 40% clinopyroxene with accessory biotite, apatite, quartz, ilmenite, magnetite, and sulfides. The pyroxenite is fine-grained, with an idiomorphic to hypidiomorphic granular texture, and consists mainly of 30-85% tremolite, 10-20% talc, and 15-30% chlorite after orthopyroxene and clinopyroxene. The olivine pyroxenite is characterized by a hypidiomorphic-granular texture and consists mainly of 40-55% talc after orthopyroxene, 20-40% tremolite after clinopyroxene, and 10-30% serpentine pseudomorphs after olivine. The core peridotite has a cumulus-intercumulus texture and consists of 40-60% 0.2-1 mm serpentine-tremolite-talc pseudomorphs, 20-30% orthopyroxene, and 10-20% clinopyroxene in a matrix of tremolite-chlorite (Zhang et al., 2006; Wang et al., 2006). The Baimazhai Ni-Cu-(PGE) mineralized intrusion is not only zoned in terms of the abundance of silicate minerals, but also in terms of sulfide abundance, with massive sulfide occurring in the center, surrounded by net-textured to disseminated sulfides, and finally by an outer zone of unmineralized mafic rocks (Wang et al., 2006; Li et al., 2019).

The mineralized rocks are pervasively altered to an assemblage of amphibole ± chlorite ± quartz ± talc ± carbonate (Zhang et al., 2006). Based on the presence of these phases and the absence of any evidence of metamorphic olivine, enstatite, or anthophyllite, regional metamorphism can be interpreted to have been less than ~550$^{o}$C under low-moderate $XCO_2$ conditions (see Gole et al., 1987).

## 3.5 Methodology

The samples used in this study were collected from adit 755 in the No. 3 intrusion and include three samples of disseminated mineralization (**Figs. 3A-B**), three samples of net-textured mineralization (**Figs. 3C-D**), and three samples of massive mineralization (**Figs. 3E-F**). They were used not only to generate mineral chemical data but were also analyzed for whole-rock geochemistry and S isotopes to provide

links back to previous data.

Whole-rock S, Ni, Cu, and PGE contents were analyzed at the National Research Center of Geoanalysis in Beijing, China. Nickel and Cu were determined by inductively coupled plasma-mass spectrometry (ICP-MS) using a Thermo Elemental X-series ICP-MS. Sulfur was determined using a LECO carbon-sulfur analyzer; detection limits are 0.005% and the accuracies are estimated to be better than 10% RSD. Platinum-group elements were concentrated by NiS fire assay, co-precipitated with Te, and analyzed via ICP-MS analysis; precision and accuracy, as demonstrated by analyzing UMT-1 and WPR-1 reference materials, are better than 10% RSD.

The compositions of base-metal sulfides were analyzed at Laurentian University by energy dispersive X-ray emission spectrometry using a JEOL 6400 scanning electron microscope equipped with an Oxford X-Max detector. Operating conditions were 20 kv accelerating voltage and 1 nA beam current. Data reduction, which included a ZAF correction, was performed using INCA software. Instrument calibration was achieved by analyzing well-characterized reference materials, including Wakefield diopside (MgKα), albite (AlKα), chalcopyrite (FeKα), synthetic $CaTiO_3$ (TiKα), synthetic $Cr_2O_3$ (CrKα), synthetic $MnNb_2O_6$ (MnKα), Ni wire (NiKα), and Zn wire (ZnKα).

Trace elements were analyzed in situ by laser ablation inductively coupled plasma mass spectrometry (LA-ICP-MS) using a Resonetics RESOlution M50 ArF excimer 193 nm laser coupled to a Thermo-Fisher XSeries II ICP-MS in the Geochemical Fingerprinting laboratory, Harquail School of Earth Sciences at Laurentian University. For sulfides, the analyzed masses were $^{33}S$, $^{55}Mn$, $^{57}Fe$, $^{59}Co$, $^{60}Ni$, $^{61}Ni$, $^{63}Cu$, $^{65}Cu$, $^{68}Zn$, $^{75}As$, $^{77}Se$, $^{99}Ru$, $^{101}Ru$, $^{103}Rh$, $^{105}Pd$, $^{108}Pd$, $^{111}Cd$, $^{118}Sn$, $^{130}Te$, $^{121}Sb$, $^{185}Re$, $^{189}Os$, $^{193}Ir$, $^{195}Pt$, $^{197}Au$, $^{208}Pb$, and $^{209}Bi$. Sulfur, Fe, and Ni were used as the internal standard depending on the mineral. For oxides, the analyzed masses were $^{25}Mg$, $^{27}Al$, $^{29}Si$, $^{34}S$, $^{44}Ca$, $^{45}Sc$, $^{47}Ti$, $^{49}Ti$, $^{51}V$, $^{52}Cr$, $^{53}Cr$, $^{55}Mn$, $^{57}Fe$ (used as internal standard), $^{59}Co$, $^{60}Ni$, $^{63}Cu$, $^{65}Cu$, $^{66}Zn$, $^{69}Ga$, $^{71}Ga$, $^{74}Ge$ $^{75}As$, $^{89}Y$, $^{90}Zr$, $^{92}Zr$, $^{93}Nb$, $^{95}Mo$, $^{107}Ag$, $^{111}Cd$, $^{118}Sn$, $^{121}Sb$, $^{178}Hf$, $^{181}Ta$, $^{182}W$, and $^{208}Pb$. Dwell times were 10 ms on Fe, 5 ms on major elements, and 15 ms on trace elements. Five line-scan analyses were performed on each phase with a laser beam diameter of 19 μm. The laser energy was 60 mJ, the fluence 5 J/cm$^2$, and the repetition rate 6 Hz. Ablated material was transferred from the laser to the mass spectrometer with high purity He at 650 ml/min and $N_2$ at 6 ml/min via 3 m of tubing. The ICP-MS was operated at a forward power of

1450 W. The laser has a fast washout dual-volume cell enabling fast ablation without causing laser induced element fractionation (Chew et al., 2017). All instruments were tuned to maximize signal at low oxide rates of < 0.5 % $ThO^+/Th^+$ and a Th/U value higher than 0.9. Certified reference material Po725 pyrrhotite (from Memorial University) was used for $^{99}Ru$, $^{101}Ru$, $^{103}Rh$, $^{189}Os$, $^{193}Ir$, $^{195}Pt$, and $^{197}Au$, and internal standards were S (for violarite), Ni (for millerite) and Fe (pyrite, chalcopyrite) from average of analyses by EPMA. The GSD was used to calibrate all other elements. The NIST 610 glass was used to tune the instrument prior to analyzing the certified reference materials and unknowns. There are some elements that are present in both reference materials, which were used to check accuracy and precision, yielding similar results. For Ni (violarite) and Cu (chalcopyrite), yields were checked based on stoichiometry. To account for the interference of $^{40}Ar^{59}Co+$, $^{40}Ar^{61}Ni^+$, $^{40}Ar^{63}Cu^+$, and $^{40}Ar^{68}Zn^+$ on $^{99}Ru$, $^{101}Ru$, $^{103}Rh$, and $^{108}Pd$, respectively, a set of natural gersdorffite-cobaltite, millerite, chalcopyrite, and sphalerite samples with metal contents below detection limits were analyzed at the beginning and at the end of each session in order to monitor signals at the relevant masses. Element distribution maps were created on selected sulfide assemblages. All analyses were processed using Iolite 2.5 for Igor-Pro 6.34A. Each time-resolved spectra obtained was inspected to assess the presence of metalloid-rich nuggets, which appeared as isolated spikes emerging from uniform spectra and became more abundant with increasing metalloid concentration. To obtain the element concentration in sulfides, only the nugget-free parts of the signal were integrated. Limits of detection were calculated in Iolite using the method of (Pettke et al., 2012).

Analyses of $^{32}S$ and $^{34}S$ were done by mass spectrometry after conversion of sulfide to $SO_2$ using a Thermo Finnigan MAT 253 spectrometer at National Research Center of Geoanalysis in Beijing, China. The results are reported in standard notation as per mil (‰) deviations from the Vienna Canyon Diablo Troilite (V-CDT) standards. Accuracy of the sample data was assessed by measuring the S isotope compositions of sulfide standards GBW-4414 ($\delta^{34}S$ = -0.07‰) and GBW-4415 ($\delta^{34}S$ = 22.15‰). The analytical uncertainty was less than ±0.1‰.

Available whole-rock lithogeochemical and isotopic data were compiled from the literature and used alongside the newly acquired data to more robustly constrain genetic models. Whole-rock data for the Baimazhai intrusion are from Wang et al. (2006) and Wang and Zhou (2006). Most samples from Wang et al. (2006) are disseminated to net-textured mineralization, whereas most samples from Wang and Zhou

(2006) are massive mineralization. Additional S isotopic data are from Wang et al. (2018) and Zhang (2006). The analyzed sulfides included pentlandite, pyrrhotite, chalcopyrite, and magnetite from disseminated to massive ores. Strontium-Nd isotopic data are from Wang et al. (2006), and Re-Os isotopic data for the massive ores are from Sun et al. (2008).

## 3.6 Results

### 3.6.1 Mineralogy

The sulfides in the Baimazhai deposit include pentlandite, pyrrhotite, and chalcopyrite, with minor oxides, violarite, cobaltite, and galena (**Figs. 4A-I**). The base metal sulfides compositions are shown in Table S3-1. Primary sulfide minerals are more abundant in the massive sulfides (samples BMZ2-2, 3-1, 3-2), whereas secondary sulfide minerals occur in the modified disseminated and net-textured sulfides (samples BMZ 7-1, 7-2, 8-1, 8-2, D2-B1, D2-B2, D2-B3). The latter cross-cut or replace primary phases and are distinguished by different geochemistry (see below).

Primary pentlandite occurs as exsolution flames in pyrrhotite, and as pentlandite veinlets along pyrrhotite grain boundaries in massive sulfides (**Figs. 4A-E**), and as veinlets, or intergranular/subhedral grains in net-textured and disseminated sulfides.

Chalcopyrite occurs as coarse subhedral primary grains in massive sulfides and as subhedral or anhedral secondary grains in net-textured and disseminated sulfides.

All violarite occurs as anhedral secondary grains with pentlandite and chalcopyrite (**Fig. 4F**), apparently replacing pentlandite. Galena occurs as euhedral or subhedral grains in massive sulfides and net-textured sulfides.

Cobaltite is euhedral to subhedral and occurs with secondary chalcopyrite and secondary pyrrhotite (**Fig. 4H, I**).

Oxides in the Baimazhai intrusion include magnetite, chromite, and ilmenite (**Figs. 4A-B, F, G, H**). Magnetite occurs as euhedral (early magmatic) or subhedral (late magmatic) crystals and is particularly abundant in massive sulfides (**Fig. 4A-B**). Chromite is more euhedral and typically rimmed by secondary magnetite (**Fig. 4G**). Ilmenite occurs as primary euhedral and secondary subhedral and typically occurs

as elongate laths in disseminated and net-textured ores (**Fig. 4I**).

### 3.6.2 Whole-Rock Chemistry

Bulk-rock S, Ni, Cu, Co, and PGE contents of this study and by Wang et al. (2006) and Wang and Zhou (2006) are presented in **Table 1**. As expected, disseminated and net-textured sulfides have relatively low S contents (0.04-17.98 wt%, median: 1.02 wt%) and massive sulfides have much higher S contents (19.1-36.5 wt%, median: 30.7 wt%). Massive sulfides have higher Co-Ni-Cu and PGE contents (median: 252 ppb Pd+Pt+Rh+Ru+Ir) than disseminated and net-textured sulfides (median: 3.2 ppb Pd+Pt+Rh+Ru+Ir). For the disseminated and net-textured sulfides, all metals correlate positively with S (**Fig. 5**), indicating that the PGEs occur in or are associated with (exsolved from) sulfides. For the massive sulfides, Ni-Cu-Rh-Ru-Ir correlate positively with S, whereas Pd-Pt correlate negatively with S (**Fig. 5**), indicating that their concentrations are controlled by phases other than sulfides.

Th/Yb and Nb/Yb values by Wang et al. (2006) are presented in Figure 6. The host rocks at Baimazhai plot well above the mantle array at high Th/Yb and Nb/Yb, intermediate to deposits in CAOB and other deposits in ELIP (**Fig. 6**). Ni, Cu, and PGE contents of picrites and basalts in ELIP are from Li et al. (2012) and Wang et al. (2011) (Fig. 7A). Pricites in the Emeishan LIP are enriched in Cu and depleted in Ir-group PGE (Os, Ir, Ru; IPGE) > Pt-group PGE (Pt, Pd, Rh; PPGE), whereas low-Ti Type 2 (LT2) basalts are depleted in Ir-Ru > Ni > Rh-Pt > Cu-Pd, high-Ti (HT) basalts are depleted in Ru > Ni > Ir-Rh-Pt-Pd, and low-Ti Type 1 (LT1) basalts are depleted in Pd-Pt-Rh-Ru-Ir >> Ni >> Cu (**Fig. 7A**).

### 3.6.3 Metal Tenors

In order to compare samples with different sulfide contents, we recalculated the metal abundances to 100% sulfide (e.g., Naldrett, 1981; Barnes and Lightfoot, 2005). When normalized to primitive mantle disseminated and net-textured sulfides are enriched in Rh-Ru-Ni-Ir-Co relative to Pd-Cu-Pt. Massive sulfides have similar Pd-Cu-Pt patterns, but generally have lower abundances of Rh-Ru-Ni-Ir-Co **(Fig. 8**). Overall, the sulfides are enriched in Cu-Ni relative to Pd-Pt-Rh-Ru-Ir (**Fig. 7B**), similar to most Chinese Ni-Cu-(PGE) deposits (Lu et al., 2019).

### 3.6.4 Mineral Chemistry of base metal sulfides

The concentrations of most PGE in the base-metal sulfides (BMS) are lower than the limits of detection (LLD) of LA-ICP-MS, except for secondary cobaltite and violarite, and a few grains of pentlandite and

pyrrhotite (**Table 2**). The mineral compositions of base metal sulfides are given in detail in Table S3-2. Secondary cobaltite contains 0.025-152 ppm Pd, <LLD-8.4 ppm Pt, 0.0057-8.9 ppm Rh, and 0.073-2.8 ppm Ru. Secondary violarite contains <LLD-4.3 ppm Pd, <LLD-9 ppm Ru, <LLD-6.3 ppm Au, 0.04-248 ppm Ag, 0.68-64 ppm Sb, 8.1-1260 ppm Pb, and no detectable Pt. Primary pentlandite contains <LLD-9.9 ppm Pd, <LLD-1.9 ppm Ru, 0.54-71 ppm Ag, 0.28-104 ppm Pb, and 0.11-110 ppm Bi, whereas secondary pentlandite contains <LLD-0.9 ppm Pd, <LLD-0.81 ppm Ru, <LLD-59 ppm Ag, 1.6-480 ppm Pb, and 0.56-48 ppm Bi. Primary chalcopyrite contains 7-11.8 ppm Ag, 3.98-42.3 ppm Sn, 4.98-104 ppm Pb, and 2.91-54 ppm Bi, whereas secondary chalcopyrite contains 12.2-181 ppm Ag, <LLD-14.7 ppm Sn, 2.6-260 ppm Pb, and 0.79-40 ppm Bi. Primary pyrrhotite contains <LLD-4.3 ppm Ag, 0.77-123 ppm Pb, and 1.13-102 ppm Bi, whereas secondary pyrrhotite contains 0.13-9 ppm Ag, 0.3-67 ppm Pb, and 1.59-1100 ppm Bi. Primitive mantle normalized patterns for the different BMS of this study based on the LA-ICP-MS results are presented in **Figure 9.** Secondary pyrrhotite and chalcopyrite have higher Ni and Co contents than primary pyrrhotite and chalcopyrite (**Fig. 10**).

### 3.6.5 Mineral Chemistry of magnetite

Primary magnetite contains 3,050-22,200 ppm Ti, 1,960-8,990 ppm V, and 30,600-118,600 ppm Cr. Evolved magnetite contains 109-387 ppm Ti, 35.1-188 ppm V, and 51.1-2,260 ppm Cr. Secondary magnetite contains <LLD-123 ppm Ti, 2.9-112 ppm V, and <LLD-21.2 ppm Cr (**Table 3**).

### 3.6.6 S Isotopes

The S isotope compositions of Ni-Cu ores and BMS from the Baimazhai deposit from this study as well as from Zhang (2006) and Wang et al. (2018) are listed in **Table 4**. Bulk ores range from 5.8 to 6.8 ‰ $\delta^{34}S$ and sulfide separates range from 6.0 to 8.6 ‰ $\delta^{34}S$. All have $\delta^{34}S$ values that are significantly greater than MORB mantle (0.1 ± 0.5‰ $\delta^{34}S$: Sakai et al., 1984; −0.91 ± 0.50‰: Labidi et al., 2012; -0.5 ± 1‰: Labidi et al. 2013) or subduction-modified mantle (-2.5 ± 0.3‰: Li et al. 2020). The $\delta^{34}S$ values of sedimentary sulfide and sandstone and are 10‰ and 6.3‰, respectively.

### 3.6.7 Nd-Os Isotopes

The Nd and Os compositions of Ni-Cu-PGE deposits in ELIP by Wang et al. (2006), Zhou et al. (2008), Sun et al. (2008), Tao et al. (2010a, 2010b), and Han (2017) are plotted in **Figure 11**. Baimazhai and most other Ni-Cu-PGE deposits in ELIP (see review by Lu et al., 2019) have high γOs and intermediate

εNd, and plot on a mixing trend between magmas derived from pyroxenitic mantle and continental crust. They are distinctly different from subcontinental lithospheric mantle (SCLM), which is characterized by lower εNd and γOs, and from peridotitic mantle (including ELIP picrite and high-Ti basalt), which is characterized by lower γOs, reflecting the more depleted nature of both reservoirs.

## 3.7 Discussion

### 3.7.1 Magma source and partial melting

Emeishan LIP basalts have been subdivided into low-Ti and high-Ti varieties (Xu et al., 2001; Xiao et al., 2004), but the relationship between magmatic sulfide deposits and their associated basalt types is still debated. Some workers suggest that magmatic sulfide deposits are derived from low-Ti basaltic magmas (e.g., Limahe, Zhubu, Jinbaoshan, Baimazhai deposits: Zhou et al., 2008; Wang et al., 2012, 2018), whereas others suggest that they are derived from high-Ti basaltic magmas (e.g., Yangliuping and Limahe: Song et al., 2005; Tao et al., 2008). The Baimazhai Ni-Cu-(PGE) deposit is believed to have formed from a low-Ti basaltic magma (Wang et al., 2006, 2018; Wang and Zhou, 2006; Zhang and Ren, 2013).

The sources of the magmas that formed the host rocks to the deposits can be further constrained by using ratios of lithophile elements that are highly to moderately incompatible (HILE: Th-Nb-Ta-LREE, MILE: MREE-Zr-Hf-Y-HREE) during mantle melting (Pearce, 2008). Although olivine and pyroxene contain only small abundances of these elements, they typically contain more MILE than HILE, so fractionation of these minerals may increase HILE/MILE ratios, whereas accumulation may decrease HILE/MILE ratios (e.g., Arndt and Lesher, 1992; Pearce, 2008). The host rocks at Baimazhai have high Th/Yb and intermediate Nb/Yb (**Fig. 6**). Such a signature may be produced by: 1) assimilation-fractional crystallization (AFC) of a magma derived from a N-MORB type source that was subsequently contaminated by continental crust, 2) low-degree partial melting of an N-MORB type source modified by subduction-related fluids, and/or 3) moderate-degree partial melting of an E-MORB type source modified by subduction-related fluids (see Pearce, 2008). The host magmas at Jinbaoshan, Yangliuping, Zhubu, and Limahe have very high Nb/Yb, and appear to be derived from a slightly more enriched magma (between E-MORB and OIB), compared to Baimazhai. The Baimazhai deposit is different from these deposits and is suggested to have formed from a magma derived from a subduction-modified

enriched (E-MORB-like) mantle (Lu et al., 2019). The Baimazhai samples have similar Nb/Yb ratios and slightly higher Th/Yb ratios as the LT1 (low-Ti) basalts of Xiao et al. (2004), and so it is likely that the Baimazhai magma was more evolved compared to LT1, but which underwent greater degrees of crustal contamination (**Fig. 6**).

Chalcophile elements provide critical constraints on the generation and evolution of mafic magmas (e.g., Barnes et al., 1985; Keays, 1995; Crocket and Paul, 2004; Mungall and Brenan, 2014; Barnes et al. 2015). LT1 basalts are enriched in Cu-Ni-Co relative to PGE with chalcophile element patterns similar to sulfide-poor gabbros in the Baimazhai intrusion (**Fig. 7A**), which has previously been interpreted to reflect removal of sulfides in a deeper staging chamber (Wang et al., 2011). However, because sulfide/melt partition coefficients are PGE >>> Cu > Ni > Co, sulfide removal should deplete the magma in PGE >>> Cu > Ni > Co, which is not what is observed (**Fig. 7A**). A better explanation for the observed enrichment in Cu-Ni-Co relative to PGE is derivation from subduction metasomatized mantle (Tonnelier, 2010; Lu et al., 2019). MORB is depleted in PGE >>> Cu > Ni > Co (e.g., Crocket, 2002; Arndt et al., 2005) and metasomatism converts olivine (which retains Ni-Co during melting) to pyroxene (which does not retain nearly as much Ni-Co). Thus, the abundances of Ni-Co in magmas derived from pyroxenitic mantle will be higher at similar degrees of partial melting than magmas derived from unmetasomatized peridotitic mantle (e.g., Sobolev et al., 2005). The source of the higher Cu is not completely clear, as MORB and arc basalts contain similar amounts of Cu (e.g., Richards, 2015), but the pervasiveness of the enriched Cu-Ni-Co and depleted PGE signature in most Chinese Ni-Cu-(PGE) deposits suggest that it is characteristic of the complex multidirectional subduction history of the North China Craton (see discussion by Lu et al., 2019). Baimazhai sulfides are compositionally similar, but more enriched in Cu-Ni-Co compared to sulfides that interacted with a LT1 magma (**Fig. 7B**), so it is likely that the parental magma of Baimazhai originated from a LT1-like source that interacted with pyroxenitic mantle (**Fig. 11**).

### 3.7.2 Source of S

The undepleted PGE signatures and negative pressure dependence on the solubility of S in most mafic-ultramafic magmas more magnesian than MORB indicate that they are unlikely to have been saturated in sulfide (e.g., Keays, 1982; Wendlandt, 1982; see also Lesher and Groves, 1986; Naldrett and Barnes, 1986; Arndt et al., 2005). For this reason, incorporation of crustal S is normally considered to be an essential process in generating magmatic Ni-Cu-(PGE) deposits (e.g., Lesher et al., 1984, 2001; Lesher

and Campbell, 1993; Naldrett, 2004; Arndt et al., 2005; Barnes and Lightfoot, 2005; Keays and Lightfoot, 2010; Ripley and Li, 2013; Barnes et al., 2016; Lesher, 2017, 2019). This is why most Ni-Cu-PGE deposits have $\delta^{34}S$ values that are different from mantle and similar or closer to their wall rocks (see reviews by Lesher, 2017; Lu et al., 2019).

Lesher and Burnham (2001) noted that it is possible for crustal sulfide xenomelts to be shifted toward mantle S isotopic compositions if the effective magma:sulfide mass ratios (R factors) are high enough. The $\delta^{34}S$ values of most Baimazhai sulfides vary between 6‰ and 8‰. If we assume that the initial $\delta^{34}S$ and S content of the parental magma were 0‰ (mantle-like) and 0.05 wt% (conservative values), respectively, and that the initial $\delta^{34}S$ and S content of the sulfide xenomelt (sedimentary sulfide) were 10‰ (analyzed in this study) and 1.5% (S content in the wall rock), the magma:sulfide mass ratios (R factors) required to produce the observed variations in Baimazhai sulfides are 100-1000 **(Fig. 12**).

### 3.7.3 Magma:sulfide ratio

The final abundance of metal i in a magmatic Ni-Cu-PGE sulfide melt ($Y_i^f$) is controlled by the abundance of metal i in the initial magma ($X_i^o$), the sulfide liquid/silicate melt partitition coefficient ($D_i^{Sul/Sil}$), the magma:sulfide mass ratio (R: Campbell and Naldrett, 1979), and the abundance of i (if any) in the crustal sulfide xenomelt ($Y_i^o$: Lesher and Burnham, 2001):

$$Y_i^f = (X_i^o R + Y_i^o) D_i^{Sul/Sil} / (R+D_i^{Sul/Sil}) \quad [4]$$

$D_i^{Sul/Sil}$ values vary with composition, temperature, $fO_2$, and $fS_2$ (see reviews by Naldrett, 2004; Barnes and Lightfoot, 2005; Barnes and Ripley, 2016), but in basaltic magmas they are of the order of 300-1000 for Ni, 900-1400 for Cu, and $10^4$-$10^6$ for Pd, Pt, Rh, Ru and Ir (Francis, 1990; Peach et al., 1990; Fleet et al.,1991; Peach and Mathez, 1996; Sattari et al., 2002; Mungall and Brenan, 2014).

The compositions of the ores in the Baimazhai deposit are best reproduced by interacting metal-poor, crustally-derived sulfides with an LT1-type Ni-Cu-Co-enriched, PGE-depleted basalt magma containing ~200 ppm Ni, ~100 ppm Cu, 0.4 ppb Pd, 0.2 ppb Pt, 0.005 ppb Rh, 0.02 ppb Ru, and 0.01 ppb Ir at magma:sulfide mass ratios of 500. These concentations are within the range of PGE contents of LT1

basalts (0.7 ppb Pd, 0.2 ppb Pt, 0.015 ppb Rh, 0.025 ppb Ru, and 0.01 ppb Ir), but LT1 basalts have much lower Ni (60 ppm) and Cu (36 ppm) contents (Wang et al., 2011).

### 3.7.4 Ore localization

The mineralization in the Baimazhai Ni-Cu-(PGE) deposit occurs in the central part of the intrusion. The inward concentric zonation from gabbro through pyroxenite and barren peridotite to mineralized peridotite has been interpreted previously to represent flowage differentiation (Wang et al., 2006; Wang and Zhou, 2006). Such a process, however, cannot explain the systematic inward change in cumulus mineralogy (Plag-Cpx → Cpx-Opx → Opx-Ol-Chr → Ol-Chr) and, therefore, magma composition (basaltic to picritic). An interpretation that is more consistent with the change in cumulus mineralogy is that the intrusion crystallized inward during emplacement, and that magma flux, temperature, and Mg content increased with time.

The central concentration of sulfides in the Baimazhai deposit has also been interpreted to have been produced by flowage differentiation (Wang and Zhou, 2006). Small (<2 cm) droplets of dense (~4.2 g $cm^{-3}$: Kress, 2008) molten sulfide melt can be transported at reasonable magma flow rates (Lesher and Groves, 1986; de Bremond d'Ars et al., 2001; Robertson et al., 2015), but flowage differentiation does not explain the observed variations in silicate mineralogy. It is possible that small sulfide melt droplets were carried in only the highest flux phase of the system and accumulated with olivine and coalesced during flow-through to form the observed massive-net-disseminated zonation in the core of the intrusion. This would not only be the phase of the intrusion that would have the high flux needed to transport sulfides, but also the high flux needed to incorporate sulfides from the crustal source.

The absence of any country-rock xenoliths, which are common in basaltic Ni-Cu-(PGE) systems (see review by Lesher, 2017), suggests that the sulfides were selectively melted out of the crustal S source, which is unlikely for reasons discussed by Robertson et al. (2015), or that the silicate components were completely assimilated under the inferred conditions of sustained magma flow and channelization, which is consistent with a flow-through emplacement and crystallization model for the intrusion.

### 3.7.5 Crystallization of sulfide liquid

The crystallization of sulfide liquid has been studied experimentally by many workers (Naldrett, 1969, 2004; Mungall, 2005, 2007; Barnes and Ripley, 2016). The first phase to crystallize at ~1190°C (lower

with increasing Ni-Cu) is monosulfide solid solution (MSS) or magnetite, depending on $fO_2$. Fe-Co-IPGE and Ni (at higher temperatures) preferentially partition more strongly into MSS, whereas Ni (at lower temperatures) Cu-PPGE-Au-Ag-Pb-Zn-Cd and Te-As-Bi-Sb-Sn (TABSS) preferentially partition into residual sulfide melt (**Fig. 13A-B**). At temperatures of 900-800°C, intermediate solid solution (ISS) crystallizes from residual melt (**Fig. 13C**) and at temperatures of 650-250°C, pentlandite and pyrrhotite exsolve from MSS, and chalcopyrite exsolves from ISS (**Fig. 13D**, see below).

Sulfide crystallization at Baimazhai can tracked using the abundances of minor and trace elements in magnetite (Dare et al et al., 2012, 2014; Boutroy et al., 2014). Chromium-Ga-Ge-Mg-Mn-V-W partition moderately strongly into magnetite and, therefore, behave compatibly during the crystallization of magnetite from the sulfide liquid. As a consequence, early-formed magnetite in MSS will be enriched in these elements, particularly Cr-Ti-V, and during sulfide fractionation lithophile elements in both sulfide melt and magnetite will decrease (Dare et al., 2012). Type I (early magmatic), Type II (late magmatic), and Type III (secondary) magnetite have been recognized in massive and net-textured ores of the Baimazhai deposit (**Fig. 14**).

The enrichments of $Pd_{100}$, $Cu_{100}$ and $Pt_{100}$, relative to $Ru_{100}$, $Ni_{100}$, $Ir_{100}$, $Co_{100}$ in most massive ores (**Fig. 8**) are consistent with massive ores containing excess residual sulfide liquid. The composition of the residual sulfide melt can be modeled as fractional crystallization (Rayleigh, 1896):

$$Y_i^{Liq} = Y_i^o \, f^{(DiMSS/Liq-1)} \qquad [1]$$

The observed variations in $Ir_{100}$ and $Pd_{100}$ (metals in 100% sulfide) are consistent with 40-60% fractional crystallization of MSS to form Ni-Co-IPGE-rich massive ores and Cu-PPGE-Au-rich residual sulfide liquids (**Fig. 15**). The broadly positive correlation between $Ir_{100}$ and $Pd_{100}$ in disseminated and net-textured ores (**Fig. 15**) indicates that the remainder of the variations are mainly controlled by magma:sulfide ratio (R factors). The calculated R factors are consistent with previous calculations based on the S isotopes.

### 3.7.6 Late-Magmatic Modification

Experimental studies have shown that late-magmatic modification of ores with bulk compositions similar to Baimazhai involves exsolution of pentlandite and minor chalcopyrite from MSS and inversion of ISS to chalcopyrite. Exsolution of pentlandite and chalcopyrite are evident in the textures of the mineralization, particularly massive sulfides (**Figs. 3-4**), but inversion of ISS to chalcopyrite can only be inferred.

Laser ablation ICP-MS results indicate that the PGE contents of most primary sulfides (pyrrhotite, pentlandite, and chalcopyrite) in the Baimazhai intrusion are lower than detection limits, except for Pd, Rh, and Ru, which are detected in few pentlandite grains. This is because IPGEs enter and remain in MSS (Naldrett, 1967; Craig, 1973) from which pentlandite exsolves. The IPGE, therefore, remain in pentlandite, and Pd will also enter into MSS as a result of diffusion from the residual sulfide liquid or peritectic reaction (e.g., Dare et al., 2010; Mansur, 2019). In the Baimazhai deposit, the PGE will, therefore, be enriched in pentlandite (**Fig. 13D**).

Cobaltite is a common accessory phase in magmatic Ni-Cu-PGE deposits (e.g., Yangliuping: Song et al., 2004; Sudbury: Dare et al., 2010; Piaohechuan: Wei et al., 2015; Sarah's Find: Le Vaillant et al., 2016). The compositions of cobaltite in Baimazhai sulfides, projected into the ternary phase diagram of the sulfarsenide solid-solution series, suggests that cobaltite crystallized at late-magmatic temperatures of 500-550°C, which is slightly lower than the crystallization temperature for cobaltite in some deposits (~600°C at Sudbury, Piaohechuan, Yangliuping) but similar to the temperature of crystallization in other deposits (e.g., Sarah's Find) (**Fig. 16**). As in the Yangliuping deposit, the cobaltite at Baimazhai also formed prior to exsolution of pentlandite from MSS and inherited Rh and Ru from MSS (**Fig. 13D**). MSS itself does not contain significant amounts of Pd (e.g., Mackovicky, 2002; Dare et al., 2010, 2011), so it is likely that Pd was derived from the surrounding sulfides. All of the cobaltite analyses have variably high concentrations of Cu-Ni, implying that minor amounts of chalcopyrite and pentlandite may have been incorporated into some of the analyses of such fine grains (**Fig. 4H**).

### 3.7.7 Hydrothermal alteration

Most magmatic sulfide deposits have experienced some degree of post-magmatic mineral-chemical modification, which may be deuteric, magmatic-hydrothermal, metamorphic-hydrothermal, or supergene.

Although Cu, Au, Pt, Pd, Pb, and TABSS are commonly mobile to varying degrees, Ni-Co-IPGE appear to be less immobile except under specific circumstances (e.g., As-rich fluids or oxidized and acidic conditions: see e.g., Lesher and Keays, 1984; Hanley, 2005; Barnes and Liu, 2012; Le Vaillant et al., 2016). For example, Ni and Co may be released from olivine during serpentinization but are typically incorporated in sulfides or oxides and are only rarely lost (e.g., Eckstrand, 1975; Donaldson, 1981; Barnes et al., 2011; Pirajno and González-Álvarez, 2013; Lu et al., 2020). Nearly all of the olivine in the Baimazhai intrusion has been altered to serpentine. As a consequence, secondary pyrrhotite and chalcopyrite have higher Ni and Co contents than primary pyrrhotite and chalcopyrite, respectively (**Fig. 10**).

The similar Pd ranges in secondary violarite (0.53-4.3 ppm) and primary pentlandite (0.61-9.9 ppm) indicate that Pd has been mobile only on small scales during alteration. Palladium is considered to be the most mobile of the PGEs and can be transported as bisulfide complexes in acidic-neutral solutions under reduced to moderately oxidizing conditions at 300°C (e.g., Barnes and Liu, 2012). Thus, there is little evidence for significant mobility of Pd at Baimazhai.

In contrast, the higher Sb, Au, and Pb contents of secondary pentlandite compared to primary pentlandite, and the higher Ag, Sb, Au, and Pb contents of secondary chalcopyrite compared to primary chalcopyrite indicate that those elements were added during alteration (**Fig. 9**). The lower Sn contents of secondary violarite, chalcopyrite, and pentlandite indicate that it was lost during alteration (**Fig. 9**).

The sources of Ag, Sb, Au, and Pb and the sink for Sn are not well constrained, but the Cu-Au-Pb-Zn-Ag-Sn-W mineralization (e.g., magmatic-hydrothermal Au-Cu-Mo-Sn-W deposits, porphyry-skarn Au-Cu-Mo deposits, volcanic massive sulfide + Mississippi Valley-type + magmatic-hydrothermal Pb-Zn-Cu-Ag deposits, and orogenic Au deposits in the region) (Zhang et al., 2014; He et al., 2015, 2016; Deng and Wang, 2016; Yang et al., 2016, 2017; Zhang et al., 2018; Deng et al., 2019) provide abundant possibilities.

## 3.8 Conclusions

1. Like many other magmatic sulfide deposits in the ELIP, the magma that formed the Baimazhai intrusion appears to have been a low-Ti basalt derived from a pyroxenitic mantle source, most likely

modified by slab-derived fluids during the Late Permian. It was not derived from SCLM or peridotitic mantle (including ELIP picrate or HT basalt sources).

2. The parental magma of the Baimazhai intrusion appears to have contained of the order of 200 ppm Ni, 100 ppm Cu, 0.4 ppb Pd, 0.2 ppb Pt, 0.005 ppb Rh, 0.02 ppb Ru, and 0.01 ppb Ir.
3. The Baimazhai intrusion appears to represent a tectonically modified (folded) channelized sill that crystallized inward with increasing flow rates to produce (from periphery to core) gabbro, pyroxenite, olivine pyroxenite, barren peridotite, and mineralized peridotite containing disseminated to massive sulfides.
4. The magma melted S-bearing upper continental crustal rocks to form sulfide xenomelts that reacted with the magma at moderate R factors (100-1000) to form the precursors to the observed Ni-Cu-(PGE) mineralization.
5. Post-magmatic metamorphic-hydrothermal alteration modified primary pentlandite, pyrrhotite, and chalcopyrite, forming secondary pentlandite, pyrrhotite, violarite, and chalcopyrite. Secondary sulfides inherited PGEs from primary sulfides, are enriched in Ni-Co and Ag-Sb-Au-Pb and depleted in Sn.
6. The Baimazhai deposit demonstrates the exploration potential for the Ailaoshan orogenic belt to host arc-related magmatic sulfide deposits.

## Acknowledgements

This paper is dedicated to the memory of A.J. Naldrett, who was a mentor to CML and an inspiration to two generations of magmatic ore deposit geologists in China and worldwide. This research has been supported by the National Natural Science Foundation of China (No. 42002110), the National Key Technologies R&D Program (2019YFA0708603), the National Key Basic Research Development Program of China (No. 2015CB452606, 2009CB421008), the Geological investigation work project of China Geological Survey (No. 12120114013501, DD20190439), 111 Project of the Ministry of Education of China (Grant No. B07011), a Natural Sciences and Engineering Council of Canada Discovery grant to CML, and a SEG Canada Foundation grant and China Scholarship Council award to YL. This is Mineral Exploration Research Centre publication MERC-2021-04. Constructive reviews from Sarah-

Jane Barnes, Malte Junge, and an anonymous reviewer are greatly appreciated.

## References

Arndt, N.T., Lesher, C.M. 1992, Fractionation of REEs by olivine and the origin of Kambalda komatiites, Western Australia: *Geochimica et Cosmochimica Acta*, v. 56, p. 4191-4204.

Arndt, N., Lesher, C.M., Czamanske, G.K., 2005, Mantle-derived magmas and magmatic Ni-Cu-(PGE) deposits: *Economic Geology 100th Anniversary Volume*, 5-24.

Bai, Z.J., Zhong, H., Naldrett, A.J., Zhu, W.G., Xu, G.W., 2012, Whole-rock and mineral composition constraints on the genesis of the giant Hongge Fe-Ti-V oxide deposit in the Emeishan Large Igneous Province, Southwest China: *ECON GEOL* 07, 507-524.

Barnes S.-J., Cox R.A., Zientek M.L., 2006, Platinum-group element, gold, silver and base metal distribution in compositionally zoned sulfide droplets from the Medvezky Creek Mine, Noril'sk, Russia: *Contributions to Mineralogy and Petrology* 152, 187-200.

Barnes, S-J., 2016, Chalcophile elements. In: White, W.M., (Ed.) Encyclopedia of Geochemistry: A Comprehensive Reference Source on the Chemistry of the Earth, *Part of the Series Encyclopedia of Earth Sciences Series*, 1-5.

Barnes, S. J., Mungall, J. E., Maier, W. D., 2015, Platinum group elements in mantle melts and mantle samples. *Lithos* 232, 395-417.

Barnes, S.-J., Lightfoot, P.C., 2005, Formation of magmatic nickel sulfide ore deposits and processes affecting their copper and platinum group element contents: Economic geology, *Economic Geology 100th Anniversary Volume* 34, 79-214.

Barnes, S.-J., Naldrett, A.J., Gorton, M.P, 1985, The origin of the fractionation of platinum-group elements in terrestrial magmas: *Chemical geology* 53, 303-323.

Barnes, S.-J., Ripley, E.M., 2016, Highly siderophile and strongly chalcophile elements in magmatic ore deposits: *Reviews in Mineralogy and Geochemistry* 81, 25-774.

Barnes, S.J., Godel, B.M., Locmelis, M., Fiorentini, M.L., Ryan, C.G., 2011, Extremely Ni-rich Fe–Ni sulfide assemblages in komatiitic dunite at Betheno, Western Australia: results from synchrotron X-ray fluorescence mapping: *Australian Journal of Earth Sciences* 58, 691-709.

Barnes, S.J., Liu, W., 2012, Pt and Pd mobility in hydrothermal fluids: Evidence from komatiites and from thermodynamic modelling: *Ore Geology Reviews* 44, 49-58.

Begg, G.C., Hronsky, J.A., Arndt, N.T., Griffin, W.L., O'Reilly, S.Y., Hayward, N., 2010, Lithospheric, cratonic, and geodynamic setting of Ni-Cu-PGE sulfide deposits: *ECON GEOL* 105, 1057-1070.

Boutroy, E., Dare, S.A., Beaudoin, G., Barnes, S.-J., Lightfoot, P.C., 2014, Magnetite composition in Ni-Cu-PGE deposits worldwide: application to mineral exploration: *Journal of Geochemical Exploration* 145, 64-81.

Campbell, I.,H., Naldrett, A.J., 1979, The influence of silicate:sulfide ratios on the geochemistry of magmatic sulfides: *ECON GEOL* 74, 1503-1506.

Cassidy, K.F., Champion, D.C., Krapez, B., Barley, M.E., Brown, S.J. A., Blewett, R.S., Groenewald, P.B., Tyler, I.M., 2006, A revised geological framework for the Yilgarn Craton, Western Australia: *Geological Survey of Western Australia*, Record, 1-8.

Champion, D.C., Cassidy, K.F., 2007, An overview of the Yilgarn Craton and its crustal evolution: *Geoscience Australia Record* 14, 8-13.

Chung, S.L., Jahn, B.M., 1995, Plume-lithosphere interaction in generation of the Emeishan flood basalts at the Permian-Triassic boundary: *Geology* 23, 889-892.

Craig, J.R., 1973, Pyrite-pentlandite assemblages and other low temperature relations in the Fe-Ni-S system: *American Journal of Science* 273, 496-510.

Crocket, J.H., 2002, Platinum-group elements in basalts from Maui, Hawai'i: Low abundances in Alkali basalts: *Canadian Mineralogist* 40, 595-609.

Crocket, J.H., Paul, D.K., 2004, Platinum-group elements in Deccan mafic rocks: a comparison of suites

differentiated by Ir content: *Chemical Geology* 208, 273–291.

Dare, S. A., Barnes, S. J., Prichard, H. M., Fisher, P. C., 2011, Chalcophile and platinum-group element (PGE) concentrations in the sulfide minerals from the McCreedy East deposit, Sudbury, Canada, and the origin of PGE in pyrite. *Mineralium Deposita*, 46(4), 381-407.

Dare, S.A.S., Barnes, S.-J., Beaudoin, G., 2012, Variation in trace element content of magnetite crystallized from a fractionating sulfide liquid, Sudbury, Canada: Implications for provenance discrimination: *Geochimica et Cosmochimica Acta* 88, 27-50.

Dare, S.A.S., Barnes, S.-J., Beaudoin, G., Méric, J., Boutroy, E., Potvin-Doucet, C., 2014, Trace elements in magnetite as petrogenetic indicators: *Mineralium Deposita* 49, 785-796.

Dare, S.A.S., Barnes, S.-J., Prichard, H.M., Fisher, P.C., 2010, The timing and formation of platinum-group minerals from the Creighton Ni-Cu-platinum-group element sulfide deposit, Sudbury, Canada: Early crystallization of PGE-rich sulfarsenides: *ECON GEOL* 105, 1071-1096.

de Bremond d'Ars, J., Arndt, N.T., Hallot, E., 2001, Analog experimental insights into the formation of magmatic sulfide deposits: *Earth and Planetary Science Letters* 186, 371-381.

Deng, J., Wang, Q., Li, G., Hou, Z., Jiang, C., Danyushevsky, L., 2015a, Geology and genesis of the giant Beiya porphyry–skarn gold deposit, northwestern Yangtze Block, China. *Ore Geology Reviews* 70, 457-485.

Deng, J., Wang, Q., Li, G., Zhao, Y., 2015b, Structural control and genesis of the Oligocene Zhenyuan orogenic gold deposit, SW China. *Ore Geology Reviews* 65, 42-54.

Deng, J., Wang, C., Bagas, L., Selvaraja, V., Jeon, H., Wu, B., Yang, L., 2017, Insights into ore genesis of the Jinding Zn–Pb deposit, Yunnan Province, China: Evidence from Zn and in-situ S isotopes. *Ore Geology Reviews* 90, 943-957.

Deng, J., Wang, Q.F., 2016, Gold mineralization in China: Metallogenic provinces, deposit types and tectonic framework. *Gondwana Research* 36, 219-274.

Deng, J., Wang, Q.F., Li, G.J., 2017, Tectonic evolution, superimposed orogeny, and composite metallogenic system in China: *Gondwana Research* 50, 216-266.

Deng, J., Wang, Q.F., Li, G.J., Li, C., Wang, C.M., 2014a, Tethys tectonic evolution and its bearing on the distribution of important mineral deposits in the Sanjiang region, SW China: *Gondwana Research* 26, 419-437.

Deng, J., Wang, Q.F., Li, G.J., Santosh, M., 2014b, Cenozoic tectono-magmatic and metallogenic processes in the Sanjiang region, southwestern China: *Earth Science Review* 138, 268-299.

Donaldson, M.J., 1981, Redistribution of ore elements during serpentinization and talc-carbonate alteration of some Archean dunites, Western Australia: *ECON GEOL* 76, 1698-1713.

Eckstrand, O.R., 1975, The Dumont serpentinite: a model for control of nickeliferous opaque mineral assemblages by alteration reactions in ultramafic rocks: *ECON GEOL* 70, 183-201.

Francis, R.D., 1990, Sulfide globules in mid-ocean ridge basalts (MORB), and the effect of oxygen abundance in Fe-S-O liquids on the ability of those liquids to partition metals from MORB and komatiite magmas: *Chemical Geology* 85, 199-213.

Fleet, M.E., Stone, W.E., and Crocket, J.H., 1991, Partitioning of palladium, iridium and platinum between sulfide liquid and basalt melt: Effects of melt composition, concentration and oxygen fugacity: *Geochimica et Cosmochimica Acta* 55, 2545−2554.

Grinenko, L.I., 1985, Sources of sulfur of the nickeliferous and barren gabbro-dolerite intrusions of the northwest Siberian platform: *International Geology Review* 27, 695-708.

Guan, T., Huang, Z.L., Xu, C., Zhang, Z.L., Yan, Z.F., Shen, B.J., 2005, REE geochemistry of lamprophyres in Baimazhai nickel deposit, Yunnan Province, China: implication for the mantle source region: *Chinese Journal of Geochemistry* 24, 273-279.

Gole, M. J., Barnes, S. J., Hill, R. E., 1987, The role of fluids in the metamorphism of komatiites, Agnew nickel deposit, Western Australia. *Contributions to Mineralogy and Petrology* 96(2), 151-162.

Han M., M, 2017, Mineralization study of Yangliuping Cu-Ni sulphide deposit in Sichuan: Master thesis, Beijing, China, *China University of Geosciences (Beijing)*, 1-62.

Hanley, J.J., 2005, The aqueous geochemistry of the platinum-group elements (PGE) in surficial, low-T hydrothermal and high-T magmatic-hydrothermal environments, *in* Mungall, J.E., ed., *Exploration for Platinum-Group Element deposits: Mineralogical Association of Canada, Short Course Series* 35, 35-56.

He, B., Xu, Y.G., Huang, X.L., Luo, Z.Y., Shi, Y.R., Yang, Q.J., Yu, S.Y., 2007, Age and duration of the Emeishan flood volcanism, SW China: geochemistry and SHRIMP zircon U-Pb dating of silicic ignimbrites, post-volcanic Xuanwei Formation and clay tuff at the Chaotian section: *Earth and Planetary Science Letters* 255, 306-323.

He, W.Y., Mo, X.X., He, Z.H., White, N.C., Chen, J.B., Yang, K.H., Wang, R., Yu, X.H., Dong, G.C., Huang, X.F., 2015, The geology and mineralogy of the Beiya skarn gold deposit in Yunnan, southwest China: *ECON GEOL* 110, 1625-1641.

He, W.Y., Yang, L.Q., Brugger, J., McCuaig, T.C., Lu, Y.J., Bao, X.S., Gao, X.Q., Lu, Y.G., Xing, Y.L., 2016, Hydrothermal evolution and ore genesis of the Beiya giant Au polymetallic deposit, western Yunnan, China: Evidence from fluid inclusions and H-O-S-Pb isotopes: *Ore Geology Reviews* 90, 847-862.

Holwell, D.A., Mcdonald, I., 2010, A Review of the Behaviour of Platinum Group Elements within Natural Magmatic Sulfide Ore Systems: *Platinum Metals Review* 54, 26-36.

Keays, R.R., 1982, Palladium and iridium in komatiites and associated rocks: Application to petrogenetic problems. in Komatiites, N.T. Arndt and E.G. Nisbet, Eds.: *George Allen and Unwin, London*, p. 435-457.

Keays, R.R., 1995, The role of komatiitic and picritic magmatism and S-saturation in the formation of the ore deposits, *Lithos* 34, 1-18.

Keays, R.R., Lightfoot, P.C., 2010, Crustal sulfur is required to form magmatic Ni–Cu sulfide deposits: evidence from chalcophile element signatures of Siberian and Deccan Trap basalts: *Mineralium*

*Deposita* 45, 241-257.

Kerrich, R., Goldfarb, R.J., and Richards, J.P., 2005, Metallogenic provinces in an evolving geodynamic framework: *Economic Geology 100th Anniversary Volume,* 1097–1136.

Klemm, D.D., 1965, Synthesen und Analysen in den Dreiecksdiagrammen FeAsS-CoAsS-NiAsS und $FeS_2$-$CoS_2$-$NiS_2$: *Neus Jahrbuch fuer Mineralogie Abhandlungen* 103, 205-255.

Kress, V., Greene, L.E., Ortiz, M.D., Mioduszewski, L. 2008, Thermochemistry of sulfide liquids IV: density measurements and the thermodynamics of O–S–Fe–Ni–Cu liquids at low to moderate pressures: *Contributions to Mineralogy and Petrology* 156, 785.

Labidi, J., Cartigny, P., Moreira, M., 2013, Non-chondritic sulphur isotope composition of the terrestrial mantle: *Nature* 501, 208-211.

Le Vaillant, M., Saleem, A., Barnes, S.J., Fiorentini, M.L., Miller, J., Beresford, S., Perring, C., 2016, Hydrothermal remobilisation around a deformed and remobilised komatiite-hosted Ni-Cu-(PGE) deposit, Sarah's Find, Agnew Wiluna greenstone belt, Yilgarn Craton, Western Australia: *Mineralium Deposita* 51, 369-388.

Lesher, C.M., 2019, Up, down, or sideways: emplacement of magmatic Fe–Ni–Cu–PGE sulfide melts in large igneous provinces: *Canadian Journal of Earth Sciences* 56, 756-773.

Lesher, C.M., 2017, Roles of xenomelts, xenoliths, xenocrysts, xenovolatiles, residues, and skarns in the genesis, transport, and localization of magmatic Fe-Ni-Cu-PGE sulfides and chromite: *Ore Geology Reviews* 90, 465-484.

Lesher, C.M., Barnes, S.J., Gillies, S.L., Ripley, E.M., 1999, Ni-Cu-(PGE) sulphides in the Raglan Block, in Lesher CM (Editor), Komatiitic Peridotite-Hosted Fe-Ni-Cu-(PGE) Sulphide Deposits in the Raglan Area, Cape Smith Belt, New Québec: Guidebook Series 2, Mineral Exploration Research Centre, *Laurentian University*, Sudbury, 177-184.

Lesher, C.M., Burnham, O.M., 2001, Multicomponent elemental and isotopic mixing in Ni-Cu-(PGE) ores at Kambalda, Western Australia: *The Canadian Mineralogist* 39, 421-446.

Lesher, C.M., Campbell, I.H., 1993, Geochemical and fluid dynamic modeling of compositional variations in Archean komatiite-hosted nickel sulfide ores in Western Australia: *ECON GEOL* 88, 804-816.

Lesher, C.M., Groves, D.I., 1986, Controls on the formation of komatiite-associated nickel copper sulfide deposits: In: Friedrich, G.H., Genkin, A.D., Naldrett, A.J. (Eds.), *Geology and Metallogeny of Copper Deposits*. Springer, 43–62.

Lesher, C.M., Keays, R.R., 1984, Metamorphically and hydrothermally mobilized Fe-Ni-Cu sulphides at Kambalda, Western Australia: Sulphide deposits in mafic and ultramafic rocks, *Institute of Mining and Metallurgy, London*, 62-69.

Lesher, C.M., Keays, R.R., 2002, Komatiite-associated Ni-Cu-(PGE) deposits: Mineralogy, geochemistry, and genesis. In: Cabri, L.J. (Ed.), The Geology, Geochemistry, Mineralogy, and Mineral Benefciation of the Platinum-Group Elements: *Canadian Institute of Mining, Metallurgy, and Petroleum* 54, 579–617

Li, B., Huang, Z.L., Guan, T., Ding, W., 2008, $^{40}Ar$-$^{39}Ar$ dating of lamprophyre dykes in the Baimazhai nickel deposit, Yunnan Province, China, and its geological significance: *Chinese Journal of Geochemistry* 27, 351-355.

Li, C., 2017, Significance of Magmatic Ni-Cu Sulfide Deposits in Convergent Tectonic Setting: Lesson from China: *SEG workshop short courses*, 1-23.

Li, C., Ripley, E.M., Tao,Y., 2019, Magmatic Ni-Cu and Pt-Pd Sulfide Deposits in China: *Society of Economic Geologists, Special Publications* 22, 483-508.

Li, C., Ripley, E.M., Tao, Y., Hu, R.Z., 2016, The significance of PGE variations with Sr-Nd isotopes and lithophile elements in the Emeishan flood basalt province from SW China to northern Vietnam: *Lithos* 248, 1-11.

Li, C., Tao, Y., Qi, L., Ripley, E.M., 2012b, Controls on PGE fractionation in the Emeishan picrites and basalts: constraints from integrated lithophile-siderophile elements and Sr-Nd isotopes: *Geochimica et Cosmochimica Acta* 90, 12-32.

Li, C., Zhang, M.J., Fu, P., Qian, Z.Z., Hu, P.Q., Ripley, E.M., 2012a, The Kalatongke magmatic Ni-Cu deposits in the Central Asian Orogenic Belt, NW China: product of slab window magmatism: *Mineralium Deposita* 47, 51-67.

Li, C., Zhang, Z.W., Li, W.Y., Wang, Y.L., Sun, T., Ripley, E.M., 2015, Geochronology, petrology and Hf-S isotope geochemistry of the newly-discovered Xiarihamu magmatic Ni-Cu sulfide deposit in the Qinghai-Tibet plateau, western China: *Lithos* 216, 224-240.

Li, J., Xu, J.F., Suzuki, K., He, B., Xu, Y.G., Ren, Z. Y., 2010, Os, Nd and Sr isotope and trace element geochemistry of the Muli picrites: insights into the mantle source of the Emeishan Large Igneous Province: *Lithos* 119, 108-122.

Li, J.L., Schwarzenbach, E.M., John, T., Ague, J.J., Huang, F., Gao, J., Klemd, R., Whitehouse, M.J., Wang, X.S., 2020, Uncovering and quantifying the subduction zone sulfur cycle from the slab perspective: *Nature communications* 11, 1-12.

Lightfoot, P.C., Evans-Lamswood, D., 2015, Structural controls on the primary distribution of mafic–ultramafic intrusions containing Ni–Cu–Co–(PGE) sulfide mineralization in the roots of large igneous provinces: *Ore Geology Reviews* 64, 354-386.

Liu, P.P., Zhou, M.F., Chen, W.T., Gao, J.F., Huang, X.W., 2015, In-situ LA-ICP-MS trace elemental analyses of magnetite: Fe-Ti-(V) oxide-bearing mafic–ultramafic layered intrusions of the Emeishan Large Igneous Province, SW China: *Ore Geology Reviews* 65, 853-871.

Lu, Y.G., Lesher, C. M., Deng, J., 2019, Geochemistry and genesis of magmatic Ni-Cu-(PGE) and PGE-(Cu)-(Ni) deposits in China: *Ore Geology Reviews* 107, 863-887.

Lu, Y.G., He, W.Y., 2018, Characteristics of S-Os isotopes and its constraints on the mineralization for the Jinbaoshan Pt-Pd deposit: *Acta Petrologica Sinica* 34, 1258-1270 (in Chinese with English abstract).

Lu, Y.G., Zhao, K., Xiong, Y.Q., Li, P., Du, D.Y., Yuan M.W., 2014, Elements geochemistry of Jinbaoshan Pt-Pd deposit, western Yunnan, China: *Acta Petrologica Sinica* 30, 2681-2694 (in Chinese with English abstract).

Lu, Y.G., Hao, B., Sun, K., He, S.F., Xu, K.K., Gong, P.H., Zhang, H., 2020, General situation of cobalt resource and its utilization analysis. *Geological Survey and Research*, 43(01):72-80 (in Chinese with English abstract).

Maier, W.D., Groves, D.I., 2011, Temporal and spatial controls on the formation of magmatic PGE and Ni-Cu deposits: *Mineralium Deposita* 46, 841-857.

Manor, M.J., Scoates, J.S., Nixon, G.T., Ames, D.E., 2016, The giant Mascot Ni-Cu-PGE deposit, British Columbia: mineralized conduits in a convergent margin tectonic setting: *ECON GEOL*, 111, 57-87.

Mansur, E.T., Barnes, S.-J., Duran, C.J., 2019, Textural and compositional evidence for the formation of pentlandite via peritectic reaction: Implications for the distribution of highly siderophile elements: *Geology* 47, 351-354.

Makovicky, E., 2002, Ternary and quaternary phase systems with PGE. *The geology, geochemistry, mineralogy and mineral Beneficiation of Platinum-group elements* 54, 131-175.

Mavrogenes, J.A., O'Neill, H.S.C., 1999, The relative effects of pressure, temperature and oxygen fugacity on the solubility of sulfide in mafic magmas: *Geochimica et Cosmochimica Acta* 63, 1173-1180.

McDonough, W.F., Sun, S.S., 1995, The composition of the Earth: *Chemical geology* 120, 223-253.

Mole, D.R., Fiorentini, M.L., Cassidy, K.F., Kirkland, C.L., Thebaud, N., McCuaig, T.C., Doublier, M.P., Romano, S.S., Belousova, E.A., Barnes, S.J., Miller, J., 2015, Crustal evolution, intra-cratonic architecture and the metallogeny of an Archaean craton: *Geological Society, London, Special Publications* 393, 23-80.

Mungall, J. E., Andrews, D. R., Cabri, L. J., Sylvester, P. J., Tubrett, M., 2005, Partitioning of Cu, Ni, Au, and platinum-group elements between monosulfide solid solution and sulfide melt under controlled oxygen and sulfur fugacities. *Geochimica et Cosmochimica Acta* 69(17), 4349-4360.

Mungall, J. E., 2007, Crystallization of magmatic sulfides: An empirical model and application to Sudbury ores. *Geochimica et Cosmochimica Acta* 71(11), 2809-2819.

Mungall, J. E., Brenan, J. M., 2014, Partitioning of platinum-group elements and Au between sulfide liquid and basalt and the origins of mantle-crust fractionation of the chalcophile elements. *Geochimica et Cosmochimica Acta* 125, 265-289.

Naldrett, A.J., 1966, The role of sulphurization in the genesis of iron-nickel sulphide deposits of the Porcupine District, Ontario. *Can. Inst. Mining Metal. Trans*. 69: 147-155.

Naldrett, A. J., 1969, A portion of the system Fe–S–O between 900 and 1080 C and its application to sulfide ore magmas. *Journal of Petrology* 10(2), 171-201.

Naldrett, A.J., 1981, Nickel sulfde deposits: classifcation, composition and genesis: *ECON GEOL*, 75, 628-655.

Naldrett, A.J., 2004, Magmatic Sulfide Deposits: *Geology, Geochemistry and Exploration: Springer,* 1-727.

Naldrett, A.J., Barnes, S.-J., 1986, The behaviour of platinum group elements during fractional crystallization and partial melting with special reference to the composition of magmatic sulfide ores. *Fortschr. Miner*. 63, 113–133.

Naldrett, A.J., Craig, J.R., Kullerud, G., 1967, The central portion of the Fe-Ni-S system and its bearing on pentlandite exsolution in iron-nickel sulfide ores: *ECON GEOL* 62, 826-847.

Pettke, T., Oberli, F., Audétat, A., Guillong, M., Simon, A. C., Hanley, J. J., Klemm, L. M., 2012, Recent developments in element concentration and isotope ratio analysis of individual fluid inclusions by laser ablation single and multiple collector ICP-MS. *Ore Geology Reviews* 44, 10-38.

Pearce, J.A., 2008, Geochemical fingerprinting of oceanic basalts with applications to ophiolite classification and the search for Archean oceanic crust: *Lithos* 100, 14-48.

Peach, C.L., Mathez, E.A., and Keays, R.R., 1990, Sulfide melt-silicate melt distribution coefficients for the noble metals as deduced from MORB: Implications for partial melting: *Geochimica et Cosmochimica Acta* 54, 3379-3389.

Peach, C.L., and Mathez, E.A., 1996, Constraints on the formation of platinum-group element deposits in igneous rocks: *ECON GEOL* 91, 439-450.

Petrus, J. A., Chew, D. M., Leybourne, M. I., Kamber, B. S., 2017, A new approach to laser-ablation inductively-coupled-plasma mass-spectrometry (LA-ICP-MS) using the flexible map interrogation tool 'Monocle'. Chemical Geology 463, 76-93.

Pina, R., Gervilla, F., Ortega, L., Lunar, R., 2008, Mineralogy and geochemistry of platinum-group elements in the Aguablanca Ni-Cu deposit (SW Spain): *Mineralogy and Petrology* 92, 259-282.

Pirajno, F., González-Álvarez, I., 2013, A re-appraisal of the Epoch nickel sulphide deposit, Filabusi Greenstone Belt, Zimbabwe: A hydrothermal nickel mineral system?: *Ore Geology Reviews* 52 58-65.

Rayleigh, J.W.S., 1896, Theoretical considerations respecting the separation of gases by diffusion and similar processes: *Philosophical Magazine* 42, 77–107.

Richards, J.P., 2015, The oxidation state, and sulfur and Cu contents of arc magmas: Implications for metallogeny: *Lithos* 233, 27–45.

Ripley, E.M., 2010, A new perspective on exploration for magmatic sulfide-rich Ni-Cu-(PGE) deposits: *Society of Economic Geologists Special Publication* 15, 437-450.

Ripley, E.M., Li, C., 2013, Sulfide saturation in mafic magmas: is external sulfur required for magmatic Ni-Cu-(PGE) ore genesis?: *ECON GEOL* 108, 45-58.

Ripley, E.M., Park, Y.R., Li, C., Naldrett, A.J., 1999, Sulfur and oxygen isotopic evidence of country rock contamination in the Voisey's Bay Ni-Cu-Co deposit, Labrador, Canada: *Lithos* 47, 53-68.

Robertson, J., Ripley, E.M., Barnes, S.J., Li, C., 2015, Sulfur liberation from country rocks and incorporation in mafic magmas: *ECON GEOL* 110, 1111-1123.

Sattari, P., Brenan, J.M., Horn, I., McDonough, W.F., 2002, Experimental constraints on the sulfide- and chromite-silicate melt partitioning behavior of rhenium and platinum-group elements: *ECON GEOL*

97, 385-398.

Shen, X., Zhang, B., Du, Q., Su, Y., 2019, Rb–Sr geochronology and geochemistry of the Xiaotongchang basalt-hosted copper deposit in the Jinping area, SW China. *Ore Geology Reviews* 112, 103021.

Sleep, N. H., 2006, Mantle plumes from top to bottom: *Earth-Science Reviews* 77, 231-271.

Sobolev, A.V., Hofmann, A.W., Sobolev, S.V., Nikogosian, I.K., 2005, An olivine-free mantle source of Hawaiian shield basalts: *Nature* 434, 590-597.

Song, X.Y., Chen, L.M., Deng, Y.F., Xie, W., 2013, Syncollisional tholeiitic magmatism induced by asthenosphere upwelling owing to slab detachment at the southern margin of the Central Asian Orogenic Belt: *Journal of the Geological Society* 170, 941-950.

Song, X.Y., Zhang, C.J., Hu, R.Z., Zhong, H., Zhou, M.F., Ma, R.Z., Li, Y.G., 2005, Genetic links of magmatic deposits in the Emeishan large igneous province with dynamics of mantle plume: *J Mineral Petrol* 25, 35-44.

Song, X.Y., Keays, R.R., Xiao, L., Qi, H.W., Ihlenfeld, C., 2009, Platinum-group element geochemistry of the continental flood basalts in the central Emeishan Large Igneous Province, SW China: *Chemical Geology* 262, 246-261.

Song, X.Y., Li, X.R., 2009, Geochemistry of the Kalatongke Ni-Cu-(PGE) sulfide deposit, NW China: implications for the formation of magmatic sulfide mineralization in a postcollisional environment: *Mineralium Deposita* 44, 303-327.

Song, X.Y., Yi, J.N., Chen, L.M., She, Y.W., Liu, C.Z., Dang, X.Y., Yang, Q.A., Wu, S.K., 2016, The giant Xiarihamu Ni-Co sulfide deposit in the East Kunlun orogenic belt, northern Tibet plateau, China: *ECON GEOL* 111, 29-55.

Song, X.Y., Zhou, M.F., Cao, Z.M., 2004, Genetic relationships between base-metal sulfides and platinum-group minerals in the Yangliuping Ni-Cu-(PGE) sulfide deposit, southwestern China: *Canadian Mineralogist* 42, 469-483.

Song, X.Y., Zhou, M.F., Cao, Z.M., Sun, M., Wang, Y.L., 2003, Ni-Cu-(PGE) magmatic sulfide deposits in the Yangliuping area, Permian Emeishan igneous province, SW China: *Mineralium Deposita* 38, 831-843.

Song, X.Y., Zhou, M.F., Tao, Y., Xiao, J.F., 2008, Controls on the metal compositions of magmatic sulfide deposits in the Emeishan large igneous province, SW China. *Chemical Geology* 253, 38-49.

Stifter, E.C., Ripley, E.M., Li, C., 2014. Silicate melt removal and sulfide liquid retention in ultramafic rocks of the Duke Island Complex, Southeastern Alaska: *Mineralogy and Petrology* 108, 727-740.

Sun, X.M., Wang, S.W., Sun, W.D., Shi, G.Y., Sun, Y.L., Xiong, D.X., Qu, W.J., Du, A.D., 2008, PGE geochemistry and Re–Os dating of massive sulfide ores from the Baimazhai Cu–Ni deposit, Yunnan province, China: *Lithos* 105, 12-24.

Tang, Q.Y., Ma, Y.S., Zhang, M.J., Li, C., Zhu, D., Tao, Y., 2013, The origin of Ni-Cu-PGE sulfide mineralization in the margin of the Zhubu mafic-ultramafic intrusion in the Emeishan large igneous province, southwestern China: *ECON GEOL* 108, 1889-1901.

Tao, Y., Li, C., Song, X.Y., Ripley, E.M., 2008, Mineralogical, petrological, and geochemical studies of the Limahe mafic–ultramafic intrusion and associated Ni-Cu sulfide ores, SW China: *Mineralium Deposita* 43, 849-872.

Tao, Y., Li, C., Hu, R.Z, Ripley, E.M., Du, A.D, Zhong, H., 2007, Petrogenesis of the Pt-Pd mineralized Jinbaoshan ultramafic intrusion in the Permian Emeishan large igneous province, SW China. *Contributions to Mineralogy and Petrology* 153, 321–337.

Tao, Y., Hu, R.Z., Qi, L., Qu, W.J., Chu, Z.Y., Gou, T.Z., 2010a, Sr-Nd-Os isotopic constraints on magma origin and evolution of the Jinbaoshan Pt-Pd deposit, Yunnan. *J. Mineral. Petrol* 30, 60–67 (in Chinese with English abstract).

Tao, Y., Li, C., Hu, R.Z, Qi, L., Qu, W.J, Du, A.D, 2010b, Re-Os isotopic constraints on the genesis of the Limahe Ni-Cu deposit in the Emeishan large igneous province, SW China: *Lithos* 119, 137–146.

Thakurta, J., Ripley, E.M., Li, C., 2014, Platinum group element geochemistry of sulfide-rich horizons in the Ural-Alaskan type ultramafic complex of Duke Island, southeastern Alaska: *ECON GEOL* 109, 643-659.

Tonnelier, N.J., 2010, Geology and genesis of the Jinchuan Ni-Cu-(PGE) deposit, China: Unpublished Ph.D. thesis, Sudbury, Canada, *Laurentian University*, 1-192.

Tornos, F., 2006, Environment of formation and styles of volcanogenic massive sulfides: The Iberian Pyrite Belt: *Ore Geology Reviews* 28, 259-307.

Tornos, F., Casquet, C., Galindo, C., Velasco, F., Canales, A., 2001, A new style of Ni-Cu mineralization related to magmatic breccia pipes in a transpressional magmatic arc, Aguablanca, Spain: *Mineralium Deposita* 36, 700-706.

Wang, C.Y., Wei, B., Zhou, M.F., Minh, D.H., Qi, L., 2018, A synthesis of magmatic Ni-Cu-(PGE) sulfide deposits in the 260 Ma Emeishan large igneous province, SW China and northern Vietnam: *Journal of Asian Earth Sciences* 154, 162-186.

Wang, C.Y., Zhou, M.F., 2006, Genesis of the Permian Baimazhai magmatic Ni-Cu-(PGE) sulfide deposit, Yunnan, SW China: *Mineralium Deposita* 41, 771-783.

Wang, C.Y., Zhou, M.F., Keays, R.R., 2006, Geochemical constraints on the origin of the Permian Baimazhai mafic-ultramafic intrusion, SW China: *Contributions to Mineralogy and Petrology*, 152, 309-321.

Wang, C.Y., Zhou, M.F., Qi, L., 2007, Permian flood basalts and mafic intrusions in the Jinping (SW China)-Song Da (northern Vietnam) district: mantle sources, crustal contamination and sulfide segregation: *Chemical Geology* 243, 317-343.

Wang, C.Y., Zhou, M.F., Qi, L., 2011, Chalcophile element geochemistry and petrogenesis of high-Ti and low-Ti magmas in the Permian Emeishan large igneous province, SW China: *Contributions to Mineralogy and Petrology*, 161, 237-254.

Wang, C.Y., Zhou, M.F., Sun, Y., Arndt, N.T., 2012, Differentiation, crustal contamination and

emplacement of magmas in the formation of the Nantianwan mafic intrusion of the ~260 Ma Emeishan large igneous province, SW China: *Contributions to Mineralogy and Petrology* 164, 281-301.

Wei, B., Wang, C.Y., Arndt, N.T., Prichard, H.M., Fisher, P. C., 2015, Textural relationship of sulfide ores, PGE, and Sr-Nd-Os isotope compositions of the Triassic Piaohechuan Ni-Cu sulfide deposit in NE China: *ECON GEOL* 110, 2041-2062.

Wei, B., Wang, C.Y., Li, C., Sun, Y., 2013, Origin of PGE-depleted Ni-Cu sulfide mineralization in the Triassic Hongqiling No. 7 orthopyroxenite intrusion, Central Asian orogenic belt, northeastern China: *ECON GEOL* 108, 1813-1831.

Wendlandt, R.F., 1982, Sulfide saturation of basalt and andesite melts at high pressure: *American Mineralogist* 67, 877–885.

Wu, C.Z., Xie, S.W., Gu, L.X., Samson, I.M., Yang, T., Lei, R.X., Zhu, Z.Y., Dang, B., 2018, Shear zone-controlled post-magmatic ore formation in the Huangshandong Ni-Cu sulfide deposit, NW China: *Ore Geology Reviews* 100, 545-560.

Xiao, L., Xu, Y.G., Mei, H.J., Zheng, Y.F., He, B., Pirajno, F., 2004, Distinct mantle sources of low-Ti and high-Ti basalts from the western Emeishan large igneous province, SW China: implications for plume–lithosphere interaction: *Earth and Planetary Science Letters* 228, 525-546.

Xie, W., Song, X.Y., Chen, L.M., Deng, Y.F., Zheng, W.Q., Wang, Y.S., Luan, Y., 2014. Geochemistry insights on the genesis of the subduction-related Heishan magmatic Ni-Cu-(PGE) deposit, Gansu, northwestern China, at the southern margin of the Central Asian Orogenic Belt. *ECON GEOL*, 109, 1563-1583.

Xu, Y.G., Chung, S.L., Jahn, B.M., Wu GY., 2001, Petrologic and geochemical constraints on the petrogenesis of Permian–Triassic Emeishan flood basalts in southwestern China: *Lithos* 58, 145-168.

Xu, Y.G., Wang, Y., Wei, X., He, B., 2013, Mantle plume-related mineralization and their principal factors: *Acta Petrologica Sinica* 29, 3307-3322 (in Chinese with English abstract).

Xu, J.F., Suzuki, K., Xu, Y.G., Mei, H. J., Li, J, 2007, Os, Pb, and Nd isotope geochemistry of the Permian Emeishan continental flood basalts: insights into the source of a large igneous province: *Geochimica et Cosmochimica Acta* 71, 2104-2119.

Yang, L.Q., Deng, J., Dilek, Y., Meng, J.Y., Gao, X., Santosh, M., Wang, D., Yan, H., 2016, Melt source and evolution of I-type granitoids in the SE Tibetan Plateau: Late Cretaceous magmatism and mineralization driven by collision-induced transtensional tectonics: *Lithos* 245, 258-273.

Yang, L.Q., Deng, J., Gao, X., He, W.Y., Meng, J.Y., Santosh, M., Yu, H.J., Yang, Z., Wang, D., 2017, Timing of formation and origin of the Tongchanggou porphyry-skarn deposit: Implications for Late Cretaceous Mo-Cu metallogenesis in the southern Yidun Terrane, SE Tibetan Plateau: *Ore Geology Reviews* 81, 1015-1032.

Yang, L.Q., Deng, J., Zhao, K., Liu, J.T., 2011, Tectono-thermochronology and gold mineralization events of orogenic gold deposits in Ailaoshan orogenic belt, Southwest China: Geochronological constraints: *Acta Petrologica Sinica* 27, 2519-2532 (in Chinese with English abstract).

Zhang, J., Deng, J., Chen, H.Y., Yang, L.Q., Cooke, D., Danyushevsky, L., Gong, Q.J., 2014, LA-ICP-MS trace element analysis of pyrite from the Chang'an gold deposit, Sanjiang region, China: Implication for ore-forming process: *Gondwana Research* 26, 557-575.

Zhang, J., Wang, H., Li, S., Li, T., 2017, Paleogene magmatism and gold metallogeny of the Jinping terrane in the Ailaoshan ore belt, Sanjiang Tethyan Orogen (SW China): Geology, deposit type and tectonic setting: *Ore Geology Reviews* 91, 620-637.

Zhang, L., Ren, Z.Y., 2013, Quantitative simulation for the formation of Baimazhai Ni-Cu sulfide deposit in Yunnan Province: *Acta Petrologica Sinica* 29, 3581-3591 (in Chinese with English abstract).

Zhang, M., Zhao, F., Chen, F., Li, J., Lv, P.H., 2018, Mineralization and metallogenic epoch of the Mengnuo Pb-Zn deposit in Yunnan province. *Geological Survey and Research* 4, 280-288 (in Chinese with English abstract).

Zhang, X.S., 2006, Mafic-ultramafic rocks, metallogenetic series and prospecting targeting in the Jinping-Song Da rift: *Doctoral dissertation of Kunming University of Science and Technology*, 1-

263 (in Chinese with English abstract).

Zhang, X.S., Pirajno, F., Qin, D.X., Fan, Z.G., Liu, G.L., Nian, H., 2006, Baimazhai, Yunnan province, China: a hydrothermally modified magmatic nickel-copper-PGE sulfide deposit: *International Geology Review* 48, 725-741.

Zhang, Z, C., Mahoney, J.J., Wang, F.S., Zhao, L., Ai, Y., Yang, T.Z. 2006. Geochemistry of picritic and associated basalts flows of the western Emeishan flood basalts province, China: evidence for a plume-headed origin. *Acta Petrologica Sinica* 22(6): 1538-1552.

Zhong, H., Zhu, W.G., Chu, Z.Y., He, D.F., Song, X.Y., 2007, SHRIMP U-Pb zircon geochronology, geochemistry, and Nd–Sr isotopic study of contrasting granites in the Emeishan large igneous province, SW China: *Chemical Geology* 236, 112-133.

Zhou, M.F., Robinson, P.T., Lesher, C.M., Keays, R.R., Zhang, C.J., Malpas, J., 2005, Geochemistry, petrogenesis and metallogenesis of the Panzhihua gabbroic layered intrusion and associated Fe–Ti–V oxide deposits, Sichuan Province, SW China. *Journal of Petrology* 46, 2253-2280.

Zhou, M.F., Arndt, N.T., Malpas, J., Wang, C.Y., Kennedy, A.K., 2008, Two magma series and associated ore deposit types in the Permian Emeishan large igneous province, SW China: *Lithos* 103, 352-368.

Zhou, M.F., Lesher, C.M., Yang, Z.X., Li, J.W., Sun, M., 2004, Geochemistry and petrogenesis of 270 Ma Ni-Cu-(PGE) sulfide-bearing mafic intrusions in the Huangshan district, Eastern Xinjiang, Northwest China: implications for the tectonic evolution of the Central Asian orogenic belt: *Chemical Geology* 209, 233-257.

Zhou, M.F., Malpas, J., Song, X.Y., Robinson, P.T., Sun, M., Kennedy, A.K., Lesher, CM., Keays, R.R., 2002, A temporal link between the Emeishan large igneous province (SW China) and the end-Guadalupian mass extinction: *Earth Planetary Science Letters* 196, 113-122.

## Figure captions

**Fig. 1 Distribution of continental flood basalts and contemporaneous magmatic sulfide deposits in the Emeishan large igneous province, SW China (after Song et al., 2008, 2009; Li et al., 2016).**

**Fig. 2 Sketch geological map (A) and section (B) of the Baimazhai No.3 intrusion (after Zhang, 2006).**

**Fig. 3 Photographs and photomicrographs (plane-polarized incident light) of selected sulfide ore samples from the Baimazhai deposit. (A-B) Disseminated ore; (C-D) Net-textured ore; (E-F) Massive ore. Srp-serpentine; Po-Pyrrhotite; Pn-pentlandite; Cp-chalcopyrite; Mag-magnetite**

**Fig. 4 Photomicrographs of ores from the Baimazhai deposit. A-C: massive, D-H disseminated. Po - Pyrrhotite; Pn - pentlandite; Cp - chalcopyrite; Vio - violarite; Cbt - cobaltite; Gd - gersdorffite; Gn – galena; Mag - magnetite; Chr - chromite; Ilm – ilmenite.**

**Fig. 5 Plots of chalcophile element concentrations vs S content in whole rocks from the Baimazhai deposit.**

**Fig. 6 Th/Yb vs Nb/Yb in weakly-mineralized rocks ELIP. Data for deposits in the Central Asian Orogenic Belt (CAOB) as compiled by Lu et al. (2019); data for Baimazhai, Limahe, Yangliuping, Zhubu, and Jinbaoshan from Wang et al. (2006), Tao et al. (2008), Song et al. (2003), Tang et al. (2013), and Tao et al. (2007), respectively; data for LT1, LT2, HT from Xiao et al., (2004), and data for picrite from Zhang et al. (2006). Crustal reservoirs (P – Phanerozoic crust, A –Archean crust, UC –upper crust, MC – middle crust, LC – lower crust) from Rudnick and Fountain (1995), primitive mantle from McDonough and Sun (1995), and mantle array from Pearce (2008).**

**Fig. 7 Primitive mantle-normalized chalcophile element patterns for (A) different rock series in the ELIP (see descriptions in text); (B) average composition of ores from the Baimazhai deposit (black pattern) and LT1 interacting with different amounts of magma (grey patterns). Picrites are from Li et al. (2012). LT1, LT2 and HT are from Wang et al. (2011). Normalizing values after McDonough and Sun (1995).**

**Fig. 8 Primitive mantle-normalized chalcophile element patterns for the sulfide ores from the Baimazhai deposit. Elements are in order of increasing compatibility during mantle melting (modified from Lesher and Keays, 2002). Same colours as in Figure 5.**

**Fig. 9 Multi-element diagrams of trace element composition of primary and secondary base-metal sulfides analyzed by LA-ICP-MS. Elements are plotted from left to right in increasing order of incompatibility with picritic basalt mantle sources (Barnes, 2016). Pri-Cp = primary chalcopyrite, Sec-Cp = secondary chalcopyrite; Pri-Pn = primary pentlandite, Sec-Pn = Secondary pentlandite; Pri-Po = primary pyrrhotite; Sec-Po = secondary pyrrhotite; Viol = violarite.**

**Fig. 10 Ni vs. Co in the base-metal sulfides from the Baimazhai deposit. Cp = chalcopyrite, Po = pyrrhotite, Pn = pentlandite, Cbt = cobaltite, Viol = violarite, Co-Viol = cobaltian violarite.**

**Fig. 11 εNd vs. γOs for Ni-Cu-PGE deposits in ELIP. The plot is modified after Lu et al. (2019). Data of Ni-Cu-PGE deposits in ELIP are from Wang et al. (2006), Zhou et al. (2008), Sun et al. (2008), Tao et al. (2010a, 2010b), Han (2017). Data of picrite, LT basalt, and HT basalt are from Xu et al., (2007), Li et al. (2010). BMZ Baimazhai, LMH Limahe, JBS Jinbaoshan, YLP Yangliuping.**

**Fig. 12 $\delta^{34}S$ data for 23 samples/spots of sulfide ores from the Baimazhai intrusion (orange bars) and compositions calculated at varying magma:sulfide ratios (R factor) assuming 0 ‰ $\delta^{34}S$ in a magma containing 0.1% S and 10‰ $\delta^{34}S$ in a sulfide xenomelt (derived from country-rock sandstone) containing 38% S. All but one of the samples appear to have formed at R factors between 100 and 1000.**

**Fig. 13 Schematic model for the formation of base metal sulfides and magnetite from the Baimazhai deposit.**

**Fig. 14 Cr-Ti-V contents of different types of magnetite in the Baimazhai intrusion.**

**Fig. 15 Modeled variations of Ir and Pd in 100% sulfides in Baimazhai ores with varying magma:sulfide mass ratio (R factor: open squares) and fractional crystallization of monosulfide solid-solution from sulfide liquid (open circles). F = fraction of sulfide liquid.**

**Fig. 16 Ternary phase diagram of sulfarsenide solid-solution series (CoAsS-FeAsS-NiAsS) for the Baimazhai deposit and other Ni-Cu-PGE deposits. Temperature contours are after Klemm (1965). Data for Piaohechuan, Yangliuping, Sudbury, and Sarah's Find are from Wei et al. (2015), Song et al. (2004), Dare et al. (2010), and Le Vaillant et al. (2016), respectively.**

**Table captions**

**Table 1. S, Ni, Cu, Co and PGE concentrations in whole rocks from the Baimazhai deposit from this study, Wang et al. (2006), and Wang and Zhou (2006).**

**Table 2. Maximum, minimum, and median values of metal contents for sulfides in the Baimazhai No.3 intrusion.**

**Table 3 Ti, V, and Cr contents of magnetite in the Baimazhai No.3 intrusion.**

**Table 4. Sulfur isotope composition of sulfides and whole rocks from the Baimazhai deposit from this study, Zhang (2006), and Wang et al. (2018).**

## Figures

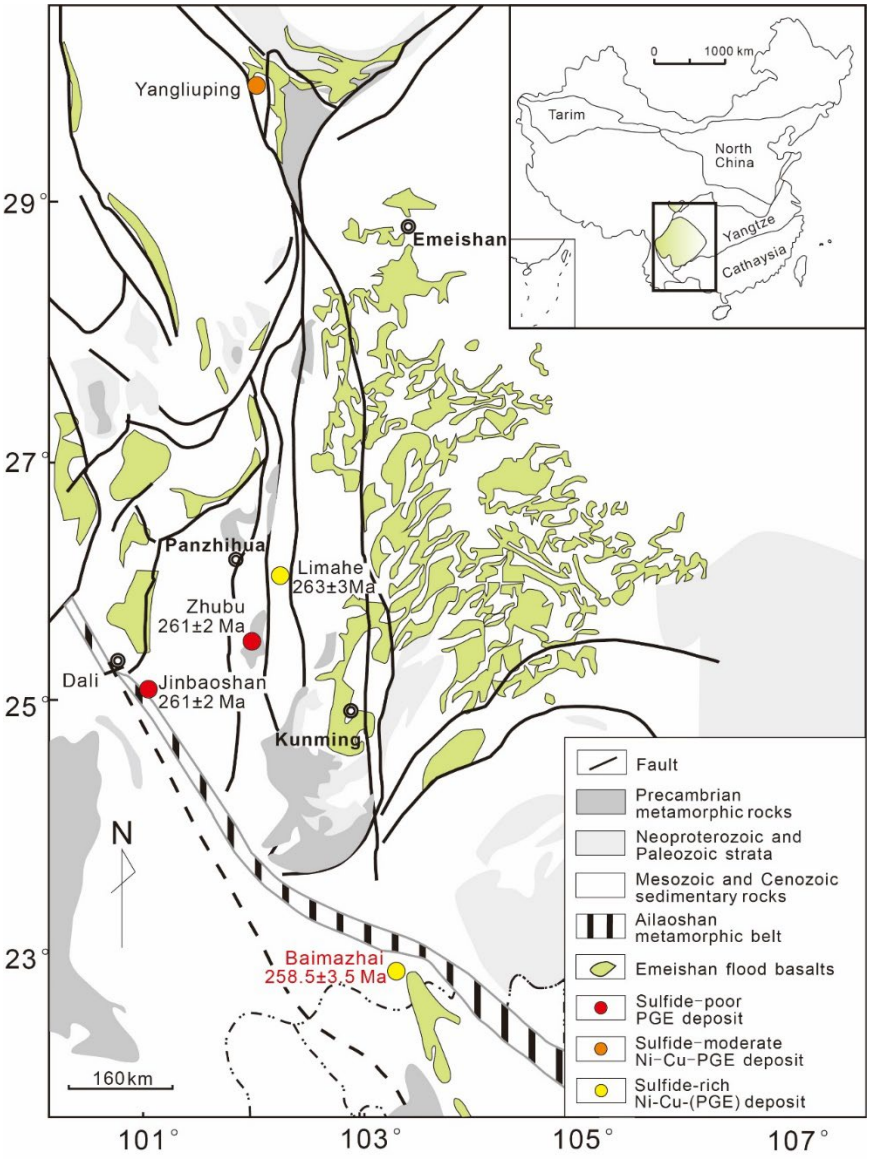


**Figure 1**

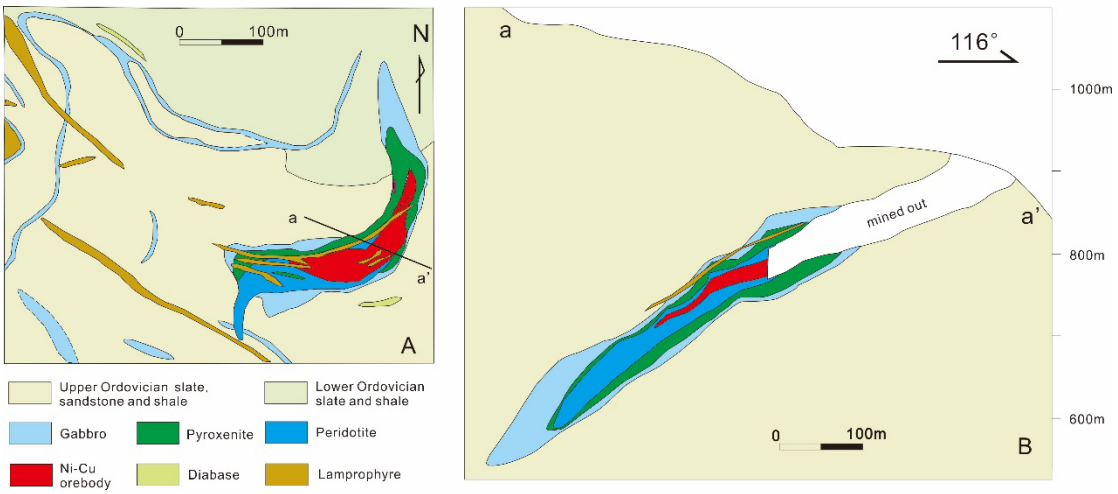
0
100m
N
a
a'
A
Upper Ordovician slate, sandstone and shale
Lower Ordovician slate and shale
Gabbro
Pyroxenite
Peridotite
Ni-Cu orebody
Diabase
Lamprophyre
a
116°
1000m
mined out
a'
800m
600m
0
100m
B

**Figure 2**

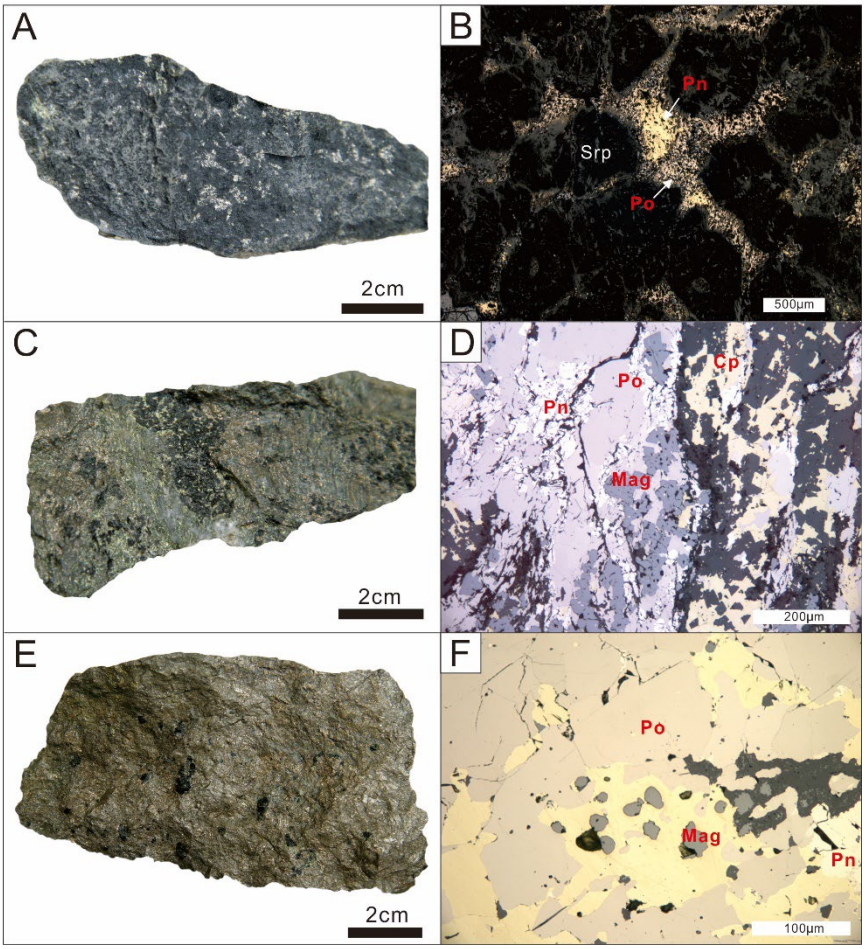
A
2cm
B
Pn
Srp
Po
500μm
C
2cm
D
Po
Pn
Mag
Cp
200μm
E
2cm
F
Po
Mag
Pn
100μm

**Figure 3**

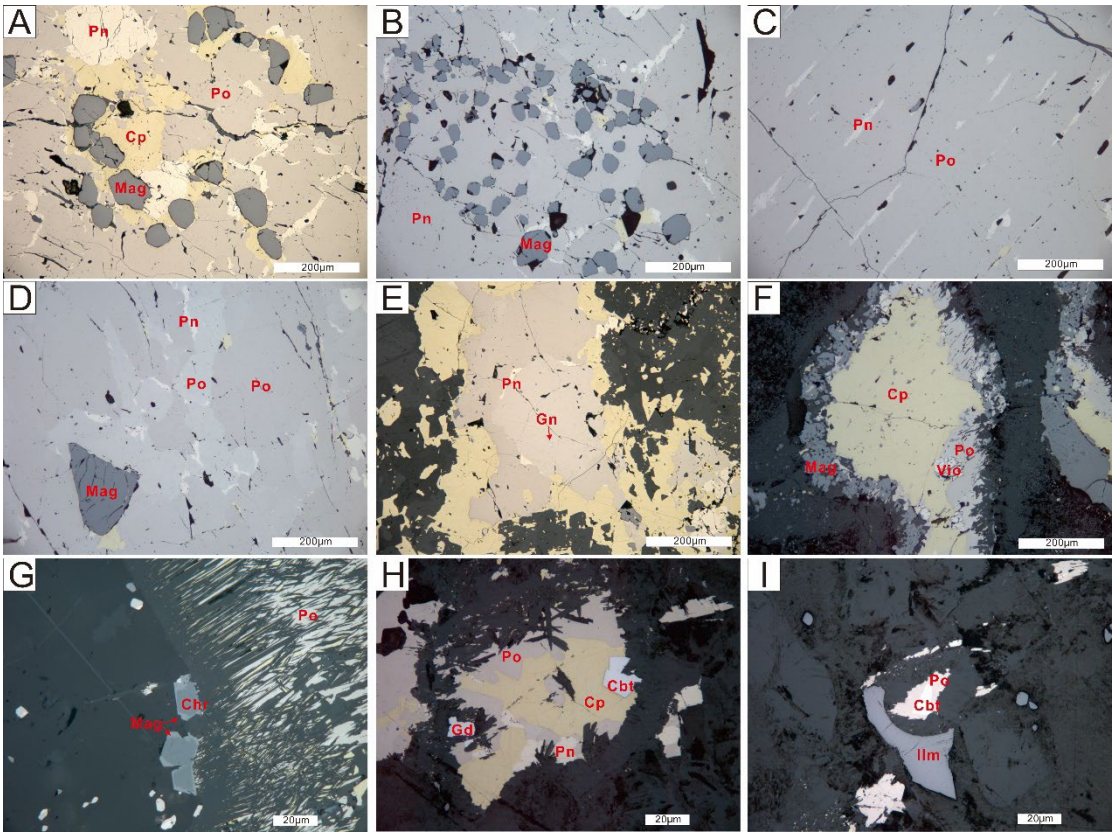
A
Pn
Po
Cp
Mag
200µm
B
Pn
Mag
200µm
C
Pn
Po
200µm
D
Pn
Po
Po
Mag
200µm
E
Pn
Gn
200µm
F
Cp
Po
Mag
Vio
200µm
G
Po
Chl
Mag
20µm
H
Po
Cbt
Cp
Gd
Pn
20µm
I
Po
Cbt
Ilm
20µm

**Figure 4**

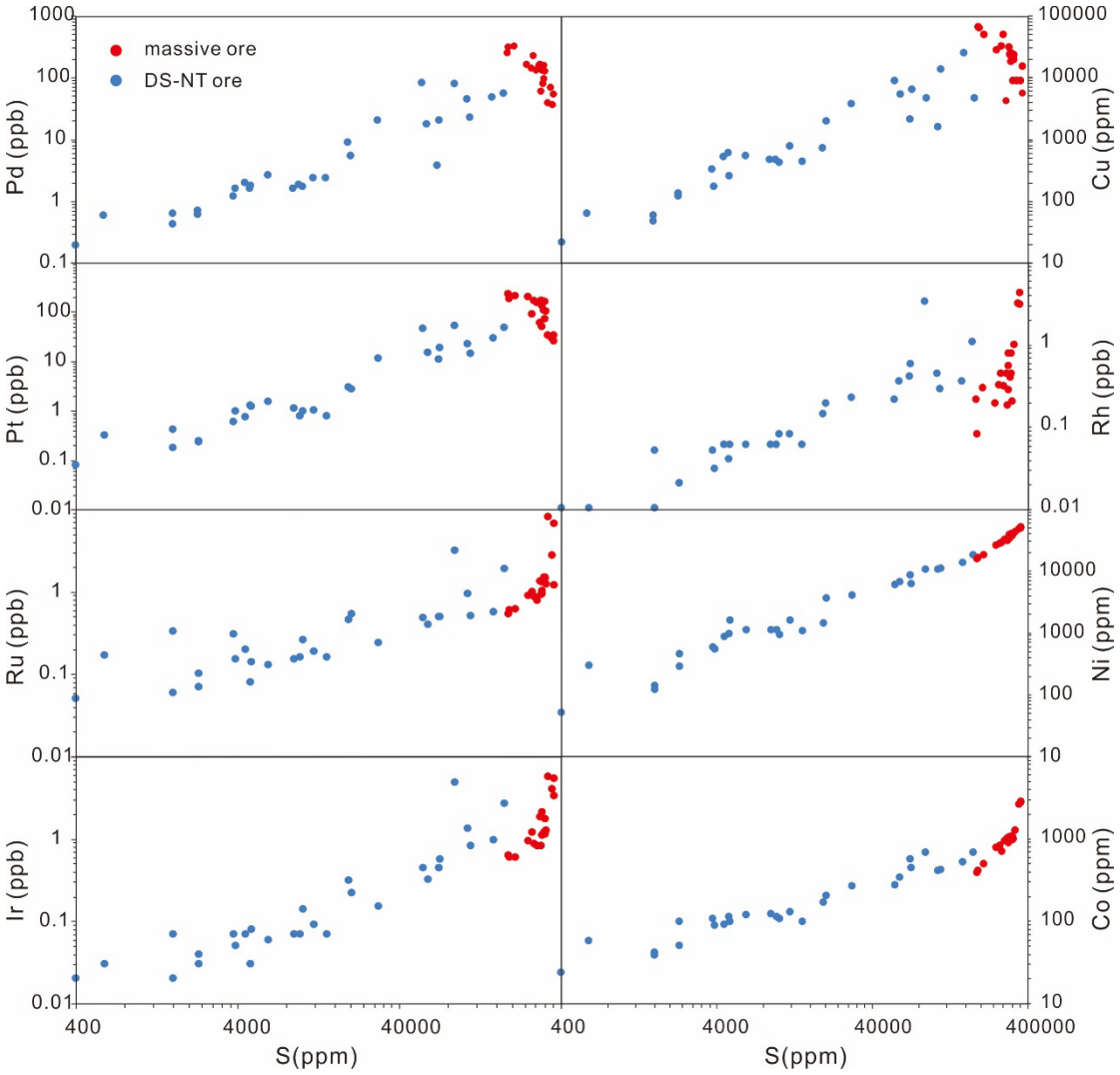
massive ore
DS-NT ore
Pd (ppb)
Pt (ppb)
Ru (ppb)
Ir (ppb)
Cu (ppm)
Rh (ppb)
Ni (ppm)
Co (ppm)
S(ppm)
S(ppm)

**Figure 5**

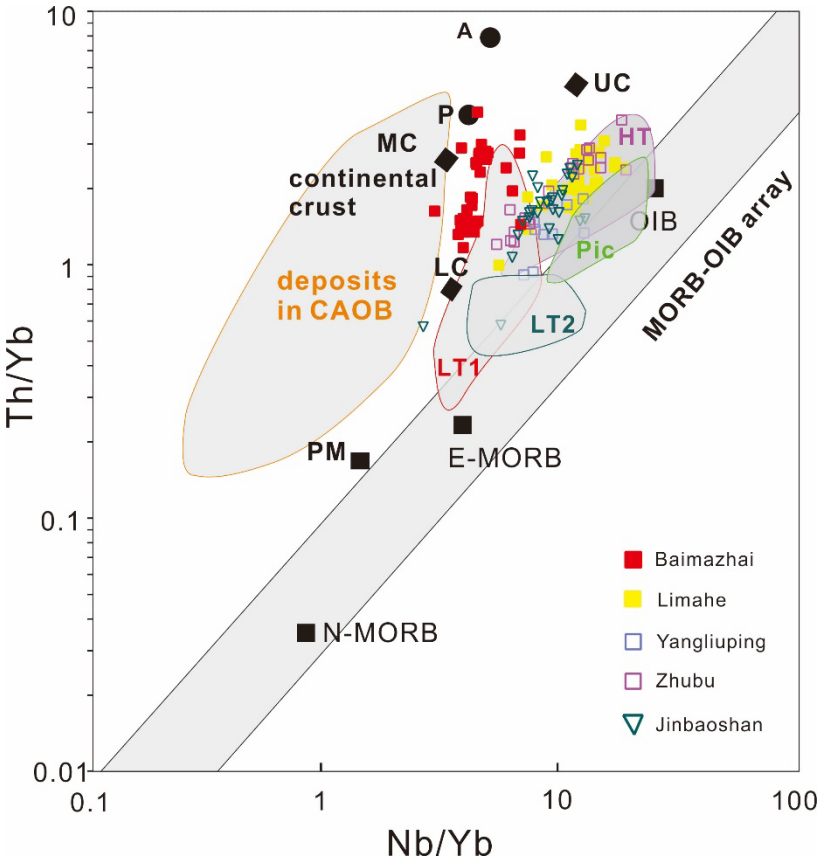
10
1
0.1
0.01
Th/Yb
0.1
1
10
100
Nb/Yb
A
UC
P
MC
continental
crust
HT
OIB
Pic
LC
deposits
in CAOB
LT2
LT1
MORB-OIB array
PM
E-MORB
N-MORB
Baimazhai
Limahe
Yangliuping
Zhubu
Jinbaoshan

**Figure 6**

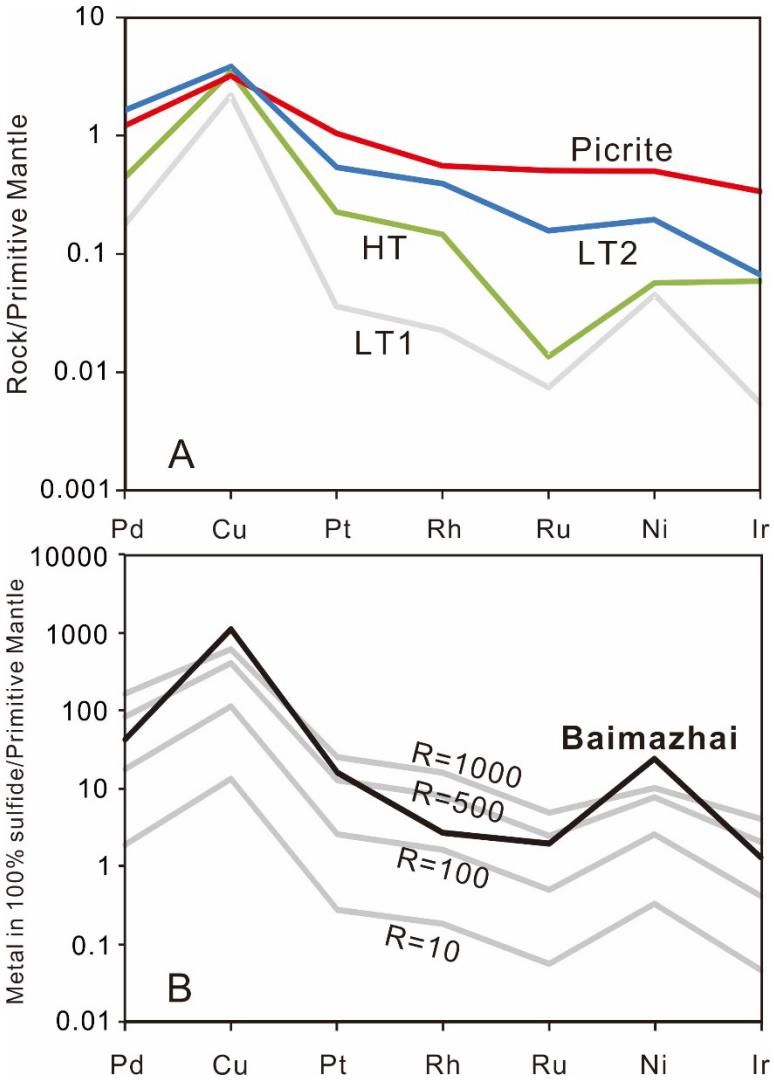
10
1
0.1
0.01
0.001
Rock/Primitive Mantle
Picrite
HT
LT2
LT1
A
Pd
Cu
Pt
Rh
Ru
Ni
Ir
10000
1000
100
10
1
0.1
0.01
Metal in 100% sulfide/Primitive Mantle
Baimazhai
R=1000
R=500
R=100
R=10
B
Pd
Cu
Pt
Rh
Ru
Ni
Ir

**Figure 7**

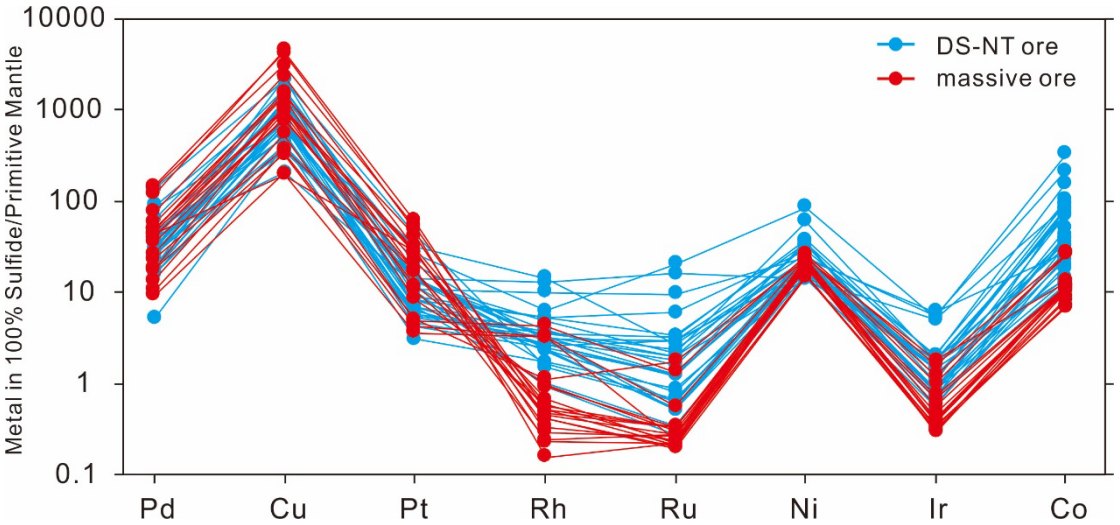
10000
1000
100
10
1
0.1
Metal in 100% Sulfide/Primitive Mantle
DS-NT ore
massive ore
Pd
Cu
Pt
Rh
Ru
Ni
Ir
Co

**Figure 8**

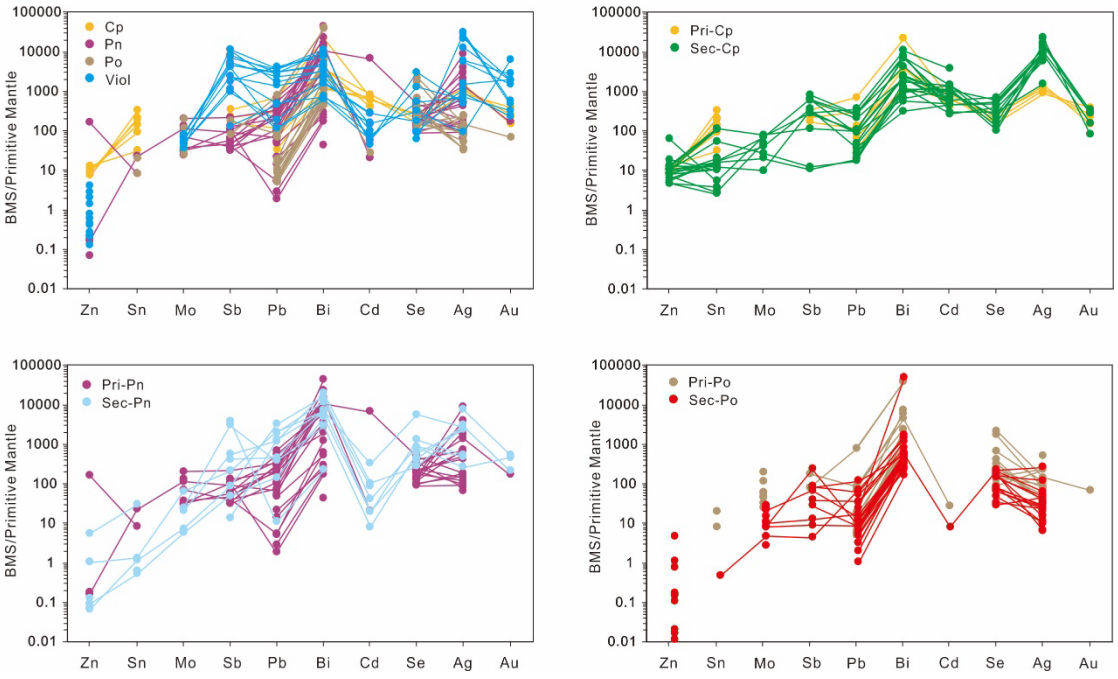
Cp
Pn
Po
Violl
Pri-Cp
Sec-Cp
Pri-Pn
Sec-Pn
Pri-Po
Sec-Po
BMS/Primitive Mantle
100000
10000
1000
100
10
1
0.1
0.01
Zn
Sn
Mo
Sb
Pb
Bi
Cd
Se
Ag
Au

**Figure 9**

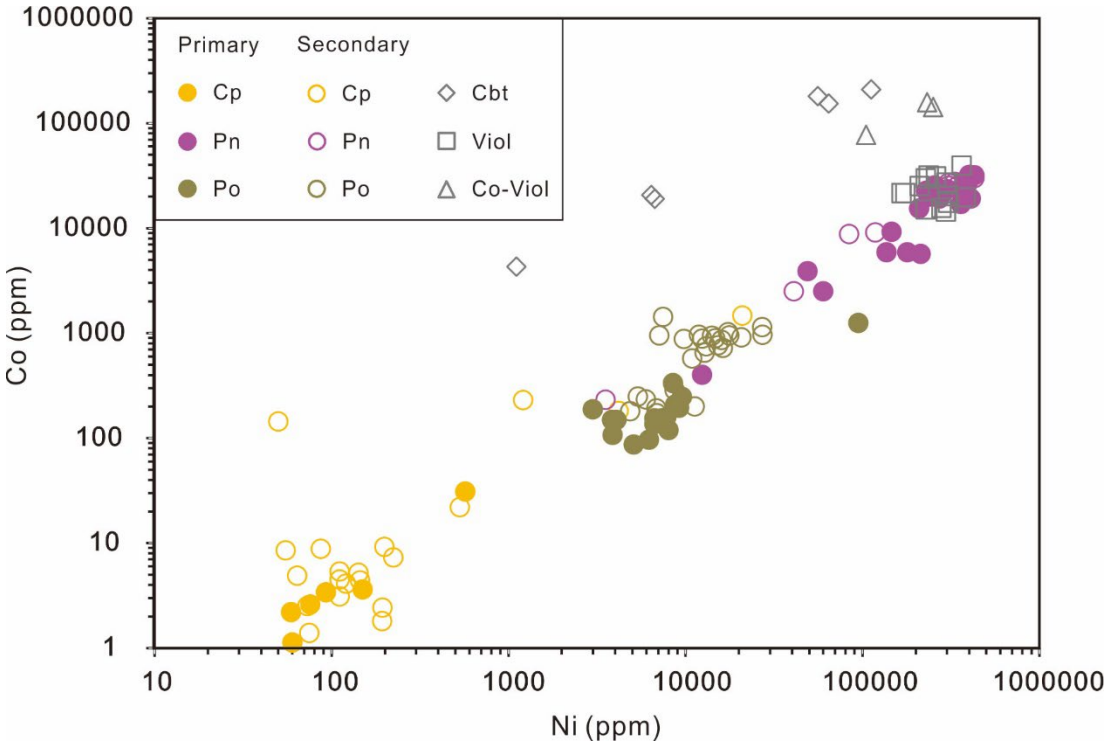
Primary
Secondary
Cp
Cp
Cbt
Pn
Pn
Viol
Po
Po
Co-Viol
Co (ppm)
Ni (ppm)
1000000
100000
10000
1000
100
10
1
10
100
1000
10000
100000
1000000

**Figure 10**

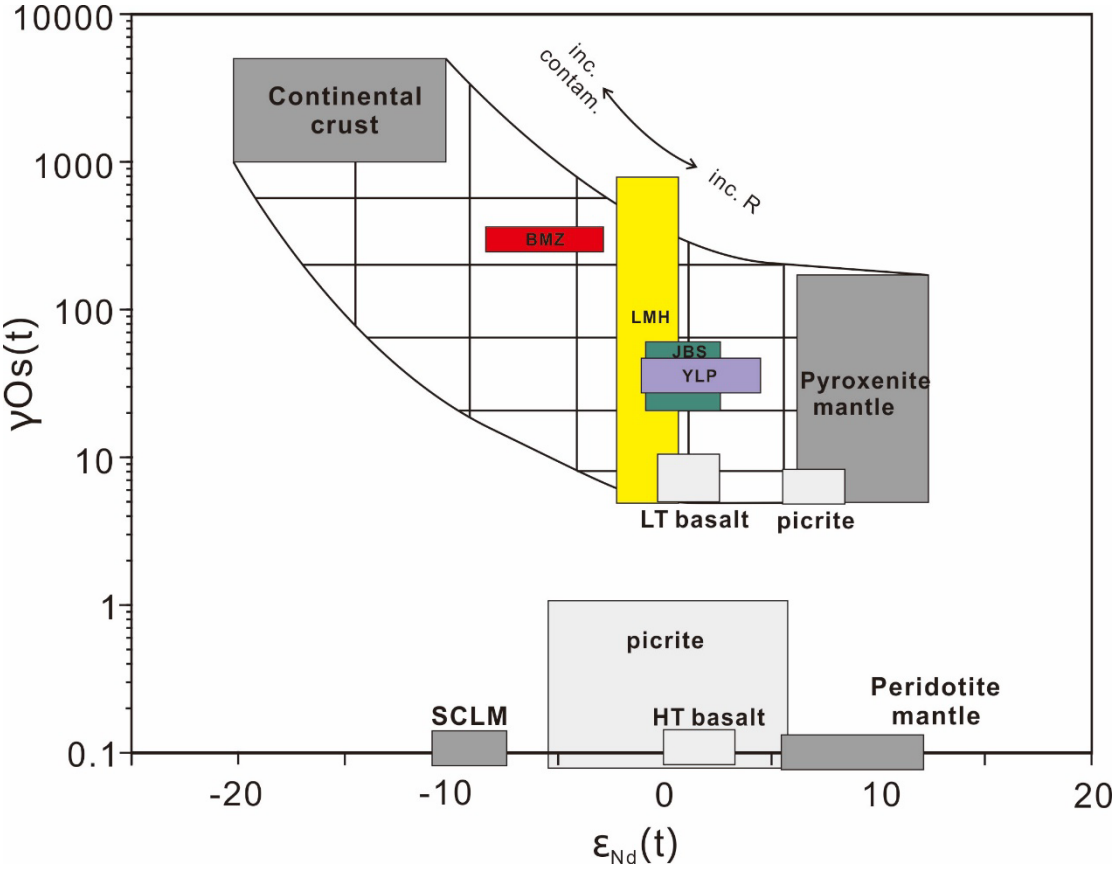
10000
1000
100
10
1
0.1
γOs(t)
-20
-10
0
10
20
εNd(t)
Continental crust
inc. contam.
inc. R
BMZ
LMH
JBS
YLP
Pyroxenite mantle
LT basalt
picrite
picrite
SCLM
HT basalt
Peridotite mantle

**Figure 11**

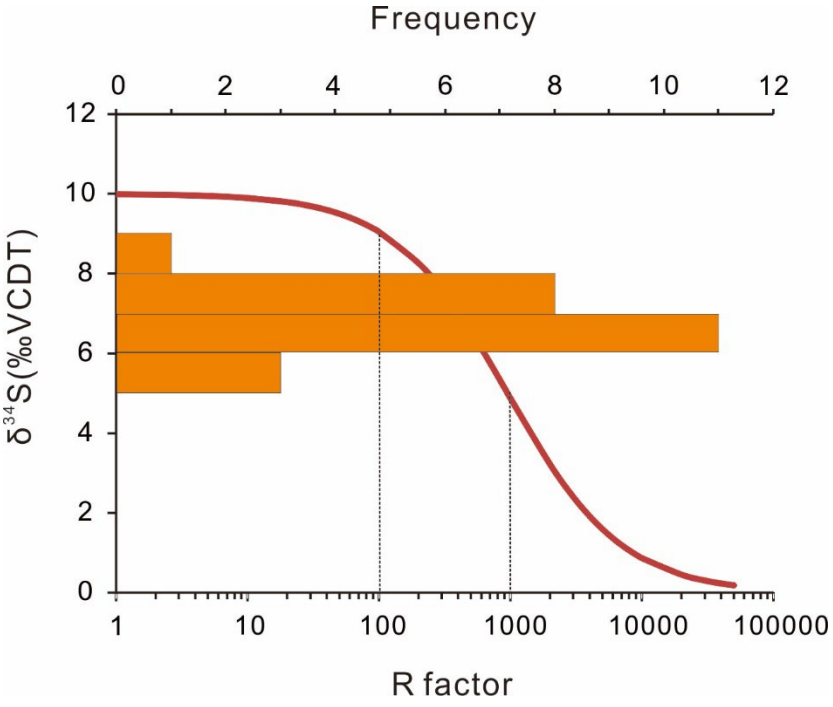
Frequency
0
2
4
6
8
10
12
δ34S(‰VCDT)
1
10
100
1000
10000
100000
R factor

**Figure 12**

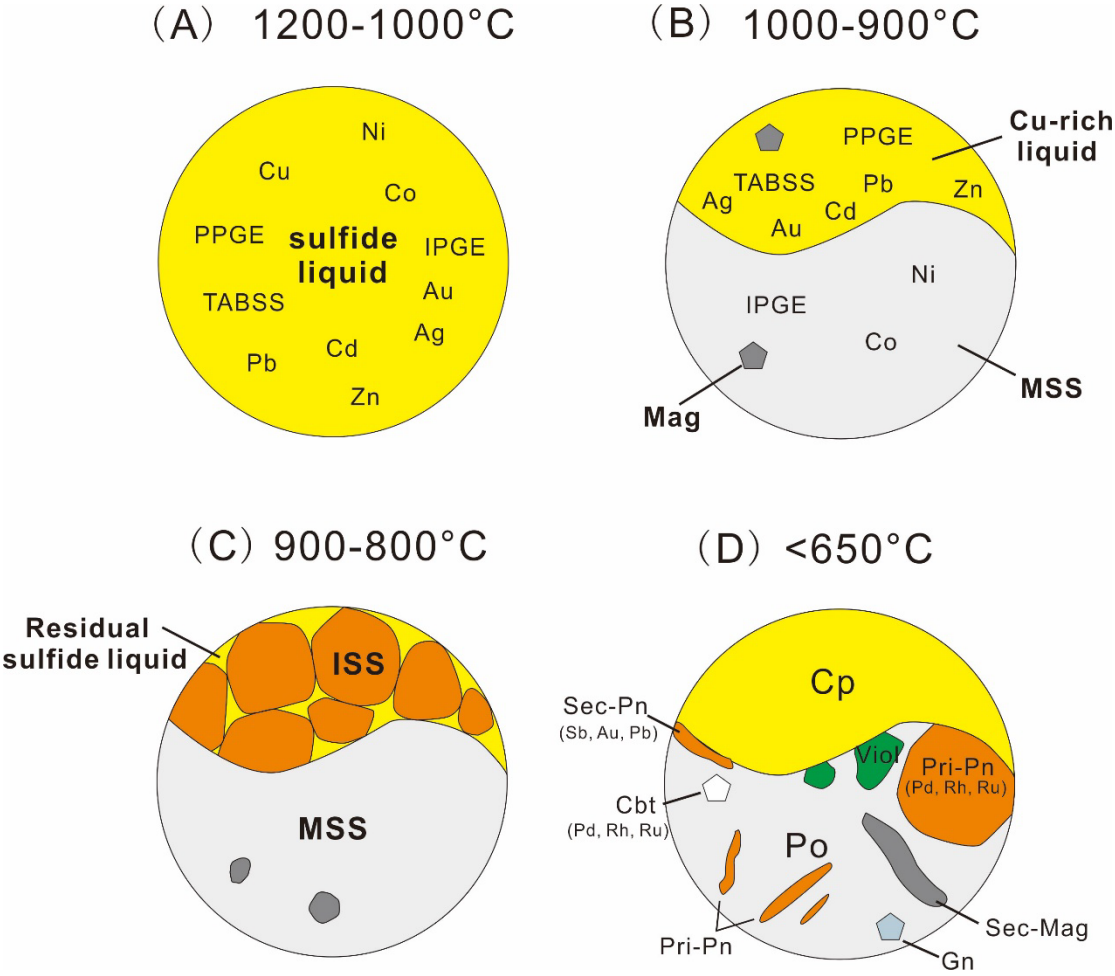
(A) 1200-1000°C
Ni
Cu
Co
PPGE
sulfide liquid
IPGE
TABSS
Au
Ag
Pb
Cd
Zn
(B) 1000-900°C
PPGE
Cu-rich liquid
TABSS
Pb
Zn
Ag
Cd
Au
Ni
IPGE
Co
MSS
Mag
(C) 900-800°C
Residual sulfide liquid
ISS
MSS
(D) <650°C
Cp
Sec-Pn
(Sb, Au, Pb)
Viol
Pri-Pn
(Pd, Rh, Ru)
Cbt
(Pd, Rh, Ru)
Po
Sec-Mag
Pri-Pn
Gn

**Figure 13**

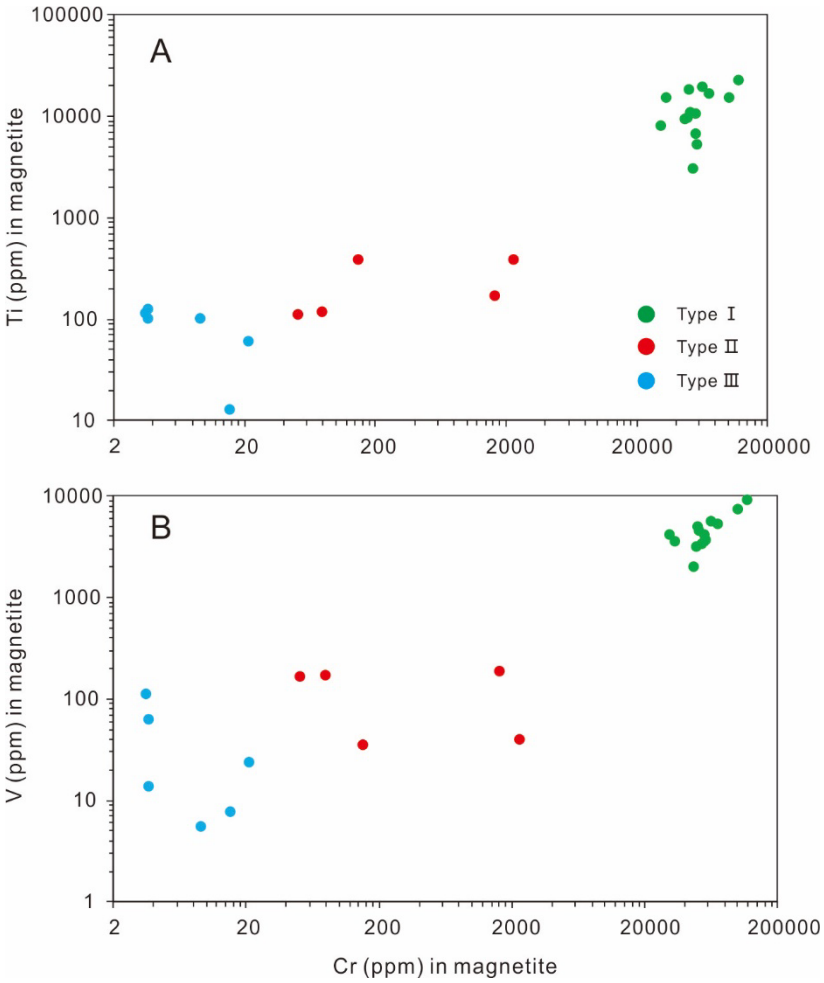
A
B
Ti (ppm) in magnetite
V (ppm) in magnetite
Cr (ppm) in magnetite
Type Ⅰ
Type Ⅱ
Type Ⅲ
100000
10000
1000
100
10
1
2
20
200
2000
20000
200000

**Figure 14**

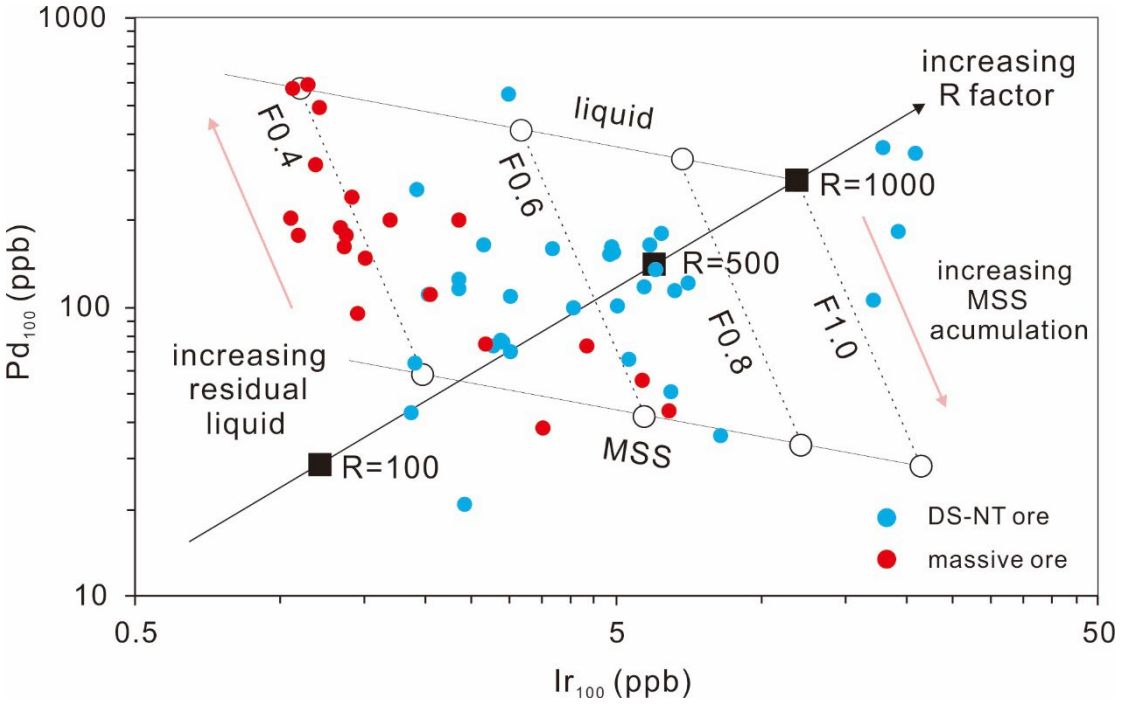
1000
100
10
0.5
5
50
Pd100 (ppb)
Ir100 (ppb)
increasing
R factor
liquid
F0.4
F0.6
F0.8
F1.0
R=1000
R=500
R=100
increasing
MSS
acumulation
increasing
residual
liquid
MSS
DS-NT ore
massive ore

**Figure 15**

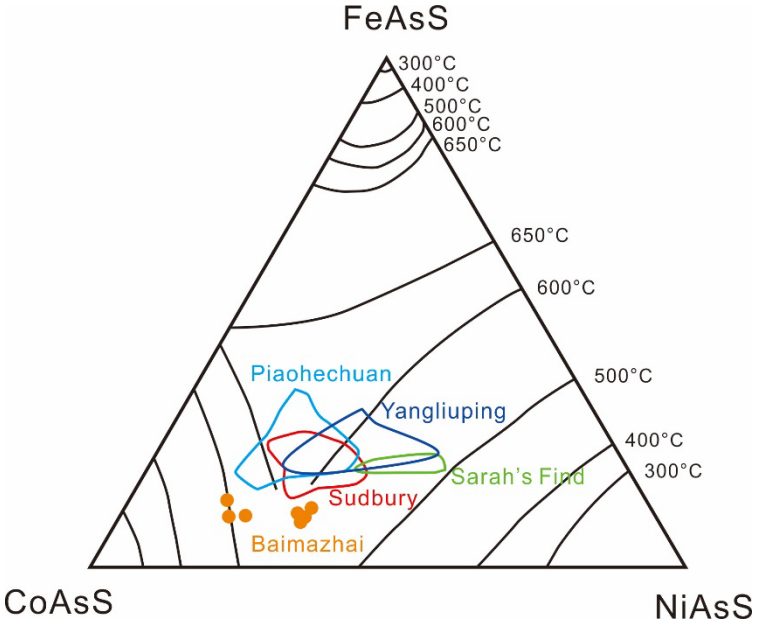
FeAsS
300°C
400°C
500°C
600°C
650°C
650°C
600°C
500°C
400°C
300°C
Piaohechuan
Yangliuping
Sarah's Find
Sudbury
Baimazhai
CoAsS
NiAsS

**Figure 16**

## Tables

**Table 1 S, Ni, Cu, Co and PGE concentrations in whole rocks from the Baimazhai deposit from this study, Wang et al. (2006), and Wang and Zhou (2006).**

| Ore type | Sample No. | S_ wt% | Pd_ ppb | Cu_ wt% | Pt_ ppb | Rh_ ppb | Ru_ ppb | Ni_ wt% | Ir_ ppb | Co_ ppm | References |
|---|---|---|---|---|---|---|---|---|---|---|---|
| DS-NT ore | BMZ-82 | 18.0 | 54.3 | 0.461 | 47.1 | 1.04 | 1.9 | 1.76 | 2.65 | 679 | |
| DS-NT ore | BMZ-84 | 10.6 | 44.3 | 0.157 | 22.3 | 0.43 | 0.94 | 1.05 | 1.34 | 411 | |
| DS-NT ore | BMZ-86 | 11.1 | 22 | 1.32 | 14 | 0.28 | 0.5 | 1.06 | 0.83 | 418 | |
| DS-NT ore | BMZ-88 | 15.3 | 46.6 | 2.44 | 28.5 | 0.35 | 0.56 | 1.32 | 0.95 | 513 | |
| DS-NT ore | BMZ-109 | 0.49 | 1.76 | 0.025 | 1.2 | 0.06 | 0.14 | 0.16 | 0.08 | 99 | |
| DS-NT ore | BMZ-111 | 6.03 | 17.4 | 0.525 | 14.6 | 0.35 | 0.4 | 0.659 | 0.32 | 334 | |
| DS-NT ore | BMZ-113 | 5.61 | 80.2 | 0.884 | 44.6 | 0.21 | 0.48 | 0.588 | 0.44 | 276 | |
| DS-NT ore | BMZ-115 | 0.62 | 2.6 | 0.054 | 1.52 | 0.06 | 0.13 | 0.108 | 0.06 | 119 | |
| DS-NT ore | BMZ-117 | 0.45 | 1.94 | 0.051 | 0.74 | 0.06 | 0.2 | 0.084 | 0.07 | 90.7 | |
| DS-NT ore | BMZ-119 | 0.23 | 0.69 | 0.012 | 0.23 | 0.02 | 0.1 | 0.045 | 0.04 | 98.4 | |
| DS-NT ore | BMZ-121 | 1.94 | 8.9 | 0.071 | 2.9 | 0.14 | 0.46 | 0.14 | 0.31 | 167 | Wang et al., 2006 Contrib. Miner. Petrol. |
| DS-NT ore | BMZ-123 | 1.02 | 1.72 | 0.041 | 0.98 | 0.08 | 0.26 | 0.09 | 0.14 | 108 | |
| DS-NT ore | BMZ-125 | 0.89 | 1.61 | 0.047 | 1.11 | 0.06 | 0.15 | 0.109 | 0.07 | 121 | |
| DS-NT ore | BMZ-127 | 0.97 | 1.83 | 0.046 | 0.76 | 0.06 | 0.16 | 0.108 | 0.07 | 112 | |
| DS-NT ore | BMZ-129 | 2.04 | 5.32 | 0.194 | 2.65 | 0.19 | 0.53 | 0.352 | 0.22 | 202 | |
| DS-NT ore | BMZ-131 | 1.19 | 2.35 | 0.075 | 1.02 | 0.08 | 0.19 | 0.156 | 0.09 | 128 | |
| DS-NT ore | BMZ-133 | 1.43 | 2.34 | 0.044 | 0.78 | 0.06 | 0.16 | 0.105 | 0.07 | 99.8 | |
| DS-NT ore | BMZ-135 | 0.39 | 1.56 | 0.017 | 0.97 | 0.03 | 0.15 | 0.054 | 0.05 | 88.7 | |
| DS-NT ore | BMZ-136 | 0.06 | 0.59 | 0.006 | 0.31 | 0.01 | 0.17 | 0.029 | 0.03 | 57.5 | |
| DS-NT ore | BMZ-71 | 0.04 | 0.19 | 0.002 | 0.08 | 0.01 | 0.05 | 0.005 | 0.02 | 23.5 | |
| DS-NT ore | BMZ-73 | 0.16 | 0.43 | 0.005 | 0.41 | 0.05 | 0.33 | 0.012 | 0.07 | 38.3 | |
| DS-NT ore | BMZ-75 | 0.16 | 0.63 | 0.006 | 0.18 | 0.01 | 0.06 | 0.014 | 0.02 | 41.6 | |
| DS-NT ore | BMZ-77 | 0.23 | 0.6 | 0.013 | 0.24 | 0.02 | 0.07 | 0.028 | 0.03 | 50.1 | |
| DS-NT ore | BMZ12-D2-B1 | 8.91 | 78.2 | 0.455 | 52.4 | 3.18 | 3.16 | 1.048 | 4.85 | 675 | This study |
| DS-NT ore | BMZ14-755-3 | 7.02 | 3.78 | 0.209 | 11 | 0.4 | 0.49 | 0.842 | 0.44 | 563 | |

| | | | | | | | | | | | |
|---|---|---|---|---|---|---|---|---|---|---|---|
| DS-NT ore | BMZ14-8 | 7.17 | 20.2 | 0.635 | 18.1 | 0.56 | 0.49 | 0.617 | 0.56 | 448 | |
| DS-NT ore | BMZ14-7 | 2.96 | 19.9 | 0.371 | 11.2 | 0.22 | 0.24 | 0.401 | 0.15 | 267 | |
| DS-NT ore | BMZ14-755-2 | 0.48 | 1.6 | 0.059 | 1.25 | 0.04 | 0.08 | 0.093 | 0.03 | 113 | |
| DS-NT ore | BMZ12-D2-B6 | 0.38 | 1.2 | 0.032 | 0.59 | 0.05 | 0.3 | 0.057 | 0.07 | 106 | |
| massive ore | BMZ-90 | 30.6 | 59.4 | 2.37 | 48.8 | 0.75 | 1.29 | 3.28 | 2.12 | 1035 | |
| massive ore | BMZ-91 | 29.8 | 154 | 3.06 | 59.6 | 0.43 | 1.34 | 3.07 | 1.84 | 1003 | |
| massive ore | BMZ-92 | 26.8 | 140 | 3.12 | 87.5 | 0.31 | 1 | 2.73 | 1.19 | 812 | |
| massive ore | BMZ-93 | 25.1 | 157 | 2.72 | 195 | 0.19 | 0.89 | 2.56 | 0.93 | 769 | |
| massive ore | BMZ-94 | 28.6 | 130 | 0.41 | 148 | 0.3 | 0.78 | 3.11 | 0.81 | 946 | |
| massive ore | BMZ-95 | 20.9 | 313 | 4.85 | 210 | 0.29 | 0.61 | 1.77 | 0.59 | 495 | |
| massive ore | BMZ-96 | 30.2 | 159 | 2.28 | 167 | 0.18 | 0.91 | 3.27 | 0.83 | 890 | |
| massive ore | BMZ-97 | 19.2 | 302 | 6.19 | 180 | 0.08 | 0.59 | 1.59 | 0.59 | 408 | Wang et al., 2006 Contrib. Miner. Petrol. |
| massive ore | BMZ-98 | 19.1 | 249 | 6.5 | 222 | 0.21 | 0.53 | 1.56 | 0.62 | 385 | |
| massive ore | BMZ-99 | 27.5 | 223 | 4.87 | 162 | 0.43 | 0.86 | 2.81 | 0.86 | 703 | |
| massive ore | BMZ-100 | 32.3 | 123 | 1.91 | 103 | 0.2 | 1.21 | 3.87 | 1.26 | 1001 | |
| massive ore | BMZ-101 | 31.7 | 78 | 0.88 | 104 | 0.39 | 1.46 | 3.95 | 1.2 | 1048 | |
| massive ore | BMZ-102 | 30.9 | 141 | 1.76 | 130 | 0.53 | 0.93 | 3.82 | 1.1 | 1001 | |
| massive ore | BMZ-103 | 32.1 | 156 | 2.31 | 159 | 0.43 | 1.44 | 3.68 | 1.12 | 972 | |
| massive ore | BMZ-104 | 30.9 | 130 | 2.44 | 163 | 0.27 | 1.01 | 3.64 | 1.1 | 990 | |
| massive ore | BMZ-105 | 32.2 | 91.8 | 2.26 | 71.1 | 0.76 | 1.48 | 3.76 | 1.72 | 1080 | |
| massive ore | BMZ-106 | 33.6 | 37.8 | 0.87 | 32.3 | 0.96 | 8.06 | 4.21 | 5.61 | 1266 | |
| massive ore | BMZ14-9 | 36.5 | 52.9 | 1.47 | 33.7 | 4.07 | 6.71 | 5.09 | 5.37 | 2820 | |
| massive ore | BMZ14-3 | 36.4 | 35.7 | 0.544 | 24.7 | 2.99 | 1.18 | 4.85 | 3.33 | 2758 | This study |
| massive ore | BMZ14-2 | 35.3 | 66.6 | 0.856 | 28.4 | 3.01 | 2.72 | 4.73 | 4 | 2589 | |

**Table 2 Maximum, minimum, and median values of metal contents for sulfides in the Baimazhai No.3 intrusion**

| Mineral | | Co ppm | Ni ppm | Cu ppm | Zn ppm | Se ppm | Mo ppm | Ru ppm | Rh ppm | Pd ppm | Ag ppm | Cd ppm | Sn ppm | Sb ppm | Pt ppm | Au ppm | Pb ppm | Bi ppm |
|---|---|---|---|---|---|---|---|---|---|---|---|---|---|---|---|---|---|---|
| Cbt | Max | 209000 | 112000 | 35000 | 53.3 | 98 | 20 | 2.81 | 8.9 | 152 | 30.1 | 5.2 | 2.64 | 1130 | 8.4 | 5.5 | 182 | 790 |
| | Min | 4300 | 1110 | 4 | 0.12 | <LLD | <LLD | 0.073 | 0.006 | 0.025 | 0.18 | <LLD | <LLD | 19.7 | <LLD | <LLD | 3 | 5.3 |
| | Median | 87350 | 31350 | 1683 | 11.3 | 13.7 | 1.75 | 1.11 | 0.43 | 6.3 | 2.32 | 2.33 | 1.44 | 112 | 7.6 | 2.86 | 13.4 | 64.8 |
| pri-Cp | Max | 31 | 570 | 480000 | 710 | 20.4 | <LLD | <LLD | <LLD | <LLD | 11.8 | 33 | 42.3 | 1.88 | <LLD | 0.39 | 104 | 54 |
| | Min | 1.13 | 59 | 256000 | 408 | <LLD | <LLD | <LLD | <LLD | <LLD | 7 | 16 | 3.98 | <LLD | <LLD | <LLD | 4.98 | 2.91 |
| | Median | 3 | 84.5 | 279000 | 522 | 17 | <LLD | <LLD | <LLD | <LLD | 9.6 | 25.7 | 21.3 | 1.21 | <LLD | 0.235 | 18.5 | 7.3 |
| sec-Cp | Max | 1470 | 21000 | 499000 | 102000 | 51.8 | 3.9 | <LLD | <LLD | <LLD | 181 | 8800 | 14.7 | 4.5 | <LLD | 0.34 | 260 | 40 |
| | Min | 1.39 | 50 | 145000 | 259 | <LLD | <LLD | <LLD | <LLD | <LLD | 12.2 | 10.6 | <LLD | <LLD | <LLD | <LLD | 2.57 | 0.79 |
| | Median | 5.28 | 132 | 317000 | 565 | 21.8 | 2.2 | <LLD | <LLD | <LLD | 78.5 | 29.4 | 2 | 1.64 | <LLD | 0.235 | 13.5 | 5.48 |
| pri-Pn | Max | 32100 | 429000 | 7900 | 8900 | 37 | 10.3 | 1.9 | 0.47 | 9.9 | 71 | 270 | 2.9 | 1.2 | <LLD | 0.17 | 104 | 110 |
| | Min | 400 | 12400 | <LLD | <LLD | <LLD | <LLD | <LLD | <LLD | <LLD | 0.54 | <LLD | <LLD | <LLD | <LLD | <LLD | 0.28 | 0.106 |
| | Median | 20150 | 249500 | 47.3 | 9.25 | 14.9 | 1.87 | 1.1 | 0.305 | 5.26 | 4 | 135 | 1.99 | 0.285 | <LLD | 0.17 | 16 | 12.4 |
| sec-Pn | Max | 29900 | 429000 | 44000 | 298 | 416 | 3.2 | 0.81 | 0.61 | 0.92 | 59 | 12.7 | 3.8 | 21.2 | <LLD | 0.53 | 480 | 48 |
| | Min | 232 | 3540 | <LLD | 3.6 | <LLD | <LLD | <LLD | 0.008 | <LLD | <LLD | <LLD | <LLD | 0.073 | <LLD | <LLD | 1.6 | 0.56 |
| | Median | 25300 | 306000 | 1130 | 6 | 53.1 | 1 | 0.62 | 0.076 | 0.215 | 20 | 1.62 | 0.149 | 2.27 | <LLD | 0.45 | 176 | 17.4 |
| pri-Po | Max | 1250 | 95000 | 50 | <LLD | 168 | 10.1 | <LLD | 0.24 | <LLD | 4.3 | 1.1 | 2.7 | 1 | <LLD | 0.07 | 123 | 102 |
| | Min | 87 | 2990 | <LLD | <LLD | <LLD | <LLD | <LLD | <LLD | <LLD | <LLD | <LLD | <LLD | <LLD | <LLD | <LLD | 0.77 | 1.13 |
| | Median | 154 | 7040 | 9.9 | <LLD | 19.3 | 2.7 | <LLD | 0.24 | <LLD | 0.735 | 1.1 | 1.89 | 0.73 | <LLD | 0.07 | 1.66 | 3.57 |
| sec-Po | Max | 1430 | 27300 | 20000 | 621 | 69.9 | 4.4 | <LLD | 0.35 | 0.54 | 9 | 0.82 | 0.108 | 5.4 | <LLD | <LLD | 67 | 1100 |
| | Min | 143 | 4880 | <LLD | <LLD | <LLD | <LLD | <LLD | <LLD | <LLD | 0.13 | <LLD | <LLD | <LLD | <LLD | <LLD | 0.299 | 1.59 |
| | Median | 813 | 12155 | 11.5 | 12 | 21.9 | 2.65 | <LLD | 0.31 | 0.54 | 0.595 | 0.82 | 0.108 | 0.68 | <LLD | <LLD | 4.38 | 5.32 |
| sec-Viol | Max | 158000 | 383000 | 4800 | 224 | 232 | 4.12 | 9 | 0.25 | 4.33 | 248 | 11.7 | <LLD | 63.7 | <LLD | 6.26 | 1260 | 57 |
| | Min | 14300 | 105000 | 7.4 | <LLD | <LLD | <LLD | <LLD | <LLD | <LLD | 0.04 | <LLD | <LLD | 0.68 | <LLD | <LLD | 8.1 | 1.62 |
| | Median | 25100 | 251000 | 58.2 | 24.6 | 32.5 | 2.55 | 1.49 | 0.25 | 1.44 | 12.2 | 3.6 | <LLD | 13.8 | <LLD | 1.74 | 265 | 11.5 |

**Table 3 Ti, V, and Cr contents of magnetite in the Baimazhai No.3 intrusion**

| Spot | Type | Ti_ppm | V_ppm | Cr_ppm |
|---|---|---|---|---|
| BMZ-2-2 area 4 mg1 | primary | 14900 | 7290 | 100500 |
| BMZ-2-2 area 4 mg2 | primary | 7950 | 4180 | 30600 |
| BMZ-2-2 area 5 mg3 | primary | 10630 | 4080 | 55800 |
| BMZ-2-2 area 5 mg4 | primary | 10890 | 4470 | 51300 |
| BMZ-2-2 area 1 mg5 | primary | 6670 | 3550 | 56400 |
| BMZ-2-2 area 1 mg6 | primary | 5210 | 3660 | 57200 |
| BMZ-3-1 area 1 mg1 | primary | 14900 | 3520 | 33600 |
| BMZ-3-1 area 1 mg2 | primary | 9600 | 3140 | 49200 |
| BMZ-3-1 area 2 mg3 | primary | 9190 | 1960 | 46700 |
| BMZ-3-1 area 5 mg4 | evolved | 381 | 39.1 | 2260 |
| BMZ-3-1 area 5 mg5 | evolved | 387 | 35.1 | 149 |
| BMZ-3-2 area 1 mg 1 | primary | 19100 | 5550 | 63300 |
| BMZ-3-2 area 1 mg 2 | primary | 17900 | 4910 | 49400 |
| BMZ-3-2 area 1 mg 3 | primary | 22200 | 8990 | 118600 |
| BMZ-3-2 area 3 mg 4 | primary | 16500 | 5190 | 71400 |
| BMZ-3-2 area 4 mg 5 | primary | 3050 | 3350 | 54000 |
| BMZ-3-2 area 5 mg 6 | evolved | 170 | 188 | 1620 |
| BMZ-3-2 area 5 mg 7 | evolved | 116 | 171 | 79 |
| BMZ-3-2 area 5 mg 8 | evolved | 109 | 165 | 51.1 |
| BMZ-8-1 area 1 mg1 | secondary | 123 | 62 | 3.7 |
| BMZ-8-1 area 1 mg2 | secondary | 113 | 112 | 3.5 |
| BMZ-8-1 area 2 mg3 | secondary | 101 | 5.5 | 9.1 |
| BMZ-8-1 area 2 mg4 | secondary | <LLD | 2.9 | <LLD |
| BMZ-8-1 area 2 mg5 | secondary | 101 | 13.5 | 3.7 |
| BMZ-8-2 area 1 mg 1 | secondary | 59 | 23.3 | 21.2 |
| BMZ-8-2 area 1 mg 2 | secondary | 12.8 | 7.6 | 15.3 |
| BMZ-8-2 area 2 mg 3 | secondary | 107 | 12 | <LLD |
| BMZ-8-2 area 2 mg 4 | secondary | 89 | 13.6 | <LLD |

**Table 4 S isotope compositions of the Baimazhai deposit from this study, Zhang (2006), and Wang et al. (2018)**

| Rock/Ore type | Sample No. | Mineral | $\delta^{34}S$（VCDT‰） | References |
|---|---|---|---|---|
| sedimentary sulfide | BMZ14-1 | Whole rock | 10 | |
| massive | BMZ14-3 | Whole rock | 6.5 | |
| net-textured | BMZ14-755-3 | Whole rock | 6.8 | This study |
| disseminated | BMZ14-7 | Whole rock | 5.8 | |
| sandstone | BMZ14-755-1 | Whole rock | 6.3 | |
| massive | BM4 | Po | 6.81 | |
| massive | BM4 | Mag | 7.23 | |
| massive | BM4 | Pn | 7.59 | |
| massive | BM4 | Ccp | 6.68 | |
| massive | BM-7 | Mag | 7.2 | Zhang, 2006 |
| massive | BM-7 | Po | 6.82 | |
| massive | BM-7 | Po | 7.01 | |
| disseminated | BM-19 | Mag | 7.23 | |
| disseminated | BM-19 | Po | 7.38 | |
| net-textured | BMZ-82 | Po | 6.7 | |
| net-textured | BMZ-82 | Pn | 7.1 | |
| net-textured | BMZ-82 | Cpy | 6.5 | |
| net-textured | BMZ-88 | Po | 6.8 | |
| net-textured | BMZ-88 | Pn | 7.1 | |
| net-textured | BMZ-88 | Cpy | 6 | |
| disseminated | BMZ-125 | Po | 6.7 | Wang et al., 2018 Asian Earth Sci. |
| disseminated | BMZ-125 | Pn | 7.4 | |
| disseminated | BMZ-125 | Cpy | 6.5 | |
| disseminated | BMZ-80 | Po | 7 | |
| disseminated | BMZ-80 | Pn | 6 | |
| disseminated | BMZ-80 | Cpy | 6.5 | |
| disseminated | BMZ-187 | Py | 8.6 | |
| disseminated | BMZ-187 | Cpy | 7.3 | |

# Chapter 4: Geochemistry and genesis of magmatic Ni-Cu-(PGE) and PGE-(Cu)-(Ni) deposits in China

**Yiguan Lu[1,2,3,*], C. Michael Lesher[1], Jun Deng[2]**

[1] Mineral Exploration Research Centre, Harquail School of Earth Sciences, Goodman School of Mines, Laurentian University, 935 Ramsey Lake Road, Sudbury, Ontario P3E 2C6, Canada

[2] State Key Laboratory of Geological Processes and Mineral Resources, China University of Geosciences, Beijing 100083, China

[3] Current Address: Tianjin Center, China Geological Survey, Tianjin 300170, China

* Corresponding Author email: mlesher@laurentian.ca;

## 4.1 Abstract

Magmatic sulfide deposits can be subdivided into: 1) Ni-Cu-PGE deposits, which have relatively smooth mantle-normalized metal patterns; 2) Ni-Cu-(PGE) deposits, which are depleted in PGE relative to Ni-Cu-Co; and 3) PGE-(Cu)-(Ni) deposits, which are enriched in PGE relative to Ni-Cu-Co. China contains almost exclusively deposits in the second group, including the world's largest semi-continuous ore body (Jinchuan) and the largest known deposit in a possible arc setting (Xiarihamu), but which are less common elsewhere (e.g., Pechenga, Voisey's Bay). Unlike other magmatic Ni-Cu-PGE, Ni-Cu-(PGE), and PGE-(Cu)-(Ni) deposits, many of which are Neoarchean or Paleo-Mesoproterozoic and formed primarily in rifted-related settings, all known Chinese deposits are younger (some Neoproterozoic, but mainly mid-late Paleozoic) and many are inferred to have formed in settings that previously experienced subduction. Based on mineralization age, tectonic setting, and spatial distribution, most deposits occur

in three tectono-magmatic settings: 1) Neoproterozoic belts related to the breakup of the Rodinian supercontinent (e.g., Jinchuan, Zhouan); 2) Devonian to Triassic magmatism in the Central Asian (CAOB) and East Kunlun (EKOB) orogenic belts (e.g., Huangshan, Hongqiling, Kalatongke, Xiarihamu); and 3) the late Permian Emeishan large igneous province (ELIP) (e.g., Jinbaoshan, Zhubu, Baimazhai). Many deposits (Huangshandong, Huangshannan, Huangshanxi, Jinchuan, Jingbulake, Kalatongke #1, Hongqiling #1, Limahe, Qingkuangshan, Zhubu) are hosted by small intrusions with diamond-shaped surface sections and funnel-shaped cross sections that have been interpreted to represent subvertical transtensional structures, but which are asymmetrically differentiated and are more likely sections through subhorizontal blade-shaped dikes. A few are hosted by subhorizontal chonoliths (e.g., Kalatongke #2). Only a few are hosted by subhorizontal sills (e.g., Jinbaoshan, Yangliuping). Mineral chemical, whole-rock lithogeochemical, ore geochemical, and S-Nd-Sr-Os isotopic data for 18 typical deposits are used here to aid in the assessment of their genesis and metallogeny. Most deposits in orogenic belts appear to be hosted by rocks derived from magmas generated from subduction-enriched, but originally depleted mantle sources with minor crustal contamination. Most deposits in the ELIP appear to be hosted by rocks derived from magmas generated from subduction-enriched, but originally more enriched mantle sources with variable degrees of crustal contamination. Deposits related to the breakup of Rodinia exhibit transitional geochemical characteristics. Relatively high Ni-Cu-Co and relatively low PGE tenors, high-Ni in olivine at a given Fo content, high $\gamma$Os, and intermediate $\varepsilon$Nd values suggest that many Chinese Ni-Cu-(PGE) deposits were derived by melting Ni-Co-Cu-rich PGE-poor pyroxenitic mantle, most likely produced by interaction of recycled oceanic crust with depleted mantle peridotite. Variable PGE tenors that correlate inversely with $\delta^{34}S$ and $\gamma$Os values suggest that most deposits formed at low-moderate (10-1000) magma:sulfide mass ratios (R factors). Some deposits exhibit fractionations of $Ni_{100}$-$Co_{100}$-$IPGE_{100}$ from $Cu_{100}$-$Au_{100}$-$PPGE_{100}$ (metals in 100% sulfides) indicating that the sulfide melts experienced variable degrees of MSS fractionation/accumulation. Compared to Archean and Proterozoic magmatic Ni-Cu-PGE deposits elsewhere in the world, most of which appear to have formed primarily in rifted continental and rifted continental margin settings and to have been derived from peridotitic mantle, most of the Phanerozoic Ni-Cu-(PGE) deposits in China appear to have formed in convergent or formerly convergent settings and to have had variable amounts of metasomatized pyroxenitic mantle in their sources.

**Key words**: magmatic sulfide deposits; Ni-Cu-(PGE), Ni-Cu-PGE, PGE-(Cu)-(Ni), tectonic setting;

pyroxenitic mantle; ore genesis; China

## 4.2 Introduction

Magmatic sulfide deposits can be subdivided into: 1) Ni-Cu-PGE deposits, which have relatively smooth mantle-normalized Ni-Cu-Co-PGE metal patterns (e.g., Duluth, Kambalda-Mt Keith-Perseverance, Noril'sk-Talnakh, Raglan, Sudbury, Thompson); 2) Ni-Cu-(PGE) deposits, which are depleted in PGE relative to Ni-Cu-Co (e.g., Jinchuan, Pechenga, Voisey's Bay); and 3) PGE-(Cu)-(Ni) deposits, which are enriched in PGE relative to Ni-Cu-Co (e.g., Bushveld, Great Dyke, Stillwater). Together, these deposits contain 56% of global Ni resources (the remainder are in lateritic deposits) and 96% of global PGE resources (Mudd and Jowitt 2014; Barnes et al., 2017).

Giant Ni-Cu-PGE, Ni-Cu-(PGE), and PGE-(Cu)-(Ni) deposits/camps are distributed unevenly and significant deposits have been discovered in only a few countries (Australia, Canada, China, Russia, South Africa, USA) (Naldrett, 2004, 2010, 2011). Chinese resources in 2017 (USGS) were 2.5 Mt Ni (3.2% of global Ni resources) and 28 Mt Cu (3.9% of global Cu resources). Most Chinese deposits are relatively small (<1 Mt Ni, except Jinchuan and Xiarihamu), have relatively low grades (<1% Ni, except Hongqiling) (**Table 1**, **Fig. 1**), and are variably depleted in PGE relative to Ni-Cu-Co. Magmatic Ni-Cu-(PGE) and PGE-(Cu)-(Ni) deposits in China account for 93% of total Ni resources (Sun et al., 2015), 6.4% of total Cu resources (Ying et al., 2014), and more than 98% of total PGE resources (Zhou et al., 2002a).

Although the super-giant Noril'sk-Talnakh deposits formed at the Permian-Triassic boundary, most of the world's largest Ni-Cu-PGE, Ni-Cu-(PGE), and PGE-(Cu)-(Ni) deposits formed in the Neoarchean (e.g., Kambalda-Mt Keith-Perseverance, Great Dyke), Paleoproterozoic (e.g., Bushveld, Pechenga, Sudbury, Thompson), and Mesoproterozoic (e.g., Duluth, Voisey's Bay). The Jinchuan and Zhouan Ni-Cu-(PGE) deposits in China formed in the Neoproterozoic, but all other known Ni-Cu-(PGE) and PGE-(Cu)-(Ni) deposits in China formed between the Early Devonian and Late Triassic (**Table 1**)

Like many Ni-Cu-PGE and Ni-Cu-(PGE) deposits worldwide, most Ni-Cu-(PGE) deposits in China are hosted by relatively small mafic-ultramafic intrusions. The Jinchuan Ni-Cu-(PGE) deposit, the largest single originally semi-continuous magmatic sulfide deposit in the world, occurs in a steeply-dipping

intrusion with a surface cross-section of only 1.34 $km^2$ (Tang et al., 2009, 2012). Like some Ni-Cu-PGE deposits elsewhere in the world (e.g., Aguablanca, Ban Phuc Eagle, Expo-Méquillon, Santa Rita), many of the Ni-Cu-(PGE)-bearing intrusions in China have diamond-shaped surface sections and funnel-shaped cross sections (e.g., Huangshandong, Huangshannan, Huangshanxi, Jinchuan, Jingbulake, Kalatongke #1, Hongqiling #1, Limahe, Qingkuangshan, Zhubu) and have been interpreted to have filled subvertical transtensional features (Lightfoot and Evans-Lamswood, 2015).

The geology, mineralogy, petrology, geochemistry, and isotope geochemistry of Chinese Ni-Cu-(PGE) have been reported extensively in the literature (e.g., Zhou et al., 2002a, 2008; Song et al., 2009, 2012, 2016; Li et al., 2005, 2012; Wang et al., 2018). However, most papers describe single deposits or several deposits in a single region, leading to divergent interpretations regarding their genesis and metallogenesis. In particular, there is no interpretation of why Chinese Ni-Cu-(PGE) deposits as a whole are so different from those in other areas.

To aid in the interpretation of these deposits, we have compiled mineral chemical, whole-rock lithogeochemical, ore geochemical, and S-Nd-Sr-Os isotopic data from 18 representative Ni-Cu-(PGE) and PGE-(Cu)-(Ni) deposits in China and use the data to generate a comparative view that provides better constraints on the genesis and metallogenesis of Chinese Ni-Cu-(PGE) and PGE-(Cu)-(Ni) deposits.

## 4.3 Geological, Temporal, and Spatial Distribution

There are at least 80 magmatic Ni-Cu-(PGE) and PGE-(Cu)-(Ni) deposits in China, including two giant deposits, 14 large deposits, 20 intermediate deposits, and many small deposits and occurrences (Lu et al., 2007). Some of the larger and more important deposits are shown in **Figure 2**. Some appear to be isolated (e.g., Jinchuan), but many occur as clusters of individual deposits in the same area. For example, the Huangshan camp in the Eastern Tianshan district of the Xinjiang province includes several large- to medium-sized deposits, including Huangshandong, Huangshannan, and Huangshanxi, and the Pobei camp in the Beishan district of the Xinjiang province includes several cogenetic intrusions, including Poyi, Posan, Poqi, and Poshi. Bulk tonnages, bulk Ni grades, and contained Ni for Chines Ni-Cu-(PGE) and PGE-(Cu)-(Ni) deposits are shown in **Figure 1**. The resources for many deposits are not well characterized and many are low-grade deposits, but we include all for which we have data.

China is a collage of cratons and fragmental continental blocks and arcs, welded by ophiolitic mélange (Deng et al., 2014a, 2014b, 2017). The principal tectonic provinces of China are shown in **Figure 2**. The formation ages of the main magmatic sulfide deposits in China range from Neoproterozoic to Triassic with peaks in the Neoproterozoic and Permian (**Fig. 3**). The Neoproterozoic deposits occur along the margin of the North China Craton (e.g., Jinchuan) and the Yangtze Craton (e.g., Zhouan, Lengshuiqing). The Permian deposits occur mainly in the Central Asian Orogenic Belt (e.g., Huangshan, Tianyu, Kalatongke, Pobei) and the Emeishan Large Igneous Province (e.g., Baimazhai, Jinbaoshan, Limahe, Yangliuping, Zhubu). These locations represent rifted continental margins (e.g., Jinchuan), subduction and post-subduction of orogenic belts (e.g., Heishan, Huangshan, Kalatongke), and mantle plumes (e.g., Baimazhai, Jinbaoshan, Zhubu). Thus, based on mineralization age, tectonic setting, and spatial distribution, most deposits occur in three tectono-magmatic settings (Zhou et al., 2004; Lu et al., 2007; Sun et al., 2015): 1) Neoproterozoic deposits related to magmatic activity accompanying breakup of Rodinia (e.g., Jinchuan, Lengshuiqing, Zhouan); 2) Devonian to Triassic deposits related to post-collisional extension and magmatism in the orogenic settings (e.g., Chajianling, Erbutu, Jingbulake, Heishan, Hongqiling, Huangshan, Kalatongke, Lashuixia, Piaohechuan, Tianyu, Xiarihamu); and 3) Permian deposits related to plume magmatism in the Emeishan Large Igneous Province (e.g., Baimazhai, Jinbaoshan, Limahe, Yangliuping, Zhubu).

### 4.3.1 Neoproterozoic deposits related to breakup of Rodinia

The supercontinent Rodinia assembled 1.3-0.9 billion years ago and broke up 750-600 million years ago, triggered by an 830-820 Ma mantle plume beneath South China (Li et al., 1999, 2003, 2008). According to Wang and Mo (1995), the North China, Tarim, and Yangtze Cratons appear to have been geographically closed during the assembly of the Rodinia supercontinent by ~1.0 Ga. The Ni-Cu-(PGE) deposits in the Baotan district, Guangxi province have been dated at 982 ± 21 Ma by whole-rock Re-Os n-TIMS methods, interpreted to represent an event that occurred during late assembly or early breakup of Rodinia (Mao and Du, 2001). The ~828 Ma Jinchuan and ~817 Ma Lengshuiqing Ni-Cu-(PGE) deposits have been interpreted to be related to a 830-820 mantle superplume accompanying the main phase of breakup of Rodinia (Li et al., 2005; Yang et al., 2005; Zhu et al., 2007; Zhang et al., 2010) and the ~637 Zhouan Ni-Cu-(PGE) deposit may represent the last magmatism related to the breakup of the Rodinia supercontinent in the Neoproterozoic in the northern margin of the Yangtze Craton (Wang et al., 2013a).

The Jinchuan intrusion is located in the uplifted Longshoushan Terrane along the southwestern margin of the North China Craton. It intrudes Proterozoic (>2 Ga) upper amphibolite facies orthogneisses, paragneisses, and marbles of the Baijiazhuizi Formation (Tang and Li, 1995; Lehmann et al., 2007; Tonnelier, 2010). There are four major groups of faults at Jinchuan: 1) steeply-dipping NW-SE striking regional thrust faults, 2) steeply-dipping NEE-SWW striking sinistral strike-slip faults, 3) NNW-SSE striking dextral strike-slip faults, and 4) steeply-dipping NE-SW striking normal faults, the second group of which divides the intrusion into four segments (from west to east): Mining Areas III, I, II, and IV (Tang, 1993; Tang and Li, 1995; Song et al., 2012).The predominant rock types in the Jinchuan intrusion are heteradcumulate olivine-sulfide (net-textured mineralization), mesocumulate lherzolite, orthocumulate olivine websterite, and minor plagioclase lherzolite and gabbro (Tonnelier, 2010; Duan et al., 2016). Zircons from a dolerite dike cutting the intrusion and a lherzolite sample from the intrusion have been dated at 828 ± 3 Ma and 831 ± 0.6 Ma, respectively by U-Pb SHRIMP and U-Pb ID-TIMS single zircon methods, suggesting that the emplacement of the Jinchuan intrusion was related to the breakup of Rodinia (Li et al., 2005; Zhang et al., 2010).

The Zhouan intrusion is located along the northern margin of the Yangtze Block (Wang et al., 2013a, 2013b). Is it one of numerous mafic-ultramafic bodies occurring in the Southern Qinling orogenic belt and along margin of Yangtze Craton, which range 820-632 Ma in age and which are considered to have formed from a magma derived from upwelling asthenosphere mantle during Neoproterozoic extension related to breakup of Rodinia in that region (Gao et al., 1992, 1996; Li et al., 2003; Zeng et al., 2016). The Zhouan intrusion, dated at 637±4 Ma and associated with several other ~635 Ma mafic-ultramafic intrusions in the Suizao basin, appears to represent some of the last magmatism related to the breakup of Rodinia along the northern margin of the Yangtze Craton (Wang et al., 2013a). The intrusion is a 2450 m long sill-like body that is 700 m wide in the western part and 1500 m wide in the eastern part. It consists of lherzolite and olivine gabbronorite and intrudes the Meso- to Neoproterozoic Zhujiashan Formation, which is overlain by 30-120 m thick Cenozoic sedimentary rocks (Wang et al., 2013b).

### 4.3.2 Permian to Triassic deposits in the Central Asian Orogenic belt (CAOB) and an early Devonian deposit in the East Kunlun Orogenic belt

The Central Asian Orogenic Belt (CAOB) extends over 5000 km, from the Urals Mountains in Russia in the west through Kazakhstan, Uzbekistan, Tajikistan, Kyrgyzstan, the Xinjiang province in northwestern

China, and parts of Mongolia and Inner Mongolia to Northeast China (**Fig. 2**). It is a complex collage containing continental fragments, island arc assemblages, remnants of oceanic crust, and continental margins that is sandwiched between the Siberian craton to the north and the Tarim-North China craton to the south. It appears to have formed by multiple subduction-accretion and collision processes between the Neoproterozoic and Late Paleozoic, and contains considerable amounts of Cu, Au, Pb-Zn, and Ni-Cu-(PGE) mineralization (Sengör et al., 1993; Xiao et al., 2003, 2008, 2009; Windley et al., 2007; Xie et al., 2014; Deng and Wang, 2016). The CAOB in China can be subdivided into a western Tianshan-Altay segment (Mao et al., 2008) and an eastern segment in Inner Mongolia and northeastern China (Zhou and Wilde, 2013). Both parts contain numerous mafic-ultramafic intrusions, most of which appear to have formed in the late Permian to Triassic (e.g., Huangshan, Kalatongke, Pobei, Tianyu, Hongqiling, Piaohechuan), although some intrusions and minor magmatic sulfide deposits formed in the Silurian and Carboniferous, including the ~431 Ma Jingbulake Ni-Cu-(PGE) deposit and the ~357 Ma Heishan Ni-Cu-(PGE) deposit (Yang and Zhou, 2009; Xie et al., 2014).

The western part of the CAOB can be subdivided into 4 areas from north to south: 1) The Altay orogenic belt is bounded to the south by the Ulungar fault and the Junggar block and to the north by the Sayan and associated belts, and has been interpreted to represent a late Cambrian to Carboniferous magmatic arc built upon a microcontinent (Sengör et al., 1993; Windley et al., 2002; Xiao et al., 2009). The ~287 Ma Kalatongke Ni-Cu-(PGE) deposit is located in this belt, hosted in a mafic intrusion consisting of norite, troctolite, gabbro, and diorite (Han et al., 2004; Gao et al., 2012). 2) The Eastern Tianshan district is located between the Junggar block and Tarim block and contains ~120 mafic-ultramafic intrusions, at least six of which host significant Ni-Cu-(PGE) mineralization, including the Huangshandong, Huangshanxi, Huangshannan, Hulu, Tulaergen, and Xiangshan deposits (Zhou et al., 2004; Mao et al., 2008; Qin et al., 2011; Gao et al, 2012; Tang et al., 2012). It is considered to be the most important Ni-Cu-(PGE) belt in northwestern China and great success has been achieved recently in the exploration for additional mineralization in this district (Mao et al., 2008; Han et al., 2010; Tang et al., 2012). 3) The Central Tianshan district is located between the Kawabulak fault, which marks the northern boundary of the South Tianshan orogen and the Aqikkuduk fault, which marks the southern boundary of the Jueluotage orogenic belt (Chai et al., 2008; Song et al., 2013). Several mafic-ultramafic intrusions occur on the southern side of the Shaquanzi fault, some of which contain Ni-Cu-(PGE) mineralization, including the ~280 Ma Tianyu and ~281 Ma Baishiquan deposits (Tang et al., 2009; Mao et al., 2006).

4) The Beishan district is an E-W trending mountain range located along the northeastern margin of the Tarim Craton, associated with several mafic-ultramafic intrusions containing significant Ni-Cu-(PGE) mineralization. The Pobei complex is the largest and is composed of a gabbroic unit and two ultramafic bodies (Poshi and Poyi). Zircon U-Pb dates range from 270 to 278 Ma and it is considered to have formed by multiple pulses of olivine and sulfide-charged magma (Li et al., 2006; Yang et al., 2014; Xue et al., 2016).

The Hongqiling-Chajianling-Piaohechuan district in the most eastern part of the CAOB contains nearly 200 mafic-ultramafic intrusions, many of which have been dated between ~216 and ~239 Ma and contain Ni-Cu-(PGE) mineralization (Wu et al., 2004; Hao et al., 2014; Wei et al., 2015). The ~216 Ma Hongqiling Ni-Cu-(PGE) deposit, the largest in this district and prior to 2006 the second largest producer of Ni after Jinchuan (Lu et al., 2011; Wei et al., 2013), is located in the southeastern part of the CAOB adjacent to the North China Craton, and is composed mainly of orthopyroxenite, harzburgite, and norite (Wei et al., 2013). The ~216 Ma Piaohechuan Ni-Cu-(PGE) deposit occurs 80 km northeast of Hongqiling (Lu et al., 2007) and is hosted by a very small (~0.07 $km^2$) intrusion composed of hornblende-olivine gabbro and hornblende gabbro (Wei et al., 2015).

The 431-405 Ma (Li et al., 2015; Peng et al., 2016; Song et al., 2016) Xiarihamu Ni-Cu-(PGE) deposit was discovered in 2011 by the Qinghai Bureau of Geology and Mineral Resources during a regional exploration program for hydrothermal base and precious metal mineralization in the East Kunlun orogenic belt. The East Kunlun orogenic belt merges with the Qinling-Dabie orogenic belt in the east, separating the North China Craton and South China Block (Li et al., 2015; Yang et al., 2015a, 2015b). The Xiarihamu deposit is not only the second largest Ni-Cu deposit in China (after Jinchuan) but is also the largest magmatic Ni-Cu±PGE deposit discovered thus far in a possible arc setting (Li et al., 2015; Song et al., 2016). The host intrusion is ~500 m wide and 1600 m long and is composed of lherzolite and olivine websterite with minor dunite, websterite, and orthopyroxenite. Mineralization occurs mainly as disseminated to net-textured zones within the ultramafic body and near the contact with older gabbro (Li et al., 2015; Zhang et al., 2017). The age suggests a genetic linkage with Early Devonian regional magmatism (Song et al., 2016).

### 4.3.3 Permian deposits in the Emeishan Large Igneous Province

The ~260 Ma Emeishan Large Igneous Province (ELIP) is located along the western margin of the Yangtze craton in southern China and is composed of voluminous flood basalts and associated mafic-ultramafic intrusions extending over an area of ~$3\times10^5$ $km^2$ (Xu et al., 2001, 2004; Zhou et al., 2002b, 2008; Deng et al., 2010; Wang et al., 2007, 2011; Li et al., 2016). It is bounded to the west by the Ailaoshan-Red River (ASRR) fault and to the northwest by the Longmenshan-Xiaojinghe River fault (Xu and Chung, 2001). ELIP basalts can be geochemically subdivided into low-Ti and high-Ti types based on Ti contents and Ti/Y values (Xu et al., 2001; Xiao et al., 2004). The high-Ti basalts have been linked to Fe-Ti-V oxide deposits (e.g., Panzhihua), whereas the low-Ti basalts have been linked to Ni-Cu-(PGE) magmatic sulfide deposits (Zhou et al., 2008; Wang et al., 2011, 2018). The ELIP hosts a wide variety of magmatic sulfide deposits in China, including Ni-Cu-(PGE) deposits (e.g., Baimazhai, Limahe, Qingkuangshan, Yangliuping, Zhubu) and one PGE-(Cu)-(Ni) deposit (e.g., Jinbaoshan) (Zhou et al. 2002b; Song et al., 2003; Wang and Zhou et al., 2006; Tao et al., 2008; Song et al., 2008; Wang et al., 2010; Zhu et al., 2011; Lu et al., 2014).

The ~260 Ma Jinbaoshan PGE-(Cu)-(Ni) deposit is located in the central zone of the ELIP and is the largest PGE-(Ni)-(Cu) deposit in China (**Table 1**). It is hosted by a sill-like ultramafic intrusion that is ~5 km long, up to 1.2 km wide, and up to 170 m thick that is composed mainly of wehrlite (92%) with minor gabbro that intrudes Devonian dolostone (Tao et al., 2007; Wang et al., 2010). The mineralization is dominated by a violarite(polydymite)-pyrite-millerite-chalcopyrite mineral assemblages and has been referred to in the literature as a Pt-Pd deposit, but it contains proportional amounts of other PGE, including Ir, which has important genetic implications (Lu et al., 2021)

The Ni-Cu-(PGE)-bearing ~261 Ma Zhubu Ni-Cu-PGE intrusion, also located in the central zone, is composed of lherzolite, olivine websterite, and contaminated gabbroic rocks (Zhou et al., 2008; Tang et al., 2013). The sulfide mineralization occurs mainly as disseminated pyrrhotite, pentlandite, and chalcopyrite within the marginal zone (Tang et al., 2013).

The Yangliuping Ni-Cu-(PGE) camp is located in southeastern part of the Mesozoic Songpan-Ganzi orogenic belt. The currently known economic deposits occur in the Yangliuping and Zhengziyanwo sills, which are 2-3 km long, up to 300 m thick, extend 300-500 m along dip, and are composed by serpentinite,

talc schist, tremolite schist, and metagabbro (Song et al., 2003). The sulfides in Yangliuping vary from massive sulfides with up to ~34% S to disseminated sulfides with as little as 1% S.

The ~263 Ma Limahe Ni-Cu-(PGE) deposit is located in the central zone. The surface exposure of the intrusion is about 900 m long and 180 m wide (Zhou et al., 2008; Tao et al., 2008). It is a multiphase intrusion with an ultramafic (wehrlite and olivine gabbro) lower part and a mafic (diorite and gabbro) upper part (Tao et al., 2008).

The ~259 Ma Baimazhai Ni-Cu-(PGE) deposit is located in the Jinping area, on the southwest margin of the Yangtze Plate, near the Ailaoshan-Red River (ASRR) fault zone. The deposit is hosted in a lens-shaped mafic-ultramafic body that is ~530 m long, ~190 m wide, up to 64 m thick, and intrudes Ordovician metasandstone and slate. It contains significant amounts of Ni-Cu-(PGE), occurring as massive to net-textured sulfides in a zoned orthopyroxenite-websterite-gabbro body (Wang and Zhou, 2006).

## 4.4 Geochemistry

### 4.4.1 Lithophile geochemistry

Lithophile geochemistry are shown in Table S4-1. Major and trace elements for samples from 16 representative mineralized intrusions for which high-quality data are available have been recalculated to 100% on an anhydrous basis and plotted in **Figure 4**. Only samples with Ni+Cu ≤ 0.5 wt% have been included, filtering out samples containing significant amounts of Fe-Ni-Cu sulfides. The low-sulfide host rocks include dunites, lherzolites, websterites, wehrlites, gabbros, and norites, exhibiting a wide range of MgO (up to 44%) and $SiO_2$ (up to 61%). To aid in evaluating the broader mineralogical controls, we have also plotted the average compositions of olivine, orthopyroxene, clinopyroxene, and plagioclase at Jinchuan from Tonnelier (2010). Most sulfide-poor samples fall in the field outlined by the compositions Ol-Opx-Cpx-Pl, consistent with their observed cumulus mineralogy. Samples from Pobei have very high $Na_2O+K_2O$ contents because they contain hornblende and plagioclase (Su et al., 2011). On the $TiO_2$ and $FeO_t$ vs MgO plots (**Fig. 4**), many sulfide-poor samples plot outside the Ol-Opx-Cpx-Pl field, because of the presence of Fe ± Ti ± Cr oxides (magnetite, ilmenite, chromite).

The Ni-Co-Cr contents of sulfide-poor samples decrease with decreasing Mg (**Fig. 5**), consistent with

fractional crystallization/accumulation of olivine and minor chromite, except for several samples at Xiarihamu, which show a trend consistent with fractional crystallization/accumulation of only olivine (see discussion by Lesher and Stone, 1996; Barnes, 1998). Jinbaoshan samples are enriched in Cr because they contain cumulus chromite.

Highly incompatible lithophile elements (HILE: U-Th-Nb-Ta-Zr-Hf-REE-Y) generally increase with decreasing Mg (**Fig. 6**), reflecting fractional crystallization/accumulation of olivine ± Opx. Kalatongke and localities in the ELIP have higher La and La/Sm, and lower Ba/Nb than other deposits in the CAOB or associated with Rodinia. Some of the variation in Ba/Nb may reflect mobility of Ba, but some appears to be magmatic. Localities in the ELIP other than Baimazhai have somewhat higher Gd/Yb values. Deposits associated with the breakup of Rodinia, especially Jinchuan, exhibit quite variable Ba/Nb and La/Sm, some of which may mobility of Ba and La, but much of which appears to be magmatic.

Sr and Nd isotopic compositions are shown in **Figure 7**. Huangshannan, Huangshandong, and Kalatongke have εNd(t) values close to MORB, suggesting minor crustal contamination or significant amounts of magma replenishment (see discussion Lesher and Arndt, 1995; Lesher and Burnham, 2001). Heishan, Hongqiling, Jingbulake, Piaohechuan, Pobei, and Tianyu have slightly lower εNd(t) values, consistent with some crustal contributions. Host rocks in the CAOB (Heishan, Huangshandong, Huangshangnan, Hongqiling, Jingbulake, Pobei, Tianyu) generally have higher εNd(t) and lower $^{87}Sr/^{86}Sr_{(i)}$, consistent with mantle sources, whereas host rocks in the ELIP (Baimazhai, Jinbaoshan, Limahe, Zhubu) have lower εNd(t) and higher $^{87}Sr/^{86}Sr_{(i)}$ values, defining a trend from ELIP flood basalts towards upper continental crust or EM Ⅱ. Deposits associated with the break-up of Rodinia (Jinchuan and Zhouan) also have lower εNd(t), consistent with an enriched mantle source and/or crustal contamination but show a different trend than towards upper continental crust. These data provide clear evidence for variable degrees of crustal contamination and indicate that the Nd isotopic composition of the crust sampled by the host magmas was different in different areas, as would be expected.

εNd and γOs data are plotted in **Figure 8**. Most samples from Chinese deposits except Jinchuan have high γOs and intermediate εNd, plotting on a mixing trend between magmas derived from pyroxenitic mantle and continental crust, similar to Voisey's Bay and Eagle, but distinct for the most part from komatiite-associated deposits, which have low γOs and intermediate εNd, plotting on a mixing trend

between magmas derived from peridotitic mantle and continental crust. All are distinctly different from subcontinental lithospheric mantle (SCLM), which has lower εNd and lower γOs reflecting its depleted nature, and OIB sources (EMI, EMII), which also have low εNd but higher γOs reflecting their enriched nature. Samples from Jinchuan plot at lower εNd values but equally high γOs values, plotting on a mixing trend between continental crust and magmas derived from either peridotitic or pyroxenitic mantle (or a hybrid). Deposits in the CAOB plot closer to pyroxenitic mantle than deposits in ELIP and deposits related to Rodinia breakup. γOs values are typically more variable than εNd values, reflecting the higher Os contents of sulfides: removing sulfides will increase Re/Os, evolving over time to higher $^{187}Os/^{186}Os$ and γOs, whereas adding sulfides will decrease Re/Os, evolving over time to lower $^{187}Os/^{186}Os$ and γOs. Overall, deposits in the CAOB exhibit higher εNd and lower εSr (i.e., lower $^{87}Sr/^{86}Sr_{(i)}$), and therefore appear to be less contaminated than those in the ELIP, but there are no systematic differences in γOs.

### 4.4.2 Metal geochemistry

Metal geochemistry are shown in Table S4-2. Ni, Cu, Co, and PGE in mineralized samples correlate positively with S in most deposits (**Fig. 9**), suggesting that these elements were originally housed in sulfide melts. However, the PGE contents vary more widely than Ni-Co-Cu, likely reflecting differences in magma:sulfide ratio (R factor: Campbell and Naldrett, 1979) and some sulfide-rich samples (e.g., Baimazhai) show negative correlations, reflecting accumulation of MSS (see below). Among the PGEs, Pt generally shows weaker correlations and some deposits (e.g., Huangshandong, Piaohechuan, Xiarihamu) show more scatter, which is also obvious in their primitive mantle-normalized PGE patterns (**Fig. 10**) and may reflect accumulation of MSS or residual sulfide liquid and/or "nugget" effects.

In order to compare samples with different sulfide contents, we have recalculated the metal abundances to 100% sulfide (Naldrett, 1981; Barnes and Lightfoot, 2005):

$$C^i_{100} = 100\ C^i_{WR} / (2.527\ S + 0.3408\ Cu + 0.4715\ Ni) \quad [1]$$

where $C^i_{100}$ = concentration of element i in 100% sulfides, $C^i_{WR}$ = concentration of the element in the whole rock, and S, Cu, and Ni = concentrations of those elements in the whole rock in wt%. This calculation assumes that all of the Cu is in stoichiometric chalcopyrite ($CuFeS_2$), that all of the Ni is in pentlandite containing 34% Ni, and that the remaining S is in pyrrhotite containing 63% Fe, and it does not include a correction for silicate Ni. The Ni contents of pentlandite and Fe contents of pyrrhotite will

obviously vary from deposit to deposit and sample to sample, but this calculation is sufficient for the purposes of comparison. Because the Jinbaoshan PGE deposit contains mainly violarite, chalcopyrite, and pyrite, we assume that all of Cu is in chalcopyrite, all of the Ni is in violarite, and the remaining S is in pyrite.

$PGE_{100}$ values generally correlate positively between Ir and other PGEs (**Fig. 11**), although parts of some deposits show negative correlations (e.g., Baimazhai, Jinchuan, and Piaohechuan), confirming accumulation of MSS or residual sulfide liquid.

The abundances of chalcophile elements in 100% sulfides have been normalized to primitive mantle (Barnes and Maier, 1999) and plotted in terms of increasing compatibility during mantle melting in **Figures 10-11**. Baimazhai, Hongqiling, Huangshandong, Huangshannan, Huangshanxi, Jingbulake, Kalatongke, Limahe, Tianyu, and Xiarihamu are more enriched in Ni-Cu relative to PGE, whereas Heishan, Pobei, Yangliuping, and Piaohechuan are less enriched in Ni-Cu relative to PGE. Jinchuan, Zhouan, and Zhubu exhibit a range of patterns, but include some that are enriched in Ni-Cu relative to PGE. Jinbaoshan is enriched in Pd-Pd-Rh-Ir relative to Ru and Cu-Ni, similar to other PGE deposits (e.g., Bushveld, Great Dyke, Stillwater).

S isotopic compositions of mineralized samples are shown in **Figure 12**. Most (e.g., Hongqiling, Huangshannan, Huangshandong, Jinbaoshan, Jinchuan, Kalatongke, Pobei, and Yangliuping) range between -2 to 2‰ $\delta^{34}S$ and are close to – but in many cases significantly different from – the 0.1 ± 0.5‰ value expected for high-degree melting of asthenospheric mantle (Lesher, 2017) and therefore require some contributions by crustal S, which may have exchanged with magmatic S at moderate-high magma:sulfide ratios (see Lesher and Stone, 1996; Lesher and Burnham, 2001). Some (e.g., Baimazhai, Limahe, and Xiarihamu) have more positive $\delta^{34}S$ values, even more clearly requiring crustal S. The No. 1 body at Heishan ranges from 0.43 to 1.0‰ $\delta^{34}S$, whereas the No. 4 body at Heishan ranges from 1.9 to 6.1‰ $\delta^{34}S$, indicating different S sources or different magma:sulfide ratios (higher in No. 1 and lower in No. 4).

## 4.5 Discussion

Magmatic Ni-Cu-PGE, Ni-Cu-(PGE), and PGE-(Cu)-(Ni) deposits form through the concentration of

large (former two) and small (latter) amounts of immiscible sulfide melts. Small amounts of sulfide melt can exsolve from magmas during crystallization, which is the likely source of the small amounts of sulfides in PGE-(Cu)-(Ni) deposits, but the larger amounts required to form Ni-Cu-PGE and Ni-Cu-(PGE) deposits must be incorporated by thermomechanical erosion of S-bearing crustal rocks country rocks during ascent and/or emplacement (e.g., Lesher et al., 1984; Lesher and Groves, 1986; Lesher, 1989; Lesher and Keays, 2002; Naldrett, 2004, 2010; Arndt et al., 2005; Barnes and Lightfoot, 2005; Keays and Lightfoot, 2010; Ripley and Li, 2013). Crustal components are normally assimilated, but the solubility of sulfide is very low, so the sulfides are left as xenomelts (Lesher and Campbell, 1993; Lesher and Burnham, 2001). The assimilated silicate components may have a small effect on sulfide solubility and a small to intermediate effect on the metal budget but is normally not a governing process in generating sulfide-rich Ni-Cu-PGE or Ni-Cu-(PGE) deposits.

A fundamental requirement of a system capable of thermomechanical erosion is a high-flux magmatic plumbing system (e.g., Lesher et al., 1984; Lesher, 1989; Barnes et al., 2016). Such systems are commonly, but not exclusively, fed by mantle plumes (e.g., Arndt et al., 2005; Barnes and Lightfoot, 2005) and localized near craton margins (e.g., Begg et al., 2010) in continental rift or rifted continental margin settings.

The compositions of the ores are controlled by: 1) the metal abundances of the mantle source and the degree of partial melting (e.g., Naldrett and Barnes, 1986; Arndt et al., 2005; Maier et al., 2009), 2) the degree of fractional crystallization ± crustal contamination experienced by the magma during ascent (e.g., Lesher et al., 2001; Barnes et al., 2008), 3) the amount of magma that equilibrates with the sulfide (e.g., Campbell and Naldrett, 1979; Naldrett, 1981; Lesher and Burnham, 2001), 4) the degree of fractional crystallization of MSS (e.g., Hawley, 1962; Ebel and Naldrett, 1997; Barnes and Naldrett, 1987), and in some cases 5) interactions with magmatic-hydrothermal fluids (e.g., Hinchey and Hattori, 2005; Su and Lesher, 2012) or metamorphic-hydrothermal fluids (Lesher and Keays, 1984; 2002).

Below we discuss these processes as they apply to Ni-Cu-(PGE) and PGE-(Ni)-(Cu) deposits in China.

### 4.5.1 Temporal and Tectonic Settings

Ni-Cu-(PGE) and PGE-(Cu)-(Ni) deposits in China have formed during over a relatively wide range of time in at least three fundamentally different tectono-magmatic settings:

1) **828-637 Ma Plume-Initiated Rifting and Breakup of Rodinia**: The largest semi-continuous Ni-Cu±PGE deposit in the world, Jinchuan, appears to have formed during the initial stages of breakup of the Chinese portion of the supercontinent Rodina, which has been proposed to have been initiated by a superplume that produced mafic dikes and sills extending into South China and (then adjacent) south-central Australia (e.g., Li et al., 1999, 2008; Li et al., 2005; Xu et al., 2005; Xu et al., 2016; Pirajino, 2012; Wang et al., 2013a). The much smaller Zhouan deposit formed during the later stages of breakup, perhaps during a phase of lower magma flux. It is possible – if not likely – that much more mineralization formed during this event and remains to be found, but the breakup and dispersion of Rodinia may have destroyed much of it through erosion and subduction.
2) **431, 406, 357,** and **287-269 Ma Arc-Related Magmatism in the Central Asian and East Kunlun Orogenic Belts**: Larger numbers of smaller deposits were generated over an equally wide range of time during the complex history of the CAOB. There is some debate whether the mafic magmatism resulted from a mantle plume (e.g., Tarim LIP: Qin et al., 2011; Yuan et al., 2012; Yang et al., 2013; Yu et al., 2017) or arc magmatism (e.g., Li et al., 2012, 2015; Xie et al., 2014; Mao et al., 2016), but the latter seems to be gaining favour and is more consistent with the small sizes of the deposits and the geochemical and isotopic signatures of the host rocks.
3) **263-259 Ma Plume-Related Magmatism in the ELIP**: This event produced several deposits over a more restricted time interval. The relatively small ELIP has been proposed to be related to the much larger Siberian LIP, which generated the supergiant Noril'sk-Talnakh camp (see review by Naldrett, 2004). The reasons for the differences in endowment may be magma flux (higher at Noril-sk-Talnakh, lower at Emeishan) and/or accessibility to crustal S (S-rich evaporites at Noril'sk-Talnakh vs S-poor Yangtze upper crust at Emeishan).

All three tectonic settings contain Ni-Cu-(PGE) deposits and may well all contain PGE-(Cu)-(Ni) deposits, although only the large Jinbaoshan PGE-(Cu)-(Ni) deposit has been discovered thus far. The range of ages and multiple tectonic settings highlight the fact that Ni-Cu±PGE deposits formed throughout geological time in more than one tectonic setting (e.g., Arndt et al., 2005; Barnes and Lightfoot, 2005; Naldrett, 2004, 2011; Ripley and Li, 2013; Lesher, 2019). The deposits in China formed during continent assembly (CAOB and EKOB), during the initial (Jinchuan) and (Zhouan) final stages of continental breakup, and in an environment where the continent was not completely disassembled (ELIP deposits). A fertile magma in a high-flux conduit (lava channel or magma conduit) encountering a

S source does not care about the tectonic setting or when it forms in a tectonic cycle, as long as those key ingredients are satisfied.

83% of the deposits in **Table 1** occur within ~120 km of the margins of the North China and Yangtze cratons, and 61% occur within ~90 km of the margins, which is consistent with the roots of the cratons "steering" mantle plumes toward their margins (e.g., Kerrich et al., 2005; Sleep, 2005; Begg et al., 2010). There are other models that explain this association (e.g., edge-driven mantle convection: King and Anderson, 1998), but breakup of the entire supercontinent of Rodinia seems difficult to explain without a plume. There are also many deposits in China that occur in orogenic belts, so it is clear that plumes and rifting are not necessary to form Ni-Cu-(PGE) or Ni-Cu-PGE deposits, however, most are smaller and lower grade than the deposits in continental rifts (e.g., Duluth, Kambalda-Mt Keith-Perseverance, Noril'sk-Talnakh) and along rifted continental margins (e.g., Pechenga, Raglan, Thompson) probably because of lower magma fluxes and possibly lower amounts of crustal S.

### 4.5.2 Mantle source compositions

Geochemical and Nd-Os isotopic data indicate that the mafic-ultramafic magmas that formed most world-class magmatic Ni-Cu-PGE (e.g., Kambalda-Mt Keith-Perseverance, Noril'sk-Talnakh, Raglan, Thompson) and PGE-(Cu)-(Ni) (e.g., Bushveld, Great Dyke, Stillwater) deposits were derived by partial melting of HILE-depleted peridotitic (i.e., normal convecting asthenospheric) mantle (e.g., Lesher and Stone, 1996; Lesher and Keays, 2002; Arndt et al., 2005). The composition of peridotitic mantle varies with pressure, but generally consists of olivine with lesser orthopyroxene and clinopyroxene, an aluminous phase (spinel, garnet, or plagioclase depending on pressure), and small amounts of Fe-Ni-Cu-(PGE) sulfide (e.g., Naldrett and Barnes, 1986; Arndt et al., 2005). The mafic-ultramafic host magmas that host magmatic Ni-Cu-PGE deposits typically formed at moderate to high degrees of melting, leaving olivine ± minor Opx as the only residual phase(s) (e.g., Naldrett and Barnes, 1986). Because Ni-Co-IPGE partition strongly into olivine and Cu-PPGE-Au partition strongly into the melt, the Ni-Co-IPGE and Cu-PPGE-Au contents of melts derived from peridotitic mantle increase and decrease with degree of partial melting, respectively (e.g., Naldrett and Barnes, 1986; Barnes and Naldrett, 1987).

However, if the olivine in peridotitic mantle is consumed by reaction with melts derived from recycled (e.g., subducted) ocean crust, the mantle will be pyroxenitic (Sobolev et al., 2005, 2007, 2009). Melts

derived from pyroxenitic mantle will be characterized by enrichments in Ni-Co (because they will not be held back in olivine during partial melting) and Cu (which appears to be added metasomatically: Tonnelier, 2010) relative to PGE (which are depleted in MORB: Crocket, 2002). This suggests that the Ni-Co-Cu enriched, PGE-depleted patterns of many if not all of the Ni-Cu-(PGE) deposits in China (Fig. 13) are attributable to melting of pyroxenitic mantle (e.g., Tonnelier, 2010; Xu et al., 2013; Xie et al., 2013; Zhao et al., 2016b; Song et al., 2016).

Pyroxenitic and eclogitic mantle are thought to contain significantly more radiogenic Os than peridotitic mantle (Pearson and Nowell, 2004; Luguet et al., 2008) and if the mantle incorporated pyroxenetic melts the magma will be characterized by high γOs values (Lassiter et al., 2000; Huang et al., 2017). All of the Ni-Cu-(PGE) and PGE-(Cu)-(Ni) deposits in China have significantly higher γOs(t) than deposits derived from peridotitic mantle (e.g., Raglan, Alexo, Kambalda, Thompson: **Fig. 8**) and plot on a mixing trend between magmas derived from pyroxenitic mantle and continental crust, suggesting these deposits were derived from a pyroxenitic source.

To further evaluate mantle source compositions we have plotted the Fo and Ni contents of olivine in several Chinese magmatic sulfide deposits and some typical komatiite Ni-Cu-(PGE) deposits in **Figure 14A**, and have modeled the compositions of olivines crystallized from a magma derived from a peridotitic source containing 18% MgO, 10.6% $FeO_t$, and 526 ppm Ni (Straub et al., 2008) and from a magma derived from a pyroxenitic source containing 10% MgO, 8.6% $FeO_t$, and 540 ppm Ni (Straub et al., 2008). The olivine/magma partition coefficient for Ni is assumed to be 7 for the magma derived from a peridotitic source (Li et al., 2003) and 12 for the magma derived from a pyroxenitic (Straub et al., 2008). We have also modeled removal of sulfide, which will lower Ni at a given Fo content (e.g., Duke and Naldrett, 1978; Lesher and Stone, 1996), regardless of the source. It is possible to enrich the Ni content of a magma by assimilating Ni-Cu-rich sulfides (not shown), but this would normally also result in proportionately high PGE contents.

Olivine in komatiite-associated Ni-Cu-PGE deposits and barren equivalents fall on or near the model for a peridotitic source in the Fo-Ni diagram (**Fig. 14B**). However, the olivines in many Chinese magmatic sulfide deposits (particularly Heishan, Huangshannan, and Zhouan) have relatively high Ni contents at intermediate-low Fo contents, suggesting that they crystallized from a mama derived from pyroxenitic

mantle or experienced olivine-sulfide Fe-Ni exchange (see e.g., Brenan, 2003). Although we cannot exclude some loss of Ni due to removal of small amounts of sulfide, removal of large amounts of sulfide (as required to account for the very large amounts of sulfide in larger deposits like Xiarihamu), will result in a near-vertical trend toward much lower Ni contents (**Fig. 14A**). The olivines at Huangshannan and Zhouan have particularly high Ni contents, well above the 10% MgO pyroxenitic magma fractional crystallization curve, as noted by Wang et al. (2012) and Zhao et al. (2016b). Most samples fall in the range between the models for magmas derived from peridotitic and pyroxenite mantle (**Fig. 14C**), but olivines at Huangshanxi and Tianyu have lower Ni contents consistent with removal of Ni in sulfide, as noted by Tang et al. (2009) and Zhang et al. (2011). Thus, it appears that the Ni contents of olivines in most Chinese deposits are consistent with them having crystallized from magmas derived from pyroxenitic sources. Xiarihamu is more complex, as the Ni contents vary widely (500-4500 ppm) within a very narrow Fo range, which has been interpreted to indicate that multiple pulses of sulfide-laden magma were involved (Li et al., 2015). The Fo and Ni contents of olivines are given in detail in Table S4-3.

There are other factors other than source composition than can influence the Ni contents in olivine, including variations in Si content (e.g., Wang and Gaetani, 2008), differences in melting and crystallization temperatures (e.g., Hart and Davis, 1978; Kinzler et al., 1990; Matzen et al., 2013), and differences in crustal magmatic processes (e.g., Herzberg et al., 2014, 2016). Lynn et al. (2017) examined the effects of crustal processes (fractional crystallization, magma mixing, diffusive re-equilibration) on the Ni content in olivine from Hawaiian basalts and suggested that diffusive re-equilibration, crystal size, and sectioning effects can strongly affect the characterization of mantle source lithologies. However, taken together with the other geochemical and isotopic evidence presented above and discussed below, the olivine compositions are consistent with many of the magmas having been derived from pyroxenitic sources. This is consistent with the relatively young age of Chinese deposits in environments where there were many opportunities to metasomatize the underlying mantle (**Fig. 15**).

### 4.5.3 Fractional crystallization and crustal contamination

Determining the degree of fractionation crystallization and establishing primary magma compositions is difficult in mafic-ultramafic systems dominated by cumulate rocks, however, most cumulus minerals contain low to very low abundances of HILE, and Sr-Nd isotopes do not fractionate significantly during

fractional crystallization, so they can be used to assess the degree of contamination. Because assimilating other materials consumes heat and because most magmas are not superheated (komatiites being a probable exception: Lesher and Groves, 1986), assimilation normally involves fractional crystallization. The maximum assimilation:fractionation ratio varies from ~0.3 in basalts (DePaolo, 1981) to ~0.5 in high-Mg komatiites (Lesher and Arndt, 1995).

Because magmas derived by partial melting of depleted peridotite (e.g., N-MORB), slightly-enriched peridotite (e.g., E-MORB), and moderately-enriched peridotite (e.g., OIB) are progressively enriched in Th relative to Nb and Yb, and because these elements are least-mobile during metamorphism, the Nb/Yb vs Th/Yb diagram (**Fig. 16**) provides a powerful way to evaluate: 1) the sources of mantle-derived magmas (which will be reflected in similar degrees of Nb-Th enrichment), 2) the degree of subduction-related enrichment (which will be reflected in systematic enrichment in Th relative to Nb in all rocks from a given area), and 3) the degree of assimilation of continental crustal rocks (which will be reflected in variable degrees of enrichment in Th relative to Nb).

Most samples in the orogenic belts (CAOB and EKOB) have consistently high Th/Yb values and low Nb/Yb values (**Fig. 16A**). The amount of AFC required to generate such high Th/Yb values is too great for most of the samples (they would not still be basaltic; **Fig. 16B**) and it would need to be relatively constant to form an array parallel to the mantle array. Together, they suggest derivation from depleted-enriched mantle that has been enriched in Th by subduction-related fluids/melts with minor amounts of crustal contamination. Models by Pearce (2008) suggest that 3-5% subduction component is required (**Fig. 16C**). The host rocks at Heishan, Huangshandong, Huangshanxi, Huangshannan, Pobei, Jingbulake, Hongqiling, and Xiarihamu appear to have crystallized from magmas derived from subduction-modified depleted (N-MORB-like) mantle, whereas the host rocks at Jinchuan, Zhouan, Kalatongke, Piaohechuan, and Baimazhai appear to have crystallized from magmas derived from subduction-modified enriched (E-MORB-like) mantle and to have incorporated variable amounts of continental crust. The host rocks at Jinchuan have extremely high Nb/Yb and very high Th/Yb ratios and anomalously low εNd(t) and high $^{87}Sr/^{86}Sr$, so have likely also been contaminated by rocks more evolved than upper continental crustal rocks, such as the adjacent marbles (Lehmann et al., 2007; Tonnelier, 2010; Song et al., 2012). The host magmas at Jinbaoshan, Limahe, Yangliuping, and Zhubu in the ELIP plot subparallel to the mantle array with slightly high Th/Yb and very high Nb/Yb. On this diagram they appear to be derived from a more

enriched magma, possibly formed by interaction between an enriched plume source and a small amount of subducted crust, with minor crustal contamination.

Sr and Nd isotopic data provide additional constraints. The host rocks in the CAOB have positive εNd(t) values, suggesting that they formed from magmas derived from depleted mantle sources and experienced only minor crustal contamination. ELIP flood basalts have lower εNd(t) and higher $^{87}Sr/^{86}Sr_{(i)}$ values, suggesting that they were derived from a more enriched source than those in the CAOB. The host rocks in the ELIP have lower εNd(t) and trend to higher $^{87}Sr/^{86}Sr_{(i)}$ and have been interpreted to have experienced greater degrees of crustal contamination with Yangtze upper/middle crust (Zhou et al., 2008; Wang et al., 2012). Sr-Nd isotopes indicate that the degree crustal contamination degree for deposits in the ELIP is Baimazhai > Limahe > Jinbaoshan, consistent with differences in S isotopes (**Fig. 7, Fig. 12**). Thus, variations in both degree of source enrichment and crustal contamination have produced the differences in trace element and S-Nd-Sr isotopic compositions of deposits in the ELIP and CAOB, respectively. Host rocks related to the break-up of Rodinia (e.g., Jinchuan and Zhouan) exhibit a different mantle enrichment signature (toward EMI) and crustal contamination signature (toward lower continental crust). This has been suggested to represent involvement of subcontinental lithosphere mantle (Li and Ripley, 2011; Wang et al., 2013b), but a significant contribution from SCLM is not supported by Os isotopic data (**Fig. 8**).

### 4.5.4 Parental magma compositions

Determining the major element compositions of parental magmas is also difficult in mafic-ultramafic systems dominated by cumulate rocks and many of the samples in the literature contain sulfides but have not been analyzed for S, precluding corrections for Fe in sulfide. Filtering for samples containing < 0.5 wt% Ni + Cu helps but does not completely eliminate this problem. Even at Jinchuan, which has been the topic of several detailed studies and for which S data are available, it is not clear if the parental magma was a high-Mg basalt with 11.5% MgO and 11.2% FeO (Chai and Naldrett, 1992) or 12.3% MgO and 12.4% FeO (Li and Ripley, 2011), or a ferropicrite with 15.4% MgO and 13.7% FeO (Tonnelier, 2010). Part of the problem is that many studies have used regressions or averages, but that assumes all of the variations are sampling or analytical errors.

A detailed analysis at each location is beyond the scope of this contribution, but the key to constraining

parental magma compositions in ultramafic rocks is to recognize that most samples will be derived from fractionated liquids and to identify the samples that must have accumulated the most magnesian olivine, which must have crystallized from the most magnesian liquid. In this case, all areas contain at least some samples that define or lie on olivine-chromite-only control lines (**Figs. 4, 5, and 17**), indicating that most of the host rocks were derived from chromite-saturated picritic to high-Mg basaltic magmas. Only Xiarihamu, which contains high-Mg low-Cr (Ol-only) cumulates (**Fig. 5**) and highly magnesian olivine (up to $Fo_{90}$: Li et al., 2015), appears to have been derived from a chromite-undersaturated magma (see discussion by Lesher and Stone, 1996). This requires higher degrees of partial melting and/or a source with lower Cr contents than the other deposits.

### 4.5.5 Host unit olivine ± Opx enrichment and degree of differentiation

The host units range from poorly differentiated adcumulate-mesocumulate units with weighted bulk compositions that are strongly enriched in olivine ± Opx relative to their parental liquids to strongly differentiated units with thin lower cumulate zones and thick upper gabbroic-dioritic zones (**Fig. 17, Table 2**).

The bodies that are poorly differentiated and enriched in olivine (e.g., Jinchuan) have been interpreted by some authors (e.g., Tang 1993; de Waal et al. 2004) to have formed from olivine-sulfide rich "mushes". However, olivine and sulfide are very dense and olivine-sulfide loaded magmas would not be capable of rising through the crust (see Lesher, 2017). It is more likely that these units – like those in many other Ni-Cu ± PGE systems – represent magma conduits in which olivine ± Opx accumulated during flow (Lesher et al., 1984; Lesher, 1989; Barnes, 2006; Arndt et al., 2008). Such systems are typically more prospective for Ni-Cu ± PGE mineralization than unenriched, differentiated units because they represent systems with higher magma fluxes that are more capable of thermomechanically eroding country rocks "upstream" (to incorporate crustal S) and maintaining high magma:sulfide ratios (to upgrade metal tenors) (e.g., Lesher et al., 1984; Lesher and Keays, 2002; Arndt et al., 2008). The bodies that are less enriched in olivine ± Opx and more strongly differentiated may have also had high magma fluxes at an early stage and "ponded" and differentiated after ore formation but before much olivine ± Opx accumulated, but there is clearly a correlation between the degree of olivine ± Opx accumulation and total Ni resource in Chinese and other Ni-Cu±PGE deposits.

### 4.5.6 Host unit geometry

Although the focus of this paper is on geochemistry, the host units of Ni-Cu±PGE deposits in China exhibit a wide range of geometries, reflecting different modes of emplacement and therefore ore localization.

Jinchuan has been interpreted as a subvertical dike (Tang, 1993), a rotated sill (Lehmann et al., 2007; Tonnelier, 2010), and a subvertical elongate funnel (Lightfoot and Evans-Lamswood, 2015). We find the arguments for structural rotation by Lehmann et al. (2007) and the evidence for asymmetric differentiation (requiring the same sense of rotation) by Tonnelier (2010) compelling, so we have classified Jinchuan as a channelized sill. However, if it has not been rotated, Jinchuan is more likely a blade-shaped dike than a subvertical funnel (see discussion by Lesher 2019).

Branquet et al. (2012) and Lightfoot and Evans-Lamswood (2015) classified several more of the bodies as subvertical funnels with diamond-shaped surface sections, but Hongqiling, Huanshannan, Huanshandong, Huanshanxi, Kalatongke, and Limahe are highly elongate subparallel to the surface, appear to close off at both ends, and are asymmetrically-differentiated. Although the former two aspects can be attributed to deformation, the latter cannot. For this reason, we have interpreted most of them as variably eroded subhorizontal chonoliths (Kalatongke #2) or blade-shaped dikes (remainder). Only Jingbulake is asymmetrically zoned and may resemble a subvertical Alaskan-Uralian type intrusion.

The differences in the interpretations have important consequences for the mode of sulfide transport (subhorizontal rather than subvertical) and the sources of S (same stratigraphic level rather than deeper). More work is required to better distinguish between the different interpretations, but reinterpreting many of these bodies as subhorizontal channelized sills, blade-shaped dikes, and chonoliths eliminates all of the many problems inherent in transporting large abundances of dense sulfides vertically and suspending them in the throats of subvertical funnels while the host rocks crystallize (see Lesher, 2017; 2019).

### 4.5.7 S sources

Most magmas can dissolve and therefore exsolve only very small amounts of S (0.1-0.3%), so although very small amounts of sulfide (<1-2%) can exsolve during crystallization, larger amounts require the addition of external S (e.g., Lesher and Groves, 1986; Lesher, 1989; Lesher and Keays, 2002; Lightfoot and Keays, 2005; Keays and Lightfoot, 2010; Ripley and Li, 2013). S, Os, and Pb isotopes can be used

to evaluate the degree of crustal S addition, although they are all susceptible to being overprinted by replenishment in dynamic magmatic systems (see Lesher and Burnham, 2001).

Some of the deposits (Huangshannan, Huangshandong, Kalatongke, Pobei, Hongqiling) have $\delta^{34}S$ values close to the 0.1 ± 0.5‰ $\delta^{34}S$ range of MORB (asthenospheric peridotitic) mantle (see discussion by Lesher, 2017), but most exhibit variations well outside that range to more negative (e.g., Hongqiling, Kalatongke, Pobei, Yangliuping) or more positive values (e.g., Huangshandong, Huangshannan, Jinbaoshan, Jinchuan) or much more positive values (e.g., Heishan, Xiarihamu, Limahe, Baimazhai). Significantly, the ores in the CAOB and ELIP both range widely from slightly negative to moderately positive (CAOB) or strongly positive (ELIP). The sulfides with S isotopic compositions near MORB may have 1) exsolved from a MORB-like magma and been modified only slightly by interaction with crustal S, or 2) incorporated S from a non-mantle source (discussed below) and exchanged S with the magma (e.g., Lesher and Stone, 1996; Lesher and Burnham, 2001; Ripley and Li, 2013), shifting their compositions varying degrees toward mantle. The low R factors deduced above for the sulfides at Huangshandong and Hongqiling suggest that the S isotopes in those deposits more likely approach that of their sources, whereas the higher R factors deduced above for Jinbaoshan, Yangliuping, and Jinchuan suggest that the S isotopes in those deposits more likely reflect exchange with the magma: in the case of Yangliuping an even lighter (more negative) source and in the case of Jinbaoshan an even heavier (more positive) source.

Given the trace element and Sr-Nd-Os isotopic evidence for a significant subduction component in the magmas that formed the host rocks at most of the deposits (e.g., Huangshandong, Huangshannan, Huangshanxi, Jingbulake, Tianyu, Xiarihamu) and for a significant crustal component in some of the deposits (e.g., Baimazhai, Jinchuan), there are at least three potential sources of non-mantle S: 1) isotopically heavy subduction-influenced arc mantle (e.g., Woodhead et al., 1987), 2) isotopically heavy continental crustal rocks, and/or 3) isotopically light continental crustal rocks. The latter is potentially the only option for Hongqiling, Kalatongke, Pobei, and Yangliuping, but the former two are difficult to distinguish. Trace element data suggest that the magmas in the CAOB and EKOB (e.g., Heishan, Hongqiling, Huangshandong, Huangshannan, Kalatongke, Pobei) originated from subduction-modified arc mantle ($\delta^{34}S$ > 2‰: Woodhead et al., 1987), so the ~0 or slightly negative S isotopes for some of

these deposits (Hongqiling, Huangshandong, Huangshannan, Pobei) was likely caused by crustal contamination (**Fig. 12**).

The S and Os isotope geochemistry of the ores suggest that the Ni-Cu-(PGE) and PGE-(Cu)-(Ni) deposits in China include S and metals derived from at least two sources. 1) Deposits in the ELIP are characterized by variable S and Os isotopes. These data can be interpreted in two ways: for the deposits that are sulfide-rich and appear to have formed at relatively low R factors, this suggests a crustal source, but for the deposits that are sulfide-poor and appear to have formed at high R factors, the source may be the mantle-derived magma or it may be a crustal source modified by reaction with the magma as discussed above. 2) Deposits in the CAOB and EKOB are characterized by lower $PGE_{100}$ and higher $^{187}Os/^{188}Os$ values, and clearly incorporated crustal S. The sources of crustal S are not well understood, so this is an area where more research is required to determine whether the S came from deeper sources and was physically transported from depth, whether the S came from more-or-less the same stratigraphic levels and was transported only horizontally, or whether the S came from shallower sources and settled backwards (see discussion by Lesher, 2017; Lesher, 2019).

### 4.5.8 Ore localization

Most of the mineralization in Chinese Ni-Cu-(PGE) deposits occurs as low-grade disseminated sulfides, although some deposits (e.g., Baimazhai, Jinchuan, Xiarihamu) contain significant amounts of net-textured sulfides and minor massive sulfides.

The different locations of the mineralized zones – basal/marginal vs. single internal vs. multiple internal – indicate that the mineralization formed during the early, intermediate, and intermediate-late stages of emplacement and crystallization of the host units (see Lesher and Keays, 2002) in different areas:

1) Early basal/marginal mineralization: lateral parts of Jinchuan, Heishan, Hongqiling, Limahe, central parts of parts of Piaohechuan, parts of Yangliuping, Zhubu
2) Intermediate internal mineralization: Baimazhai, Jingbulake, central parts of Jinchuan, Kalatongke, Pobei, lateral parts of Piaohechuan, parts of Yangliuping
3) Intermediate-late multiple internal mineralization: Huangshannan, Huangshandong, Huangshanxi, Jinbaoshan, Tianyu, Xiarihamu

Although some workers have suggested that massive ores have been emplaced later than disseminated-

net textured mineralization, this likely reflects late mobility of massive sulfides, which remain molten at temperatures well below the crystallization temperatures of the silicate minerals (e.g., Tonnelier, 2010; Barnes et al. 2016).

The mode of sulfide emplacement is still being debated. Tang (1993), de Waal et al. (2004), Li et al. (2015), Song et al. (2016), Lightfoot and Evans-Lamswood (2015), and Wang et al. (2018) have suggested that the Ni-Cu-(PGE) deposits in China formed by mobilization of sulfide-rich magmas from deeper chambers. The motivation for such models appears to be: 1) a paucity of S in local country rocks; and/or 2) depletion of PGE relative to Ni-Co-Cu in the ores, which is interpreted to reflect prior removal of small amounts of sulfides. There are several problems with such models:

1) The S source need not be at depth, it may have been along strike in the plumbing system. Many of the deposits occur in sedimentary sequences that likely contained at least some sulfidic pelites or evaporites and many of the host units appear to have subhorizontal orientations (as discussed above).
2) Depletion of PGE relative to Ni-Co-Cu can also be attributed to the mantle source and parental magma being depleted in PGE and enriched in Ni-Co-Cu (as discussed above). However, a more serious problem with this model is that it requires unrealistically high R factors (up to $10^6$ in the case of some elements) to model the observed ore compositions.
3) Sulfide melts are very dense (~4.2 g $cm^{-3}$) and very fluid (~0.1 g cm $sec^{-1}$) compared to silicate magmas (~2.7 g $cm^{-3}$ and 10-1000 g cm $sec^{-1}$), so any more than 10-15% is impossible to transport in magmas ascending buoyantly through continental crust (ave <2.9 g $cm^{-3}$) (e.g., Lesher and Groves, 1986; Lesher, 2017).
4) It is possible for fine, dilute suspensions of sulfide droplets to be transported and collected on "filter beds" in overlying chambers (Lesher, 2017), but that does not explain why significant amounts of Ni-Cu ± PGE mineralization or PGE enrichment have not been reported in volcanic rocks other than in situations where there is evidence for it having formed at that stratigraphic level (e.g., Alexo, Kambalda, Raglan; see discussion in Lesher, 2017, 2019).
5) It is possible for greater amounts of sulfide droplets to be transported in the presence of volatile bubbles (Mungall et al., 2015) or felsic xenoliths (Lesher, 2017), which can reduce the bulk density of the magma, but none of the deposits in China contain abundant vesicles like those observed at

Noril'sk (e.g., Barnes et al., 2017; Lesher, 2017) or abundant xenoliths like those observed at Aguablanca (e.g., Tornos et al., 2001) or Voisey's Bay (e.g., Li and Naldrett, 2000).

6) It is feasible to transport sulfide-rich magmas via seismic pumping (Lesher, 2013a, 2013b, 2017, 2019) and Lightfoot and Evans-Lamswood (2015) have suggested that dense sulfide-rich magmas were pumped from depth through a subvertical conduit system undergoing alternating transtension and transpression and localized in dilations and traps created by cross-linking structures in strike-slip fault zones. However, such a model does not explain the absence of any sulfides in areas where overlying volcanic equivalents are exposed (e.g., ELIP), some of which are consistent with being near-primary compositions that have not fractionated significantly *en route* to the surface and none of which are depleted in PGE (Lesher, 2019).

It is equally possible, if not probable, that the sulfides were generated at more-or-less the same stratigraphic level and were trapped at those levels (Lesher, 2017, 2019).

The abundance of low-grade mineralization in many deposits can likely be attributed to a paucity of available S. Very high magma fluxes would also favour disseminated rather than net-textured or semi-massive mineralization (e.g., Lesher and Keays, 2002), but most of the low-grade systems do not appear to be olivine-rich high-flux systems.

### 4.5.9 R factor

Although the abundances of Ni-Co-Cu in most mafic-ultramafic magmas are high enough that the small amounts of sulfide that typically exsolve from magmas may extract enough metals to generate reasonable metals tenors without severely depleting the magma, because the partition coefficients (~30, = 100-500, = 500-1000, and = $10^5$-$10^6$) are so high (see reviews by Lesher and Stone, 1996; Naldrett, 2004; Barnes and Lightfoot, 2005), there are limitations on how much Ni-Co-Cu can enter moderate-large amounts of sulfide and limitations on how much PGE can enter even very small amounts of sulfide. The mass balance varies, depending on whether sulfide is exsolved from the magma (Campbell and Naldrett, 1979), incorporated from a barren external source (Naldrett, 1981), or incorporated from an external source containing metals (Lesher and Burnham, 2001). The general form of the mass balance is (Lesher and Burnham, 2001):

$$Y_i^f = \frac{(X_i^o R + Y_i^o) D_i^{Sul/Sil}}{R + D_i^{Sul/Sil}} \quad [1]$$

where $X_i^o$ is the initial concentrations of metal *i* in the silicate liquid, $Y^0{}_i$ is the initial concentration of metal *i* in the sulfide melt, *R* is the magma/sulfide mass ratio, $D_i^{Sul/Sil}$ is the sulfide/silicate partition coefficient, and $Y^f{}_i$ is the final concentration of metal in the sulfide melt.

The major unknown is the amount of metal in the magma, which is better constrained in areas where chilled margins or contemporaneous volcanic rocks are present (e.g., ELIP), but poorly constrained in areas containing only cumulate rocks (e.g., Jinchuan). We are less confident than some authors in our ability to estimate these values, particularly given the spectrum of mantle sources indicated by the lithogeochemical, Ni in olivine, and Sr-Nd-Os isotopic data. For example, ores depleted in PGE relative to Ni-Cu-Co have been interpreted by some authors to have formed by prior extraction of small amounts of sulfide from a peridotitic source (see Song et al., 2008; Gao et al., 2012, 2013; Zhao et al., 2015) and by other authors to have formed by equilibration with a magma derived from a Ni-Cu-Co-enriched, PGE-depleted pyroxenitic source (see Tonnelier, 2010; Xu et al., 2013; Xie et al., 2013; Zhao et al., 2016b; Song et al., 2016). As noted above, the Os isotopic data are fairly definitive and in the case of Jinchuan the former model predicts factors that are much too high (up to $10^6$ in the case of Ir) for a such a sulfide-rich deposit, and the latter model predicts factors that are much more reasonable (~500) (Tonnelier, 2010).

We have modelled R factor variations in a peridotite-derived picritic magma and a pyroxenite-derived ferropicritic magma in **Figures 13E-F**. It is clear that variations in R factor can increase PGE relative to Ni-Cu-Co, but cannot decrease PGE relative to Ni-Cu-Co. As discussed below, crystallization of MSS from sulfide melt will fractionate Ni-Co-IPGE from Cu-Au-PPGE, not all PGE from Ni-Cu-Co. Thus, high R factors can erase or reduce the pyroxenite signature and MSS fractionation can modify the pyroxenite signature, but only a magma depleted in PGE > Ni-Cu-Co can produce an ore that is depleted in PGE > Ni-Cu-Co.

Ir is virtually insoluble in magmatic-hydrothermal and metamorphic-hydrothermal fluids (Keays et al., 1982; Lesher and Keays, 1984, 2002; Su and Lesher, 2011) and nearly all samples have tight positive correlations in Ir vs Rh and Ir vs Ru diagrams (**Fig. 11**). The Jinbaoshan PGE deposit has the highest abundance of PGE in sulfides, suggesting a very high factor (up to $10^5$: Lu et al., 2014). Pobei and Zhouan

have moderate PGE content in sulfides, consistent with moderate to high R factors (up to 6000: Wang et al., 2013b; Yang et al., 2014). Other Ni-Cu deposits in China have been proposed to have formed at low-moderate R factors (30-1000) resulting in systematic PGE depletion relative to Co-Ni-Cu (Tao et al., 2008; Zhang et al., 2009; Yang et al., 2012; Wei et al., 2013; Sun et al., 2013). However, the calculated factors vary depending on the abundances of PGE in the chosen parental magma. A magma derived from a pyroxenitic source, for example, will have higher Ni-Cu-Co and lower PGE (e.g., Lesher and Stone, 1996; Tonnelier, 2010), increasing – with all else equal – the apparent factor than for a magma derived from a peridotitic source.

The decoupling of Os from Sr-Nd isotopes in Jingbulake deposit has been attributed to selective incorporation of Os-rich, Sr-Nd-poor sulfides relative to Os-poor, Sr-Nd-rich silicate components (Yang et al., 2012). This seems logical given the lower melting point of sulfides, but there is no evidence for selective incorporation of sulfides relative to silicates in other deposits where this has been studied in detail (e.g., Duluth, Kambalda, Raglan, Thompson, Voisey's Bay). Furthermore, massive sulfides at Limahe and Jingbulake have high $\gamma Os_{(t)}$ values and low PGE tenors, both consistent with low R factors, and disseminated and sulfide-poor samples have low $\gamma Os_{(t)}$ values and high PGE tenors, both consistent with high R factors. It is more likely that the decoupling of Os isotopes from Sr-Nd isotopes can be attributed to their relative abundances in sulfide melt (Os >>> Sr-Nd) and silicate magma (Sr > Nd >> Os) (Lesher and Burnham, 1999, 2001). As a result of the R factor effect, these deposits show variable $\gamma Os_{(t)}$ over a limited range of Nd (**Fig. 8**).

### 4.5.10 Fractional crystallization of sulfide liquid

Experimental studies have shown that the first phase to crystallize from a sulfide liquid is Fe-Ni-IPGE rich, Cu-PPGE-Au-poor monosulfide solid solution (MSS), leaving a residual sulfide melt that is enriched in Cu-PPGE-Au (e.g., Barnes and Naldrett, 1987; Fleet and Pan, 1994; Ebel and Naldrett, 1997; Sinyakova and Kosyakov 2009). In the $Ir_{100}$ vs $PGE_{100}$ plots (**Fig. 11**), most samples have tight positive correlations between Ir, Ru, and Rh because these elements have similar partition coefficients between MSS and sulfide liquid. Samples from Jinbaoshan and Huangshandong have lower Ru/Ir values, which may indicate crystallization of chromite, as Ru is known to partition into chromite (e.g., Brenan et al., 2012; Pagé and Barnes, 2016). In the $Ir_{100}$ vs $Pd_{100}$ and $Pt_{100}$ plots (**Fig. 11**), however, quite a few samples depart from the positive trend. $Pt_{100}$ is decoupled from $Pd_{100}$ and decreases at more-or-less constant $Ir_{100}$

in many Xiarihamu samples and some Jinchuan and Piaohechuan samples, suggesting that Pt (which commonly occurs as Pt alloys rather than in PGMs) has segregated or been mobile (see Song et al., 2009; Chen et al., 2013). Pd and Ir are inversely correlated significantly only at Jinchuan and possibly Zhouan, consistent with accumulation of MSS (samples with higher Ir and lower Pd) or residual sulfide liquid (samples with lower Ir and higher Pd). For the most part, most other deposits have relatively consistent Cu-Ni-Co patterns and relatively consistent PPGE-IPGE patterns. This suggests that the majority of the deposits have not fractionated significantly and/or that the sampling has homogenized any fractionation.

The finer details of MSS fractionation are well illustrated at Jinchuan. The positive correlation between $Ir_{100}$ and $Ru_{100}$-$Pt_{100}$ in disseminated ores (**Fig. 18**) indicates that the variations are controlled by magma:sulfide ratios (R factors), not MSS fractionation. However, some of the net-textured and massive ores are enriched in Fe-Ni-IPGE and depleted in Cu-PPGE-Au (i.e., enriched in MSS) and some are depleted in Fe-Ni-IPGE and enriched in Cu-PPGE-Au (i.e., enriched in residual sulfide melt). Thus, there are three different mantle-normalized PGE patterns for Jinchuan mineralized samples (**Fig. 10**) and only the disseminated ores reflect the composition of the original sulfide melts.

## 4.6 Conclusions

1) Nearly all Chinese Ni-Cu-(PGE) and PGE-(Cu)-(Ni) deposits occur along or near the margins of cratons (e.g., North China craton, Yangtze Craton) or in orogenic belts (e.g., Central orogenic belt, East Kunlun orogenic belt) that likely represented craton margins, consistent with those locations representing areas where magmas were able to preferentially rise through the crust.
2) Olivine, chalcophile element, and Nd-Sr-Os isotopic compositions suggest that many host magmas formed by melting of metasomatized pyroxenitic mantle, likely produced by the interaction of recycled oceanic crust with variably-enriched peridotitic mantle, but the compositions of the parental magmas have been modified by minor to significant degrees of crustal contamination.
3) Although many deposits appear to have been derived from a pyroxenite source, the composition of the original peridotitic mantle, the degree of mantle metasomatism, and the degree of crustal contamination appear to have been different. Most deposits in the CAOB and EKOB appear to have been derived from magmas formed by partial melting a metasomatized but originally depleted mantle source with minor crustal contamination. Most deposits in the ELIP appear to have been

derived from magmas formed by partial melting of more enriched sources than in the other metallogenic provinces. Those related to the breakup of Rodinia exhibit transitional geochemical characteristics.

4) The deposits appear to be hosted by subhorizontal blade-shaped dikes, chonoliths, and channelized sills, not subvertical funnels as proposed by other workers.
5) S isotopic data indicate a wide range of crustal S sources, modified by interaction with variable amounts of mantle-derived magmas.
6) The compositions of most Chinese Ni-Cu-(PGE) deposits have been modified to some degree – in some cases significant degrees (e.g., Jinchuan) – by MSS fractionation. Averaging samples without weighting them will not properly compensate for this process and even net-textured ores are susceptible to fractionation. Only disseminated ores are reliable indicators of original sulfide melt compositions, but care must be taken to ensure that low-grade samples have not experienced modifications in Ni contents accompanying serpentinization of olivine.
7) The wide variations in tectonic-magmatic setting (breakup of Rodinia vs CAOB vs ELIP), host rock composition (dunite to diorite), geochemistry (HILE-enriched to HILE-depleted), and isotope geochemistry (high to low $^{87}Sr/^{86}Sr/\varepsilon Nd/\gamma Os$, positive to negative $\delta^{34}S$) indicate that these factors were not critical to the formation of magmatic Ni-Cu-(PGE) and PGE-(Cu)-(Ni) deposits in China, but that the key factors are channelized magma flow to thermomechanically erode country rocks upstream in the system, to access crustal S, and to achieve at least moderate R factors.

## Acknowledgements

This research has been supported by grants from the National Key Basic Research Development Program (Nos. 2015CB452606 and 2009CB421008) to JD; a Natural Sciences and Engineering Council of Canada Discovery grant to CML (#203171-2012); and China Scholarship Council and SEG Canada Foundation grants to YL. We are very grateful to Peter Lightfoot and two anonymous Ore Geology Reviews reviewers for helpful comments on the manuscript.

## References

Amelin, Y., Li, C., Valeyev, O., Naldrett, A. J., 2000. Nd-Pb-Sr isotope systematics of crustal assimilation in the Voisey's Bay and Mushuau intrusions, Labrador, Canada. Econ. Geol. 95, 815-830.

Arndt, N.T., Lesher, C.M., Barnes, S.J., 2008. Komatiite. Cambridge university press, 1-487.

Arndt, N.T., Lesher, C.M., Czamanske, G.K., 2005. Mantle-derived magmas and magmatic Ni-Cu-(PGE) deposits. 100th Anniversary Volume, Society of Economic Geologists, 5-24.

Barnes, S.J. 1998. Chromite in komatiites, 1. Magmatic controls on crystallization and composition. J. Petrol. 39, 1689-1720.

Barnes, S.J., Cruden, A.R., Arndt, N., Saumur, B.M., 2016. The mineral system approach applied to magmatic Ni-Cu-PGE sulphide deposits. Ore Geol. Rev. 76, 296-316.

Barnes, S. J., van Achterbergh, E., Makovicky, E., Li, C., 2001. Proton microprobe results for the partitioning of platinum-group elements between monosulphide solid solution and sulphide liquid. South Afri J. Geol, 104(4), 275-286.

Barnes, S.-J., Lightfoot, P.C., 2005. Formation of magmatic nickel sulfide ore deposits and processes affecting their copper and platinum group element contents. 100th Anniversary Volume, Society of Economic Geologists, 179-214.

Barnes, S.-J., Maier, W. D., 1999. The fractionation of Ni, Cu and the noble metals in silicate and sulfide liquids. Geological Association of Canada Short Course Notes, 13, 1-52.

Barnes, S.J., Mungall, J.E., Le Vaillant, M., Godel, B., Lesher, C.M., Holwell, D., Lightfoot, P.C., Krivolutskaya, N., Wei, B., 2017. Sulfide-silicate textures in magmatic Ni-Cu-PGE sulfide ore deposits: Disseminated and net-textured ores Am. Mineral. 102, 473-506.

Barnes, S.-J., Naldrett, A.J., 1987. Fractionation of the platinum-group elements and gold in some komatiites of the Abitibi greenstone belt, northern Ontario. Econ. Geol. 82, 165-183.

Barnes, S.-J., Prichard, H.M., Cox, R.A., Fisher, P.C., Godel, B., 2008. The location of the chalcophile

and siderophile elements in platinum-group element ore deposits (a textural, microbeam and whole rock geochemical study): implications for the formation of the deposits. Chem. Geol. 248, 295-317.

Begg, G.C., Hronsky, J.A., Arndt, N.T., Griffin, W.L., O'Reilly, S.Y., Hayward, N., 2010. Lithospheric, cratonic, and geodynamic setting of Ni-Cu-PGE sulfide deposits. Econ. Geol. 105, 1057-1070.

Branquet, Y., Gumiaux, C., Sizaret, S., Barbanson, L., Wang, Bo, Cluzel, D., Li, G., Delaunay, A., 2012. Synkinematic mafic/ultramafic sheeted intrusions: Emplacement mechanism and strain restoration of the Permian Huangshan Ni–Cu ore belt (Eastern Tianshan, NW China), J. Asian Earth Sci. 56, 240–257

Brenan, J.M., 2003, Effects of $fO_2$, $fS_2$, temperature, and melt composition on Fe-Ni exchange between olivine and sulfide liquid: Implications for natural olivine–sulfide assemblages. Geochim. Cosmochim. Acta 67 (14), 2663–2681.

Brenan, J.M., Finnigan, C.F., McDonough, W.F., Homolova, V., 2012. Experimental constraints on the partitioning of Ru, Rh, Ir, Pt and Pd between chromite and silicate melt: the importance of ferric iron. Chem. Geol. 302: 16-32.

Campbell, I.H., Naldrett, A.J., 1979. The influence of silicate: sulfide ratios on the geochemistry of magmatic sulfides. Econ. Geol. 74, 1503-1506.

Chai, F.M., Zhang, Z.C., Mao, J.W., Dong, L.H., Zhang, Z.H., Wu, H., 2008. Geology, petrology and geochemistry of the Baishiquan Ni-Cu-bearing mafic-ultramafic intrusions in Xinjiang, NW China: implications for tectonics and genesis of ores. J. Asian Earth Sci. 32, 218-235.

Chai, G., Naldrett, A.J., 1992. The Jinchuan ultramafic intrusion: cumulate of a high-Mg basaltic magma. J. Petrol. 33, 277-303.

Chen, L.M., Song, X.Y., Keays, R.R., Tian, Y.L., Wang, Y.S., Deng, Y.F., Xiao, J. F., 2013. Segregation and fractionation of magmatic Ni-Cu-PGE sulfides in the western Jinchuan intrusion, northwestern China: Insights from platinum group element geochemistry. Econ. Geol. 108, 1793-1811.

Crocket, J.H., 2002. Platinum-group element geochemistry of mafic and ultramafic rocks. The Geology,

Geochemistry and Mineral Beneficiation of Platinum-Group Elements. Special Volume, 54, 177-210.

De Waal, S.A., Xu, Z., Li, C., Mouri, H., 2004. Emplacement of viscous mushes in the Jinchuan ultramafic intrusion, western China. Can. Mineral. 42, 371-392.

Deng, J., Wang, Q., Yang, S.J., Liu, X.F., Zhang, Q.Z., Yang, L.Q., Yang, Y.H., 2010. Genetic relationship between the Emeishan plume and the bauxite deposits in Western Guangxi, China: constraints from U-Pb and Lu-Hf isotopes of the detrital zircons in bauxite ores. J. Asian Earth Sci. 37, 412-424.

Deng, J., Wang, Q., 2016. Gold mineralization in China: Metallogenic provinces, deposit types and tectonic framework. Gondwana Res. 36, 219-274.

Deng, J., Wang, Q.F., Li, G.J., 2017. Tectonic evolution, superimposed orogeny, and composite metallogenic system in China. Gondwana Res. 50, 216–266.

Deng, J., Wang, Q.F., Li, G.J., Li, C., Wang, C.M., 2014a. Tethys tectonic evolution and its bearing on the distribution of important mineral deposits in the Sanjiang region, SW China, Gondwana Res. 26, 419-437.

Deng, J., Wang, Q.F., Li, G.J., Santosh, M., 2014b. Cenozoic tectono-magmatic and metallogenic processes in the Sanjiang region, southwestern China. Earth Sci. Rev. 138, 268-299.

Deng, Y.F., Song, X.Y., Zhou, T.F., Yuan, F., Chen, L.M., Zheng, W.Q., 2012. Correlations between Fo number and Ni content of olivine of the Huangshandong intrusion, eastern Tianshan, Xinjiang, and the genetic significances. Acta Petrol. Sin. 28, 2224-2234 (in Chinese with English abstract).

DePaolo, D.J., 1981. Trace element and isotopic effects of combined wallrock assimilation and fractional crystallization. Earth Planet. Sci. Lett. 53, 189-202.

Ding, X., Ripley, E.M., Shirey, S.B., Li, C., 2012. Os, Nd, O and S isotope constraints on country rock contamination in the conduit-related Eagle Cu-Ni-(PGE) deposit, Midcontinent Rift System, Upper Michigan. Geochim. Cosmochim. Acta. 89, 10-30.

Dong, G.Z., Ye, M.H., Dai, X.G., Sun, C., 2012. Petrology and geochemistry characteristics of the Cu-Ni sulfide deposits of the 3rd rocks in Hongqiling area, Jilin. Miner. Explor. 2012, 3, 297-304 (in Chinese with English abstract).

Duan, J., Li, C., Qian, Z.Z., Jiao, J.G., Ripley, E.M., Feng, Y.Q., 2016. Multiple S isotopes, zircon Hf isotopes, whole-rock Sr-Nd isotopes, and spatial variations of PGE tenors in the Jinchuan Ni-Cu-PGE deposit, NW China. Mineral. Deposita 51, 557-574.

Duke, J.M., Naldrett, A.J., 1978. A numerical model of the fractionation of olivine and molten sulfide from komatiite magma. Earth Planet. Sci. Lett. 39, 255-266.

Dupré, B., Chauvel, C., Arndt, N.T., 1984. Pb and Nd isotopic study of two Archean komatiitic flows from Alexo, Ontario. Geochim. Cosmochim. Acta. 48, 1965-1972.

Ebel, D.S., Naldrett, A.J., 1997. Crystallization of sulfide liquids and the interpretation of ore composition. Can. J. Earth Sci. 34, 352-365.

Fleet, M.E., Pan, Y., 1994. Fractional crystallization of anhydrous sulfide liquid in the system Fe-Ni-Cu-S, with application to magmatic sulfide deposits. Geochim. Cosmochim. Acta. 58, 3369-3377.

Foster, J.G., Lambert, D.D., Frick, L.R., Maas, R., 1996. Re-Os isotopic evidence for genesis of Archaean nickel ores from uncontaminated komatiites. Nature 382, 703-706.

Gangopadhyay, A., Walker, R. J., 2003. Re-Os systematics of the ca. 2.7-Ga komatiites from Alexo, Ontario, Canada. Chem. Geol. 196, 147-162.

Gao, J.F., Zhou, M.F., Lightfoot, P.C., Wang, C.Y., Qi, L., 2012. Origin of PGE-poor and Cu-rich magmatic sulfides from the Kalatongke deposit, Xinjiang, Northwest China. Econ. Geol. 107, 481-506.

Gao, J.F., Zhou, M.F., Lightfoot, P.C., Wang, C.Y., Qi, L., Sun, M., 2013. Sulfide saturation and magma emplacement in the formation of the Permian Huangshandong Ni-Cu sulfide deposit, Xinjiang, Northwestern China. Econ. Geol. 108, 1833-1848.

Gao, S., Zhang, B.R., Luo, T.C., Li, Z.J., Xie, Q.L., Gu, X.M., Gao, C.L., 1992. Chemical composition of the continental crust in the Qinling Orogenic Belt and its adjacent North China and Yangtze Cratons. Geochim. Cosmochim. Acta. 56, 3933-3950.

Gao, S., Zhang, B.R., Wang, D.P., Ouyang, J.P., Xie, Q.L., 1996. Geochemical evidence for the Proterozoic tectonic evolution of the Qinling Orogenic Belt and its adjacent margins of the North China and Yangtze cratons. Precambrian Res. 80, 23-48.

Han, B.F., Ji, J.Q., Song, B., Chen, L.H., Li, Z.H., 2004. SHRIMP zircon U-Pb ages and implications of the Kalatongke and Huangshandong sulfide-bearing mafic-ultramafic intrusions. Chin Sci Bull. 49, 2324-2328 (in Chinese with English abstract)

Han, C.M., Xiao, W.J., Zhao, G.C., Ao, S.J., Zhang, J.E., Qu, W.J., Du, A.D., 2010. In-situ U-Pb, Hf and Re-Os isotopic analyses of the Xiangshan Ni-Cu-Co deposit in Eastern Tianshan (Xinjiang), Central Asia Orogenic Belt: constraints on the timing and genesis of the mineralization. Lithos 120, 547-562.

Han, C.M., Xiao, W.J., Zhao, G.C., Qu, W.J., Du, A.D., 2007. Re-Os dating of the Kalatongke Cu-Ni deposit, Altay Shan, NW China, and resulting geodynamic implications. Ore Geol. Rev. 32, 452-468.

Hanski, E.J., Huhma, H., Melezhik, V.A., 2014. New isotopic and geochemical data from the Palaeoproterozoic Pechenga greenstone belt, NW Russia: Implication for basin development and duration of the volcanism. Prec. Res. 245: 51-65.

Hao, L.B., Sun, L.J., Zhao, Y.Y., Lu, J.L., 2013. Shrimp Zircon U-Pb Dating of Chajian Mafic-Ultramafic Rocks in Hongqiling Mine Field, Jilin Province, and its implications. Earth Sci. (J. China Univ. Geosci), 38, 233-240 (in Chinese with English abstract).

Hao, L.B., Zhao, X.Y., Boorder, H., Lu, J.L., Zhao, Y.Y., Wei, Q.Q., 2014. Origin of PGE depletion of Triassic magmatic Cu-Ni sulfide deposits in the central-southern area of Jilin province, NE China. Ore Geol. Rev. 63, 226-237.

Hart, S.R., Davis, K.E., 1978. Nickel partitioning between olivine and silicate melt. Earth Planet. Sci.

Lett. 40, 203-219.

Hawley, J.E., 1962. The Sudbury ores, their mineralogy and origin; Part 1, The geological setting. The Can. Mineral. 7, 1-29.

Herzberg, C., Cabral, R.A., Jackson, M.G., Vidito, C., Day, J. M.D., Hauri, E.H., 2014. Phantom Archean crust in Mangaia hotspot lavas and the meaning of heterogeneous mantle. Earth Planet. Sci. Lett. 396, 97-106.

Herzberg, C., Vidito, C., Starkey, N.A., 2016. Nickel-cobalt contents of olivine record origins of mantle peridotite and related rocks. Am. Mineral. 101, 1952-1966.

Hinchey, J. G., Hattori, K. H., 2005. Magmatic mineralization and hydrothermal enrichment of the High Grade Zone at the Lac des Iles palladium mine, northern Ontario, Canada. Mineral. Deposita 40, 13-23.

Huang, F., Xu, J .F., Liu, Y.S., Li, J., Chen, J.L., Li, X. Y., 2017. Re–Os isotope evidence from Mesozoic and Cenozoic basalts for secular evolution of the mantle beneath the North China Craton. Contrib. Miner. Petrol. 172(5): 28.

Hulbert, L.J., Hamilton, M.A., Horan, M.F., Scoates, R.F.J., 2005. U-Pb zircon and Re-Os isotope geochronology of mineralized ultramafic intrusions and associated nickel ores from the Thompson Nickel Belt, Manitoba, Canada. Econ. Geol. 100, 29-41.

Jahn, B. M., Wu, F., Lo, C. H., Tsai, C. H., 1999. Crust-mantle interaction induced by deep subduction of the continental crust: geochemical and Sr-Nd isotopic evidence from post-collisional mafic-ultramafic intrusions of the northern Dabie complex, central China. Chem. Geol. 157, 119-146.

Keays, R.R., Lightfoot, P.C., 2010. Crustal sulfur is required to form magmatic Ni-Cu sulfide deposits: evidence from chalcophile element signatures of Siberian and Deccan Trap basalts. Mineral. Deposita 45, 241-257.

Kerrich, R., Goldfarb, R.J., Richards, J.P., 2005. Metallogenic provinces in an evolving geodynamic framework. 100th Anniversary Volume, Society of Economic Geologists, 1097-1136.

King, S.D., Anderson, D.L., 1998. Edge-driven convection. Earth Planet. Sci. Lett. 160, 289-296.

Kinzler, R.J., Grove, T.L., Recca, S.I., 1990. An experimental study on the effect of temperature and melt composition on the partitioning of nickel between olivine and silicate melt. Geochim. Cosmochim. Acta. 54, 1255-1265.

Lambert, D.D., Foster, J.G., Frick, L.R., Li,C., Naldrett, A.J., 1999. Re-Os isotopic systematics of the Voisey's bay Ni-Cu-Co magmatic ore system, Labrador, Canada. Lithos 47, 69-88.

Lambert, D.D., Frick, L.R., Foster, J.G., Li, C., Naldrett, A.J., 2000. Re-Os isotope systematics of the Voisey's Bay Ni-Cu-Co magmatic sulfide system, Labrador, Canada: II. Implications for parental magma chemistry, ore genesis, and metal redistribution. Econ. Geol. 95, 867-888.

Lassiter, J.C., Hauri, E.H., Reiners, P.W., Garcia, M.O., 2000. Generation of Hawaiian post-erosional lavas by melting of a mixed lherzolite/pyroxenite source. Earth Planet. Sci. Lett. 178, 269-284.

Lehmann, J., Arndt, N., Windley, B., Zhou, M.F., Wang, C.Y., Harris, C., 2007. Field relationships and geochemical constraints on the emplacement of the Jinchuan intrusion and its Ni-Cu-PGE sulfide deposit, Gansu, China. Econ. Geol. 102, 75-94.

Lesher, C.M., 2019, Up, down, or sideways: Emplacement of magmatic Fe-Ni-Cu-PGE sulfide melts in Large Igneous Provinces. Can. J Earth Sci.

Lesher C.M., 2017. Roles of xenomelts, xenoliths, xenocrysts, xenovolatiles, residues, and skarns in the genesis, transport, and localization of magmatic Fe-Ni-Cu-PGE sulfides and chromite. Ore Geol. Rev. 90, 465-484.

Lesher, C.M., 1989. Komatiite-associated nickel sulfide deposits. Rev. Econ. Geol. 4, 45-101.

Lesher, C.M., Arndt, N.T., 1995. REE and Nd isotope geochemistry, petrogenesis and volcanic evolution of contaminated komatiites at Kambalda, Western Australia. Lithos 34, 127-157.

Lesher, C.M., Arndt, N.T., Groves, D.I., 1984. Genesis of komatiite-associated nickel sulphide deposits at Kambalda, Western Australia: A distal volcanic model. Sulphide deposits in mafic and ultramafic

rocks. Institute of Mining and Metallurgy, London, 70-80.

Lesher, C.M., Burnham, O.M., 1999. Mass balance and mixing in dynamic ore-forming magmatic system. Dynamic processes in magmatic ore deposits and their application in mineral exploration. Geological Associations of Canada Short Course Notes, 13, 413-450.

Lesher, C.M., Burnham, O.M., 2001. Multicomponent elemental and isotopic mixing in Ni-Cu-(PGE) ores at Kambalda, Western Australia. Can. Mineral. 39, 421-446.

Lesher, C.M., Burnham, O.M., Keays, R.R., Barnes, S.J., Hulbert, L., 2001. Trace-element geochemistry and petrogenesis of barren and ore-associated komatiites. Can. Mineral. 39, 673-696.

Lesher, C.M., Groves, D.I., 1986. Controls on the formation of komatiite-associated nickel-copper sulfide deposits. In: Friedrich, G.H., Genkin, A.D., Naldrett, A.J. (Eds.), Geology and Metallogeny of Copper Deposits. Springer, pp. 43-62.

Lesher, C.M., Keays, R.R., 1984. Metamorphically and hydrothermally mobilized Fe-Ni-Cu sulphides at Kambalda, Western Australia. In: Buchanan, D.L., Jones, M.J. (Eds.), Sulphide Deposits in Mafic and Ultramafic Rocks. Institution of Mining and Metallurgy, London, pp. 62-69.

Lesher, C.M., Keays, R.R., 2002. Komatiite-associated Ni-Cu-(PGE) deposits: Mineralogy, geochemistry, and genesis. In: Cabri, L.J. (Ed.), The Geology, Geochemistry, Mineralogy, and Mineral Beneficiation of the Platinum-Group Elements. Special vol. 54. Canadian Institute of Mining, Metallurgy, and Petroleum, pp. 579-617.

Lesher, C.M., Stone, W.E., 1996. Igneous trace element geochemistry: applications for massive sulphide exploration, Geol Assoc Can, Short Course Notes. Exploration geochemistry of komatiites. 12, 153-204.

Lesher, C.M., 2013a. The roles of local incorporation, in-situ segregation, and physical transport in the genesis of magmatic sulfide and oxide deposits, GAC-MAC Annual Meeting, Winnipeg, Abstract Volume, 128-129.

Lesher, C.M., 2013b. Physical transport and localization of magmatic Fe-Ni-Cu sulfide melts. In:

Conference Proceedings, SEG 2013: Geoscience for Discovery, Whistler BC, Society of Economic Geologists, abstract (p18) and poster (P1.12), ISBN 978-1-629492-66-7.

Lesher C M, Campbell I H. Geochemical and fluid dynamic modeling of compositional variations in Archean komatiite-hosted nickel sulfide ores in Western Australia. Economic Geology, 1993, 88(4): 804-816.

Li, A., Wang, J., Song, Y., Liu, J.G., Xue, S.C., 2018. Geochemistry characteristics of the ore-bearing mafic-ultramafic intrusions in the Hongqiling Ni-Cu sulfide deposit, NE China and its petrogenesis significance. Acta Geol. Sin. 92(2), 263-277 (in Chinese with English abstract).

Li, C., Naldrett, A.J. 2000. Melting reactions of gneissic inclusions with enclosing magma at Voisey's Bay, Labrador, Canada: Implications with respect to ore genesis. Econ. Geol. 95, 801-814.

Li, C., Naldrett, A.J., 1999. Geology and petrology of the Voisey's Bay intrusion: reaction of olivine with sulfide and silicate liquids. Lithos 47, 1-31.

Li, C., Ripley, E.M., 2011. The giant Jinchuan Ni-Cu-(PGE) deposit: tectonic setting, magma evolution, ore genesis and exploration implications. Rev. Econ. Geol. 17, 163-180.

Li, C., Ripley, E.M., Naldrett, A.J., 2003. Compositional variations of olivine and sulfur isotopes in the Noril'sk and Talnakh intrusions, Siberia: implications for ore-forming processes in dynamic magma conduits. Econ. Geol. 98, 69-86.

Li, C., Ripley, E.M., Tao, Y., Hu, R.Z., 2016. The significance of PGE variations with Sr-Nd isotopes and lithophile elements in the Emeishan flood basalt province from SW China to northern Vietnam. Lithos 248, 1-11.

Li, C., Xu, Z., Waal, S.A., Ripley, E.M., Maier, W.D., 2004. Compositional variations of olivine from the Jinchuan Ni-Cu sulfide deposit, western China: implications for ore genesis. Mineral. Deposita 39, 159-172.

Li, C., Zhang, M.J., Fu, P., Qian, Z.Z., Hu, P.Q., Ripley, E.M., 2012. The Kalatongke magmatic Ni-Cu deposits in the Central Asian Orogenic Belt, NW China: product of slab window magmatism?

Mineral. Deposita 47, 51-67.

Li, C., Zhang, Z., Li, W., Wang, Y., Sun, T., Ripley, E.M., 2015. Geochronology, petrology and Hf-S isotope geochemistry of the newly-discovered Xiarihamu magmatic Ni-Cu sulfide deposit in the Qinghai-Tibet plateau, western China. Lithos 216, 224-240.

Li, H.Q., Chen, F.W., Mei, Y.P., Wu, H., Cheng, S.L., Yang, J.Q., Dai, Y.C., 2006, Dating of the No. 1 intrusion of Pobei basic-ultrabasic rocks belt, Xinjiang, and its geological significance: Mineral Deposits, 25, 63-469 (in Chinese with English abstract).

Li, X.H., Su, L., Chung, S.L., Li, Z.X., Liu, Y., Song, B., Liu, D.Y., 2005. Formation of the Jinchuan ultramafic intrusion and the world's third largest Ni-Cu sulfide deposit: Associated with the 825 Ma south China mantle plume? Geochem., Geophys. Geosyst. 10(4).

Li, Z.X., Bogdanova, S.V., Collins, A.S., Davidson, A., Waele, B., Ernst, R. E., Karlstrom, K.E., 2008. Assembly, configuration, and break-up history of Rodinia: a synthesis. Precambrian Res. 160, 179-210.

Li, Z.X., Li, X.H., Kinny, P.D., Wang, J., 1999. The breakup of Rodinia: did it start with a mantle plume beneath South China? Earth Planet. Sci. Lett. 1999, 173, 171-181.

Li, Z.X., Li, X.H., Kinny, P.D., Wang, J., Zhang, S., Zhou, H., 2003. Geochronology of Neoproterozoic syn-rift magmatism in the Yangtze Craton, South China and correlations with other continents: evidence for a mantle superplume that broke up Rodinia. Precambrian Res. 122, 85-109.

Lightfoot, P. C., Evans-Lamswood, D., 2015. Structural controls on the primary distribution of mafic-ultramafic intrusions containing Ni-Cu-Co-(PGE) sulfide mineralization in the roots of large igneous provinces. c 64, 354-386.

Lightfoot, P.C., Keays, R.R., 2005. Siderophile and chalcophile metal variations in flood basalts from the Siberian Trap, Noril’sk Region: implications for the origin of the Ni-Cu-PGE sulfide ores. Econ. Geol. 100, 439-462.

Ling, J.L., 2014. Petrogenesis of Mafic-ultramafic Intrusions and Minerogenesis of Nickel Sulfide

Deposit in the Periphery of Qaidam Block, Qinghai China. Ph.D. thesis, Chang'an University, 1-178 (in Chinese with English abstract).

Lu, L.S, Mao, J.W., Li, H.B., Pirajno, F., Zhang, Z.H., Zhou, Z.H., 2011. Pyrrhotite Re-Os and SHRIMP zircon U-Pb dating of the Hongqiling Ni-Cu sulfide deposits in Northeast China. Ore Geol. Rev. 43, 106-119.

Lu, L.S., Liu, J., Zhang, Z.H., Xie, G.Q., 2007. Temporal-spatial distribution and geodymanic settings of magmatic Ni-Cu-(PGE) Sulfide deposits in china. Acta Petrologica Sinica, 23(10) (in Chinese with English abstract)

Lu, L.S., Mao.J.W., Zhou, Z.H., Li, H.B, Zhang, Z.H., and Wang, Y.F., 2012. Mineral chemistry of ore-bearing ultramafic rocks from Hongqiling No.1 and 7 intrusions in Jilin province: Constrains on the magmatic process and the metallogenesis of Ni-Cu sulfide deposit: Acta Petrol. Sin. 28, 319-344 (in Chinese with English abs.).

Lu, Y.G., Zhao, K., Xiong, Y.Q., Li, P., Du, D.Y., Yuan, M.W., 2014. Elements geochemistry of Jinbaoshan Pt-Pd deposit, western Yunnan, China. Acta Petrol. Sin. 30, 2681-2694 (in Chinese with English abstract).

Lu, Y., Lesher, C. M., Yang, L., Leybourne, M. I., He, W., Yuan, M., Yang, Z., Gao, X., 2021. Genesis of the Jinbaoshan PGE-(Cu)-(Ni) deposit: Distribution of chalcophile elements and platinum-group minerals. Can. Mineral. 59(6), 1511-1542.

Luguet, A., Pearson, D.G., Nowell, G.M., Dreher, S.T., Coggon, J.A., Spetsius, Z.V., Parman, S.W., 2008. Enriched Pt-Re-Os isotope systematics in plume lavas explained by metasomatic sulfides. Science, 319(5862): 453-456.

Lynn, K.J., Shea, T., Garcia, M.O., 2017. Nickel variability in Hawaiian olivine: Evaluating the relative contributions from mantle and crustal processes. Am. Mineral. 102, 507-518.

Maier, W.D., Barnes, S.J., Campbell, I.H., Fiorentini, M.L., Peltonen, P., Barnes, S.J., Smithies, R. H., 2009. Progressive mixing of meteoritic veneer into the early Earth's deep mantle. Nature 460, 620-623.

Mao, J.W., Du, A.D., 2002. The 982 Ma Re-Os age of copper-nickel sulfide ores in the Baotan area, Guangxi and its geological significance. Science in China (Series D) 31, 992-998 (in Chinese with English abstract).

Mao, J.W., Pirajno, F., Zhang, Z.H., Chai, F.M., Wu, H., Chen, S.P., Zhang, C.Q., 2008. A review of the Cu-Ni sulphide deposits in the Chinese Tianshan and Altay orogens (Xinjiang Autonomous Region, NW China): principal characteristics and ore-forming processes. J. Asian Earth Sci. 32, 184-203.

Mao, Q.G., Xiao, W. J., Han, C. M., Sun, M., Yuan, C., Yan, Z., Li, J. Z., Yong, Y., Zhang, J. E., 2006. Zircon U-Pb age and the geochemistry of the Baishiquan mafic-ultramafic complex in the Eastern Tianshan, Xinjiang province: constraints on the closure of the Paleo-Asian Ocean. Acta Petrol. Sin. 22, 153-162 ( (in Chinese with English abstract).

Mao, Y.J., Qin, K.Z., Barnes, S.J., Tang, D.M., Xue, S.C., Le Vaillant, M., 2017. Genesis of the Huangshannan high-Ni tenor magmatic sulfide deposit in the Eastern Tianshan, northwest China: Constraints from PGE geochemistry and Os-S isotopes. Ore Geol. Rev. 90, 591-606.

Mao, Y.J., Qin, K.Z., Li, C., Xue, S.C., Ripley, E.M., 2014. Petrogenesis and ore genesis of the Permian Huangshanxi sulfide ore-bearing mafic-ultramafic intrusion in the Central Asian Orogenic Belt, western China. Lithos 200, 111-125.

Matzen, A.K., Baker, M.B., Beckett, J.R., Stolper, E.M., 2013. The temperature and pressure dependence of nickel partitioning between olivine and silicate melt. J. Petrol. 54, 2521-2545.

Mudd, G.M., Jowitt, S.M., 2014. A detailed assessment of global nickel resource trends and endowments. Econ. Geol. 109, 1813-1841.

Mungall, J.E., Brenan, J.M., Godel, B., Barnes, S.J., Gaillard, F., 2015. Transport of metals and sulphur in magmas by flotation of sulphide melt on vapour bubbles. Nat. Geosci. 8, 216.

Naldrett, 2004. Magmatic sulfide deposits—geology, geochemistry and exploration: Berlin, Heidelberg, New York, Springer, 1-727.

Naldrett, A.J., 1981. Nickel sulfide deposits: classification, composition and genesis. Econ. Geol, 75:

628-655.

Naldrett, A.J., 1999. World-class Ni-Cu-PGE deposits: key factors in their genesis. Mineral. Deposita 34, 227-240.

Naldrett, A.J., 2010. Secular variation of magmatic sulfide deposits and their source magmas. Econ. Geol. 105, 669-688.

Naldrett, A.J., 2011. Fundamentals of magmatic sulfide deposits. Rev. Econ. Geol. 17, 1-50.

Naldrett, A.J., Barnes, S.-J. 1986. The behaviour of platinum group elements during fractional crystallization and partial melting with special reference to the composition of magmatic sulfide ores. Fortschr. Miner. 63, 113-133.

Pagé, P., Barnes, S.-J., 2016. The influence of chromite on osmium, iridium, ruthenium and rhodium distribution during early magmatic processes. Chem. Geol. 420, 51-68.

Pearce, J.A., 2008. Geochemical fingerprinting of oceanic basalts with applications to ophiolite classification and the search for Archean oceanic crust. Lithos 100, 14-48.

Pearson, D.G., Nowell, G.M., 2004. Re-Os and Lu-Hf isotope constraints on the origin and age of pyroxenites from the Beni Bousera peridotite massif: implications for mixed peridotite-pyroxenite mantle sources. J. Petrol. 45, 439-455.

Peng, B., Sun, F., Li, B., Wang, G., Li, S., Zhao, T., Zhi, Y., 2016. The geochemistry and geochronology of the Xiarihamu II mafic-ultramafic complex, Eastern Kunlun, Qinghai Province, China: Implications for the genesis of magmatic Ni-Cu sulfide deposits. Ore Geol. Rev. 73, 13-28.

Peng, R.M., Zhai, Y.S., Li, C., Ripley, E.M., 2013. The Erbutu Ni-Cu deposit in the Central Asian orogenic belt: A Permian magmatic sulfide deposit related to boninitic magmatism in an arc setting. Econ. Geol. 108, 1879-1888.

Pirajno, F., 2012. The Geology and Tectonic Settings of China's Mineral Deposits. Springer Science & Business Media.

Qin, K. Z., Su, B. X., Sakyi, P. A., Tang, D. M., Li, X. H., Sun, H., Xiao, Q. H., Liu, P. P., 2011. SIMS zircon U-Pb geochronology and Sr-Nd isotopes of Ni-Cu-bearing mafic-ultramafic intrusions in Eastern tianshan and Beishan in correlation with flood basalts in Tarim basin (NW China): Constraints on a Ca. 280 Ma mantle plume. Am. J. Sci. 311, 237-260.

Ripley, E.M., Li, C., 2013. Sulfide saturation in mafic magmas: is external sulfur required for magmatic Ni-Cu-(PGE) ore genesis? Econ. Geol. 108, 45-58.

Ripley, E.M., Sarkar, A., Li, C., 2005. Mineralogic and stable isotope studies of hydrothermal alteration at the Jinchuan Ni-Cu deposit, China. Econ. Geol. 100, 1349-1361.

Rudnick, R.L., Fountain, D.M., 1995. Nature and composition of the continental crust: a lower crustal perspective. Rev. Geophys. 33(3), 267–309.

Rudnick, R.L., Gao, S., Ling, W.L., Liu, Y.S., McDonough, W.F., 2004. Petrology and geochemistry of spinel peridotite xenoliths from Hannuoba and Qixia, North China craton. Lithos 77, 609-637.

Sengör, A.M.C., Natal'In, B.A., Burtman, V.S., 1993. Evolution of the Altaid tectonic collage and Palaeozoic crustal growth in Eurasia. Nature 364, 299-307.

Shirey, S.B., Barnes, S.-J. 1994. Re-Os and Sm-Nd isotopic constraints on basaltic komatiitic volcanism and magmatic sulphide formation in the Cape Smith Foldbelt, Quebec. DELTA, 2, 3.

Shirey, S.B., Walker, R.J., 1998. The Re-Os isotope system in cosmochemistry and high-temperature geochemistry. Annual Review of Earth and Planetary Sciences, 26(1): 423-500.

Sinyakova, E.F., Kosyakov, V.I., 2009. Experimental modeling of zonality of copper-rich sulfide ores in copper-nickel deposits//Doklady Earth Sciences. SP MAIK Nauka/Interperiodica, 427(1): 787-792.

Sleep, N.H., 2005. Evolution of the continental lithosphere. Annu. Rev. Earth Planet. Sci., 33, 369-393.

Sobolev, A.V., Hofmann, A.W., Kuzmin, D.V., Yaxley, G.M., Arndt, N.T., Chung, S.L., Gurenko, A.A., 2007. The amount of recycled crust in sources of mantle-derived melts. Science 316, 412-417.

Sobolev, A.V., Hofmann, A.W., Sobolev, S.V., Nikogosian, I.K., 2005. An olivine-free mantle source of

Hawaiian shield basalts. Nature 434, 590-597.

Sobolev, A.V., Krivolutskaya, N.A., Kuzmin, D.V., 2009. Petrology of the parental melts and mantle sources of Siberian trap magmatism. Petrology 17, 253-286.

Song, X. Y., Chen, L. M., Deng, Y. F., Xie, W., 2013. Syncollisional tholeiitic magmatism induced by asthenosphere upwelling owing to slab detachment at the southern margin of the Central Asian Orogenic Belt. Journal of the Geological Society, 170, 941-950.

Song, X.Y., Danyushevsky, L.V., Keays, R.R., Chen, L M., Wang, Y.S., Tian, Y.L., Xiao, J.F., 2012. Structural, lithological, and geochemical constraints on the dynamic magma plumbing system of the Jinchuan Ni-Cu sulfide deposit, NW China. Mineral. Deposita 47, 277-297.

Song, X.Y., Keays, R.R., Zhou, M.F., Qi, L., Ihlenfeld, C., Xiao, J.F., 2009. Siderophile and chalcophile elemental constraints on the origin of the Jinchuan Ni-Cu-(PGE) sulfide deposit, NW China. Geochim. Cosmochim. Acta. 73, 404-424.

Song, X. Y., Li, X. R., 2009. Geochemistry of the Kalatongke Ni-Cu-(PGE) sulfide deposit, NW China: implications for the formation of magmatic sulfide mineralization in a postcollisional environment. Mineral. Deposita 44, 303-327.

Song, X.Y., Yi, J.N., Chen, L.M., She, Y.W., Liu, C.Z., Dang, X.Y., Yang, Q.A., Wu, S.K., 2016. The giant Xiarihamu Ni-Co sulfide deposit in the East Kunlun orogenic belt, northern Tibet plateau, China. Econ. Geol. 111, 29-55.

Song, X.Y., Zhou, M.F., Cao, Z.M., Sun, M., Wang, Y. L., 2003. Ni-Cu-(PGE) magmatic sulfide deposits in the Yangliuping area, Permian Emeishan igneous province, SW China. Mineral. Deposita 38(7), 831-843.

Song, X.Y., Zhou, M.F., Tao, Y., Xiao, J.F., 2008. Controls on the metal compositions of magmatic sulfide deposits in the Emeishan large igneous province, SW China. Chem. Geol. 253, 38-49.

Straub, S.M., Gomez-Tuena, A., Stuart, F.M., Zellmer, G.F., Espinasa-Perena, R., Cai, Y., Iizuka, Y., 2011. Formation of hybrid arc andesites beneath thick continental crust. Earth Planet. Sci. Lett. 303, 337-

347.

Straub, S.M., LaGatta, A.B., Pozzo, M.D., Lillian, A., Langmuir, C.H., 2008. Evidence from high-Ni olivines for a hybridized peridotite/pyroxenite source for orogenic andesites from the central Mexican Volcanic Belt. Geochem., Geophys. Geosyst. 9, 1-33.

Su, B.X., Qin, K.Z., Tang, D.M., Deng, G., Xiao, Q.H., Sun, H., Lu, H.F., Dai, Y.C., 2011. Petrological features and implications for mineralization of the Poshi mafic-ultramafic intrusion in Beishan area, Xinjiang. Acta Petrol. Sin. 27, 3627-3639 (in Chinese with English abstract).

Su, S.G., Lesher, C.M., 2012. Genesis of PGE mineralization in the Wengeqi mafic-ultramafic complex, Guyang County, Inner Mongolia, China. Mineral. Deposita 47, 197-207.

Sun, L.J., 2013. Geological and Geochemical Characteristics of Hongqiling Cu-Ni Sulfide Deposit and Prospecting Techniques for the Same Type Deposit. Ph.D. thesis, Jilin University, 1-157 (in Chinese with English abstract).

Sun, S.-S., and McDonough, W.F., 1989. Chemical and isotopic systematics of oceanic basalts: implications for mantle composition and processes. *in* Saunders, A.D., Norry, M.J. (eds), Magmatism in the Ocean Basins, Geol. Soc. Spec. Publ. 42, 313-345.

Sun, T., 2011. The Magmatic Sulfide Deposit in the Huangshan Mafic-ultramafic Rocks Belt, Eastern Tianshan, and its Mineralization. Ph.D. thesis, Chang'an University, 1-117 (in Chinese with English abstract).

Sun, T., Qian, Z.Z., Deng, Y.F., Li, C., Song, X.Y., Tang, Q., 2013. PGE and isotope (Hf-Sr-Nd-Pb) constraints on the origin of the Huangshandong magmatic Ni-Cu sulfide deposit in the Central Asian orogenic belt, northwestern China. Econ. Geol. 108, 1849-1864.

Sun, T., Wang, D.H., Qian, Z.Z., Fu, Y., Chen, Z.H., Lou, D.B., 2015. A Preliminary Review of the Metallogenic Regularity of Nickel Deposits in China. Acta Geol. Sin. (English Edition), 89(4): 1375-1397.

Sun, X.M, Wang, S.W., Sun, W.D., Shi, G.Y., Sun, Y.L., Xiong, D.X., Qu, W.J., Du, A.D., 2008. PGE

geochemistry and Re-Os dating of massive sulfide ores from the Baimazhai Cu-Ni deposit, Yunnan province, China. Lithos 105, 12-24.

Tang, D.M., Qin, K.Z., Li, C., Qi, L., Su, B.X., Qu, W.J., 2011. Zircon dating, Hf-Sr-Nd-Os isotopes and PGE geochemistry of the Tianyu sulfide-bearing mafic-ultramafic intrusion in the Central Asian Orogenic Belt, NW China. Lithos 126, 84-98.

Tang, D.M., Qin, K.Z., Sun, H., Qi, L., Xiao, Q.H., Su, B.X., 2009. PGE geochemical characteristics of Tianyu magmatic Cu-Ni deposit: implications for magma evolution and sulfide segregation. Acta Geol. Sin. 83, 680-697 (in Chinese with English abstract)

Tang, D.M., Qin, K.Z., Sun, H., Su, B.X., Xiao, Q.H., 2012. The role of crustal contamination in the formation of Ni-Cu sulfide deposits in Eastern Tianshan, Xinjiang, Northwest China: Evidence from trace element geochemistry, Re-Os, Sr-Nd, zircon Hf-O, and sulfur isotopes. J. Asian Earth Sci. 49, 145-160.

Tang, Q.Y., Ma, Y.S., Zhang, M.J., Li, C., Zhu, D., Tao, Y., 2013. The origin of Ni-Cu-PGE sulfide mineralization in the margin of the Zhubu mafic-ultramafic Intrusion in the Emeishan large igneous province, southwestern China. Econ. Geol. 108, 1889-1901.

Tang, Z. L, 1993. Genetic model of the Jinchuan nickel-copper deposit. Geol Assoc Can Special Paper, 40, 389-401.

Tang, Z.L., Li, W.Y., 1995. Mineralisation model and geology of the Jinchuan Ni-Cu sulfide deposit bearing PGE. Geological, Beijing, 210.

Tang, Z.L., Song, X.Y., Su, S.G., 2009. Ni-Cu deposits related to high-Mg basaltic magma, Jinchuan, Western China. New developments in magmatic Ni-Cu and PGE deposits. Geological Publishing House, Beijing, 121-140.

Tang, Z.L., Xu, G., Wang, Y.L., Qiu, G.L., Dai, J.F., 2012. The New Exploration of Magmatic Mineralization: Small Intrusion Mineralization and Geological prospecting breakthrough. Northwestern Geology, 45, 1-16 (in Chinese with English abstract)

Tao, Y., Hu, R.Z., Qi, L., Qu, W.J., Chu, Z.Y., Gou, T.Z., 2010a. Sr-Nd-Os isotopic constraints on magma origin and evolution of the Jinbaoshan Pt-Pd deposit, Yunnan, J. Mineral. Petrol. 30, 60-67 (in Chinese with English abstract).

Tao, Y., Li, C., Hu, R., Qi, L., Qu, W., Du, A., 2010b. Re-Os isotopic constraints on the genesis of the Limahe Ni-Cu deposit in the Emeishan large igneous province, SW China. Lithos 119, 137-146.

Tao, Y., Li, C., Hu, R., Ripley, E.M., Du, A., Zhong, H., 2007. Petrogenesis of the Pt-Pd mineralized Jinbaoshan ultramafic intrusion in the Permian Emeishan large igneous province, SW China. Contrib. Miner. Petrol. 153, 321-337.

Tao, Y., Li, C., Song, X.Y., Ripley, E.M., 2008. Mineralogical, petrological, and geochemical studies of the Limahe mafic-ultramatic intrusion and associated Ni-Cu sulfide ores, SW China. Mineral. Deposita 43, 849-872.

Tao, Y., Ma, Y.S., Miao, L.C., Zhu, F.L, 2009. SHRIMP U-Pb zircon age of the Jinbaoshan ultramafic intrusion, Yunnan Province, SW China. Chin. Sci. Bull. 54, 168-172.

Thakurta, J., Ripley, E.M., Li, C., 2008. Geochemical constraints on the origin of sulfide mineralization in the Duke Island Complex, southeastern Alaska. Geochem., Geophys. Geosyst. 9(7).

Tonnelier, N.J., 2010. Geology and genesis of the Jinchuan Ni-Cu-(PGE) deposit, China: Unpublished Ph.D. thesis, Sudbury, Canada, Laurentian University, 1-192.

Tornos, F., Casquet, C., Galindo, C., Velasco, F., Canales, A., 2001. A new style of Ni-Cu mineralization related to magmatic breccia pipes in a transpressional magmatic arc, Aguablanca, Spain. Mineral. Deposita 36, 700-706.

Walker, R.J., Morgan, J.W., Hanski, E., and Smolkin, V.F., 1994. The role of the Re-Os isotope system in deciphering the origin of magmatic sulphide ores: A tale of three ores. Ontario Geological Survey Special Volume 5, 343-355.

Wang, C.Y., Wei, B., Zhou, M.F., Minh, D.H., Qi, L., 2018. A synthesis of magmatic Ni-Cu-(PGE) sulfide deposits in the 260 Ma Emeishan large igneous province, SW China and northern Vietnam. J. Asian

Earth Sci. 154, 162-186.

Wang, C.Y., Zhou, M.F., 2006. Genesis of the Permian Baimazhai magmatic Ni-Cu-(PGE) sulfide deposit, Yunnan, SW China. Mineral. Deposita 41, 771-783.

Wang, C.Y., Zhou, M.F., Keays, R.R., 2006. Geochemical constraints on the origin of the Permian Baimazhai mafic-ultramafic intrusion, SW China. Contrib. Miner. Petrol. 152, 309-321.

Wang, C.Y., Zhou, M.F., Qi, L., 2007. Permian flood basalts and mafic intrusions in the Jinping (SW China)-Song Da (northern Vietnam) district: mantle sources, crustal contamination and sulfide segregation. Chem. Geol. 243, 317-343.

Wang, C.Y., Zhou, M.F., Qi, L., 2010. Origin of extremely PGE-rich mafic magma system: an example from the Jinbaoshan ultramafic sill, Emeishan large igneous province, SW China. Lithos 119, 147-161.

Wang, C.Y., Zhou, M.F., Qi, L., 2011. Chalcophile element geochemistry and petrogenesis of high-Ti and low-Ti magmas in the Permian Emeishan large igneous province, SW China. Contrib. Miner. Petrol. 161, 237-254.

Wang, C.Y., Zhou, M.F., Sun, Y.L, Arndt, N.T., 2012. Differentiation, crustal contamination and emplacement of magmas in the formation of the Nantianwan mafic intrusion of the~260 Ma Emeishan large igneous province, SW China. Contrib. Miner. Petrol. 161, 164(2), 281-301.

Wang, H., Qu, W.J., Li, H.Q., Chen, S.P., 2007. Dating and discussion on the rockforming and ore-forming age of newly-discovered Cu-Ni-sulfide deposits in Hami, Xinjiang. Acta Geol. Sin. 81, 526-530 (in Chinese with English abstract).

Wang, M.X., Wang, C.Y., 2012. Mineral chemistry of Zhouan ultramafic intrusion on northern margin of the Yangtze Block: implications for origin of intrusion and Ni-Cu-(PGE) sulfide mineralization. Mineral Deposits 31, 179-194 (in Chinese with English abstract).

Wang, M.X., Wang, C.Y., Sun, Y., 2013b. Mantle source, magma differentiation and sulfide saturation of the 637Ma Zhouan mafic-ultramafic intrusion in the northern margin of the Yangtze Block, Central

China. Precambrian Res. 228, 206-222.

Wang, M.X., Wang, C.Y., Zhao, J.H., 2013a. Zircon U/Pb dating and Hf-O isotopes of the Zhouan ultramafic intrusion in the northern margin of the Yangtze Block, SW China: Constraints on the nature of mantle source and timing of the supercontinent Rodinia breakup. Chin. Sci. Bull. 58, 777-787.

Wang, Y.P., Mo, X.Y., 1995. Basic characteristics of active tectonics in China. Episodes 18, 73-82.

Wang, Z.R, Gaetani, G.A., 2008. Partitioning of Ni between olivine and siliceous eclogite partial melt: experimental constraints on the mantle source of Hawaiian basalts. Contrib. Miner. Petrol. 156, 661-678.

Wei, B., Wang, C.Y., Arndt, N.T., Prichard, H.M., Fisher, P.C., 2015. Textural Relationship of Sulfide Ores, PGE, and Sr-Nd-Os Isotope Compositions of the Triassic Piaohechuan Ni-Cu Sulfide Deposit in NE China. Econ. Geol. 110, 2041-2062.

Wei, B., Wang, C.Y., Li, C., Sun, Y., 2013. Origin of PGE-depleted Ni-Cu sulfide mineralization in the Triassic Hongqiling No. 7 orthopyroxenite intrusion, Central Asian orogenic belt, northeastern China. Econ. Geol. 108, 1813-1831.

Windley, B. F., Alexeiev, D., Xiao, W., Kröner, A., Badarch, G., 2007. Tectonic models for accretion of the Central Asian Orogenic Belt. J. Geol. Soc. 164, 31-47.

Windley, B.F., Kröner, A., Guo, J., Qu, G., Li, Y., Zhang, C., 2002. Neoproterozoic to Paleozoic geology of the Altai orogen, NW China: new zircon age data and tectonic evolution. J. Geol. 110, 719-737.

Windley B F, Maruyama S, Xiao W J. Delamination/thinning of sub-continental lithospheric mantle under Eastern China: The role of water and multiple subduction. American J. Sci, 2010, 310(10): 1250-1293.

Woodhead, J.D., Harmon, R.S., & Fraser, D.G., 1987. O, S, Sr, and Pb isotope variations in volcanic rocks from the Northern Mariana Islands: implications for crustal recycling in intra-oceanic arcs. Earth Planet. Sci. Lett. 83, 39-52.

Wu F.Y., Wilde S.A., Zhang G.L., Sun, D.Y., 2004. Geochronology and petrogenesis of the post-orogenic Cu-Ni sulfide-bearing mafic-ultramafic complexes in Jilin Province, NE China. J. Asian Earth Sci. 23, 781-797.

Xia, M.Z., Jiang, C.Y., Li, C., Xia, Z.D., 2013. Characteristics of a newly discovered Ni-Cu sulfide deposit hosted in the Poyi ultramafic intrusion, Tarim Craton, NW China. Econ. Geol. 108, 1865-1878.

Xiao, L., Xu, Y.G., Mei, H.J., Zheng, Y.F., He, B., Pirajno, F., 2004. Distinct mantle sources of low-Ti and high-Ti basalts from the western Emeishan large igneous province, SW China: implications for plume-lithosphere interaction. Earth Planet. Sci. Lett. 228, 525-546.

Xiao, W.J., Han, C.M., Yuan, C., Sun, M., Lin, S.F., Chen, H.L., Li, Z.L., Li, J.L., Sun, S., 2008. Middle Cambrian to Permian subduction-related accretionary orogenesis of Northern Xinjiang, NW China: implications for the tectonic evolution of central Asia. J. Asian Earth Sci. 32, 102-117.

Xiao, W.J., Windley, B.F., Hao, J., Zhai, M.G., 2003. Accretion leading to collision and the Permian Solonker suture, Inner Mongolia, China: termination of the central Asian orogenic belt. Tectonics 22(6).

Xiao, W.J., Windley, B.F., Huang, B.C., Han, C.M., Yuan, C., Chen, H.L., Li, J.L., 2009. End-Permian to mid-Triassic termination of the accretionary processes of the southern Altaids: implications for the geodynamic evolution, Phanerozoic continental growth, and metallogeny of Central Asia. Int. J. Earth Sci. 98, 1189-1217.

Xie, H.Q., Zhang, F.Q., Miao, L.C., Li, T.S., Liu, D.Y., 2007. Characteristics of the Piaohechuan mafic-ultramafic complex, central Jilin, Northeast China: Constrains on the nature and evolution of the northeastern North China marginal tectonic belt. Geol. Bull. China, 26(7): 810- 822 (in Chinese with English abstract).

Xie, W., Song, X.Y., Chen, L.M., Deng, Y.F., Zheng, W.Q., Wang, Y.S., Luan, Y., 2014. Geochemistry insights on the genesis of the subduction-related Heishan magmatic Ni-Cu-(PGE) deposit, Gansu, northwestern China, at the southern margin of the Central Asian Orogenic Belt. Econ. Geol. 109,

1563-1583.

Xie, W., Song, X.Y., Deng, Y.F., Chen, L.M., Zhang, X.Q., Zheng, W.Q., Wei, X., 2013. Geology and olivine geochemistry of the Heishan Ni-Cu-(PGE) sulfide deposit, Gansu, NW China. Acta Petrol. Sin. 29, 3487-3502 (in Chinese with English abstract).

Xie, W., Song, X.Y., Deng, Y.F., Wang, Y.S., Ba, D.H., Zheng, W.Q., Li, X.B., 2012. Geochemistry and petrogenetic implications of a Late Devonian mafic-ultramafic intrusion at the southern margin of the Central Asian Orogenic Belt. Lithos 144, 209-230.

Xu, B., Jian, P., Zheng, H.F., Zou, H.B., Zhang, L.F., Liu, D. Y., 2005. U-Pb zircon geochronology and geochemistry of Neoproterozoic volcanic rocks in the Tarim Block of northwest China: implications for the breakup of Rodinia supercontinent and Neoproterozoic glaciations. Precambrian Res. 136, 107-123.

Xu, X., Song, S.G., Allen, M. B., Ernst, R. E., Niu, Y.L., Su, L., 2016. An 850-820 Ma LIP dismembered during breakup of the Rodinia supercontinent and destroyed by Early Paleozoic continental subduction in the northern Tibetan Plateau, NW China. Precambrian Res. 282, 52-73.

Xu, Y.G., Chung, S.L., Jahn, B.M., Wu, G.Y., 2001. Petrologic and geochemical constraints on the petrogenesis of Permian-Triassic Emeishan flood basalts in southwestern China. Lithos 58, 145-168.

Xu, Y.G., He, B., Chung, S.L., Menzies, M.A., Frey, F.A., 2004. Geologic, geochemical, and geophysical consequences of plume involvement in the Emeishan flood-basalt province. Geology 32, 917-920.

Xu, Y.G., Wang, Y., Wei, X., He, B., 2013. Mantle plume-related mineralization and their principal controlling factors. Acta Petrol. Sin. 29, 3307-3322 (in Chinese with English abstract).

Xue, S.C., Qin, K.Z., Li, C., Tang, D.M., Mao, Y.J., Qi, L., Ripley, E. M., 2016. Geochronological, petrological, and geochemical constraints on Ni-Cu sulfide mineralization in the Poyi ultramafic-troctolitic intrusion in the northeast rim of the Tarim Craton, Western China. Econ. Geol. 111, 1465-1484.

Yang, G., Du, A., Lu, J., Qu, W.J., Chen, J.F., 2005. Re-Os (ICP-MS) dating of the massive sulfide ores

from the Jinchuan Ni-Cu-PGE deposit. Science in China (Series D) 48, 1672-1677.

Yang, L.Q., Deng, J., Dilek, Y., Qiu, K.F., Ji, X.Z., Li, N., Taylor, R.D., Yu, J.Y., 2015a. Structure, geochronology, and petrogenesis of the Late Triassic Puziba granitoid dikes in the Mianlue Suture Zone, Qinling Orogen, China. Geol. Soc. Am. Bull. 11, 1831-1854

Yang, L.Q., Ji, X.Z., Santosh, M., Li, N., Zhang, Z.C., & Yu, J.Y., 2015b. Detrital zircon U-Pb ages, Hf isotope, and geochemistry of Devonian chert from the Mianlue suture: Implications for tectonic evolution of the Qinling orogen. J. Asian Earth Sci. 113, 589-609.

Yang, S.F., Chen, H.L., Li, Z.L., Li, Y.Q., Yu, X., Li, D, X., Meng, L.F., 2013. Early Permian Tarim large igneous province in northwest China. Science China Earth Sciences, 56, 2015-2026.

Yang, S.H, Qu, W., Tian, Y., Chen, J., Yang, G., Du, A., 2008. Origin of the inconsistent apparent Re-Os ages of the Jinchuan Ni-Cu sulfide ore deposit, China: Post-segregation diffusion of Os. Chem. Geol. 247, 401-418.

Yang, S.H., Zhou, M.F., 2009. Geochemistry of the~ 430-Ma Jingbulake mafic-ultramafic intrusion in Western Xinjiang, NW China: Implications for subduction related magmatism in the South Tianshan orogenic belt. Lithos 113, 259-273.

Yang, S.H., Zhou, M.F., Lightfoot, P.C., Malpas, J., Qu, W.J., Zhou, J.B., Kong, D.Y., 2012. Selective crustal contamination and decoupling of lithophile and chalcophile element isotopes in sulfide-bearing mafic intrusions: An example from the Jingbulake intrusion, Xinjiang, NW China. Chem. Geol. 302, 106-118.

Yang, S.H., Zhou, M.F., Lightfoot, P.C., Xu, J.F., Wang, C.Y., Jiang, C.Y., Qu, W.J., 2014. Re-Os isotope and platinum-group element geochemistry of the Pobei Ni-Cu sulfide-bearing mafic-ultramafic complex in the northeastern part of the Tarim Craton. Mineral. Deposita 49, 381-397.

Ying, L.J., Chen, Y.C., Wang, D.H., Tang, J.X., Chen, Z.H., Wang, C. H., 2014. Metallogenic regularity of copper ore in China. Acta Geol. Sin. 88, 2216-2226 (in Chinese with English abstract).

You, M.X., 2014. Geological, geochemical and metallogenic characteristics of the ultramafic intrusions

in Panxi district. Master thesis. Chinese Academy of Geological Sciences: 1-88 (in Chinese with English abstract).

Yu, X., Yang, S.F., Chen, H.L., Li, Z.L., Li, Y. Q., 2017. Petrogenetic model of the Permian Tarim Large Igneous Province. Science China Earth Sciences, 60, 1805-1816.

Yuan, F., Zhou, T.F., Zhang, D.Y., Jowitt, S. M., Keays, R. R., Liu, S., Fan, Y., 2012. Siderophile and chalcophile metal variations in basalts: Implications for the sulfide saturation history and Ni-Cu-PGE mineralization potential of the Tarim continental flood basalt province, Xinjiang Province, China. Ore Geol. Rev. 45, 5-15.

Zeng, W., Sima, X.Z., Wang, J.S., Wang, J.M., Ran, H., Liu, X.X., Duan, M., Chen, J.Q., 2016. Geochronology, geochemistry and Sr-Nd isotope characteristics of Zhou'an Cu-Ni-PGE deposit: Genesis of mafic-ultramafic rock and ore deposit. Acta Petrol. Sin. 32, 1232-1248 (in Chinese with English abstract).

Zhang, M.J, Kamo, S.L., Li, C., Hu, P., Ripley, E.M., 2010. Precise U-Pb zircon-baddeleyite age of the Jinchuan sulfide ore-bearing ultramafic intrusion, western China. Mineral. Deposita 45, 3-9.

Zhang, M.J, Li, C., Fu, P., Hu, P.Q, Ripley, E.M., 2011. The Permian Huangshanxi Cu-Ni deposit in western China: intrusive-extrusive association, ore genesis, and exploration implications. Mineral. Deposita 46, 153-170.

Zhang, X.S., 2005. Mafic-ultramafic rocks, metallogenetic series and prospecting targeting in the Jinping-Song Da rift. PhD thesis. Kunming University of Science and Technology: 1-263 (in Chinese with English abstract).

Zhang, Z.C., Mao, J.W., Chai, F.M., Yan, S.H., Chen, B.L., Pirajno, F., 2009. Geochemistry of the Permian Kalatongke mafic intrusions, northern Xinjiang, northwest China: implications for the genesis of magmatic Ni-Cu sulfide deposits. Econ. Geol. 104, 185-203.

Zhang, Z.H., Mao, J.W., Du, A.D., Pirajno, F., Wang, Z.L., Chai, F.M., Zhang, Z.C., Yang, J.M., 2008. Re-Os dating of two Cu-Ni sulfide deposits in northern Xinjiang, NW China and its geological significance. J. Asian Earth Sci. 32, 204-217.

Zhang, Z.W., 2013. The Geological and Geochemical Characteristics of Mafic-ultramafic Intrusions in the Hualong area, Southern Qilian Mountains, and its Ni-Cu Mineralization. PhD thesis. Chang'an University: 1-178 (in Chinese with English abstract).

Zhang, Z.W., Tang, Q.Y., Li, C., Wang, Y.L., Ripley, E.M., 2017. Sr-Nd-Os-S isotope and PGE geochemistry of the Xiarihamu magmatic sulfide deposit in the Qinghai-Tibet plateau, China. Mineral. Deposita 52, 51-68.

Zhao Y., Yang, Y.Q., Ke, J.J., 2016a. Origin of Cu- and Ni-bearing magma and sulfide saturation mechanism: A case study of Sr-Nd-Pb-S isotopic composition and element geochemistry on the Huangshannan magmatic Ni-Cu sulfide deposit, Xinjiang. Acta Petrol. Sin. 32, 2086-2098 (in Chinese with English abstract).

Zhao, Y., Xue, C.J., Zhao, X.B., Yang, Y.Q., Ke, J., Zu, B., Zhang, G.Z., 2016b. Origin of anomalously Ni-rich parental magmas and genesis of the Huangshannan Ni-Cu sulfide deposit, Central Asian Orogenic Belt, Northwestern China. Ore Geol. Rev. 77, 57-71.

Zhao, Y., Xue, C.J., Zhao, X.B., Yang, Y.Q., Ke, J.J., 2015. Magmatic Cu-Ni sulfide mineralization of the Huangshannan mafic-untramafic intrusion, Eastern Tianshan, China. J. Asian Earth Sci. 105, 155-172.

Zhou, J.B., Wilde, S.A., 2013. The crustal accretion history and tectonic evolution of the NE China segment of the Central Asian Orogenic Belt. Gondwana Res. 23, 1365-1377.

Zhou, M.F., Arndt, N.T., Malpas, J., Wang, C.Y., Kennedy, A.K., 2008. Two magma series and associated ore deposit types in the Permian Emeishan large igneous province, SW China. Lithos 103, 352-368.

Zhou, M.F., Lesher, C.M., Yang, Z.X., Li, J.W., Sun, M., 2004. Geochemistry and petrogenesis of 270 Ma Ni-Cu-(PGE) sulfide-bearing mafic intrusions in the Huangshan district, Eastern Xinjiang, Northwest China: implications for the tectonic evolution of the Central Asian orogenic belt. Chem. Geol. 209, 233-257.

Zhou, M.F., Malpas, J., Song, X.Y., Robinson, P.T., Sun, M., Kennedy, A.K., Lesher, CM., Keays, R.R., 2002b. A temporal link between the Emeishan large igneous province (SW China) and the end-

Guadalupian mass extinction. Earth Planet. Sci. Lett. 196, 113-122.

Zhou, M.F., Yang, Z.X., Song, X.Y, Keays, R.R., Lesher, C.M., 2002a. Magmatic Ni-Cu-(PGE) sulfide deposits in China. The geology, geochemistry, mineralogy, mineral beneficiation of the platinum-group elements. Canadian Institute of Mining, Metallurgy and Petroleum, 54: 619-636.

Zhu, F.L., Tao, Y., Hu, R.Z., Yu, S.Y., Qu, W.J., Du, A.D., 2011. Re-Os isotopic constraints on the ore-forming mechanism for the Qingkuangshan Ni-Cu-PGE deposit in the Huili County, Sichuan Province. Acta Petrol. Sin. 27, 2655-2664 (in Chinese with English abstract).

Zhu, W. G., Zhong, H., Li, X. H., Liu, B. G., Deng, H. L., Qin, Y. 2007. $^{40}Ar$-$^{39}Ar$ age, geochemistry and Sr-Nd-Pb isotopes of the Neoproterozoic Lengshuiqing Cu-Ni sulfide-bearing mafic-ultramafic complex, SW China. Precambrian Res. 155, 98-124

Zi, J.W., Fan, W.M., Wang, Y.J., Cawood, P.A., Peng, T.P., Sun, L.H., Xu, Z.Q., 2010. U-Pb geochronology and geochemistry of the Dashibao Basalts in the Songpan-Ganzi Terrane, SW China, with implications for the age of Emeishan volcanism. Am. J. Sci, 310, 1054-1080.

Zindler, A., Hart, S., 1986. Annual review of earth and planetary sciences. Chemical geodynamics.14: 493-571.

Zwanzig, H.V., 2005. Geochemistry, Sm-Nd isotope data and age constraints of the Bah Lake assemblage, Thompson Nickel Belt and Kisseynew Domain margin: relation to Thompson-type ultramafic bodies and a tectonic model (NTS63J, O and P). Report of activities, 40-53.

## Figure captions

**Fig. 1. Plot of Ni grade vs. tonnage of deposit for Chinese Ni-Cu-(PGE) and PGE-(Cu)-(Ni) deposits and other Ni-Cu-PGE deposits worldwide. Data sources: Naldrett (2004), Wang and Zhou (2006), Lu et al., (2007), Tao et al. (2008), Song and Li (2009), Ding et al. (2010), Zhang et al. (2011), Tang et al. (2012), Gao et al. (2013), Xie et al. (2014), Wei et al. (2015), and Song et al. (2016).**

**Fig. 2. Simplified geological map of continental China showing major terrains and shield areas, the locations of magmatic sulfide deposits, and the relative sizes of their Ni resources. The ages of dated deposits are from Han et al. (2004), Wu et al. (2004), Zhou et al. (2004), Li et al. (2005), Wang et al. (2006), Zhou et al. (2008), Tao et al. (2009), Yang and Zhou (2009), Zi et al. (2010), Tang et al. (2011), Zhang et al. (2011), Xie et al. (2012), Zhang (2013), Hao et al. (2013), Wang et al. (2013a), Peng et al. (2013), Xia et al. (2013), Zhao et al. (2015), and Song et al. (2016). BMZ Baimazhai, BT Baotan; CJL Chajianling; EBT Erbutu; HS Heishan; HSDXN camp Huangshandong, Huangshanxi, and Huangshannan; HQL Hongqiling; JBS Jinbaoshan; JC Jinchuan; JBLK-Jingbulake; KLTK Kalatongke; LMH Limahe; LSX Lashuixia; PHC Piaohechuan; PB Pobei; TY-Tianyu; XRHM Xiarihamu; YLP Yangliuping; ZB Zhubu; ZA Zhouan.**

**Fig. 3. Ages of Chinese magmatic sulfide deposits. Data sources in Fig. 1.**

**Fig. 4. Whole-rock $SiO_2$, $TiO_2$, $Al_2O_3$, $FeO_t$, CaO, and $Na_2O+K_2O$ vs MgO. Data from Song et al. (2003), Wang et al. (2006), Tao et al. (2007, 2008), Xie et al. (2007), Yang and Zhou (2009), Tang et al. (2011), Li et al. (2012, 2015), Xie et al. (2012), Song et al. (2012), Sun et al. (2013), Tang et al. (2013), Xia et al. (2013), Wang et al. (2013b), Mao et al. (2014), Zhao et al. (2015), and Li et al. (2018). Olivine, orthopyroxene, clinopyroxene, and plagioclase data are average compositions at Jinchuan (Tonnelier, 2010). Samples with Ni+Cu > 0.5% have been excluded.**

**Fig. 5. Whole-rock Cr, Co, Ni, and Cu vs MgO. Data sources as in Fig. 4.**

**Fig. 6. Whole-rock La, Ba/Nb, La/Sm, and Gd/Yb vs MgO. Data sources as in Fig. 4**

**Fig. 7. εNd(t) versus $^{87}Sr/^{86}Sr(i)$ for Chinese Ni-Cu-(PGE) and PGE-(Cu)-(Ni) deposits. Data sources: magmatic sulfide deposits from Wang et al. (2006), Zhou et al. (2008), Song and Li (2009), Tang et al. (2011), Yang et al. (2012), Xia et al. (2013), Tang et al. (2013), Sun et al. (2013), Wang et al. (2013b), Wei et al. (2013, 2015), Duan et al. (2016), and Peng et al. (2016); MORB, EMI, EMII, and mantle array from Zindler and Hart (1986); LCC and UCC from Jahn et al. (1999).**

**Fig. 8. εNd vs γOs for Chinese Ni-Cu-(PGE) and PGE-(Cu)-(Ni) deposits. Data sources: Nd isotopes of Chinese deposits from references in Figs. 7; Os isotopes of Chinese deposits from Yang et al. (2005), Wang et al. (2007), Han et al. (2007), Zhang et al. (2008), Sun et al. (2008), Tao et al. (2010a, 2010b), Tang et al. (2011), Yang et al. (2008, 2012, 2014), Gao et al. (2013), Wang et al. (2013b), Wei et al. (2013, 2015), Ling (2014), Zhang et al. (2017), Mao et al. (2017). Eagle from Ding et al. (2012); Pechenga from Walker et al. (1994) and Hanski et al. (2014); Voisey's Bay from Amelin et al. (2000) and Lambert et al. (2000); Kambalda and Thompson from Lesher and Arndt (1995), Foster et al. (1996), Zwanzig (2005), and Hulbert and Hamilton (2005); Alexo and Raglan from Shirey and Barnes (1994), Gangopadhyay and Walker (2003), and Dupré et al. (1984); peridotite mantle from Rudnick et al. (2004); pyroxenite mantle from Lassiter et al. (2000) and Pearson and Nowell (2004); EMI and EMII from Zindler and Hart (1986) and Shirey and Walker (1998); SCLM from Ding et al. (2012); continental crust from Jahn et al. (1999) and Lambert et al. (1999).**

**Fig. 9. Whole-rock Ni, Cu, Ru, Rh, Pt, and Pd vs S. Data sources: Wang et al. (2006), Wang and Zhou (2006), Tao et al. (2007, 2008), Song et al. (2008, 2016), Tang et al. (2011), Yang et al. (2012, 2014), Li et al. (2012), Tang et al. (2013), Wei et al. (2013); Gao et al. (2013), Wang et al. (2013b), Chen et al. (2013), Mao et al. (2014), Xie et al. (2014), Zhao et al. (2015), Wei et al. (2015).**

**Fig. 10. Primitive mantle-normalized chalcophile element patterns for Chinese Ni-Cu-(PGE) and PGE-(Cu)-(Ni) deposits. Concentrations recalculated to 100% sulfide using normalization values from Barnes and Maier (1999). Data sources as in Fig. 9.**

**Fig. 11. Pd, Pt, Rh, and Ru in 100% sulfides vs Ir in 100% sulfides. Calculation method in text. Data sources as in Fig. 9.**

**Fig. 12. Box and whisker plot of $\delta^{34}S$ for parts of the Chinese magmatic sulfide deposits. Coloured bars span range, black bar indicates median value, coloured box span 25th and 75th percentiles (second and third quartiles); circles are outliers (1.5*(Q3-Q1)) and far outliers (3*(Q3-Q1)). YLP Yangliuping; KL Kalatongke; PB Pobei; HQL Hongqiling; HSN Huangshannan; HSD Huangshandong; JC Jinchuan; JBS Jinbaoshan; HS Heishan; LMH Limahe; XR Xiarihamu; BMZ Baimazhai. Data sources: Ripley et al. (2005), Zhang (2005), Tao et al. (2007), Wang (2010), Sun (2011), Dong et al. (2012), Jiang et al. (2012), Sun (2013), Xie et al. (2014), You (2014), Li et al. (2015), and Zhao et al. (2016a).**

**Fig. 13. Primitive mantle-normalized chalcophile element patterns with elements in order of increasing compatibility during mantle melting (Lesher and Keays, 2002). A) and B) Chinese Ni-Cu-(PGE) deposits; C) Chinese PGE deposit; D) komatiite-associated Ni-Cu-(PGE) deposits, E) modeled patterns for ores derived from a typical picrite at various R factors, and F) modeled patterns for ores derived from a typical ferropicrite at various R factors. Note that variations in R factor can increase PGE relative to Ni-Cu-Co, but cannot decrease PGE relative to Ni-Cu-Co. Data sources: Chinese deposits from references in Fig. 9; komatiite-associated deposits data from Lesher and Keays (2002); picrite composition and $D^{Sul/Sil}$ values from Barnes and Lightfoot (2005); ferropicrite composition and $D^{Sul/Sil}$ values from Barnes et al. (2001).**

**Fig. 14. Ni vs forsterite contents (Fo) of olivine (Ol) in Chinese magmatic sulfide deposits (A, C) and several komatiite-associated Ni-Cu-(PGE) deposits (A-B) for comparison. Blue curve represents fractional crystallization of Ol from a magma derived from a pyroxenitic source; green curve represents 2% crystallization of Ol from the same parental magma, followed by crystallization of Ol and segregation of sulfide (olivine:sulfide = 50:1); purple curve represents fractional crystallization of Ol from a magma derived from a peridotite source. Pyroxenite melts and peridotite melt compositions are from Straub et al. (2008, 2011). Data sources: Chinese deposits (A, C) from Li et al. (2004, 2012, 2015), Tao et al. (2007, 2008), Tang et al. (2009), Zhang et al. (2011), Deng et al. (2012), Lu et al. (2012), Wang and Wang (2012), Xie et al. (2013), Zhao et al. (2016b); Duke island deposit data from Thakurta et al. (2008); Eagle deposit from Ding (2010); Voisey's Bay from Li and Naldrett (1999); komatiite-associated deposits from Lesher and Stone (1996).**

**Fig. 15. A three-dimensional model illustrating a schematic formation process for Chinese Ni-Cu-(PGE) deposits related tectonic settings (after Windley et al., 2010).**

**Fig. 16. Th/Yb vs Nb/Yb for A) Chinese deposits and major reservoirs, B) Chinese deposits and two model assimilation-fractionation crystallizations trajectories, and C) Chinese deposits and two models for subduction zone enrichment. SZ: subduction zone. Data sources in Fig. 4. Mantle array after Pearce (2008). N-MORB, E-MORB, OIB, and Primordial Mantle (PM) after Sun and McDonough (1989); average lower crust (LC), upper crust (UC), total continental crust (CC) and felsic Phanerozoic (P) and Archean (A) crust are from Rudnick and Fountain (1995).**

**Fig. 17. Molar Sr/Zr vs molar ((Fe+Mg)/2)/Zr. Data sources in Fig. 4.**

**Fig. 18. $Pt_{100}$ and $Ru_{100}$ vs $Ir_{100}$ vs for Jinchuan. Data from Chen et al. (2013). Modelling parameters: $D_{Ir}^{Sul/Sil} = 35000$, $D_{Pd}^{Sul/Sil} = 35000$; $D_{Ir}^{MSS/Liq} = 5$, $D_{Pd}^{MSS/Liq} = 0.01$.**

## Table captions

**Table 1. Ages, mineralization types, tectonic settings, tectonic locations, morphologies, tonnages, grades, magma types, distances to craton margin, host rocks, associated rocks, and selected references for Chinese Ni-Cu-(PGE), Ni-Cu-PGE, and PGE-(Cu)-Ni deposits**

**Table 2. Variations in degree of olivine enrichment and degree of differentiation for Chinese Ni-Cu±PGE deposits (adapted from Lesher et al., 1984; Lesher and Keays, 2002; Arndt et al., 2008).**

# Figures

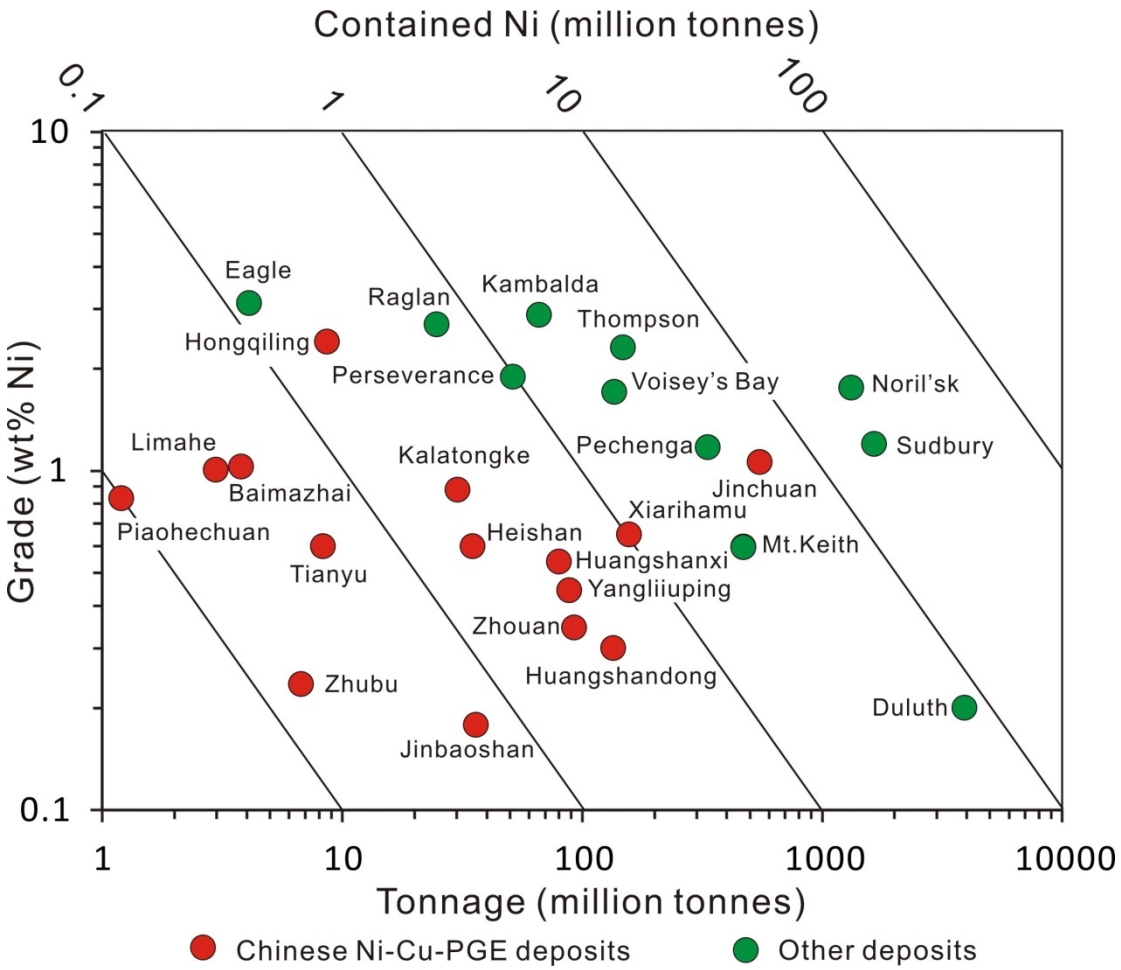


**Figure 1**

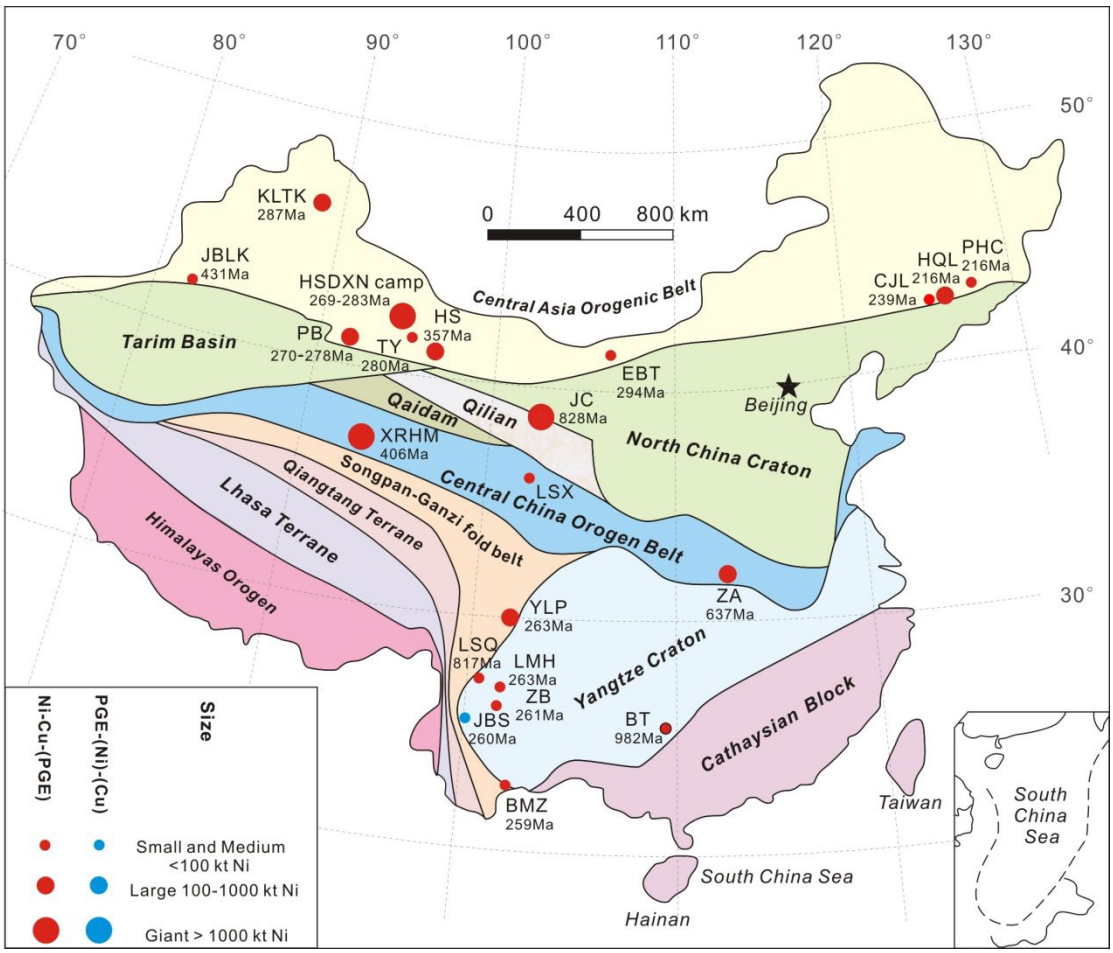
70°
80°
90°
100°
110°
120°
130°
50°
40°
30°
0
400
800 km
KLTK
287Ma
JBLK
431Ma
HSDXN camp
269-283Ma
HS
357Ma
PB
270-278Ma
TY
280Ma
Central Asia Orogenic Belt
Tarim Basin
EBT
294Ma
Beijing
JC
828Ma
Qaidam
Qilian
XRHM
406Ma
North China Craton
Songpan-Ganzi fold belt
Central China Orogen Belt
LSX
Qiangtang Terrane
Lhasa Terrane
Himalayas Orogen
ZA
637Ma
YLP
263Ma
LSQ
817Ma
LMH
263Ma
ZB
261Ma
JBS
260Ma
BT
982Ma
Yangtze Craton
Cathaysian Block
BMZ
259Ma
Taiwan
South China Sea
Hainan
PHC
216Ma
HQL
216Ma
CJL
239Ma
Ni-Cu-(PGE)
PGE-(Ni)-(Cu)
Size
Small and Medium
<100 kt Ni
Large 100-1000 kt Ni
Giant > 1000 kt Ni

**Figure 2**

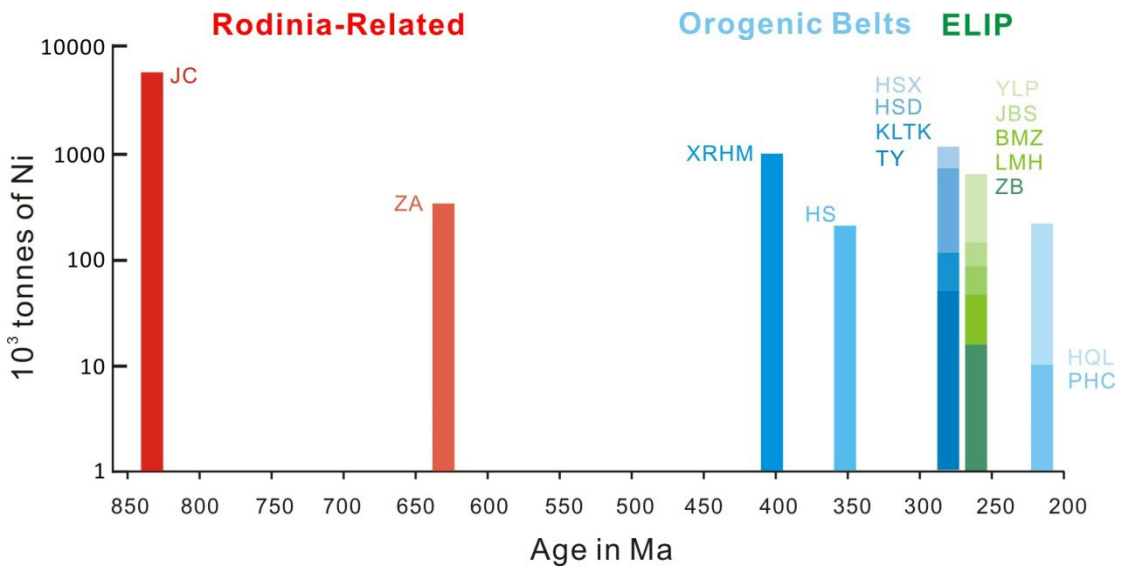
Rodinia-Related
Orogenic Belts
ELIP
10000
1000
100
10
1
$10^3$ tonnes of Ni
JC
ZA
XRHM
HS
HSX
HSD
KLTK
TY
YLP
JBS
BMZ
LMH
ZB
HQL
PHC
850
800
750
700
650
600
550
500
450
400
350
300
250
200
Age in Ma

**Figure 3**

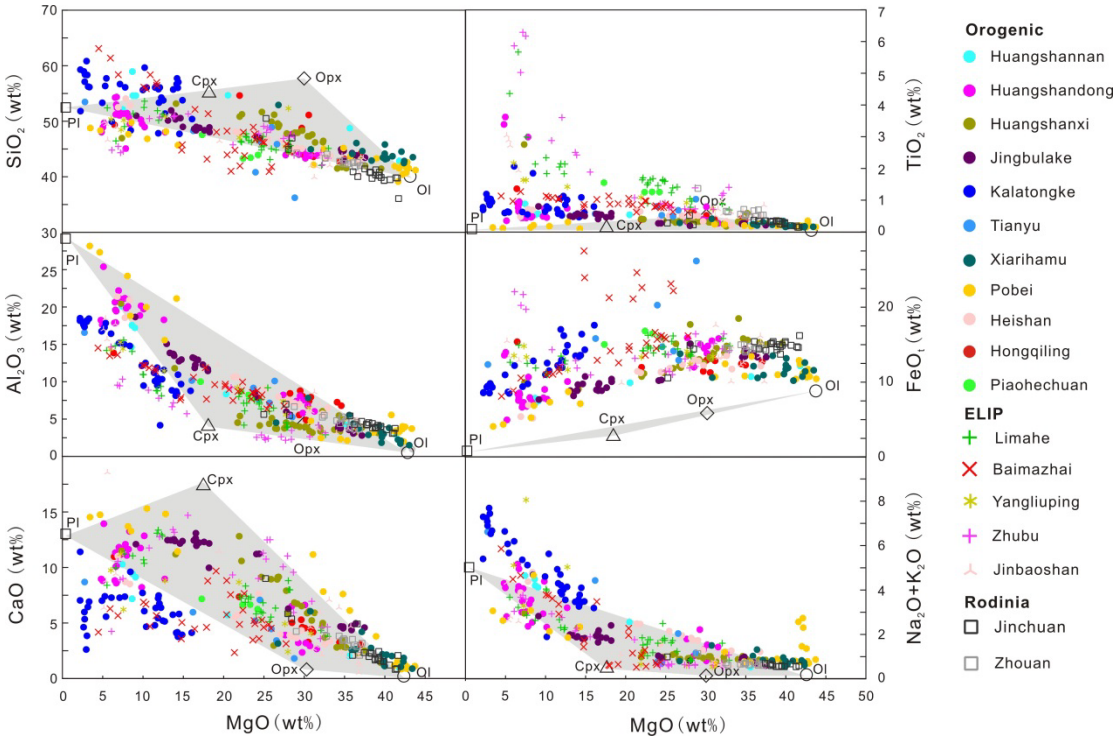
SiO2 (wt%)
TiO2 (wt%)
Al2O3 (wt%)
FeOt (wt%)
CaO (wt%)
Na2O+K2O (wt%)
MgO (wt%)
MgO (wt%)
Pl
Cpx
Opx
Ol
Orogenic
Huangshannan
Huangshandong
Huangshanxi
Jingbulake
Kalatongke
Tianyu
Xiarihamu
Pobei
Heishan
Hongqiling
Piaohechuan
ELIP
Limahe
Baimazhai
Yangliuping
Zhubu
Jinbaoshan
Rodinia
Jinchuan
Zhouan

**Figure 4**

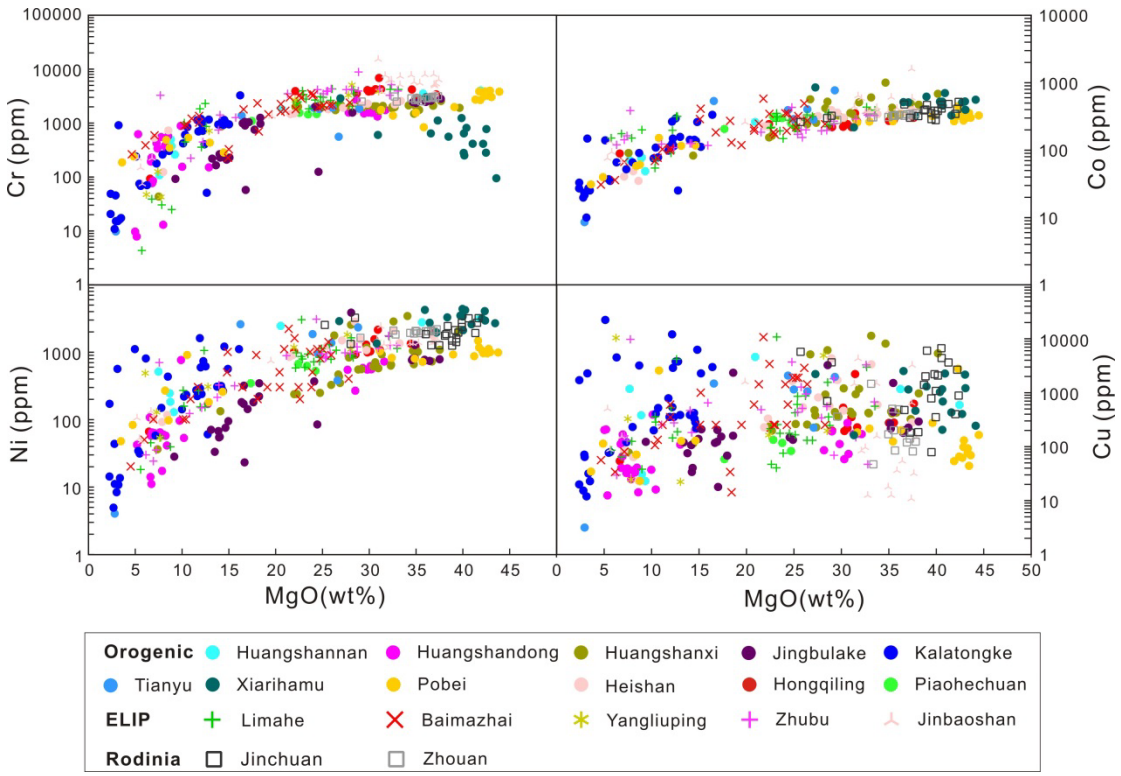
Cr (ppm)
Co (ppm)
Ni (ppm)
Cu (ppm)
MgO(wt%)
MgO(wt%)
Orogenic
Huangshannan
Huangshandong
Huangshanxi
Jingbulake
Kalatongke
Tianyu
Xiarihamu
Pobei
Heishan
Hongqiling
Piaohechuan
ELIP
Limahe
Baimazhai
Yangliuping
Zhubu
Jinbaoshan
Rodinia
Jinchuan
Zhouan

**Figure 5**

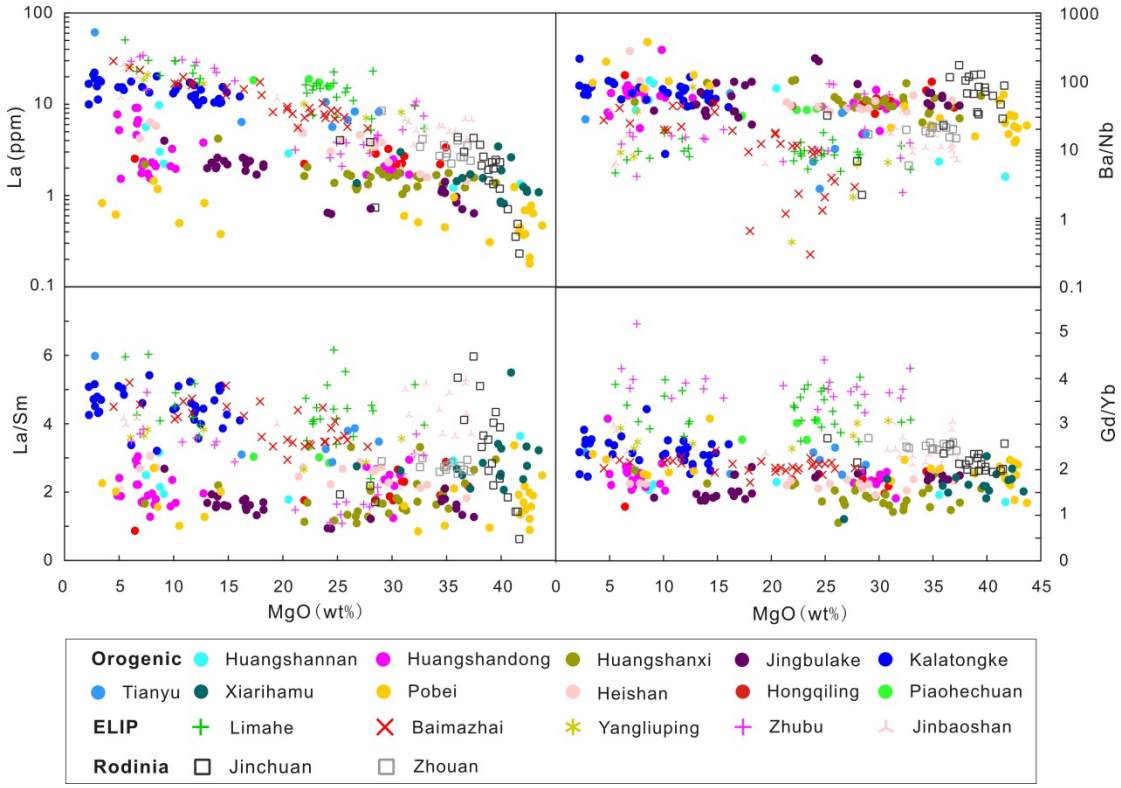
La (ppm)
Ba/Nb
La/Sm
Gd/Yb
MgO (wt%)
MgO (wt%)
Orogenic
Huangshannan
Huangshandong
Huangshanxi
Jingbulake
Kalatongke
Tianyu
Xiarihamu
Pobei
Heishan
Hongqiling
Piaohechuan
ELIP
Limahe
Baimazhai
Yangliuping
Zhubu
Jinbaoshan
Rodinia
Jinchuan
Zhouan

**Figure 6**

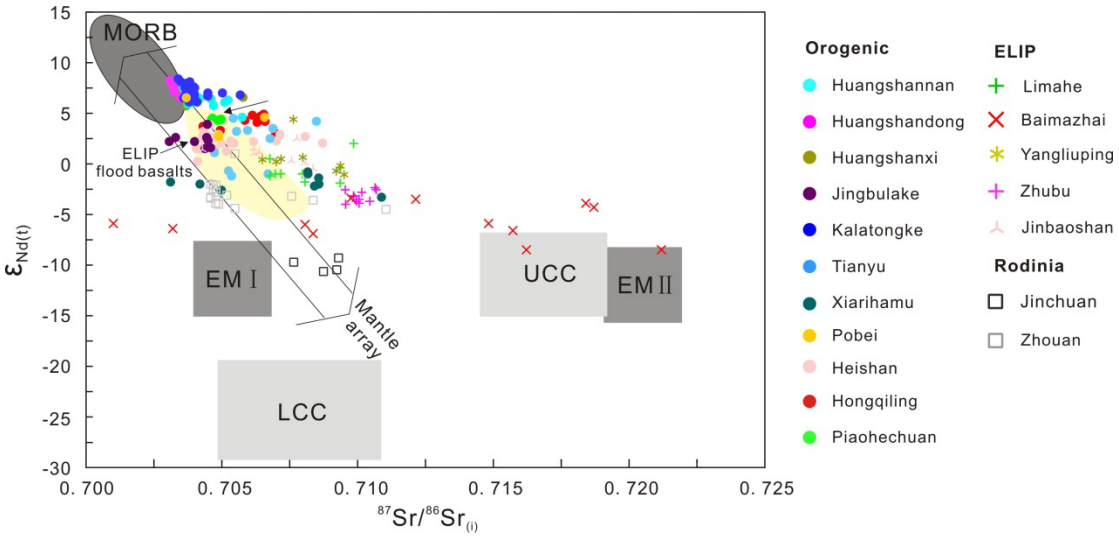
MORB
ELIP
flood basalts
EM I
EM II
UCC
LCC
Mantle
array
15
10
5
0
-5
-10
-15
-20
-25
-30
0. 700
0. 705
0. 710
0. 715
0. 720
0. 725
$\varepsilon_{Nd(t)}$
$^{87}Sr/^{86}Sr_{(i)}$
Orogenic
Huangshannan
Huangshandong
Huangshanxi
Jingbulake
Kalatongke
Tianyu
Xiarihamu
Pobei
Heishan
Hongqiling
Piaohechuan
ELIP
Limahe
Baimazhai
Yangliuping
Zhubu
Jinbaoshan
Rodinia
Jinchuan
Zhouan

**Figure 7**

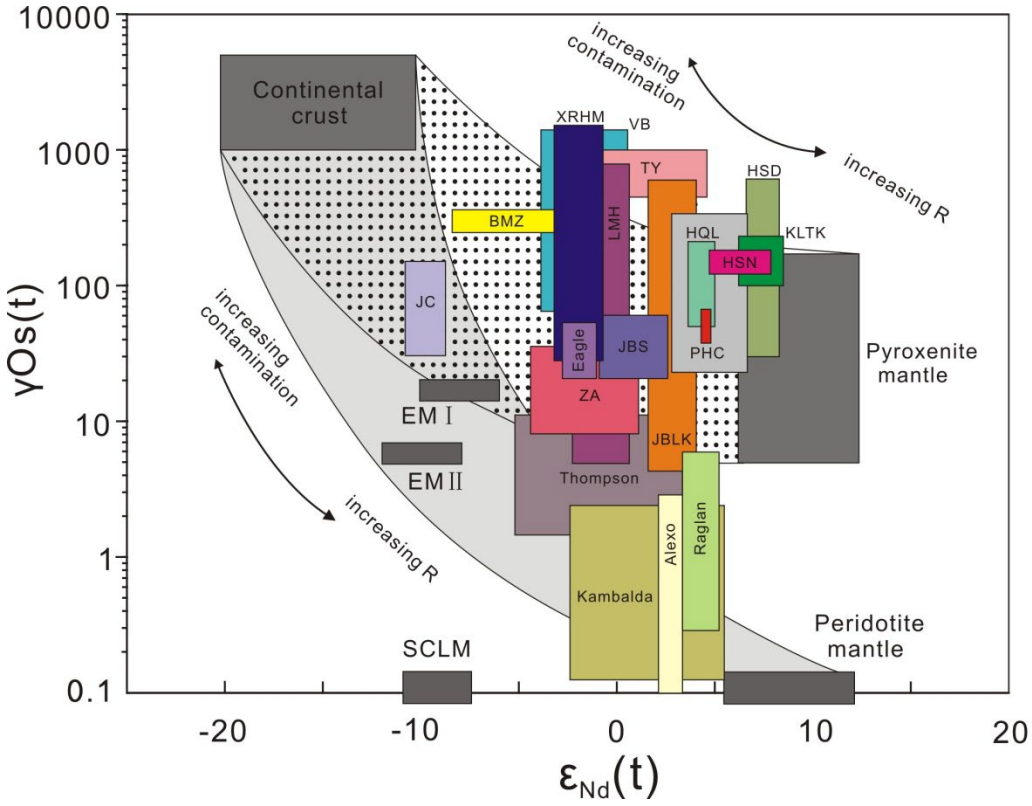
10000
1000
100
10
1
0.1
γOs(t)
-20
-10
0
10
20
εNd(t)
Continental crust
increasing contamination
increasing R
XRHM
VB
TY
HSD
BMZ
LMH
HQL
KLTK
HSN
JC
Eagle
JBS
PHC
Pyroxenite mantle
ZA
EM I
JBLK
EM II
Thompson
Alexo
Raglan
Kambalda
Peridotite mantle
SCLM

**Figure 8**

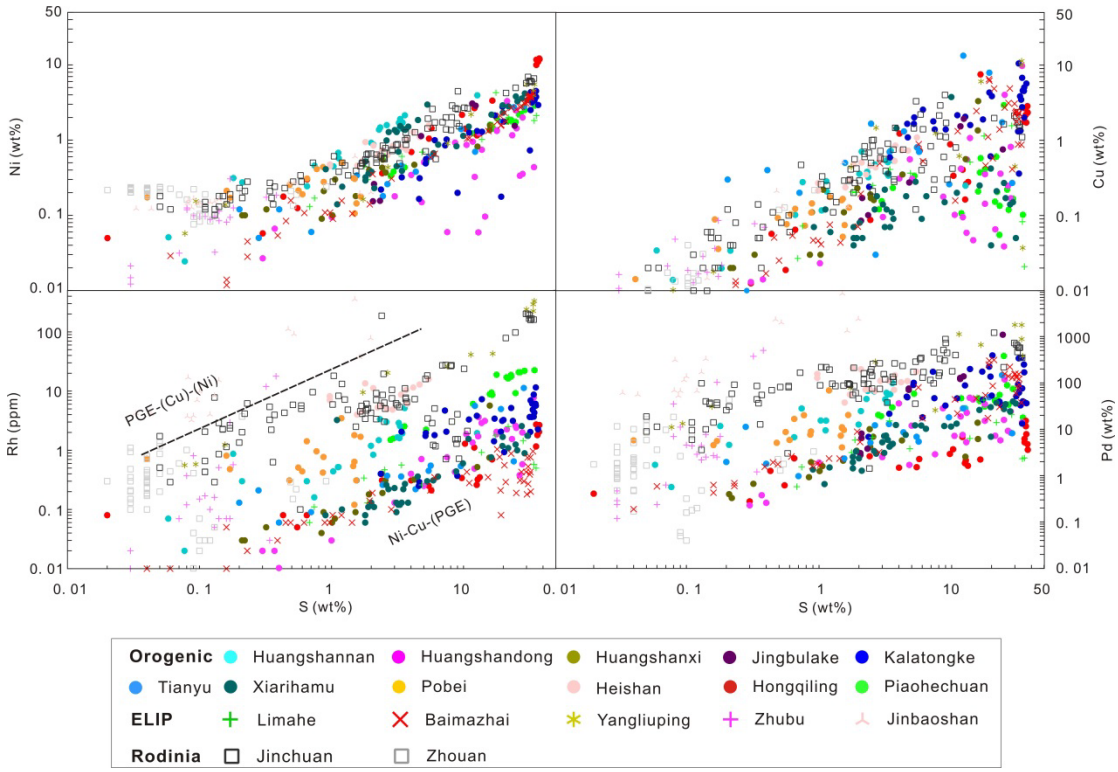
Ni (wt%)
Cu (wt%)
Rh (ppm)
Pd (wt%)
S (wt%)
S (wt%)
PGE-(Cu)-(Ni)
Ni-Cu-(PGE)
Orogenic
Huangshannan
Huangshandong
Huangshanxi
Jingbulake
Kalatongke
Tianyu
Xiarihamu
Pobei
Heishan
Hongqiling
Piaohechuan
ELIP
Limahe
Baimazhai
Yangliuping
Zhubu
Jinbaoshan
Rodinia
Jinchuan
Zhouan

**Figure 9**

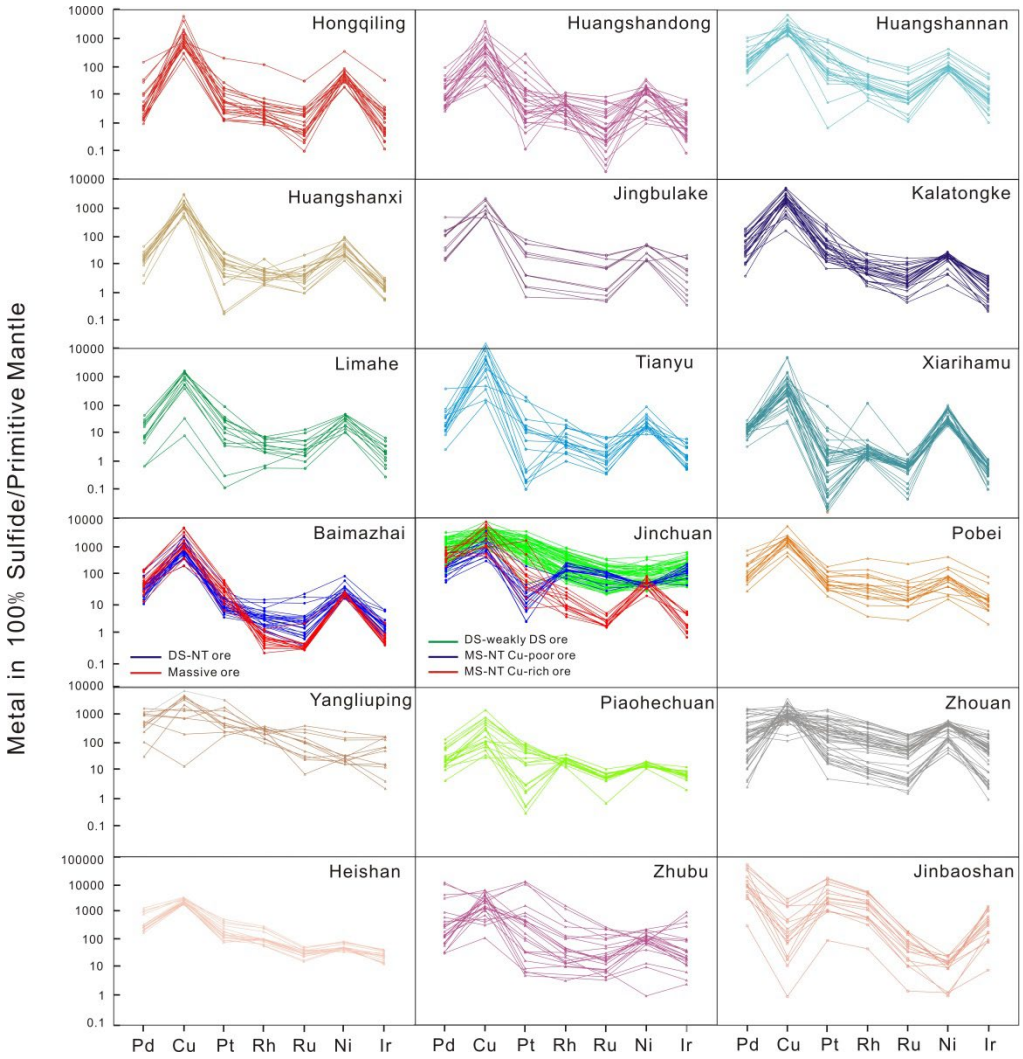
Metal in 100% Sulfide/Primitive Mantle
Hongqiling
Huangshandong
Huangshannan
Huangshanxi
Jingbulake
Kalatongke
Limahe
Tianyu
Xiarihamu
Baimazhai
Jinchuan
Pobei
Yangliuping
Piaohechuan
Zhouan
Heishan
Zhubu
Jinbaoshan
DS-NT ore
Massive ore
DS-weakly DS ore
MS-NT Cu-poor ore
MS-NT Cu-rich ore
Pd Cu Pt Rh Ru Ni Ir

**Figure 10**

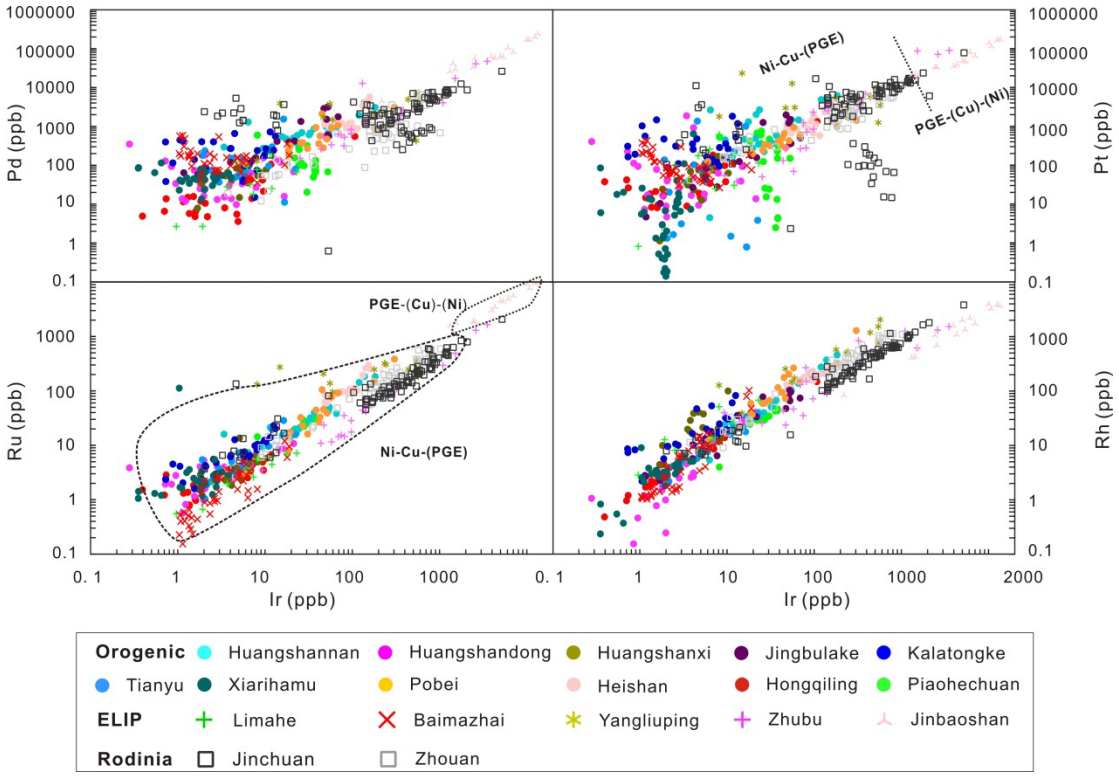
Pd (ppb)
Pt (ppb)
Ru (ppb)
Rh (ppb)
Ir (ppb)
Ir (ppb)
Ni-Cu-(PGE)
PGE-(Cu)-(Ni)
PGE-(Cu)-(Ni)
Ni-Cu-(PGE)
Orogenic
Huangshannan
Huangshandong
Huangshanxi
Jingbulake
Kalatongke
Tianyu
Xiarihamu
Pobei
Heishan
Hongqiling
Piaohechuan
ELIP
Limahe
Baimazhai
Yangliuping
Zhubu
Jinbaoshan
Rodinia
Jinchuan
Zhouan

**Figure 11**

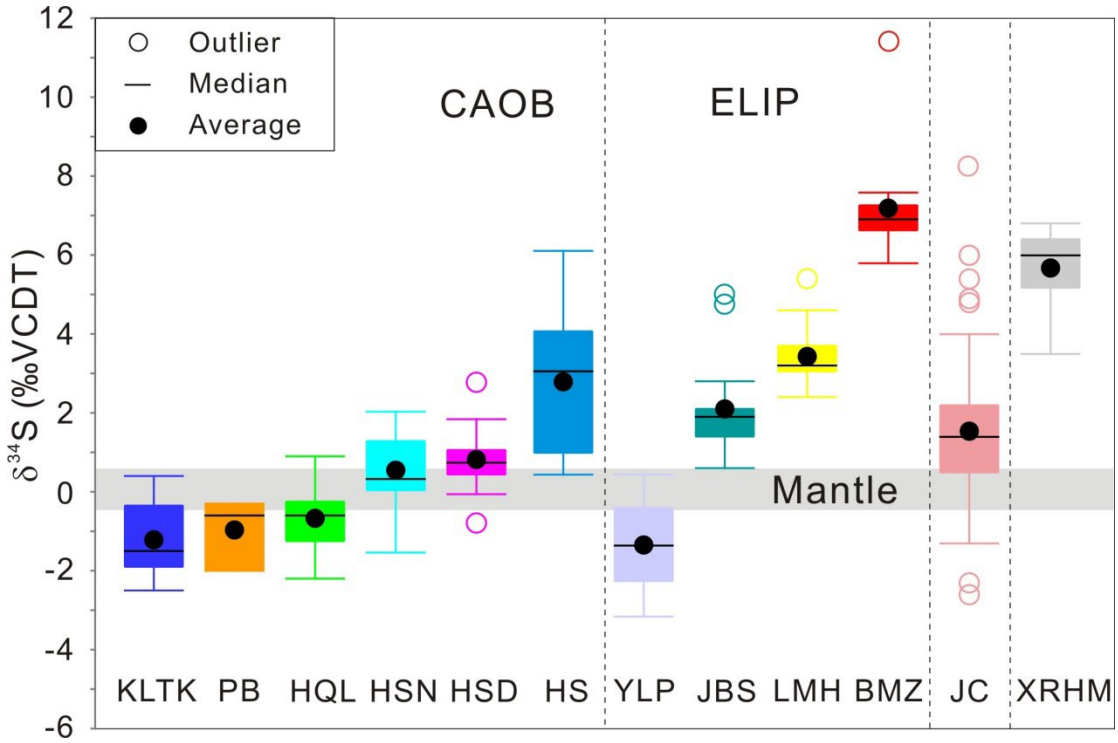
Outlier
Median
Average
CAOB
ELIP
Mantle
δ34S (‰VCDT)
12
10
8
6
4
2
0
-2
-4
-6
KLTK
PB
HQL
HSN
HSD
HS
YLP
JBS
LMH
BMZ
JC
XRHM

**Figure 12**

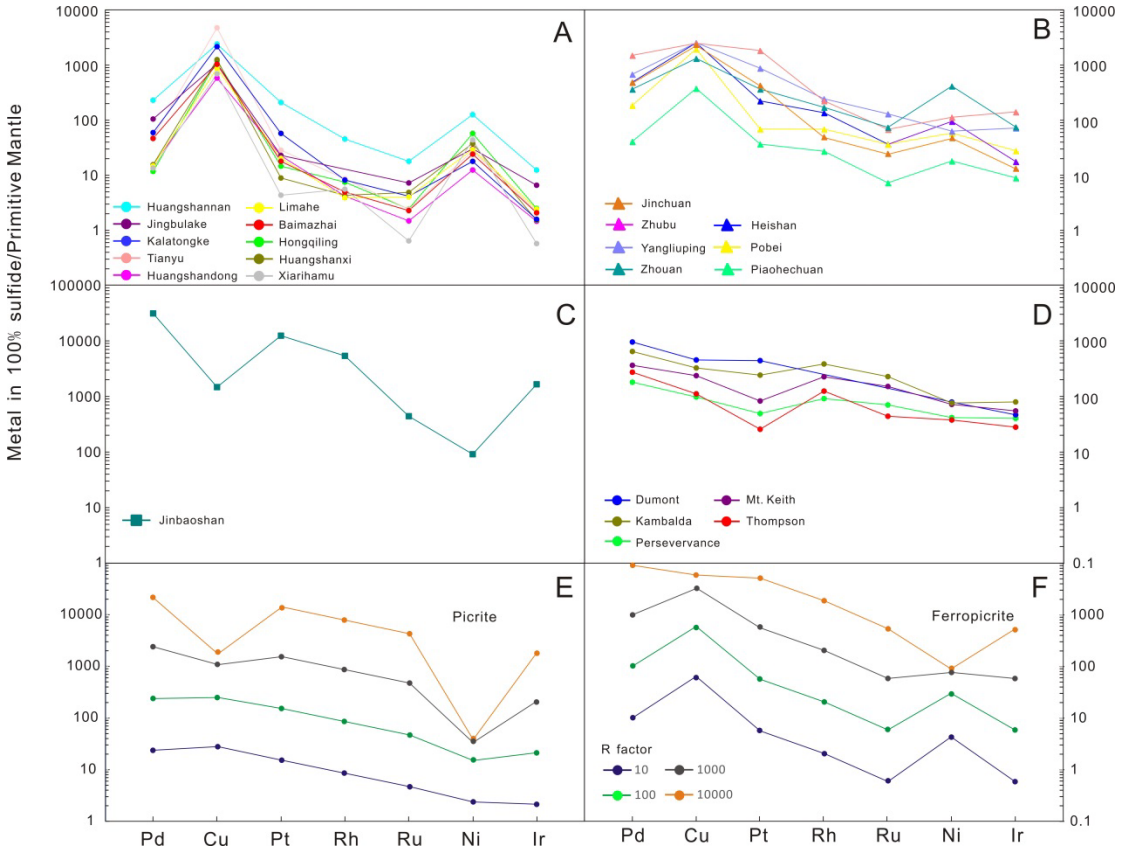
Metal in 100% sulfide/Primitive Mantle
A
B
C
D
E
F
Huangshannan
Jingbulake
Kalatongke
Tianyu
Huangshandong
Limahe
Baimazhai
Hongqiling
Huangshanxi
Xiarihamu
Jinchuan
Zhubu
Yangliuping
Zhouan
Heishan
Pobei
Piaohechuan
Jinbaoshan
Dumont
Kambalda
Perseverance
Mt. Keith
Thompson
Picrite
Ferropicrite
R factor
10
100
1000
10000
Pd
Cu
Pt
Rh
Ru
Ni
Ir

**Figure 13**

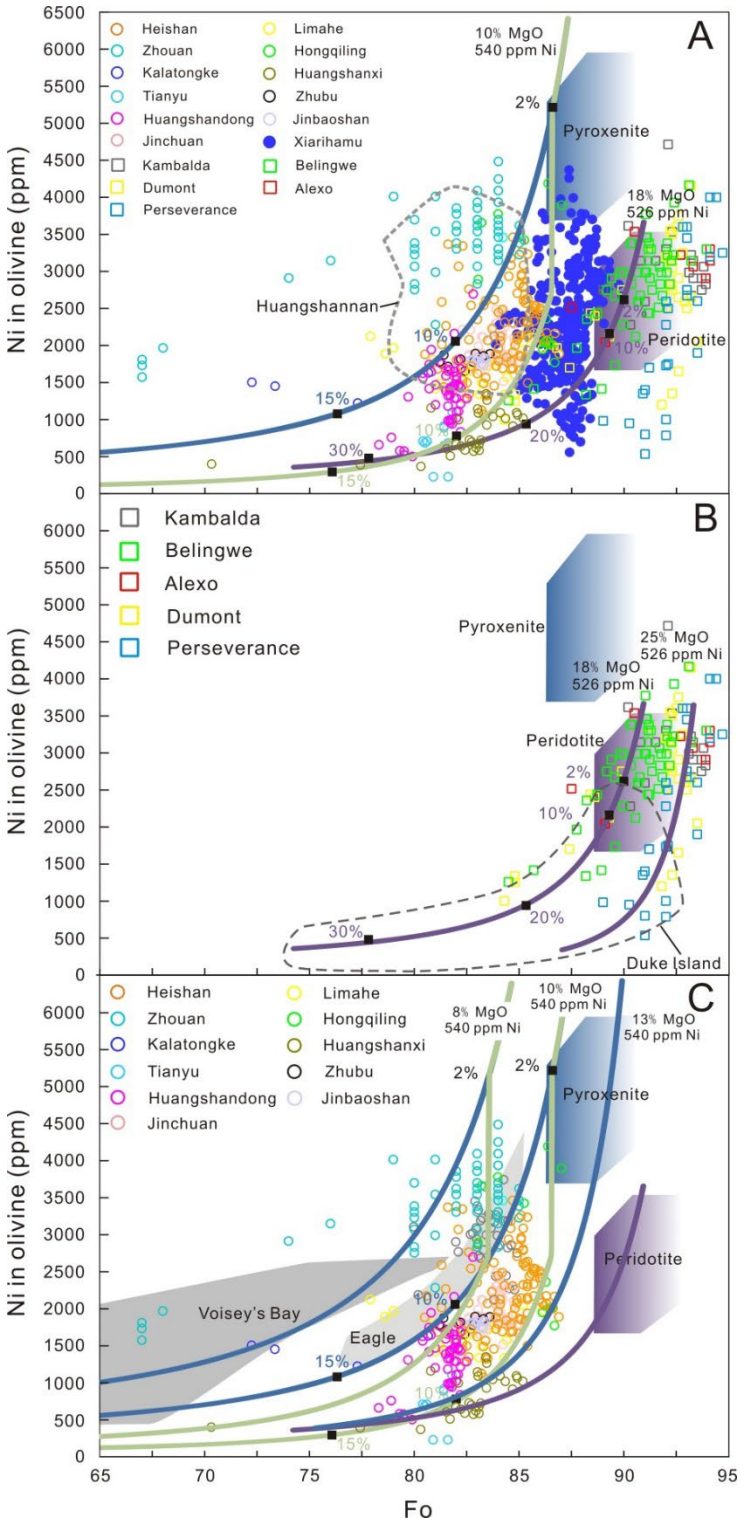
A
Heishan
Zhouan
Kalatongke
Tianyu
Huangshandong
Jinchuan
Kambalda
Dumont
Perseverance
Limahe
Hongqiling
Huangshanxi
Zhubu
Jinbaoshan
Xiarihamu
Belingwe
Alexo
10% MgO
540 ppm Ni
2%
Pyroxenite
18% MgO
526 ppm Ni
Huangshannan
Peridotite
10%
15%
30%
20%
B
Kambalda
Belingwe
Alexo
Dumont
Perseverance
Pyroxenite
25% MgO
526 ppm Ni
18% MgO
526 ppm Ni
Peridotite
Duke Island
C
8% MgO
540 ppm Ni
13% MgO
540 ppm Ni
Voisey's Bay
Eagle
Ni in olivine (ppm)
Fo

**Figure 14**

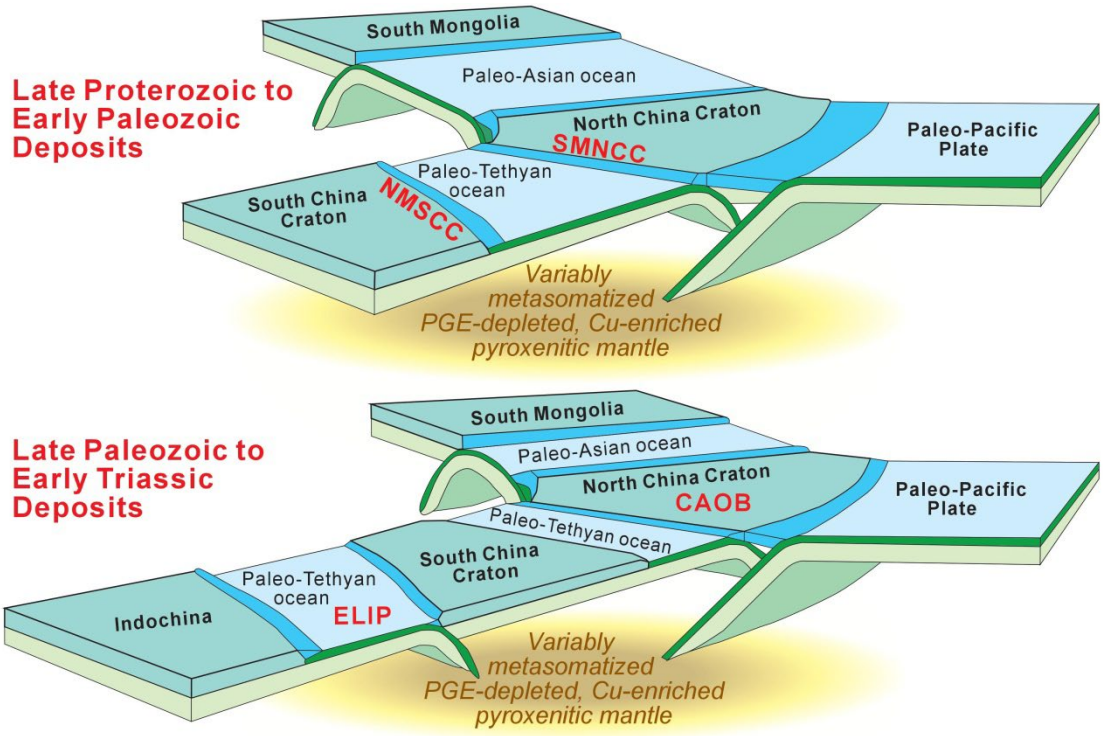
Late Proterozoic to Early Paleozoic Deposits
South Mongolia
Paleo-Asian ocean
North China Craton
SMNCC
Paleo-Pacific Plate
Paleo-Tethyan ocean
South China Craton
NMSCC
Variably metasomatized PGE-depleted, Cu-enriched pyroxenitic mantle
Late Paleozoic to Early Triassic Deposits
South Mongolia
Paleo-Asian ocean
North China Craton
CAOB
Paleo-Pacific Plate
Paleo-Tethyan ocean
South China Craton
Paleo-Tethyan ocean
ELIP
Indochina
Variably metasomatized PGE-depleted, Cu-enriched pyroxenitic mantle

**Figure 15**

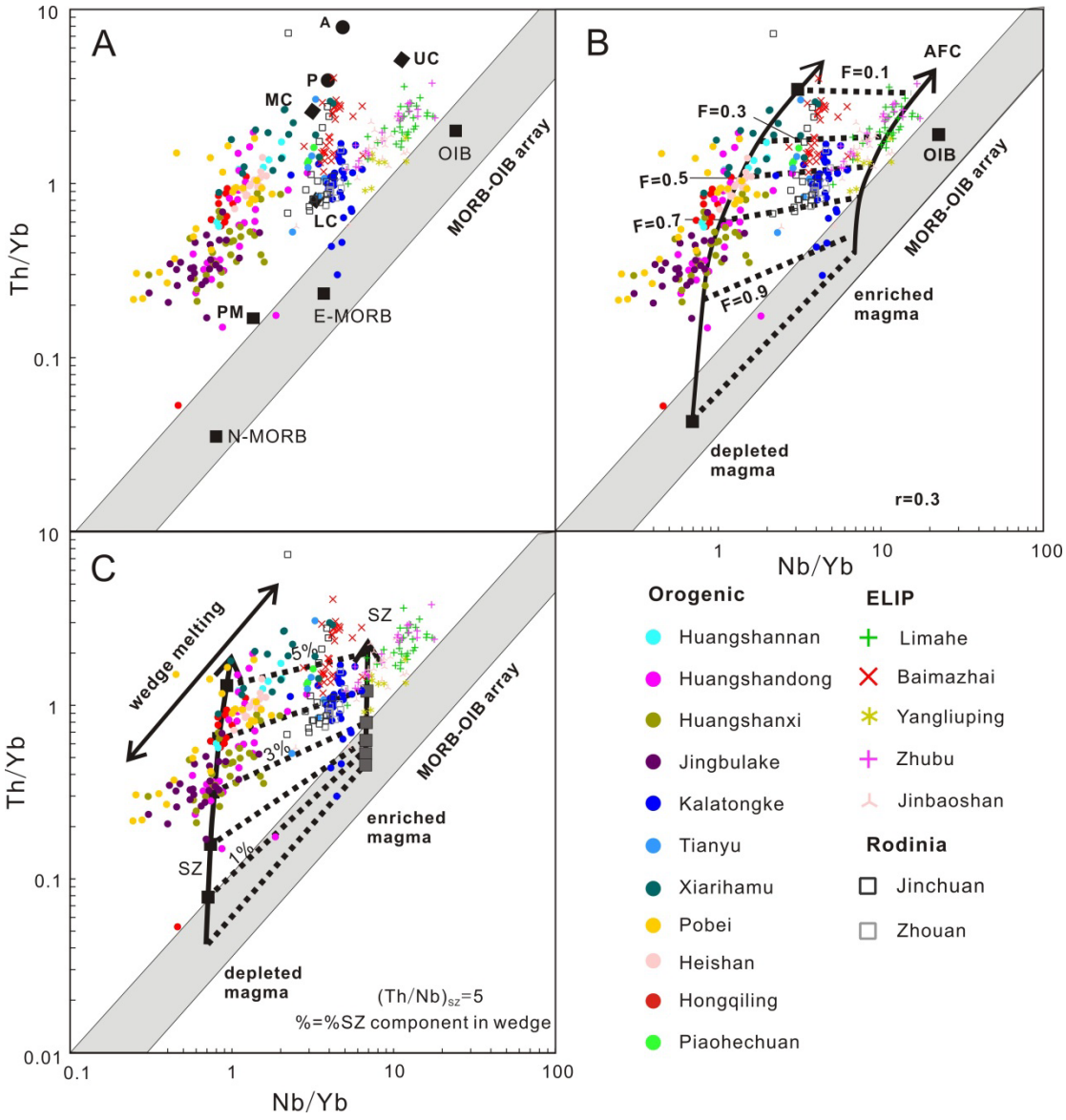
A
B
C
UC
P
MC
LC
PM
E-MORB
N-MORB
OIB
MORB-OIB array
AFC
F=0.1
F=0.3
F=0.5
F=0.7
F=0.9
enriched magma
depleted magma
r=0.3
wedge melting
SZ
5%
3%
1%
(Th/Nb)sz=5
%=%SZ component in wedge
Th/Yb
Nb/Yb
Orogenic
Huangshannan
Huangshandong
Huangshanxi
Jingbulake
Kalatongke
Tianyu
Xiarihamu
Pobei
Heishan
Hongqiling
Piaohechuan
ELIP
Limahe
Baimazhai
Yangliuping
Zhubu
Jinbaoshan
Rodinia
Jinchuan
Zhouan

**Figure 16**

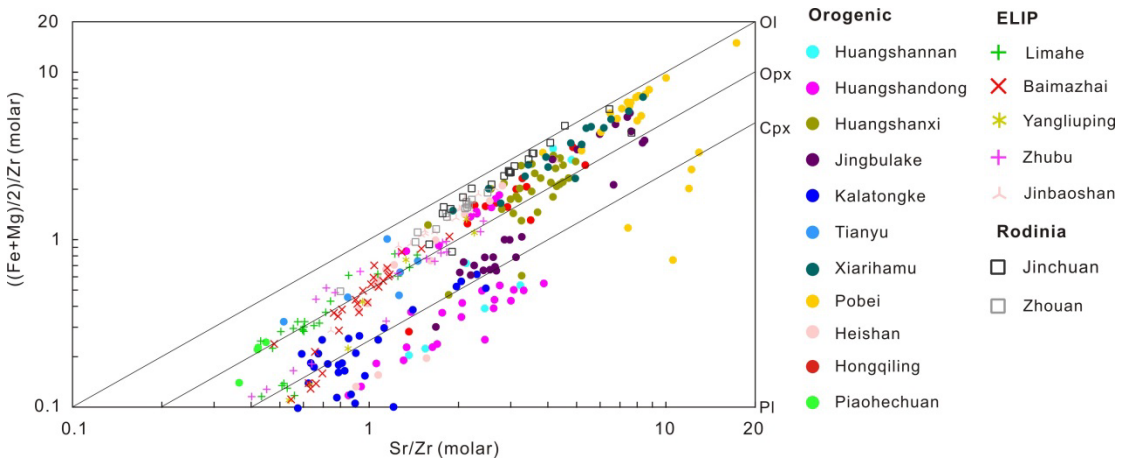
20
10
1
0.1
((Fe+Mg)/2)/Zr (molar)
0.1
1
10
20
Sr/Zr (molar)
Ol
Opx
Cpx
Pl
Orogenic
Huangshannan
Huangshandong
Huangshanxi
Jingbulake
Kalatongke
Tianyu
Xiarihamu
Pobei
Heishan
Hongqiling
Piaohechuan
ELIP
Limahe
Baimazhai
Yangliuping
Zhubu
Jinbaoshan
Rodinia
Jinchuan
Zhouan

**Figure 17**

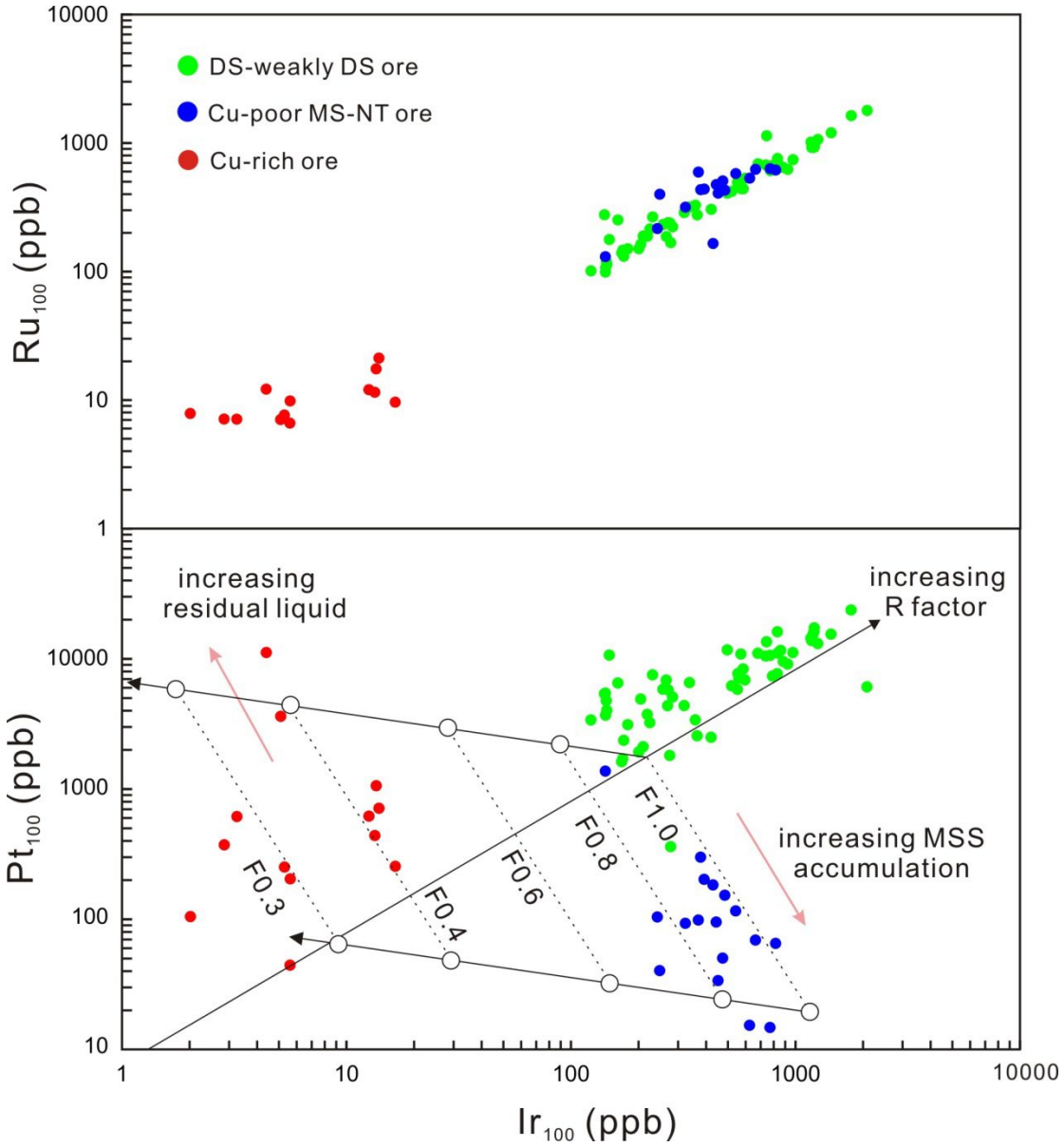
DS-weakly DS ore
Cu-poor MS-NT ore
Cu-rich ore
Ru100 (ppb)
Pt100 (ppb)
Ir100 (ppb)
increasing residual liquid
increasing R factor
increasing MSS accumulation
F0.3
F0.4
F0.6
F0.8
F1.0
10000
1000
100
10
1

**Figure 18**

# Tables

## Table 1

| **Deposit name** | **Age** (Ma) | **Mineralization type** | **Setting** | **Setting** | **Morphology** | **Surface area (km$^2$)** | **Tonnes** (Mt) | **Ni Grade** (%) | **Cu Grade** (%) |
|---|---|---|---|---|---|---|---|---|---|
| Jinchuan | 826 | Ni-Cu-(PGE) | Rift Margin | Rodinia | Segmented elongated rhomb with a narrow cone-shaped or sheet-like cross section | 1.4 | 550 | 1.05 | 0.7 |
| Zhouan | 637 | Ni-Cu-PGE | Rift Margin | Rodinia | Weakly triangle in surface with eliptical cross section | 2.7 | 96 | 0.35 | 0.11-0.17 |
| Jingbulake | 431 | Ni-Cu-(PGE) | Margin of orogenic belt | CAOB | Elongate rhomb with cross section of curved cone that narrows into the structure at each end | 3 | | 0.3-0.49 | 0.13 |
| Xiarihamu | 406 | Ni-Cu-(PGE) | Orogenic Belt | EKOB | Curved cone-like in cross section | 0.8 | 157 | 0.64 | 0.14 |
| Heishan | 357 | Ni-Cu-PGE | Margin of orogenic belt | CAOB | Elliptical shape, and curved cone-like in cross section | 0.4 | 35 | 0.6 | 0.3 |
| Kalatongke | 287 | Ni-Cu-(PGE) | Microcontinent | CAOB | Weakly elongate rhomb in surface plan with elliptical cross section | 0.25 | 30 | 0.88 | 1.3 |
| Huangshannan | 283 | Ni-Cu-(PGE) | Along fault | CAOB | Tube like in the east and a lens shaped like in the central and west | 4 | | 0.3-0.6 | 0.2-0.64 |
| Tianyu | 280 | Ni-Cu-(PGE) | Margin of terrane | CAOB | Dyke like shape, and curved cone-like in cross section | 0.2 | 8.3 | 0.6 | 0.24 |
| Pobei | 278 | Ni-Cu-PGE | Margin of orogenic belt | CAOB | Elliptical shape, and curved cone-like in cross section | 4 | | 0.3-0.6 | 0.08-0.14 |
| Huanshandong | 270 | Ni-Cu-(PGE) | Along fault | CAOB | Elongate rhomb with cross section of curved cone that narrows into the structure at each end | 5 | 135 | 0.3 | 0.16 |
| Huanshanxi | 269 | Ni-Cu-(PGE) | Along fault | CAOB | Ribbon like surface with curved cone cross section | 3 | 80 | 0.54 | 0.3 |
| Limahe | 263 | Ni-Cu-(PGE) | Intracontinent/ELIP | ELIP | Elongate rhomb with cross section of curved cone that narrows into the structure at each end and an asymmetric dyke-like keel | 1.8 | 3 | 1 | 0.6 |
| Yangliuping | 263 | Ni-Cu-PGE | Rift Margin/ELIP | ELIP | Sill | 0.6 | 90 | 0.45 | 0.16 |
| Zhubu | 261 | Ni-Cu-PGE | Intracontinent/ELIP | ELIP | Elliptical shape, and curved cone-like in cross section | 0.3 | 6.7 | 0.23 | 0.22 |
| Jinbaoshan | 260 | PGE | Rift Margin/ELIP | ELIP | Sill-like body | 5 | 34 | 0.17 | 0.14 |
| Baimazhai | 259 | Ni-Cu-(PGE) | Rift Margin/ELIP | ELIP | U-tubed shape with curved cone cross section | 0.15 | 3.8 | 1.03 | 0.81 |
| Hongqiling No.7 | 216 | Ni-Cu-(PGE) | Margin of orogenic belt | CAOB | Elongate rhomb with cross section of curved cone that narrows into the structure at each end | 0.1 | 8.9 | 2.3 | 0.63 |
| Piaohechuan | 216 | Ni-Cu-PGE | Margin of orogenic belt | CAOB | Elongate rhomb with cross section of curved cone | 0.07 | 1.2 | 0.83 | 0.05-0.39 |

## Table 1 (continued)

| Magma | MgO (%) | FeOt (%) | Distance to craton (km) | Host rock | Associated Rocks | References |
|---|---|---|---|---|---|---|
| Ferropicrite; High Mg basalt | 12.0-15.4 | 11.5-13.7 | <10 | dunite,lherzolite | Proterozoic granitoids, gneisses, and marbles | Chai and Naldrett, 1992; Tonnelier 2010;Li and Ripley, 2011 |
| High Mg basalt | >9.8 | | 60 | lherzolite | Sandstone, conglomerate, and mudstone of the Zhujiashan Formation | Wang et al.2012, 2013 |
| High-Mg tholeiitic basalt | ~12 | | 60 | Wehrlite, olivine gabbro, pyroxene diorite | Gneiss and schist with lenses of marble | Yang et al. 2009; Lightfoot and Evans-Lamswood, 2015 |
| Boninitic basalt; High Mg basaltic magma | 9.8 | | | lherzolite, harzburgite, websterite, gabbro | Precambrian schist, granitic gneiss, and marble of the Proterozoic Jinshuikou Formation | Li et al., 2015; Song et al., 2016 |
| High Mg basalt | 11.3 | 10 | 30 | lherzolite, harzburgite | Neoproterozoic dolomitic marble and siliceous slate | Xie et al. 2012 |
| High Si and high Mg basaltic magma mixing | 6.3-11.5 | 7.6 | | Diorite, Norite | Carboniferous Nanmingshu Formation clastic rocks | Zhang et al. 2009; Gao et al. 2012; Li et al. 2012 |
| Ni-rich magma; Picritic magma | 8.7-12.4 | 9.1-10 | 120 | lherzolite, websterite, gabbronorite, diorite | Lower Carboniferous quartz schist | Zhao et al. 2016; Mao et al. 2016, 2017 |
| High Mg basalt | | | 70 | Ol websterite, lherzolite | Precambrian metamorphic rocks with grades varying from greenschist to amphibolite | Tang 2009; Song 2014 |
| High Mg basalt | 11.5-14.9 | 8.4-9.3 | 25 | dunite,lherzolite, Ol websterite, gabbro, leucogabbro | Proterozoic schists, gneiss, and gneissic granite | Xia et al. 2013; Yang et al. 2014; Xue et al. 2016 |
| Basaltic magma | 7.4-10 | 8.4-9.4 | 120 | Lherzolite, Wehrlite, Gabbronorite | Lower Carboniferous Gandun Group turbidites | Sun et al. 2013; Mao et al. 2015 |
| Tholeiitic basalt | 8.7 | 8.36 | 120 | Ol websterite, lherzolite, gabbro | Carboniferous Gandu Group schists | Zhang et al.2011, Mao et al. 2014 |
| Flood basalt/Picritic magma | | | 150 | Wehrlite, Gabbro, Diorite | Neoproterozoic pyrite-bearing quartzites, graphitic slates, and siliceous limestones of the Huili Formation | Tao et al. 2008; Wang et al. 2017 |
| Flood basalt | | | 90 | Peridotite, Ol websterite, Ol clinopyroxenite, gabbro | Middle Devonian graphite-bearing schist, slate and graphite-bearing marble of the Weiguan Formation | Song et al.2003; Wang et al. 2017 |
| Flood basalt/Emeishan picrite | | | 120 | Lherzolite, Ol websterite, Gabbro, Gabbrodiorite | Precambrian gneiss of the Yuanmou Formation | Tang et al. 2013 |
| Flood basalt | 11 | 14 | <10 | Wehrlite | Devonian dolomite, sandstone and slate of the Jinbaoshan Formation | Tao et al. 2007; Wang et al. 2010 |
| Flood basalt/Mg-rich picritic magma | | | 20 | websterite, gabbro | Ordovician sandstone and slate of the Xiangyang Formation | Wang and Zhou,2006; Wang et al. 2006 |
| High Mg basalt | | | <10 | Orthopyroxenite, harzburgite, norite | Hulan Group gneiss, schist and marble | Wei et al. 2013 |
| High Mg basalt | | | <10 | Horblende olvine gabbro, Horblende gabbro | Hulan Group gneiss, schist and marble | Wei et al. 2015 |

**Table 2**

| | Poorly Differentiated | Weakly Differentiated | Strongly Differentiated |
|---|---|---|---|
| **Strongly enriched in Ol ± Opx** | Jinchuan<br>Zhouan<br>Xiarihamu<br>Jinbaoshan<br>Huangshannan<br>Pobei | | |
| **Moderately enriched in Ol ± Opx** | | Zhubu<br>Baimazhai<br>Limahe<br>Huangshanxi | |
| **Unenriched in Ol ± Opx** | | | Heishan<br>Huangshandong<br>Jingbulake<br>Kalatongke |

# Chapter 5: Summary of the thesis

The ~260 Ma Emeishan Large Igneous Province (ELIP) is located along the western margin of the Yangtze craton in southern China and is composed of voluminous flood basalts and associated mafic–ultramafic intrusions extending over an area of ~$3 \times 10^5$ $km^2$. The ELIP contains numerous magmatic Ni-Cu-(PGE) deposits hosted by small mafic-ultramafic intrusions and world-class Fe-Ti-V oxide deposits. The Jinbaoshan PGE-(Cu)-(Ni) deposit, as the only PGE-rich, sulfide-poor deposit in the ELIP, is also the largest PGE-dominant deposit in China. In contrast, the Baimazhai Ni-Cu-(PGE) deposit is the largest high-grade Ni-Cu sulfide deposit (>1 wt% Ni) in the ELIP. This study evaluated the genesis of the two deposits by a combination of light optical and scanning electron microscopy, electron probe microanalyzer and laser ablation inductively-coupled plasma mass spectrometry mineral chemistry, whole-rock major element and lithophile/chalcophile trace element geochemistry, and Nd-Os-S isotope geochemistry.

1) Both deposits appear to have formed through interaction of crustally-derived sulfide and a mafic magma derived from subduction-metasomatized pyroxenitic mantle during impingement of the Emeishan plume and the Paleo-Tethyan oceanic subduction system during the late Permian. However, the parental magma to the Jinbaoshan deposit appears to have been a hybrid picritic-ferropicritic magma, whereas the parental magma to the Baimazhai deposit appears to have been a low-Ti basalt.
2) The parental magma to the Jinbaoshan deposit contained ~970 ppm Ni, 90 ppm Cu, 4.9 ppb Pd, and 1.1 ppb Ir, and high R factors (800-40000) in a more dynamic system generated the high PGE tenors and enrichment in PGE >>> Cu > Ni. In contrast, the parental magma of the Baimazhai intrusion contained ~200 ppm Ni, 100 ppm Cu, 0.4 ppb Pd, 0.2 ppb Pt, 0.005 ppb Rh, 0.02 ppb Ru, and 0.01 ppb Ir, and lower R factors (100-1000) in a less dynamic system generated the lower PGE tenors and enrichment in Ni-Cu-Co >> PGE.
3) More than 16 different PGMs have been identified in the Jinbaoshan deposit, including moncheite $Pt(Te,Bi)_2$ (38% of total PGMs), mertieite II $Pd_8(Sb, As)_3$ (23%), atokite or rustenburgite $(Pd,Pt)_3Sn$ (6.7%), irarsite IrAsS (6.7%), sperrylite $PtAs_2$ (5.2%), native platinum (4.5%), merenskyite $(Pd,Pt)Te_2$ (2.2%), native palladium (1.5%), palarstanide $Pd_5(Sn,As)_2$ (1.5%), electrum (1.5%), hollingworthite RhAsS (0.7%), and kotulskite Pd(Te, Bi) (0.7%). PGMs are very rare in the Baimazhai deposit.

4) In the Jinbaoshan deposit, violarite, polydymite and pyrite host the majority of the PGEs, mainly Pd and IPGE. Pt is seldom hosted by BMS, which occurs mainly as discrete Pt minerals. PGE-hosted BMS are more enriched in magmatically incompatible chalcophile elements (Ag, Pb, Zn, Cd) than the Pn-Po in other PGE deposits. Post-magmatic metamorphic-hydrothermal alteration in the Baimazhai deposit modified primary pentlandite, pyrrhotite, and chalcopyrite, forming secondary pentlandite, pyrrhotite, violarite, and chalcopyrite. Secondary sulfides inherited PGEs from primary sulfides, are enriched in Ni-Co and Ag-Sb-Au-Pb and depleted in Sn.
5) S-Nd-Os isotopes indicate that crustal contamination is a key factor in forming magmatic sulfide deposits at Jinbaoshan, Baimazhai, and all other Ni-Cu-PGE deposits in China. The abundances of sulfide were low at Jinbaoshan and may have exsolved from the magma, whereas the abundances of sulfide were higher at Baimazhai most likely formed from a sulfide xenomelt.
6) Compared to Archean and Proterozoic magmatic Ni-Cu-PGE deposits elsewhere in the world, most of which appear to have formed primarily in rifted continental and rifted continental margin settings and to have been derived from peridotitic mantle, most of the Phanerozoic Ni-Cu-(PGE) deposits in China appear to have formed in convergent or formerly convergent settings, consistent with the inferred metasomatized pyroxenitic mantle sources.
7) Although Chinese Ni-Cu-PGE deposits appear to have been derived from pyroxenite sources, the inferred composition of the original peridotitic mantle, the degree of mantle metasomatism, and the degree of crustal contamination appear to have varied. Most deposits in the CAOB and EKOB appear to have been derived from magmas formed by partial melting a metasomatized but originally depleted mantle source with minor crustal contamination. Most deposits in the ELIP appear to have been derived from magmas formed by partial melting of more enriched sources than in the other metallogenic provinces. Those related to the breakup of Rodinia exhibit transitional geochemical characteristics.
8) The wide variations in tectonic-magmatic setting (breakup of Rodinia vs CAOB vs ELIP), host rock composition (dunite to diorite), geochemistry (HILE-enriched to HILE-depleted), and isotope geochemistry (high to low $^{87}Sr/^{86}Sr$-εNd-γOs, positive to negative $\delta^{34}S$) indicate that these factors were not critical to the formation of magmatic Ni-Cu-(PGE) and PGE-(Cu)-(Ni) deposits in China, but that the key factors are channelized magma flow to thermomechanically erode country rocks upstream in the system, to access crustal S, and to achieve at moderate to high R factors.